UNIVERSITAT DE BARCELONA

Deciphering the importance of heterogeneity in Myotonic Dystrophy type 1

Judit Núñez Manchón

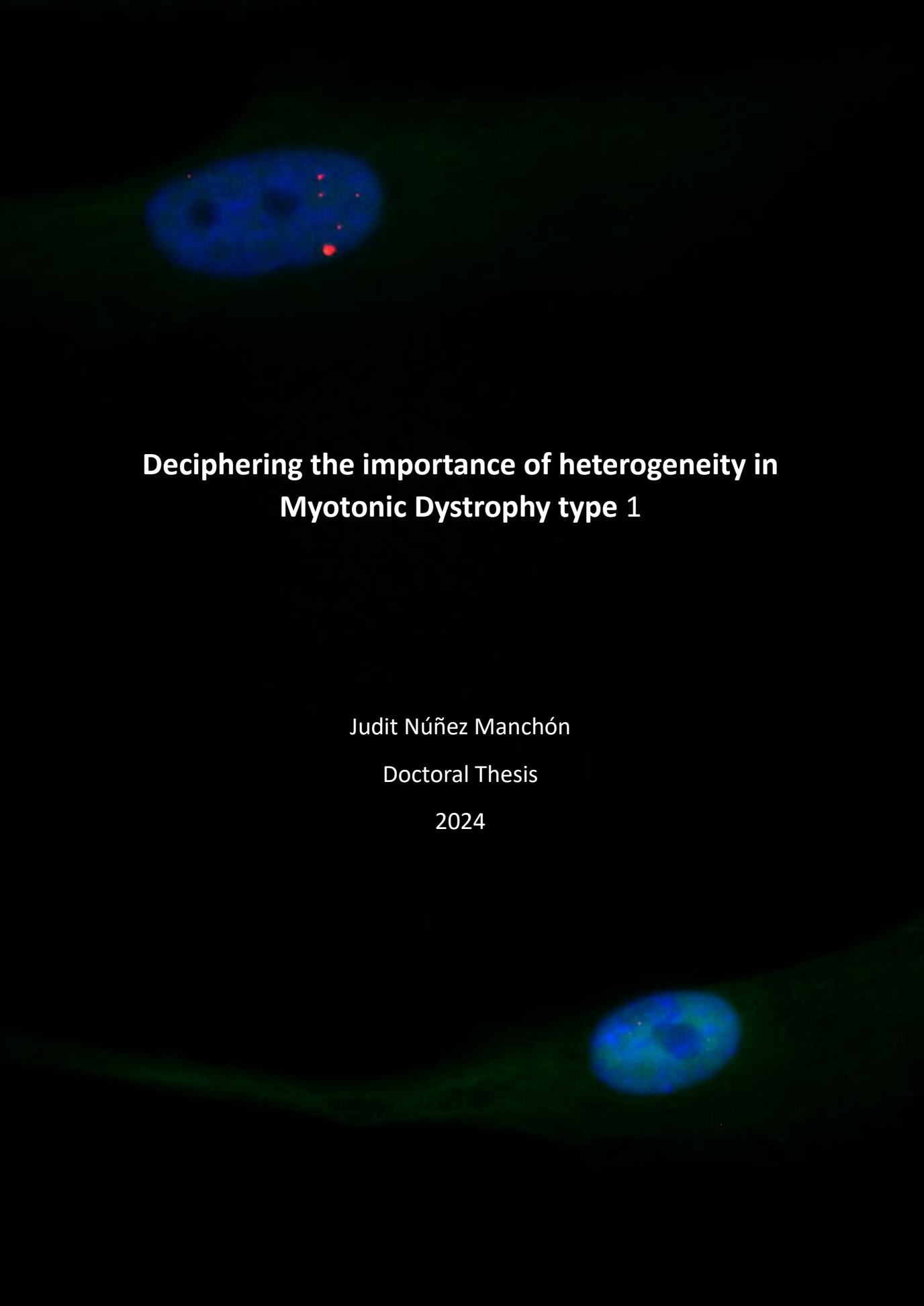

Deciphering the importance of heterogeneity in Myotonic Dystrophy type 1

Judit Núñez Manchón

Doctoral Thesis

2024

Institut d'Investigació Germans Trias i Pujol (IGTP)
Grup de Recerca en Malalties Neuromusculars de Badalona (GRENBA)

Doctorate in Genetics by the Universitat de Barcelona

Director: Dr. Gisela Nogales Gadea

Tutor: Dr. Bru Cormand Rifà

Student: Judit Núñez Manchón

Barcelona, September 2024

Memòria presentada per Judit Núñez Manchón per optar al grau de doctora per la Universitat de Barcelona

AKNOWLEDGEMENTS

Hay muchas personas que han contribuido para que esta tesis sea una realidad. No nací con el don de la palabra, pero espero que estas líneas sirvan para transmitir mi agradecimiento con todos los que la habéis hecho posible.

En primer lugar, quiero dar las gracias a Gisela por darme la oportunidad, hace casi ocho años, de formar parte de su laboratorio. Gracias por confiar en mí, por ayudarme a desarrollarme tanto personal como profesionalmente y por estar siempre dispuesta a escuchar y tener en cuenta mis opiniones. En segundo lugar, gracias a Mònica por llegar cuando más lo necesitábamos, por aportar experiencia y contagiarnos con su energía. Mi agradecimiento también a Bru por su feedback y por lo fácil que ha sido la comunicación con él.

Gracias a todas y cada una de las personas que han formado parte del grupo en algún momento a lo largo de estos años.

A l'Alfonsina, per la teva inesgotable energia, el teu positivisme i per acollir-nos a tots amb els braços oberts des del primer dia. To Emma, for your empathy, for always making time for a talk and for giving the best advices. A Ian, por tu predisposición, tu buen rollo y por hacerlo siempre todo tan fácil. To the three of you, thank you for the laughs, the support and for so many lifetime memories, in and outside the IGTP: the never-ending coffee breaks, the trips to congresses, the summer parties, Friday meetings at Emma's, Mallorca trips…. I will forever be grateful to have been able to share this journey with you.

A Renato, gracias por estar siempre dispuesto a echarme un cable con lo que hiciese falta y por las charlas a la hora del café. A Pau, Eva, Alexandra y Alicia, gracias por llenar de vida nuevamente el lab, por vuestro entusiasmo y buen hacer. Gracias también a todos los que en algún momento habéis pasado por el grupo y aportado vuestro granito de arena: Aida, Jaume, Adrián, Jorge, Marta, Shelly, Soheil, Júlia, Aina, Nacho y Paula.

Gracias a los clínicos del grupo, Alicia, Alba, Miriam, Eduard, Andrea, Giuseppe, Sebas, Jaume y Guillem, por el conocimiento que me habéis aportado en las sesiones conjuntas y por estar siempre disponibles para ayudarme con la información clínica de los pacientes.

Gracias a Bea sin la cual esta tesis un nunca hubiera sido posible. Gracias también a Fany por toda su ayuda y porque trabajar con ella en la distancia ha sido muy fácil.

Gracias a todos aquellos con los que he tenido el placer de compartir el laboratorio de la primera planta del edificio Mar durante este tiempo, por el buen ambiente y por no dudar en ayudarme cuando lo he necesitado. Gracias también a Laura por dedicar parte de tu tiempo a enseñarme a hacer análisis de célula única.

Gracias a todo el personal de las plataformas del IGTP por su ayuda. A Pilar por resolverme cualquier duda que tuviese respecto a los resultados de secuenciación. A Pilar y Jakub por ayudarme siempre que lo he necesitado con el microscopio. Y a Marco por ayudarnos a poner a punto el sorting para el análisis de célula única. Gracias también al equipo de lab managing por estar siempre disponibles y por hacer que nuestro trabajo se desarrolle de la mejor forma posible. Y por supuesto, gracias a Maribel, Emi, Montse y Noe por su ayuda y simpatía.

Thanks to Dushka and her team for welcoming me into their lab for a few weeks, it was a very nourishing experience. Special thanks to Jovan for making time in his extremely busy schedule to teach me how to do a small-pool PCR and for helping us any time we were having trouble with the sample's genetic analysis in the lab.

Finalmente, gracias a mi familia. Especialmente a mis padres, gracias al esfuerzo de los cuales esto ha sido posible y quienes siempre apoyaron mis decisiones. A Estela, por ser mi "pepito grillo" y a Raúl por tu apoyo y por tu permanente buen humor. Gracias también al pequeñajo Gabriel, a Rubén, a Irene y a mis tíos por estar ahí. Os quiero.

ABSTRACT

Myotonic dystrophy type 1 (DM1) is a genetic and multisystemic muscular dystrophy with autosomal dominant inheritance. It is caused by a CTG expansion in the 3' end of DMPK gene. Symptoms are mainly caused by the accumulation of toxic RNA aggregates, called RNA foci, which sequester MBNL1 protein, a splicing regulator. The symptoms can appear at any age and they are highly heterogeneous between patients. This heterogeneity is partially derived from the CTG repeat length, which due to both somatic and intergenerational instability, differs both between patients and between different tissues of a single patient.

In this thesis the main focus is put on DM1 heterogeneity, which is often ignored in studies. Heterogeneity is an important feature to consider because it could have an influence in the molecular DM1 alterations at cellular level and in the efficacy of a therapy, meaning that DM1 models representing said heterogeneity would be useful. The thesis is divided in three chapters, each of which, explores DM1 heterogeneity from a different perspective.

Chapter 1 is focused on the study of heterogeneity from a molecular point of view. The study analyses differences in RNA foci and MBNL1 aggregates expression between different cell types or DM1 subtypes. On the one hand, the analysis of four different cell types (lymphoblasts, fibroblasts, myoblasts and myotubes) revealed significant differences between them, being myotubes the cell type with a higher number of RNA foci and myoblasts the cell type with a higher MBNL1 sequestration. Myoblasts were also used to perform a single cell study to determine heterogeneity in expression levels and whether it correlates with the number of RNA foci expressed in the same cell. Results revealed no correlation. On the other hand, the analysis of RNA foci in the 5 subtypes of DM1 (congenital, infantile, juvenile, adult and late-onset) revealed a higher accumulation of RNA foci in patients with an earlier age of onset. In this chapter the existence of molecular heterogeneity both between and within patients is confirmed.

Chapter 2 is focused on how DM1 heterogeneity impacts the degree of efficacy of a treatment. The study assesses the therapeutic potential of antagomiRs 23b and 218, two antisense oligonucleotides that block MBNL1 repressors miRNAs 23b and 218. A previous study proved that these antagomiRs have a positive impact in DM1 pathogenesis, however DM1 heterogeneity was not

assessed. In this study eight independent human DM1 primary myoblast lines with CTG repeats ranging from 117 to 1054 were treated with both antagomiRs. It was found that miR-23b and 218 are upregulated in patient myoblasts and that miRNAs overexpression correlated with CTG expansion size. The treatment reduced the miRNAs activity, increasing MBNL1 protein levels and reducing DMPK expression and foci number. Moreover, MBNL1-dependent splicing events were significantly rescued and the degree of MBNL1 enhancement correlated with splicing rescue. In this chapter it is concluded that antagomiRs 23b and 218 have therapeutic potential across different genetic backgrounds.

Chapter 3 is focused on the need for in vitro models to study DM1 and to validate therapies that represent the clinical and genetic heterogeneity observed in DM1 patients. In the study, three DM1 muscle lines derived from patients with different DM1 subtypes and clinical backgrounds were immortalized and characterized at the genetic, epigenetic, and molecular levels. Results showed that the three immortalized cell lines displayed all the expected DM1 hallmarks with significant differences between the cell lines for several of the studied alterations. Moreover, the response of the immortalized cell lines to the previously tested therapeutics was also analysed with positive results. In this chapter it is concluded that the three immortalized DM1 cell lines developed in this study are suitable to study the pathophysiological heterogeneity of DM1 and to test future therapeutic options.

TABLE OF CONTENTS

ABBREVIATIONS

ASO = antisense oligonucleotide

AUC = area under the curve

BIN1 = the bridging integrator 1/ amphisphysin 2

CACNA1S = calcium voltage-gated channel subunit alpha 1 S

CAG – Cytosine-Adenine-Guanine

CCG – Cytosine-Cytosine-Guanine

CCND1 = cyclin D1
CDK4 = cyclin-dependent kinase 4
CGG – Cytosine-Guanine-Guanine

CELF1/CUGBP1 = CUG-binding protein 1

CLCN1 = chloride voltage-gated channel 1

CNS = central nervous system

CpG = cytosine-guanine sites

CpGi = CpG island

CRISPR-Cas9 = clustered regularly interspaced short palindromic repeats - CRISPR-associated protein 9
CTCF = CCTC-binding factor

CTC – Cytosine-Thymine-Cytosine

CTG – Cytosine-Thymine-Guanine

CUG – Cytosine-Uracil-Guanine

DM1 = myotonic dystrophy type 1

DMD = dystrophin

DMPK = dystrophia myotonica protein kinase

DMWD = dystrophia myotonica WD repeat-containing protein

DNA = desoxyribonucleic acid

DRG = disease-related genes
ePAL = estimated progenitor allele length

GSK3β = glycogen synthase kinase 3 beta

ESCs = embryonic stem cells

iPSCs = induced pluripotent stem cells

INSR = insulin receptor

iPSC = induced pluripotent stem cell
LDB3 = LIM domain binding 3

LNA – Locked Nucleic Acid

MAPT = microtubule-associated protein tau
MBNL = muscleblind-like
miRNA = microRNA
MIRS = Muscular Impairment Rating Scale

2'-MOE = 2'-O-Methoxyethyl

MRC = Medical Research Council

mRNA = Messenger Ribonucleic Acid

mRS = Modified Rankin Scale

MyoD = myoblast determination protein 1
NMDAR1 = NMDA receptor 1
2'-OMe – 2'-O-Methyl

OSKM = Reprogramming cocktail (Oct4, Sox2, Klf4 and c-Myc,)
PCR – Polymerase Chain Reaction

PKC – Protein Kinase C

PPFIBP1 = PPFI binding protein 1

pri-miRNA = Primary transcript of the miRNA
PS = Phosphorothioate

RISC = RNA-induced silencing complex

RNA = Ribonucleic acid

RNAi = RNA interference

ROC = Receptor operating curve

RyR1 = Ryanodine receptor 1

SCN5 = Sodium channel protein type 5
SERCA1 = Sarcoplasmatic/endoplasmatic reticulum calcium ATPase 1

siRNA = Small interfering RNA

SIX5 = SIX homeobox 5

SOS1 = SOS Ras/Rac Guanine Nucleotide Exchange Factor 1

SP-PCR = Small pool polymerase chain reaction

TCGA = Thymine-Cytosine- Guanine-Adenine
TERT = Catalytic subunit of human telomerase
UTR = Untranslated region

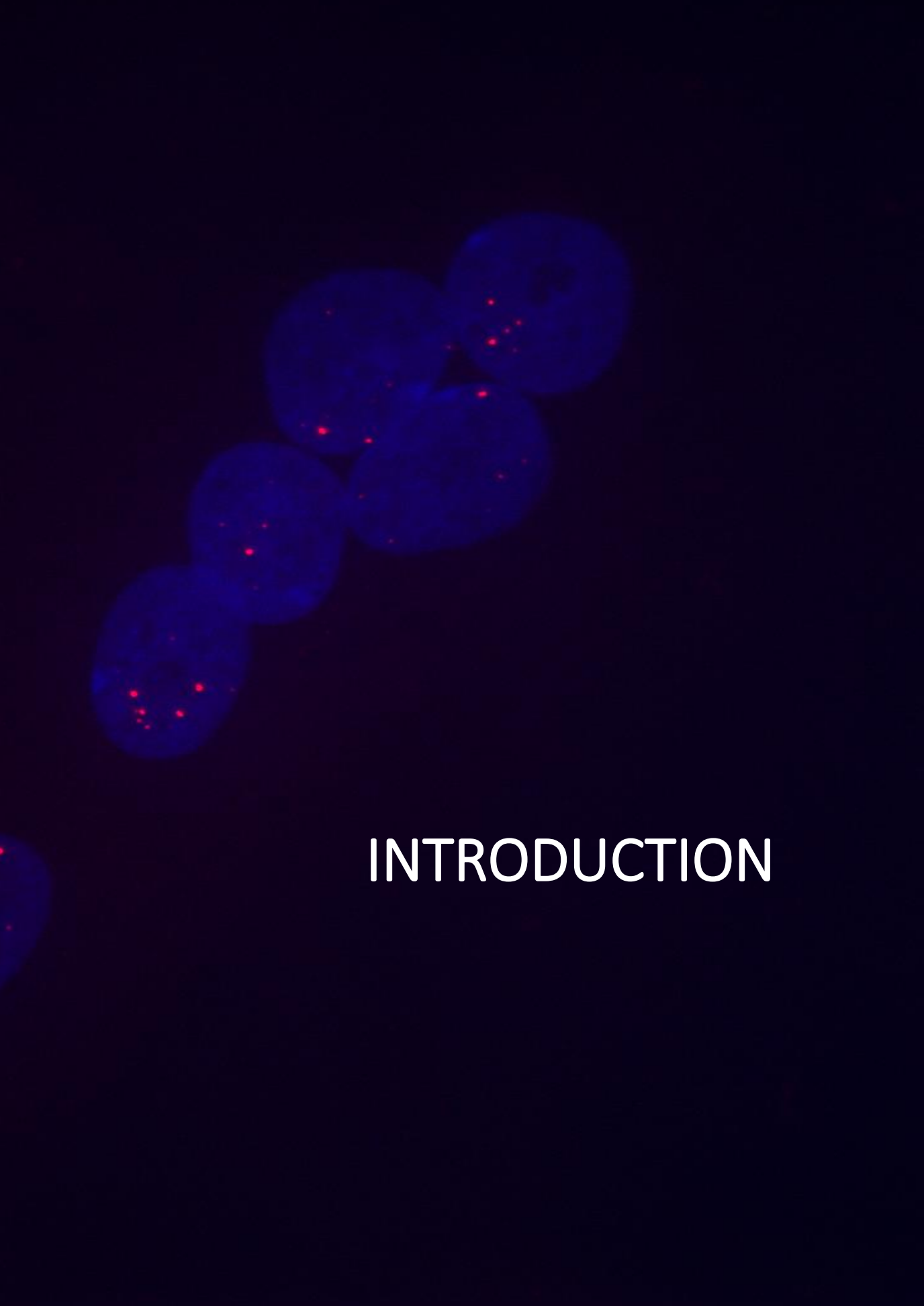

INTRODUCTION

1.- Myotonic dystrophy type 1 (DM1)

Myotonic dystrophy type 1 or Steinert Disease (DM1: OMIM: 160900) is a genetic and multisystemic muscular dystrophy with autosomal dominant inheritance [1]. It was first described from a clinical point of view in 1909 by the German doctor Hans Steinert, even though the genetic cause was not discovered until 1992[2,3]. Although it is the most prevalent muscular dystrophy in adults, it is a rare disease. The worldwide prevalence is 1 in 10.000 even though it can vary according to the region[4–6]. Nowadays, there is no cure or treatment for this progressive disease, which impairs patient's life quality and reduces life expectancy.

1.1.- Clinical features and classification

From a clinical point of view, DM1 is a very heterogeneous disease. The degree of severity and the organs affected can be extremely variable between patients. According to the symptomatology and the age of onset, DM1 has been classified in five different subtypes: congenital, infantile, juvenile, adult and late-onset[7] (Table 1).

1.1.1.- Congenital DM1

Congenital DM1 is diagnosed at birth or during the first month of life[7] and it has an estimated prevalence of 1 in 47619 births[8]. It is the most severe form of the disease with an estimated 30-40% mortality rate during the neonatal period[9].

Pregnancy symptoms, including reduced fetal movement, polyhydramnios and preterm delivery are frequent. Once born, the patients are likely to have problems breathing and feeding, hypotonia and hyporeflexia. Most of them also have facial dysmorphia, with a characteristic tent-shaped upper lips, a carp mouth and weakness. Some of them also have arthrogryposis or clubfeet[9].

Congenital DM1 is characterized by dysfunction in the central nervous system (CNS) and during development patients suffer mental and speech delay[10]. They also suffer delay in the motor development, learning to walk around the age of two. Symptoms that characterize adult DM1, usually won't appear until

adolescence or adulthood, including muscular weakness, myotonia, cardiac defects or diabetes[9].

1.1.2.- Infantile DM1

Infantile DM1 is diagnosed in children between one month and ten years old. First symptoms are usually a consequence of CNS dysfunction and most patients suffer moderate or severe cognitive delay[7]. First consultations usually occur due to language delay or to learning difficulties at school. Diagnosis can be challenging due to the inespecificity of the symptoms and family history is usually key. In some cases, there might also be motor development delay[10].

Muscular tiredness and weakness might appear during childhood or adolescence, but it is usually mild and slowly progressing. Facial dysmorphia also appears during childhood and becomes more obvious as the disease progresses. Although it is not frequent, children can also develop gastrointestinal, endocrine and cardiac alterations[10]. Infantile DM1 cases survive into adulthood, when they typically develop symptoms that are characteristic of the adult subtype[11].

1.1.3.- Juvenile DM1

The age of onset in juvenile DM1 cases is between eleven and twenty years of age[7]. This subtype is often grouped together with infantile subtype because symptomatology is similar. In this subtype, the percentage of individuals with cognitive impairment is lower than in infantile cases, but the percentage of individuals with severe myotonia is higher and they develop cardiac issues earlier. Moreover, compared to adult patients, juvenile cases have a more severe phenotype regarding dysphagia, respiratory insufficiency, muscle weakness or facial dysmorphism[7].

1.1.4.- Adult DM1

Adult DM1 is the most common subtype and its age of ranges between twenty-one and forty years old[7]. The predominant symptoms of adult DM1 are progressive distal weakness and myotonia, which may lead to patients having difficulties performing daily life activities. It is also common facial weakness, which derives in ptosis and a typical myopathic appearance. Fatigue and muscular pain are also common findings[1]. Cardiac defects are also common, including conduction abnormalities and blocks. Moreover, patients can suffer a progressive impairment of lung function which may lead to the need of

mechanical ventilation[1,12]. Indeed, cardiac arrythmias and pneumonia are the most frequent causes of death in DM1 adult patients[13].

The presence of cataracts is also frequent and they usually appear during the 30s-40s[1]. Patients can also suffer gastrointestinal abnormalities, such as constipation, diarrhoea pseudo-obstruction or dysphagia[1,14]. Moreover, endocrine alterations, such as diabetes or thyroid dysregulation can also happen[1]. Finally, adult DM1 patients may also present CNS and cognitive alterations, but not as frequently and severe as in the previously described subtypes. It is to note that patients are likely to suffer daytime sleepiness, personality disorders, anxiety and depression[1,15].

1.1.5.- Late-onset DM1

Patients with late-onset DM1 develop symptoms after forty years of age[1]. It is the mildest form of the disease and it frequently goes undiagnosed. Symptoms in this subgroup include cataracts, alopecia and mild muscle involvement[12].

Table 1. Summary of DM1 subtypes.

DM1 subtype	Age of onset	Main symptoms
Congenital	< 1 month	Hypotonia Hyporeflexia Breathing and feeding dysfunction CNS dysfunction Facial dysmorphia
Infantile	1 month – 10 years	CNS dysfunction Mild muscle weakness and tiredness Facial dysmorphia Adult subtype symptoms when they reach adulthood
Juvenile	11 years – 20 years	CNS dysfunction Myotonia Can have adult subtype symptoms but with a more severe phenotype
Adult	21 years – 40 years	Progressive distal weakness Myotonia Fatigue Cardiac defects Respiratory dysfunction Cataracts Type II diabetes Gastrointestinal abnormalities
Late-onset	>40	Cataracts Alopecia Mild muscle involvement

1.2.- Genetics

As previously said, DM1 is caused by a genetic alteration. In particular, it is due to a CTG repeat expansion in the untranslated 3' end of the Dystrophia Myotonica Protein Kinase gene (*DMPK*), which is located in the 19q13.32 chromosome and surrounded by the *DMWD* (upstream) and *SIX5* (downstream) genes. Healthy individuals have a CTG expansion range between 5 and 37 repeats, while affected patients have from 50 to thousands of repeats. Carriers of expansions with a size between 38 and 49 repeats are asymptomatic; however, the expansion is highly unstable and there is a higher risk that their offspring inherit a larger expansion that could be pathogenic[16] (Figure 1). The size of the expansion correlates with the severity of the disease, this means that usually congenital cases carry the largest expansions while late-onset carry the shortest ones[17,18].

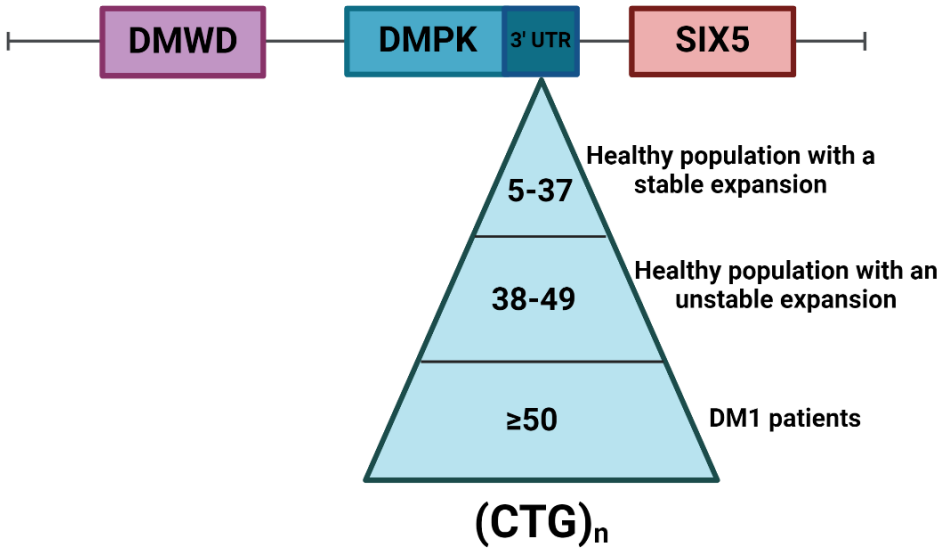

Figure 1. Scheme of *DMPK* locus and DM1 CTG expansion. *DMPK* is surrounded by *DMDW* and *SIX5* genes and contains in the 3'UTR the CTG expansion that causes the disease. Based on an image published in Visconti et al. (2023).

1.2.1.- Instability

The CTG expansion in DM1 patients is highly unstable, which results in both intergenerational and somatic instability:

Intergenerational instability

The CTG expansion has a tendency to expand in successive generations. This means that the offspring of a DM1 patient is likely to inherit a larger CTG expansion that the one the affected parent has. This is the cause of the phenomenon known as anticipation, which consists in the earlier and more severe manifestation of DM1 symptoms over successive generations[19]. There is not a stablished increase from generation to generation, as it depends on different factors such as parental age, parental sex and size of the CTG repeat. The inherited size of the CTG expansion has a tendency to increase when the parental age increases, especially if the affected parent is a male[20]. In cases where the parents carry small CTG expansions (<100) it is more likely that the inherited expansion is larger if it comes from the father than from the mother[21]. However, most congenital cases are maternally inherited (87.5-91%)[22–24]. It is hypothesized that this could be due to a negative selection of sperm containing large expansions, which could also be related to the male infertility that occurs to DM1 males[25]. Interestingly, while infantile subtype is maternally and paternally equally transmitted, juvenile, adult and late-onset subtypes are more likely to be paternally transmitted[26]. Moreover, even though it is less common, intergenerational contractions can also happen[27,28].

Somatic instability

The CTG expansion is unstable in tissue-specific manner with a tendency to increase over time. This means that DM1 patients have different CTG expansion sizes across different organs and tissues and even across different cells of the same tissue or organ. This phenomenon is known as somatic instability and it highly depends on age and the estimated progenitor allele size (ePAL)[29]. Somatic instability can be detected by analysing the CTG repeat with small-pool PCR Southern blot technique, as multiple bands corresponding to several CTG sizes can be observed in a particular tissue sample or cells pool[30,31]. Several studies have proven that blood cells have shorter CTG expansions compared to other tissues and cell types including skeletal and cardiac muscle, brain, liver, testis or fibroblasts[32–34]. It is also known that the CTG expansion in blood increases over time indicating that instability is maintained throughout life[35]. Moreover, the level of instability is modified by the ePAL of the affected individual and patients with a higher level of somatic instability correlate with an earlier age of onset. Nonetheless, there is a degree

of variability in somatic mosaicism that cannot be attributed to age and ePAL and is yet to be deciphered[29].

1.2.2.- Interruptions

The CTG repeat expansion in the DMPK gene is not always a pure CTG sequence, as it can contain variant repeats or interruptions. Currently, it is estimated that around a 3 to a 5% of the DM1 patient's present interruptions, even though this percentage could be underestimated due to difficulties analysing the deeper region of the expansion[36]. The CTG sequence can be interrupted with CCG, CTC, CGG or CAG, even though the most common one is CCG. Interruptions can be found both in the 3' and 5' end of the repeat, however they are more frequently detected in the 3' end. They can be found as isolated interruptions, in hexamers combining the interruption with the CTG sequence or in big interruption blocks. Moreover, interruptions can be either inherited or generated de novo. Some studies suggest that interruptions have a stabilizing effect by reducing both intergenerational and somatic instability. Furthermore, interruptions are associated with a delayed age of onset and with a milder or atypical phenotype, even though there are some exceptions[37–43].

1.2.3.- Methylation

DNA methylation is a heritable and reversible epigenetic modification which is involved in the regulation of gene expression, in the silencing of retroviral elements, in X chromosome inactivation and in genomic imprinting. This epigenetic modification mostly occurs in what are called CpG sites, a cytosine followed by a guanine and separated by a phosphate group. CpG sites are frequently found in CpG islands. CpG islands are regions over 200bp that contain over a 50% of GC content. They are located in many gene promoters, especially in housekeeping genes promoters. When the CpG island is methylated the gene expression is silenced[44].

The expansion's repeat in DM1 is located in a 3.5 kb CpG island, identified as CpGi 374. Moreover, in this CpG island there are two CCTC-binding factor (CTCF) sites surrounding the CTG expansion, CTCF1 and CTCF2. CTCF is a transcription factor which plays a role in transcription regulation, chromatin architecture regulation and insulation[45]. Both CTCF1 and CTCF2 have been described to show differences in methylation levels in DM1 patients compared to controls. There are controversial results regarding methylation in CTCF sites

in DM1. However, recent findings show that CTCF1 region may be methylated in blood samples from developmental cases (congenital, infantile and juvenile) while it generally remains unmethylated in non-developmental DM1 cases and controls. In the case of CTCF2 region only around half the cases that show methylation in CTCF1 present methylation in CTCF2 [46]. It has been suggested that there may be a correlation between the level of methylation in CTCF1 in blood samples and the severity of DM1, being the most methylated cases the ones with more severe symptoms, which would explain that most congenital cases are methylated. A recent study from our group, recently showed that methylation in CTCF1 may be associated with more severity in childhood cases of the disease. Moreover, it was described a muscle specific CTCF1 methylation in non-developmental cases, which however, would not affect the CpGs inside the CTCF binding sites[46]. It is not clear the effect of methylation in CTCF1 region, however, there are hypothesis that suggest that it could be affecting the expression of *DMPK* and its surrounding genes *SIX5* and *DMWD*, which have been reported to be altered in DM1[47,48].

Besides CpG 374, there are three more CpG islands in *DMPK* locus: CpGi 74, which is located in *DMWD* gene and CpGi 36 and 43, which are located in the *DMPK* gene. In the case of CpGi 74 and 36 they are methylated both in blood and muscle and in DM1 patients and healthy individuals. In the case of CpGi 43 blood samples are unmethylated both in patients and controls. However, muscle samples are methylated in healthy individuals while there is a reduction in methylation levels of DM1 patients[46]. It is hypothesized that this alteration in methylation in DM1 muscle could induce a shift from the main or strongest promoter in *DMPK* to the weak or alternative promoter in *DMPK* which overlaps with CpGi 43 by inducing a change in chromatin conformation due to the hypomethylation in CpGi 43.

1.3.- Physiopathology

There are different molecular mechanisms that have been proposed as the cause of DM1 pathogenesis[49]. The main mechanism is RNA toxicity caused by the accumulation of mutant RNA in the nucleus. However, it is a complex disease and there are other mechanisms that are thought to simultaneously contribute to the disease which are DMPK haploinsufficiency, non-coding

RNAs deregulation and the expression alteration of DMPK and its surrounding genes, SIX5 and DMWD due to methylation alterations.

1.3.1.- Main mechanism: RNA toxicity

The main mechanism of DM1 pathogenesis is RNA toxicity (Figure 2), which was first described in 1995 when it was observed that even though both alleles were transcribed into mRNA, the mutant mRNA remained in the nucleus in the shape of discrete aggregates[50]. The mutant mRNA forms hairpin-like secondary structures in which G-C base pairs matches are intercalated with U-U mismatches, forming what is known as RNA foci[50]. A transgenic mouse model with an untranslated CUG in an unrelated mRNA revealed that transcripts with CUG expansions are enough to generate a DM phenotype as they developed myotonia and myopathy[51]. RNA foci have been detected in multiple cell types and even though most of them are located in the nucleus, they can occasionally be found in the cytoplasm. RNA foci number is variable between cells within a patient and between patients and there are studies that reveal a correlation between RNA foci number and CTG expansion size[52,53].

RNA foci are involved in the dysregulation of two RNA-binding family of proteins: muscleblind-like (MBNL) and CUG-BP and ETR-3-like factors (CELF). There exist 3 MBNL paralogs, MBNL1, MBNL2 and MBNL3 of which MBNL1 is expressed in most tissues, MBNL2 is mostly expressed in brain and MBNL3 expression is restricted to placenta and muscle cell differentiation and regeneration processes[54]. In the case of CELF proteins there are six different ones, CELF1, CELF2, CELF3, CELF4, CELF5 and CELF6. The two most relevant proteins dysregulated by RNA foci in DM1 are MBNL1 and CELF1. In the case of MBNL1, it is sequestered by the hairpin-like secondary structures that form the RNA foci as they mimic the MBNL proteins natural binding site. The sequestration downregulates its expression and limits its function. In the case of CELF1, even though it is a CUG binding protein, it is not sequestered by the RNA foci. Instead, it is overexpressed due to PKC-mediated hyperphosphorylation which leads to protein stabilization and upregulation. The mechanism by which the PKC pathway is activated is not known, but it is hypothesized that the expanded RNA is involved in the activation [55,56].

Both MBNL1 and CELF1 are important splicing regulators and its dysregulation is the major cause of the spliceopathy that is observed in DM1. They are responsible of the developmental splicing switches, from embryonic to adult isoforms, of many genes. While MBNL1 levels increase during development,

CELF1 levels decrease as they have antagonistic effects in the splicings they regulate. This means that when MBNL1 induces the inclusion of a particular exon in a certain gene, CELF1 induces its exclusion. However, in DM1 there are decreased MBNL1 levels due to sequestration and increased CELF1 levels due to hyperphosphorylation, meaning that in DM1 patients the predominant isoforms of the genes they regulate are going to be the embryonic ones[57,58]. In the case of CELF1, it is not only involved in splicing alterations, but also regulates mRNA translation and stability which are altered in DM1 and contribute to the pathogenesis[58].

There are several splicings that are altered in DM1 and some of them have been directly related to symptoms of the disease. MBNL1 and CELF1 are the main splicing regulators in skeletal and cardiac muscle tissues while MBNL2 is an important splicing regulator in brain tissue[58].

In DM1 skeletal muscle more than 20 genes have been found to be misspliced, including *CLCN1*, *INSR, ATP2A1, BIN1, DMD* or *MBNL1*. *CLCN1* inclusion of exon 7a in DM1 results in the creation of a premature STOP codon which produces a channelopathy that derives in myotonia[59]. In the case of INSR, there is an aberrant exclusion of exon 11 that switches the isoform that is expressed in muscle to the one that is expressed in brain, spleen and leukocytes. This isoform codifies for a lower response insulin receptor and causes insulin resistance in DM1 patients[60]. *ATP2A1* gene encodes for a calcium channel that pumps calcium back to the lumen of the sarcoplasmic reticulum, which allows skeletal muscle relaxation. In DM1, the exclusion of exon 22 derives in the expression of the neonatal isoform, which contributes to the patient's alteration in intracellular calcium homeostasis and muscle degeneration[61]. In the case of *BIN1* there is exon 11 exclusion in DM1, while in *DMD* there is exon 78 exclusion. In both cases, the resulting isoforms would contribute to the muscle weakness that suffer DM1 patients.[62,63] MBNL1, besides regulating many other gene splicings, regulates its own splicing and the inclusion of exon 5 in MBNL1 contributes to the splicing defects in DM1[64].

There are several genes whose splicing has been described to be altered in cardiac muscle, including sodium channel protein type 5 (*SCN5*) and LIM domain binding 3 (*LDB3*). *SCN5* is a gene that codifies for a subunit of the NaV1.5 channel, which is important for the excitability of the cardiomyocytes. In DM1 the exon 6a is included in adult heart samples which causes conduction defects[65]. In the case of *LDB3*, it codifies for a sarcomere structural protein and exon 5 and 11 inclusion in DM1 patients causes dilated cardiomyopathy[66].

In brain various splicing alterations have been detected such as the ones affecting the microtubule-associated protein tau (*MAPT*) or the NMDA receptor 1 (*NMDAR1*). *MAPT* is a protein that is located in the frontal cortex. Exclusion of exons 2, 3 and 10 causes a tauopathy-like degeneration of DM1 brain[67]. In the case of NMDA, the inclusion of exon 5 in DM1 patient's brain, could contribute to the memory impairment that patients present[68].

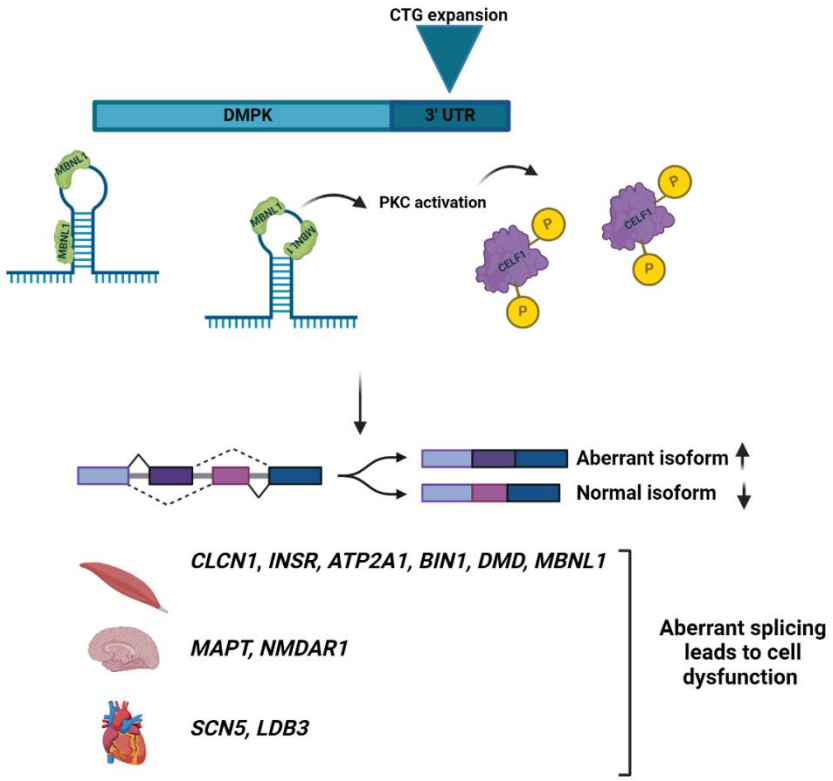

Figure 2. Scheme of the main pathogenic molecular mechanism of DM1. The expanded *DMPK* transcript forms RNA foci, which sequester MBNL1 and induce CELF1 phosphorylation. As a consequence, alternative splicing is affected which leads to cellular dysfunction. Based on a figure from López-Martínez et al. (2020).

1.3.2.- DMPK haploinsufficiency

DMPK gene encodes for a serine/threonine kinase with six different major isoforms. The predominant isoform expressed in skeletal and heart muscle codes for a protein of 80 KDa[69–71]. DMPK protein is known to have a role in skeletal muscle integrity, cardiac conduction, cell metabolism and ion-channel

gating. However, it is yet not fully understood the mechanism of action of the protein[72].

Initial studies to decipher the pathogenic mechanism of DM1 consisted in the analysis of *DMPK* mRNA and protein expression levels. The studies revealed that DM1 tissues express lower levels of both *DMPK* protein and mRNA compared to controls[73]. These results suggested that haplotype insufficiency could be the mechanism underlying disease expression, as the mutant allele expression would be highly reduced (Figure 3). However, the development of a *DMPK* knockout mouse model discarded that hypothesis. The mice displayed a mild phenotype of just some of the described DM1 symptoms. They suffered late-onset mild myopathy, cardiac conduction defects and altered calcium ion homeostasis, but they did not suffer some of the characteristic symptoms of DM1 such as myotonia[74,75]. This meant that *DMPK* haploinsufficiency was not sufficient to explain DM1 pathogenic mechanism, but it is most likely contributing to the disease phenotype.

1.3.3.- Methylation and gene expression alteration

Another mechanism that has been proposed as a cause of DM1 pathogenesis is the alteration in *DMPK* and surrounding genes *SIX5* and *DMWD* expression due to changes in methylation (Figure 3). There are studies that show that *DMPK* mRNA is downregulated[73,76,77]. This means that not only are the expanded mRNA alleles trapped in the nucleus, but the general expression levels of the transcript are also lower, which could be contributing to the decrease in DMPK protein. The surrounding genes *SIX5* and *DMWD* have also been reported to be downregulated in DM1, even though there is controversy regarding *DMWD*[78–80]. A knockout mice model for *SIX5* suggested that *SIX5* deficiency might have a role in DM1, as it was observed that SIX5 deficient mice developed cataracts[81].

It has been suggested that methylation alterations in CpG islands located in the *DMPK* locus, particularly those found in CTCF1, could be affecting the expression of these three genes by producing changes in chromatin structure. CTCF1 methylation is predominantly observed in congenital cases, which are known to be mostly maternally inherited[82]. It is hypothesized that the reduction of SIX5 expression due to hypermethylation would be responsible of that bias in inheritance in congenital cases, as SIX5 is an important gene for spermatogenic cell survival[83]. Interestingly, it has been recently generated a quadruple mutant heterozygous mouse model for SIX5, DMPK, DMWD and MBNL1 which recapitulates congenital manifestations. This finding suggests

that changes in the expression of the DMPK locus genes could be acting as disease severity modifiers[84].

1.3.4.- MicroRNAs deregulation

MicroRNAs (miRNAs) are short (20-24 bp), single-stranded, non-coding RNAs which regulate gene expression. Specifically, they repress gene expression by both translational inhibition and mRNA degradation[85]. miRNAs have important roles in many cellular processes. Deregulation in its expression or targets have been linked to several pathologies, including neuromuscular diseases, cardiac conditions, neurodegenerative diseases, metabolic diseases and cancer[86–90].

miRNAs are synthetized by RNA polymerase II, which produces a primary transcript of the miRNA (pri-miRNA). In the nucleus, pri-mRNAs are then processed by the RNase Drosha, generating a pre-miRNA, which is exported to the cytoplasm where it is further processed by RNase Dicer. Finally, one strand of the mature miRNA binds the RNA-induced silencing complex (RISC) and anneals to its target mRNA. It is known that a single miRNA can target several transcripts and that several miRNAs can act as regulators of a single mRNA[91].

Analysis in blood and serum DM1 samples have revealed alterations in miRNAs expression, making them candidates as potential biomarkers. However, contradictory results in different studies have made the search of DM1 biomarkers still unsuccessful[92]. More conclusive results could be obtained if future studies used the same normalization method and type of sample (whole blood, serum or plasma).

miRNAs levels have also been studied in other tissues, such as muscle and heart. Several miRNAs have been found to be altered either in terms of expression or localization and as it happens in blood there are some discrepancies between studies. The alteration of some of these miRNAs in DM1 has been directly related with the pathogenesis of the disease (Figure 3).[92] An example of this is miRNA1, which has been described to be downregulated in DM1 heart and skeletal muscle by most studies. Just the study conducted by Gambardella et.al suggested an upregulation of this miRNA. These different results could be explained by the CTG expansions of the samples used, the muscle biopsied or patients age, as well as by the different normalization methods used[92]. It has been suggested, by experiments carried out in Drosophila DM1 model, that MBNL1 downregulation in DM1 would be the cause of miR1 decrease, as would be involved in its biogenesis. Reduction of miRNA1 in heart has been associated with the dysregulation of gap junction proteins and cardiac channels which

would lead to conduction defects and arrythmia[93]. Other miRNAs that have been described to be dysregulated in muscle and/or heart and could be participating in the DM1 pathogenic mechanism include miR-7, miR-10, miR-29, miR133 or miR33[94].

1.3.2.- DMPK haploinsufficiency

DMPK gene encodes for a serine/threonine kinase with six different major isoforms. The predominant isoform expressed in skeletal and heart muscle codes for a protein of 80 KDa[69–71]. DMPK protein is known to have a role in skeletal muscle integrity, cardiac conduction, cell metabolism and ion-channel gating. However, it is yet not fully understood the mechanism of action of the protein[72].

Initial studies to decipher the pathogenic mechanism of DM1 consisted in the analysis of *DMPK* mRNA and protein expression levels. The studies revealed that DM1 tissues express lower levels of both *DMPK* protein and mRNA compared to controls[73]. These results suggested that haplotype insufficiency could be the mechanism underlying disease expression, as the mutant allele expression would be highly reduced (Figure 3). However, the development of a *DMPK* knockout mouse model discarded that hypothesis. The mice displayed a mild phenotype of just some of the described DM1 symptoms. They suffered late-onset mild myopathy, cardiac conduction defects and alerted calcium ion homeostasis, but they did not suffer some of the characteristic symptoms of DM1 such as myotonia[74,75]. This meant that *DMPK* haploinsufficiency was not sufficient to explain DM1 pathogenic mechanism, but it is most likely contributing to the disease phenotype.

1.3.3.- Methylation and gene expression alteration

Another mechanism that has been proposed as a cause of the DM1 pathogenesis is the alteration in *DMPK* and surrounding genes *SIX5* and *DMWD* expression due to changes in methylation (Figure 3). There are studies that show that *DMPK* mRNA is downregulated[73,76,77]. This means that not only are the expanded mRNA alleles trapped in the nucleus, but the general expression levels of the transcript are also lower, which could be contributing to the decrease in DMPK protein. The surrounding genes *SIX5* and *DMWD* have also been reported to be downregulated in DM1, even though there is controversy regarding *DMWD*[78–80]. A knockout mice model for *SIX5* suggested that *SIX5* deficiency might have a role in DM1, as it was observed that SIX5 deficient mice developed cataracts[81].

It has been suggested that methylation alterations in CpG islands located in the *DMPK* locus, particularly those found in CTCF1, could be affecting the expression of these three genes by producing changes in chromatin structure. CTCF1 methylation is predominantly observed in congenital cases, which are known to be mostly maternally inherited[82]. It is hypothesized that the reduction of SIX5 expression due to hypermethylation would be responsible of that bias in inheritance in congenital cases, as SIX5 is an important gene for spermatogenic cell survival[83]. Interestingly, it has been recently generated a quadruple mutant heterozygous mouse model for SIX5, DMPK, DMWD and MBNL1 which recapitulates congenital manifestations. This finding suggests that changes in the expression of the DMPK locus genes could be acting as disease severity modifiers[84].

1.3.4.- MicroRNAs deregulation

MicroRNAs (miRNAs) are short (20-24 bp), single-stranded, non-coding RNAs which regulate gene expression. Specifically, they repress gene expression by both translational inhibition and mRNA degradation[85]. miRNAs have important roles in many cellular processes. Deregulation in its expression or targets have been linked to several pathologies, including neuromuscular diseases, cardiac conditions, neurodegenerative diseases, metabolic diseases and cancer[86–90].

miRNAs are synthetized by RNA polymerase II, which produces a primary transcript of the miRNA (pri-miRNA). In the nucleus, pri-mRNAs are then processed by the RNase Drosha, generating a pre-miRNA, which is exported to the cytoplasm where it is further processed by RNase Dicer. Finally, one strand of the mature miRNA binds the RNA-induced silencing complex (RISC) and anneals to its target mRNA. It is known that a single miRNA can target several transcripts and that several miRNAs can act as regulators of a single mRNA[91].

Analysis in blood and serum DM1 samples have revealed alterations in miRNAs expression, making them candidates as potential biomarkers. However, contradictory results in different studies have made the search of DM1 biomarkers still unsuccessful[92]. More conclusive results could be obtained if future studies used the same normalization method and type of sample (whole blood, serum or plasma).

miRNAs levels have also been studied in other tissues, such as muscle and heart. Several miRNAs have been found to be altered either in terms of expression or localization and as it happens in blood there are some discrepancies between studies. The alteration of some of these miRNAs in DM1 has been directly related with the pathogenesis of the disease (Figure

3).[92] An example of this is miR-1, which has been described to be downregulated in DM1 heart and skeletal muscle by most studies. In contrast, just the study conducted by Gambardella et.al suggested an upregulation of this miRNA. These different results could be explained by the CTG expansions of the samples used, the muscle biopsied or patients age, as well as by the different normalization methods used[92]. It has been suggested, by experiments carried out in Drosophila DM1 model, that MBNL1 downregulation in DM1 would be the cause of miR-1 decrease, as would be involved in its biogenesis. Reduction of miR1 in heart has been associated with the dysregulation of gap junction proteins and cardiac channels which would lead to conduction defects and arrythmia[93]. Other miRNAs that have been described to be dysregulated in muscle and/or heart and could be participating in the DM1 pathogenic mechanism include miR-7, miR-10, miR-29, miR133 or miR-33[94].

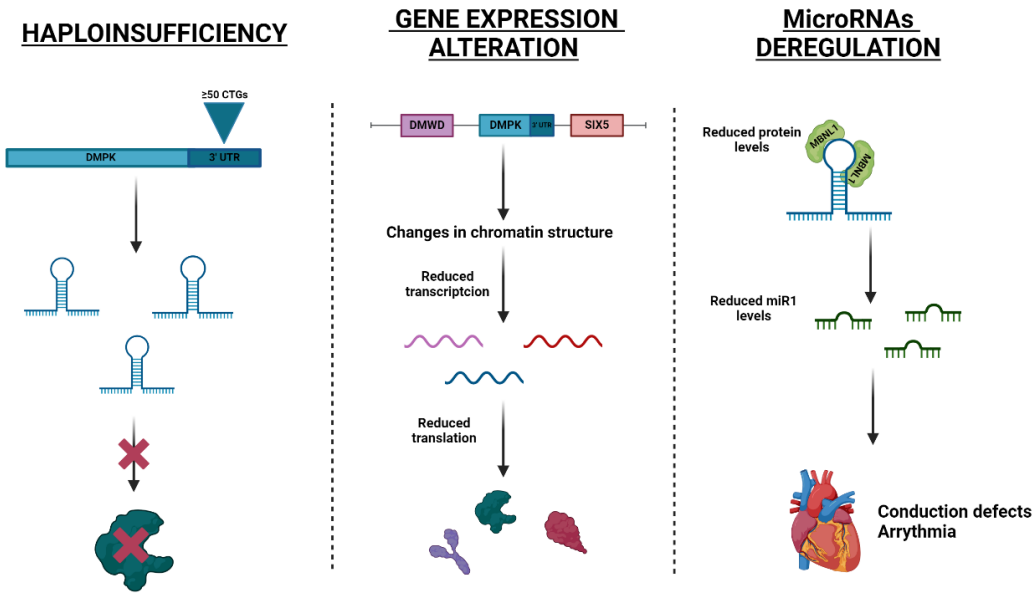

Figure 3. Schematic representation of other mechanisms contributing to DM1 pathogenesis: haploinsufficiency due to the lack of translation of the expanded transcript, gene expression alteration of *DMWD*, *DMPK* and *SIX5* due to changes in chromatin structure and microRNAs deregulation. Based on a figure from Mateos-Aierdi et al., 2015.

2.- Disease models in DM1

Disease models are animal or cell models that fully or partially reproduce the pathological mechanism of a disease. They are extremely important to study the molecular mechanisms underlaying diseases and to test the effect of potential treatments. In the case of DM1, there have been developed several models, including both animal and cellular models.

2.1.- Animal models

To date, several DM1 animal models have been developed, including vertebrate models such as mouse (Mus musculus) and fish (*Danio rerio*) and invertebrate models such as fly (*Drosophila melanogaster*) and worm (*Caenorhabditis elegans*). These models have been developed using different strategies, which include the expression of CUG repeats, the overexpression of CELF1, and the knock-out of MBNL1, SIX5, DMPK and DMWD (Table 2).

2.1.1.- Mouse models

Most DM1 models have been developed in mice and they are the most used animal model in DM1 research. The first mouse model developed is known as HSA^{LR}, which expresses the human skeletal actin (HSA) containing a 250 CTG repeat expansion in the 3' UTR. The expression of the non-coding CUG repeats in muscle results in the formation of RNA foci, the sequestration of MBNL1 and in the alteration of alternative splicing. Moreover, HSA^{LR} mice develop myotonia and mild myopathy [95]. One of the main disadvantages of this model is that the expansion expression is limited to muscle tissue. Furthermore, the mice do not have neither muscle weakness or wasting, which are commonly found in DM1. From a genetic point of view, this model does not represent the characteristic DM1 expansion instability as there isn't neither intergenerational, neither somatic instability[96].

Other mouse models based in the expression of CUG repeats, include DM300 and DMSXL. These models ubiquitously express DMPK expanded transcripts in homozygosis and under the control of the human promoter. DM300 mice have between 300 and 600 CTG repeats, while DMSXL have between 1000 and 1800 CTG repeats. Both of them display multisystemic symptoms, including myotonia, progressive muscle weakness, defects in glucose metabolism,

growth delay and a high mortality. Due to the difference in CTG size, DMSXL mice present a more severe phenotype compared to DM300 mice. One of the main drawbacks of these models is that the required homozygosis makes breeding expensive and time-consuming. Another limitation is that the splicing alterations observed are often milder than the observed in DM1 patients[96].

Inducible models have also been generated, such as EpA960, in which a Cre-lox system induces the cardiac-specific expression of a 960 untranslated and interrupted CTG repeat in DMPK gene. Expression in skeletal muscle of the CTG repeat causes myotonia, muscle wasting and myopathy. Moreover, expression in heart produces conduction defects and arrythmia which leads to death within two weeks[97]. The main disadvantages of this model are the transgene leakage in skeletal muscle, which impairs the study of tissue or cell specific DM1 mechanisms, and the high mortality rate as a consequence of cardiac dysfunction. Moreover, from a genetic point of view, the presence of interruptions could be triggering atypical DM1 manifestations[96].

There are other mouse models which are based in the inactivation of MBNL proteins. One of these models, *Mbnl1*$^{\Delta 3/\Delta 3}$ carries a modified MBNL1 gene that produces a protein unable to bind to CUG RNA repeats, mimicking what happens in DM1 when MBNL1 is sequestered by the foci and is functionally not available. These mice suffer myopathy, cataracts, cardiac defects and behavioural alterations[98]. The main inconvenience of this model is that MBNL1 inactivation does not trigger all disease pathogenesis, such as muscle weakness, meaning that other additional mechanisms would contribute to the pathogenesis of the disease[96]. In that sense, a new model carrying heterozygous mutations in *DMPK*, *SIX5* and *MBNL1* genes has been recently developed. This model displays most adult-onset DM1 symptoms, including myotonia, muscle wasting and weakness, heart defects, endocrine and digestive alterations. Furthermore, another model that adds a fourth heterozygous mutation in the *DMWD* gene, has been shown to mimic congenital DM1. Besides the typical adult symptoms, these mice present hypotonia, breathing problems and developmental delay. Despite the phenotype similarities to DM1, the model fails to reproduce some aspects of the disease, such as *CLCN1* splicing alterations[99].

Another strategy that has been used to develop a mouse model is the upregulation of *CELF1*. An inducible model, TRECUGBP1, reproduces the

myopathy and cardiopathy observed in DM1, proving its contribution to the disease. However, not all the hallmarks of the disease are present, and the mortality rate is high[96,100].

2.1.2.- Other models

Models based in the expression of CUG repeats have also been developed in *Drosophila melanogaster* and *Caenorhabditis elegans*. In the case of flies, the expression of untranslated CTG expansions triggers eye and muscle degeneration. Moreover, RNA foci, MBNL1 sequestration and splicing alterations are also detected[101]. In the case of worms, the expression of untranslated CTGs causes defects in muscle development, reduced motility and increased mortality[102].

Models based in the disruption of MBNL have also been developed in fly, worm and fish. In the case of *Drosophila melanogaster*, the disruption of its MBNL homolog induces muscle defects in the flies, but unfortunately it is lethal [103]. In *Caenorhabditis elegans,* the mutation of its MBNL homolog causes impairment of the neuromuscular junction, a decrease in the synaptic density and behavioural abnormalities [104]. In *zebrafish*, it has been developed an MBNL2 knock-out model that presents developmental abnormalities, corroborating the predominant role of MBNL2 in central nervous system observed in a MBNL2 knock-out mouse model[105].

The main disadvantages of these models are the notorious anatomic and physiologic differences between these animals and humans. However, they have a short lifespan and are easier to handle and to reproduce than mice[96].

.

Table 2. Summary of the most relevant animal models used to study DM1

Animal model		Description	Positive aspects	Negative aspects
Mus musculus	HAS^{LR}	Human skeletal actin (HAS) containing a 250 CTG repeat expansion	Presence of typical DM1 molecular alterations and symptoms in muscle	Expression limited to muscle Absence of wasting and weakness Absence of expansion instability
	DM300	Ubiquitous expression of *DMPK* with 300 to 600 CTGs	Presence of typical DM1 molecular alterations and multisystemic symptoms	Breeding is expensive and time-consuming Slicing alterations milder than in DM1 patients
	DMSXL	Ubiquitous expression of *DMPK* with 1000 to 1800 CTGs	Presence of typical DM1 molecular alterations and multisystemic symptoms	Breeding is expensive and time-consuming. Splicing alterations are milder than in patients
	EpA960	Cardiac-specific expression of a 960 CTG repeat in *DMPK* gene	Inducible presence of typical DM1 molecular alterations and multisystemic symptoms	Transgene leakage in skeletal muscle High mortality rate
	Mbnl1$^{\Delta 3/\Delta 3}$	Modified *MBNL1* gene whose protein is unable to bind to CUG RNA repeats	Splicing alterations Presence of some multisystemic symptoms	MBNL1 inactivation does not trigger all disease pathogenesis
	DSM-TKO	Heterozygous mutations in *DMPK*, *SIX5* and *MBNL1* genes	Splicing alterations Displays most adult-onset DM1 symptoms	Fails to reproduce some aspects of the disease, such as *CLCN1* splicing alterations
	DSMD-QKO	Heterozygous mutations in *DMPK*, *SIX5, MBNL1* and *DMWD* genes	Splicing alterations Mimics congenital DM1	Fails to reproduce some aspects of the disease, such as *CLCN1* splicing alterations
	TRECUGBP1	Inducible upregulation of *CELF1*	Splicing alterations Reproduces DM1 myopathy and cardiopathy	Not all the hallmarks of the disease are present Mortality rate is high
Drosophila melanogaster	CTG >480	Expression of untranslated CTG expansions >480	Presence of typical DM1 molecular alterations Shows eye and muscle phenotypes Short lifespan, easy to handle and to reproduce	Notorious anatomic and physiologic differences compared to humans
	Mbl mutant	Disruption of its MBNL homolog	Splicing alterations Reproduces muscle defects Short lifespan, easy to handle and to reproduce	It is lethal Notorious anatomic and physiologic differences compared to humans
Caenorhabditis elegans	CUG125 CUG213	Expression of untranslated CTG expansions	Shows defects in muscle development, reduced motility and increased mortality Short lifespan, easy to handle and to reproduce	Notorious anatomic and physiologic differences compared to humans
	CeMbl mutation	Mutation of its MBNL homolog	Shows impairment of the neuromuscular junction, a decrease in the synaptic density and behavioural abnormalities Short lifespan, easy to handle and to reproduce	Notorious anatomic and physiologic differences compared to humans
Zebrafish	*Mbnl2* inactivation	MBNL2 knock-out model	Splicing alterations Presents developmental abnormalities Short lifespan, easy to handle and to reproduce	Notorious anatomic and physiologic differences compared to humans

2.2.- Cellular models

There exist several cellular models developed to study DM1, all of which have its advantages and disadvantages. They can be divided in two groups: cell lines with artificially expressed CTG repeats and patient derived cell lines (Table 3).

2.2.1.- Cell lines with artificially expressed CTG repeats

Several cell lines, mostly human and murine, have been inserted with a CTG repeat to mimic the pathogenesis of DM1. The CTG repeat is frequently inserted in the 3' UTR of a truncated DMPK gene and its expression is usually controlled by a CMV promoter. One of the most used constructs is a 960 CTG repeat interrupted with TCGA sequences. The interruptions are used to maintain the stability of the CTG expansion but it is not clear whether they have an impact in the cell's pathophysiology[106]. Besides cell models expressing interrupted constructs, there are also cell models expressing short pure CTG expansion constructs[107].

These cells lines with artificially expressed CTG repeats reproduce several aspects of DM1 pathophysiology, including RNA foci, MBNL1 sequestration and splicing defects. However, they have some limitations. They lack the genomic context of the CTG expansion, including the complete *DMPK* gene and its surrounding genes *SIX5* and *DMWD*. Moreover, they also lack regulation by the *DMPK* promoter[108].

2.2.2.- Patient derived cell lines

The limitations that artificial models have are overcome with patients derived cell lines, which reproduce the pathogenesis of the disease, including other contributors besides MBNL1 sequestration in RNA foci and splicing alterations.

Primary cells

Primary cells are directly obtained from DM1 patient biopsies. Cells can be isolated either by an enzymatic digestion of the extracellular matrix or by explant culture method. The most frequently used primary cells in DM1 research are skin fibroblasts and myoblasts. Skin fibroblasts are relatively easy to obtain and to culture but they are not one of the main cell types affected by DM1 and some splicing defects may not be present. Myoblasts, are extracted from muscle, which is one of the main affected tissues in DM1. They can fuse

into myotubes which preserve most of the splicing alterations observed in muscle.

Despite primary cells being a very useful tool for DM1 study, as they are directly obtained from patients, they also have some limitations. Unfortunately, they require to perform an invasive procedure in the patient, being muscle less accessible than skin. Moreover, primary cultures can divide a limited number of times before entering into replicative senescence and DM1 primary cultures can be challenging to culture due to the disease alterations[108].

Immortalized cells

Immortalized cell lines are developed to overcome the limitation of replicative senescence that characterizes primary cells because they can divide for an unlimited number of times. This way, the number of biopsies performed in DM1 patients can be diminished. Cells are immortalized by inserting lentiviral vectors that express the catalytic subunit of human telomerase (*TERT*), cyclin-dependent kinase 4 (*CDK4*), and cyclin D1 (*CCND1*)[109].

Nowadays, DM1 immortalized fibroblast, myoblast and transdifferentiated fibroblast cell lines have been developed. In the case of myoblasts cell lines, which are the most interesting model as they are present in one of the most affected tissues in DM1, there are currently three publications in which four myoblast patient derived cell lines have been generated. All of them show the main molecular alterations that characterize DM1[110–112].

The main inconvenience of immortalized cellular models is that it needs to be proven that the insertion of the *TERT, CDK4* and *CCND1* do not produce alterations in cellular behaviour[108].

Transdifferentiated cells

Skin fibroblasts, which are relatively accessible, can be transdifferentiated into myogenic cells, which better reproduce the disease. This is done by transducing the fibroblasts with *MYOD1* and can be performed in either primary or immortalized skin fibroblasts[60]. DM1 transdifferentiated cells exhibit most of the characteristic disease pathology features, however it is known that trans-differentiation with *MYOD1* leads to an incomplete muscle cell reprogramming[108].

Pluripotent stem cells

The use of pluripotent stems cells as a DM1 cellular model is especially useful for the study of cell types that are affected in DM1 and whose availability Is limited, such as brain or heart cells[108].

Pluripotent stem cells can be obtained either by the isolation of embryonic stem cells (ESC) from the blastocyst or by the reprogramming of somatic cells into induced pluripotent stem cells (iPSC). However, ESC use is ethically controversial as it involves the destruction of an embryo[108].

iPSCs are obtained by delivering reprogramming cocktails (Oct4, Sox2, Klf4 and c-Myc, also known as OSKM) into somatic cells. These cells can then be expanded and differentiated into several cell types[113]. They reproduce the disease pathophysiology and are considered a valuable tool for DM1 study. However, one of the main disadvantages is that maturation of the cells is often incomplete. Moreover, the reprogramming process involves some challenges such as a high instability of the CTG repeat and the maintenance cost of the cells is relatively high[108].

Table 3. Summary of the main cell models used to study DM1.

Cell line type		Description	Positive aspects	Negative aspects
Artificial cell lines		Cell lines with artificially expressed CTG repeats	Show the main DM1 molecular alterations	Lack the genomic context of the CTG expansion Lack regulation by the *DMPK* promoter
Patient-derived cell lines	**Primary**	Cells directly obtained from DM1 patient biopsies	Directly obtained from patients Show the main DM1 molecular alterations	Require an invasive procedure Cell division number is limited Challenging to culture due to the disease alteration
	Immortalized	Primary DM1 cells altered with the insertion of *TERT, CDK4* and *CCND1* to proliferate indefinitely	Show the main DM1 molecular alterations Can divide for an unlimited number of times	The insertion of the *TERT, CDK4* and *CCND1* may produce alterations in cellular behaviour
	Transdifferentiated	Myogenic cells obtained by transducing DM1 skin fibroblasts with *MYOD1*	Show the main DM1 molecular alterations	Incomplete muscle cell reprogramming
	Pluripotent	Cells that can be differentiated into several cell types	Show the main DM1 molecular alterations Can then be expanded and differentiated into several cell types	Maturation of the cells is often incomplete Maintenance cost is relatively high Reprogramming process involves some challenges

3.- Therapeutic strategies in DM1

Currently there are not any therapies available that either cure DM1 or that delay or stop the progression of the disease. Available treatments are just used to treat the symptoms. For example, muscular symptoms such as myotonia and myalgia can be treated pharmacologically. Muscle weakness can be mitigated with exercise to maintain muscle mass. In the case of cardiac disfunction the use of a pacemaker is recommended. Moreover, cataracts can be surgically fixed, and diabetes can be treated with insulin sensitising drugs[114].

The search for a therapy for DM1 is focused in four main strategies: the transcriptional inhibition of *DMPK* gene, the degradation of mutant *DMPK* transcripts, the recovery of MBNL1 activity levels and the reduction of CELF1 levels. According to the type of compound used, therapeutic approaches can also be classified into three broad categories: small molecules, nucleic acid therapeutics, and genome engineering. The challenge of finding a therapy is even greater in the case of DM1, because the great heterogeneity between patients could impact the efficiency of the treatment.

3.1.- Small molecules

Small molecules mostly consist of repurposed drugs, which can be tested in patients quicker and at a lower risk and cost compared to new drugs.

Several small molecules are currently being tested in clinical trials:

- **Mexiletine (study conducted by Lupin Ltd.)** is an antiarrhythmic drug which is able to reduce myotonia blocking the sodium channels that are involved in muscle contraction and relaxation. The clinical trial is currently in phase III and results obtained in previous phases indicate a reduction in handgrip myotonia in DM1 patients.[115,116]

- **Metformin (study conducted by Assistance Publique - Hôpitaux de Paris)** is an antidiabetic drug that has been shown to correct DM1 splicing defects and to improve patient's mobility[117]. A phase II clinical trial revealed an improvement in the 6MWT and in gait's mechanical

power, however no improvement was detected neither in myotonia or muscle strength[118]. Currently, there is an ongoing phase III clinical trial.

- **Tideglusib (study conducted by AMO Pharma Limited)** is a GSK3β inhibitor originally developed to treat Alzheimer. The clinical trial evaluating this drug is currently in phase II/III and is studying its effect in congenital and infantile cases. Previous phases of the clinical trial have shown that tideglusib improves cognitive function, fatigability and patient's ability to perform daily activities[119].

- **Pitolisant (study conducted by Harmony Biosciences)** is a stimulant drug that is used in patients with narcolepsy to treat daytime sleepiness, which is a condition that also affects DM1 patients[120]. Currently there is a phase II clinical trial going on which will be finishing this year.

- **Erythromycin (study conducted by Japan Agency for Medical Research and Development)** is an antibiotic that has been proven to decrease RNA foci and rescue missplicing in both animal and cellular DM1 models[121]. A phase II clinical trial has been completed, revealing an improvement in splicing alterations and in serum creatine kinase (CK) levels in DM1 patients. A phase III clinical trial would be needed to further evaluate treatment efficacy.

3.2.- Nucleic acid therapeutics

Nucleic acid therapeutics are single or double stranded nucleic acids that are used to treat diseases by modulating gene expression. They include antisense oligonucleotides (ASOs) and small interfering RNA (siRNA). There are two main mechanisms of function for ASO: steric blocking and RNaseH mediated degradation. In the first case, the oligonucleotide binds the RNA and prevents the binding of factors but does not degrade it, while in the second one the RNA is degraded by the enzymatic activity of RNAseH. There are already 13

molecules which have been approved to treat other diseases, but not DM1[122,123].

One of the main challenges of these therapies is the delivery. To improve cell's treatment uptake and stability, the oligonucleotides are chemically modified. However, these modifications can produce toxicity and are often not enough to achieve the therapeutical dose in the affected tissue. An example of this is IONIS-DMPKRx, the first DM1 nucleic acid therapy that was tested in a clinical trial. Results in phase I/II showed that the efficacy was too low due to low drug muscle concentration. To improve delivery, the chemically modified oligonucleotides are now being conjugated with carriers such as lipids, peptides or antibodies[122,123].

Currently there are six ongoing clinical trial testing nucleic acid-based therapies for DM1, which follow three different strategies, ASOs targeting the *DMPK* gene, siRNA targeting the *DMPK* gene or antimiRs regulating MBNL1 expression (Figure 4):

- **AOC1001 (Avidity Biosciences):** It is a siRNA that targets *DMPK* mRNA, conjugated with a monoclonal antibody that binds transferrin receptor 1. It has been shown to reduce DMPK in skeletal, cardiac and smooth muscle. The drug is undergoing phase II and III clinical trial and it is being administered intravenously at different doses. Preliminary results show a significant reduction of DMPK levels in all treated individuals, improvement in splicing alterations and in myotonia in some of the patients[124].

- **DYNE-101 (Dyne Therapeutics)**: It is an ASO that targets *DMPK* by RNaseH cleavage and is conjugated with transferrin receptor 1 antibody. In preclinical studies it has been shown to reduce RNA foci, alternative missplicing and myotonia.[125] Currently it is undergoing a phase I/II clinical trial and preliminary results reported by the company Dyne Therapeutics reveal that the treatment partially corrects splcing alterations, muscle weakness and myotonia.

- **VX-670 (VERTEX)**: It is an ASO conjugated with a cyclic pepide which enhances the ASO's effective delivery. The ASO targets the CUG repeat

in an allele-specific manner and according to the sponsor VERTEX, preclinical studies in DM1 models show a reduction in RNA foci and in aberrant splicing. A phase I/II clinical trial to evaluate the safety, tolerability, pharmacokinetics and pharmacodynamics of the drug, just started earlier this year.

- **ARO-DM1 (Arrowhead Pharmaceuticals)**: It is an antibody-conjugated siRNA that targets the CUG repeats. It was developed by Arrowhead Pharmaceuticals, who earlier this year presented preclinical results at the 2024 Muscular Dystrophy Association (MDA) Clinical & Scientific Conference. The results indicated a promising reduction in DMPK levels and in missplicing. A few months ago, a phase I/II clinical trial to evaluate the safety, tolerability, pharmacokinetics and pharmacodynamics of the drug started.

- **PGN-EDOM1 (PepGen):** It is an ASO conjugated with a peptide sponsored by PepGen. It targets the CUG repeat in a steric-block manner, blocking the interaction of MBNL1 with the toxic RNA. According to the sponsor, preclinical experiments in mice show positive results up to six months after the drug administration. There is significative correction of the aberrant splicing and an improvement in myotonia.

- **ATX-01 (ARTHEx Biotech):** this nucleic acid-based therapy has a different approach compared to the others that are currently being evaluated in clinical trials. Based in the observation that overexpression of MBNL1 is well tolerated and reverts several hallmarks of DM1, it was proposed the silencing of miRNAs that regulate MBNL1 as a therapeutical option. A study identified that miRNA23b and miR218 inhibit MBNL1 translation and are highly expressed in muscle, heart, and brain cells. AntimiRs against those two miRNAs were developed and preclinical studies in a DM1 muscle cell line, mouse-derived muscle tissue and the HSA^{LR} DM1 mouse model revealed that the delivery of these two molecules improved splicing

alterations and myotonia[126–129]. Derived from these results the start-up ARTHEx Biotech, whose aim is to develop antimiR therapies, was created. After some more studies, including chapter 2 of this thesis, ATX-01 is its first developed therapy and it is an antimiR conjugated with a hydrophobic moiety which targets miR23b. The clinical trial for ATX-01 just started its phase I/II in May 2024.

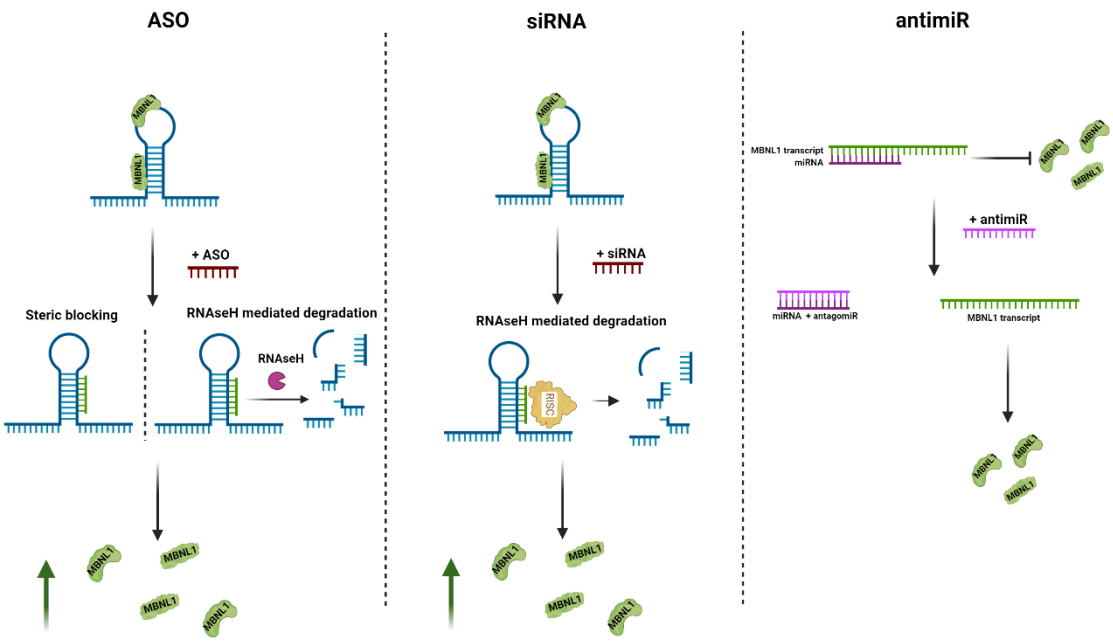

Figure 4. Schematic representation of the three mechanisms of action of acid nucleic DM1 therapies: ASOs, which induce the degradation or blockage of the RNA foci; siRNAs, which induce RISC-mediated RNA foci degradations; and antimiRs, which block miRNAs that downregulate MBNL1.

3.3.- Genome or transcriptome engineering

The most promising technique to edit the genome or transcriptome is CRISPR-Cas9 (clustered regularly interspaced short palindromic repeats - CRISPR-associated protein 9). CRISPR-Cas9 is an adapted system that is naturally found in bacteria as immune protection. This technique allows sequence-specific gene editing, which could potentially correct the defects in genetic diseases. It

works with a guide sequence that attaches to a specific target and to the enzyme Cas9, which cuts at the target site. The cut site is then repaired using the cell's repair machinery. Currently, there are no clinical trials evaluating this approach in DM1. However, there are preclinical studies going on with promising results[122].

Some studies are targeting the CTG repeats and experiments in DM1 animal and cellular models have shown a reduction of RNA foci in muscle[130,131]. Other studies are targeting the RNA CUG repeats and experiments performed both in DM1 mouse models and in DM1 human muscle cells have revealed a decrease in RNA foci number, missplicing rescue, and an improve in myotonia and muscle weakness[132,133]. The biggest concerns derived from these approaches are off-target events and unwanted effects in the target site during DNA or RNA repair[134].

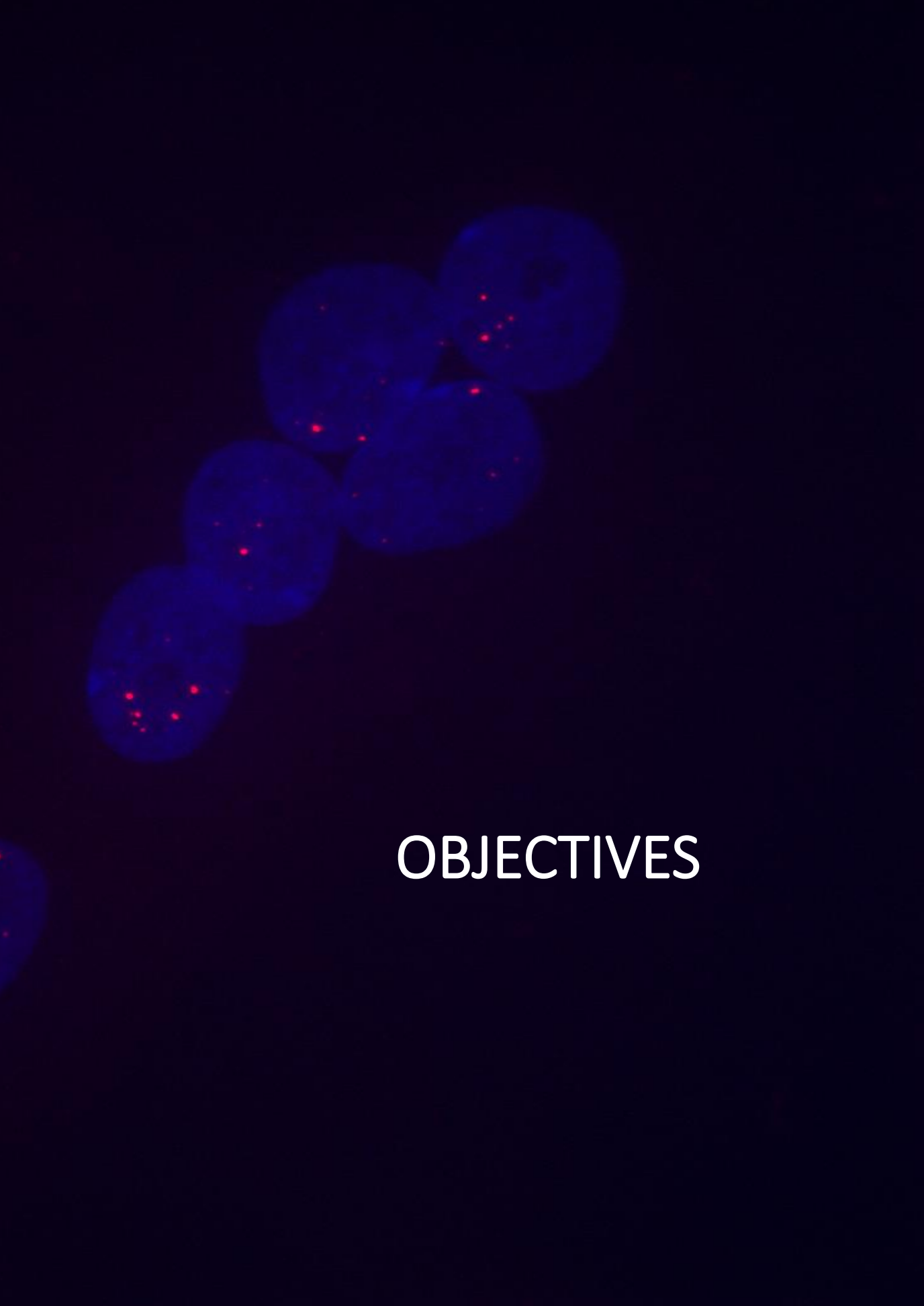

OBJECTIVES

The general objective of this doctoral thesis is to contribute to the myotonic dystrophy type 1 (DM1) research by focusing on the great heterogeneity that exists between patients and which is often ignored.

The general objective is divided into three objectives, which comprise the three chapters of the thesis:

Chapter 1: To analyse the influence of DM1 cell type and patient subtype over *DMPK* expression, RNA foci accumulation and MBNL1 sequestration.

Chapter 2: To test the effect of antagomiRs 23b and 218 in DM1 primary myotube samples derived from a heterogeneous cohort of DM1 patients.

Chapter 3: To develop, characterize and test therapies in three DM1 immortalized muscle cell models derived from three patients with different clinical characteristics.

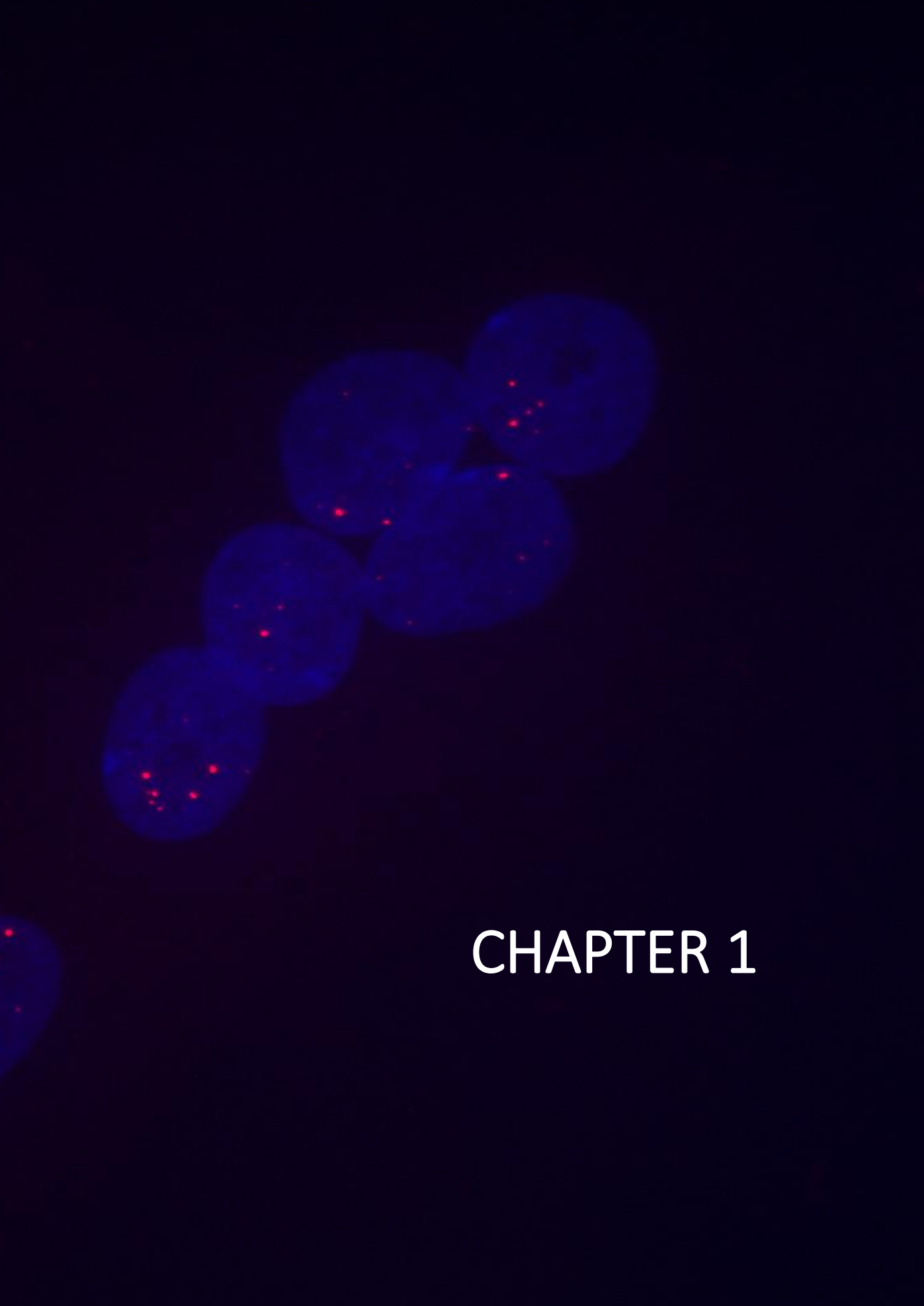

CHAPTER 1

RNA foci accumulation varies according to cell type and age of onset in Myotonic Dystrophy type 1

Judit Núñez-Manchón[1], Julia Capó[1], Alfonsina Ballester-Lopez[1, 2], Renato Odria[1], Ian Linares-Pardo[1], Emma Koehorst[1], Ana Maria Cobo[3], Jaume Coll-Cantí[1, 2, 4], Adolfo Lopez de Munain[5, 6], Alejandro Lucia[7, 8, 9], Darren G Monckton[10], Sarah A Cumming[10], Jonathan J. Magaña[11], Laura Palomo[12], Francesc Solé[12], Guillem Pintos-Morell[1, 2, 13], Giuseppe Lucente[1,4], Miriam Almendrote[1,4], Alba Ramos-Fransi[1,4*], Alicia Martínez-Piñeiro[1,4*], Gisela Nogales-Gadea[1, 2*]

Grup de REcerca Neuromuscular de BAdalona (GRENBA), Institut d'Investigació en Ciències de la Salut Germans Trias i Pujol, Campus Can Ruti, Universitat Autònoma de Barcelona, Badalona, Spain
[2]Centre for Biomedical Network Research on Rare Diseases (CIBERER), Instituto de Salud Carlos III, Madrid, Spain
[3]Centre de Compétences Neuromusculaires, Hôpital Marin APHP, Hendaye, France
[4]Neuromuscular Pathology Unit. Neurology Service. Neuroscience department, Hospital Universitari Germans Trias i Pujol, Badalona, Barcelona, Spain
[5]Neuroscience Area, Biodonostia Research Institute, Neurology Department, Donostia University Hospital, Donostia-San Sebastian, Gipuzkoa, Spain
[6]CIBERNED, Institute Carlos III, Madrid, Spain
[7]CIBER of Frailty and Healthy Aging (CIBER FES)
[8]Instituto de Investigación Hospital 12 de Octubre (i+12), Madrid, Spain
[9]Universidad Europea, Madrid, Spain, & Instituto de Investigación Hospital 12 de Octubre (i+12), Madrid, Spain
[10]Institute of Molecular, Cell and Systems Biology, College of Medical, Veterinary and Life Sciences, University of Glasgow, Glasgow, UK.

[*]Equal contribution

Corresponding author: Gisela Nogales-Gadea, Grup de REcerca Neuromuscular de BAdalona (GRENBA), Institut d'Investigació en Ciències de la Salut Germans Trias i Pujol. Ctra. de Can Ruti. Camí de les Escoles, s/n 08916 Badalona (Barcelona), Spain. Tel.: +34 93 4978684; e-mail address: gnogales@igtp.cat ORCID: 0000-0002-7414-212X

Abstract

RNA foci are one of the most relevant pathological hallmarks of DM1 as they are responsible of the sequestration of proteins relevant for splicing regulation (including MBNL1). However, despite both RNAi and MBNL1 aggregates have been described in several cell types, there aren't studies analysing the differences in expression between different cell types or between cells obtained from different DM1 patient's subtypes. Moreover, even though *DMPK*, the gene containing the pathological expansion leading to RNA foci formation, has been previously reported to be downregulated in DM1 it is not known whether RNA foci accumulation has a correlation with *DMPK* expression levels. In the first part of this study, we analysed the RNA foci and MBNL1 aggregates accumulation in different cell types (lymphoblasts, fibroblasts, myoblasts and myotubes) and observed significant differences between the cell lines, with myotubes having the highest number for RNA foci, myoblasts the highest number for MBNL1 sequestration and lymphoblastoids the lowest number for both RNA foci and MBNL1 sequestration. Furthermore, we used single cell technology to determine whether there is a correlation between DMPK expression levels and RNA foci number at single cell level. Considering muscle is one of the most affected tissues in DM1, we focused the single cell study on muscle progenitor cells. As expected, we observed a downregulation of the DMPK expression levels in patients compared to controls but no correlation between DMPK levels and RNA foci number was found. In the second part of this study, we analysed the RNA foci accumulation in lymphoblasts derived from the 5 DM1 subtypes (congenital, infantile, juvenile, adult and late-onset) and observed a higher accumulation of RNA foci in patients with an earlier onset of the disease. Overall, we can conclude that RNA foci accumulation is associated with cell type and DM1 subtype but does not correlate with DMPK expression.

Introduction

Myotonic dystrophy type I (DM1) is a multisystemic disease with an overall estimated prevalence of 1:8000[1], being the most common form of muscular dystrophy in adults. DM1 has an autosomal dominant inheritance pattern, and it is caused by a CTG repeat expansion in the 3' untranslated region (UTR) of the dystrophia myotonica-protein kinase (*DMPK*) gene[2]. More than 50 CTG repeats are considered pathogenic and this length varies from fifty to thousands of repeats in DM1 patients, with high variability between individuals[3]. The size of the CTG repeat also varies between tissues within the same patient[4–6], along a patient's lifetime[7] and produces anticipation[1].

The main pathogenic process underlying DM1 is a toxic RNA gain-of-function effect of expanded DMPK transcripts forming hairpin structured aggregates, called RNA foci[8]. RNA foci sequester splicing factors such as MBNL1 protein, leading to splicing defects affecting several genes[9]. The altered transcription of these genes in DM1 has been related to several DM1 symptoms.

DM1 is a highly heterogeneous disease affecting several tissues and systems. It affects the muscle, causing myotonia, weakness, fatigue and pain; the cardiorespiratory system, producing conduction defects, atrial fibrillation and lung function impairment; the gastrointestinal system, causing dysphagia, constipation and diarrhea; the central nervous system, producing intellectual disability, anxiety, depression or hypersomnia; the endocrine system, causing thyroid dysfunction or diabetes; the visual system, producing cataracts; and the integumentary system, causing pilomatrixomas or epitheliomas[3]. The complexity of the disease highlights the importance of studying several cellular models for a better understanding of the pathophysiology and to better assess the potential efficacy of new therapies for the disease.

DM1 symptoms can appear at any age. Based on the age of onset of the main symptoms, five clinical subtypes are defined: congenital (<1 year), childhood (1-10), juvenile (11-20), adult (21-40) and late-onset (>40). In general, disease severity increases with an earlier onset, and each subtype presents some unique features[10]. Most studies on DM1 are performed using cells derived from a single subtype of the disease, not considering the potential differences that could be found at a molecular level or in response to a treatment according to the subtype.

Therefore, the objectives of this study were: 1) to analyze the pathological hallmarks of DM1 in different cell types (myoblasts, myotubes, skin fibroblasts and lymphoblastoids) 2) to analyze the pathological hallmarks of DM1 in lymphoblastoids derived from patients of all clinical subtypes.

Materials and Methods

Participants and sample collection

This study was approved by the Ethics Committee of the University Hospital Germans Trias i Pujol and was performed in accordance with the Declaration of Helsinki for Human research. Written informed consent was obtained from all the participants. 6 controls and 24 DM1 patients were included in the study. DM1 diagnosis was confirmed with triplet primed-PCR in all the patients, as previously describe [6] d. Clinical information of patients was obtained from the medical records and updated in the last visit by neurologists. Patients were subdivided into five different categories based on age of onset: congenital= first year of life, childhood= 1-10 years, juvenile= 11-20 years, adult= 21-40 years, late-onset > 40 years[10].

Three different samples from patients were obtained, as shown in Figure 1: blood, muscle biopsy and skin biopsy. Blood was obtained from peripheral blood extraction, and lymphoblastoids were isolated. From a subset of patients, muscle biopsies were obtained from the biceps brachialis or vastus lateralis, and skin biopsies were obtained by a 0.5 cm skin punch. Myoblasts, myotubes and skin fibroblasts were obtained from biopsies. Cell isolation and subsequent culturing was performed as previously described[11].

DNA extraction and CTG expansion size analysis

Genomic DNA was extracted from peripheral blood, skin fibroblasts and muscle cells using the QIAamp DNA mini kit (Qiagen, Hilden, Germany), the PureLink genomic DNA mini kit (Thermo Fisher Scientific, Waltham, MA, USA) or a salting procedure, as previously described[12]. To estimate the length of the expanded allele, a small-pool PCR was performed using flanking primers DM-C and DM-DR, as previously described[13,14]. DNA fragments were resolved by electrophoresis on a 1% agarose gel, followed by Southern Blot as previously described (Gomes-Pereira 2004). CTG expansion sizes were estimated through comparison against the molecular weight ladder using GelAnalyzer 19.1 software (www.gelanalyzer.com, by Istvan Lazar Jr. and Istvan Lazar Sr.). We

estimated the modal allele, which is the densest part of the expanded allele distribution, thought to be the most representative size for the patient at that specific time.

RNA foci quantification and MBNL1 colocalization

Myotubes, myoblasts, skin fibroblasts and lymphoblastoids were grown on coverslips and fixed with 4% paraformaldehyde and permeabilized with 0.3% Triton X-100 at 4 ºC for 5 min (0.1% Triton X-100 for lymphoblastoids). To detect RNA foci colocalization with MBNL1, we performed fluorescence in situ hybridization (FISH) followed by immunofluorescence. Coverslips were incubated with 30% formamide in 2x SSC buffer for 30 min at room temperature, followed by an overnight incubation at 37 ºC with hybridization buffer, containing 0.01 µM Cy3-labelled (CAG)10 probe, 30% formamide, 1% dextran sulfate, 0.02% BSA and 2mM vanadyl in 2x SSC buffer. The following day, the coverslips were washed with 30% formamide in 2x SSC at 45 ºC, 1x SSC at 37 ºC and 1x PBS at room temperature. The coverslips were then blocked with 1% goat serum for 1 h, and were incubated with anti-MBNL1 antibody (sc47740, Santa Cruz Biotechnology; Dallas, TX, 1:100). Next, cells were washed and incubated with anti-mouse conjugated with Alexa Fluor 488 (A11001, Thermo Fisher Scientific, Waltham, MA, USA). Finally, coverslips were washed with PBS and mounted with ProLong Gold Anti-Fade Mountant with DAPI (Thermo Fisher Scientific, Waltham, MA, USA). Images were obtained with Zeiss Axio Observer Z1 microscope (Jena, Germany), using a 63x/1.4 NA oil immersion objective. RNA foci quantification and MNBL1 colocalization analysis were performed using ImageJ software. We analyzed at least 20 arbitrary cells per patient cell type.

For single cell analysis we developed a new FISH staining method with the aim to preserve RNA integrity as much as possible. In brief, myoblast pellets were resuspended with formamide and incubated for 20’ at 37ºC. Myoblast were then incubated with the hybridization buffer containing AT0488 labelled $(CAG)_{10}$ probe 0.01 uM and 30% formamide in 2XSSC buffer for 20’ at 37ºC. Myoblast were then washed with 30% formamide 2x SSC, 1x SSC and 1x PBS and incubated for 5’ with 5 ul of DAPI mounting solution. Finally, myoblasts were resuspended with 500 ul of 1x PBS.

Single myoblast isolation and fluorescence microscope visualization

Cells were sorted using FACSAria II flow cytometer (BD Biosciences, San Jose, CA, EEUU) into 96-Well Optical-Bottom Plates. For each participant, we sorted a total of 120 FISH stained myoblasts distributed in two plates. The cytometer could not detect the fluorescent signal of the FISH staining (probably because RNA foci fluorescence signal is small and because of their nuclear localization). Therefore, sorting was only used to isolate individual myoblasts. RNA foci signal was observed by fluorescent microscopy. To spend the least time possible, since these same cells have to go for posterior RNA analysis, and because there were two plates to analyze per participant, two independent observers simultaneously visualized one plate each, in similar fluorescence microscopes. They had the same criteria for annotating RNA foci number in every single myoblast by naked eye visualization.

RNA isolation, cDNA synthesis, preamplification and quantitative PCR (qPCR)

RNA from single myoblasts was isolated using GenElute™ Single Cell RNA Purification Kit (Sigma-Aldrich, San Luis, MO, EEUU) and cDNA was synthesized using TruScript First Strand cDNA Synthesis Kit (Norgen Biotek Corp., Thorold, ON, Canada), following the manufacturer's protocol in both. Transcripts of interest were preamplified with gene specific Taqman assays using TaqMan™ PreAmp Master Mix (ThermoFisher, Waltham, MA, EUU). This preamplification step is used in most single cell studies. Transcripts of interest included *DMPK*, *MBNL1* exon 7 inclusion (aberrant) and exclusion isoforms, *ATP2A1* exon 22 inclusion and exclusion (aberrant) isoforms and *INSR* exon 11 inclusion and exclusion (aberrant) isoforms. The design of *MBNL1*, *INSR* and *ATP2A1* Taqman assays was done with the Assay Design Tool (Thermofisher), while for *DMPK* we used a previously described Taqman assay [15]. We analyzed the expression of *DMPK* and *INSR*, *ATP2A1* and MBNL1 splicing variants by qPCR using Taqman Fast Advanced Master Mix (ThermoFisher) and the same Taqman assays as in preamplification (Thermofisher). No endogenous control was used for normalization because in single cell analysis housekeeping genes can be misleading as their expression varies from cell to cell. Expression levels are instead reported as relative quantities per cells. Data analysis was performed as previously described l[16].

Statistical analysis

The statistical analysis was performed using GraphPad Prism 9.1.2 software and the significance level was set at 0.05. Differences in RNA foci, MBNL1 colocalization and *DMPK* expression between different cell types and clinical categories were analyzed by one-way ANOVA test. Differences in *DMPK* expression were analyzed by Kruskal-Wallis test and the correlation at single cell level between *DMPK* expression and number of RNA foci was analyzed with Spearman rank correlation coefficient.

Results

Study cohort

The study is divided in two parts which are graphically represented in Figure 1. For the first part of this study, we analysed different cell types (lymphoblastoids, myoblasts, myotubes and skin fibroblasts) derived from 8 DM1 patients: 1 juvenile, 4 adults and 3 late-onset. For this group of patients, age of onset ranged from 15 to 50 years. We did not obtain skin and muscle biopsies from paediatric patients for ethical reasons. For the second part of this study 18 DM1 patients were included, 2 of which (SP6 and SP12) were also included in the first part of the study. We studied lymphoblastoids derived from those 19 patients of five different clinical categories: congenital (n=3), childhood (n=4), juvenile (n=4), adult (n=5) and late-onset (n=3). The age of onset ranged from newborns to 58. Detailed information on the clinical phenotypes of the participating patients can be found in Table 1.

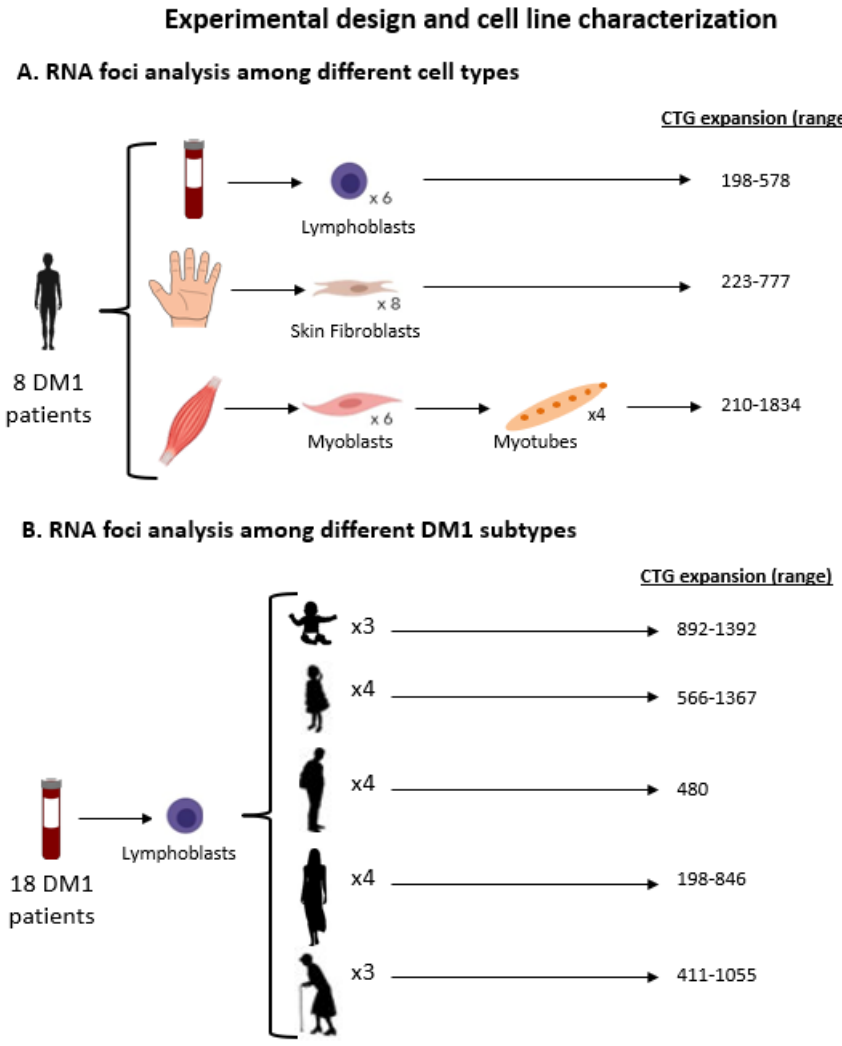

Figure 1. Experimental design and CTG expansion mode range.

Table 1. Clinical characteristics of the DM1 patients in this study

Patient	Subtype	Age of onset	Age at sampling	Gender	Myotonia	MIRS	Cardiopathy
Sp13	Congenital	At birth	10	F	NA	NA	NA
Sp107	Congenital	At birth	18	M	No	5	Yes
Sp136	Congenital	At birth	16	M	Yes	3	No
Sp69	Childhood	6	56	M	Yes	4	Yes
Sp70	Childhood	7	43	M	Yes	3	No
Sp74	Childhood	2	20	M	Yes	2	Yes
Sp77	Childhood	6	40	F	Yes	3	No
Sp3	Juvenile	15	36	F	Yes	4	Yes
Sp68	Juvenile	15	24	M	Yes	2	No
Sp104	Juvenile	15	16	M	Yes	2	No
Sp106	Juvenile	16	37	F	Yes	4	Yes
Sp163	Juvenile	14	15	M	Yes	2	No
Sp6	Adult	36	41	F	Yes	2	No
Sp10	Adult	27	39	F	Yes	4	Yes
Sp12	Adult	36	41	M	Yes	3	Yes
Sp23	Adult	35	41	F	Yes	3	Yes
Sp73	Adult	27	43	F	Yes	2	No
Sp85	Adult	30	45	F	Yes	3	No
Sp5	Late-onset	48	56	M	Yes	3	Yes
Sp9	Late-onset	42	46	F	Yes	3	Yes
Sp15	Late-onset	50	64	F	Yes	2	Yes
Sp96	Late-onset	58	65	M	No	1	Yes
Sp118	Late-onset	55	65	F	Yes	4	Yes
Sp165	Late-onset	48	68	M	Yes	4	Yes

Orange highlights the patients whose cells were used in both parts of this study, blue highlights the patients whose cells were used in the first part of this study and white highlights the patients whose cells were used in the second part of this study.

RNA foci accumulation and MBNL1 colocalization differs between DM1 patient-derived cell types

RNA foci and MBNL1 staining's were performed in 4 different cell types: lymphoblasts, fibroblasts, myoblasts and myotubes. Foci staining revealed that the average and maximum number of RNA foci/cell were significantly lower in lymphoblasts compared to myoblasts and myotubes (Fig. 2 A-C) The RNA foci average was 1.01 in lymphoblasts, 2.71 in fibroblasts, 3.92 in myoblasts and 5.44 in myotubes. The maximum RNA foci per cell was 4.17 in lymphoblasts, 6.50 in fibroblasts, 10.5 in myoblasts and 19 in myotubes. Moreover, when we analyzed the distribution of RNA foci in the cells, we observed that the percentage of lymphoblasts with foci was 58.9%, in fibroblasts 85.7%, in myoblasts 99.1% and in myotubes 91.1% (Table 2). We also observed that while in lymphoblasts most cells (>80%) had between 0 and 2 foci, in fibroblasts the cells with these low number of foci were reduced to 60% and in myoblasts and myotubes to less than 40%. Furthermore, no lymphoblasts showed more than 6 RNA foci while around 15% of the myotubes had more

than 6 RNA foci (Figure 2D). As observed in RNA foci, MBNL1 staining showed a significantly lower average of aggregates in lymphoblasts compared to myoblasts and myotubes (Fig. 3A-C). The percentage of RNA foci colocalizing with MBNL1 was 3.77 in lymphoblasts, 14.7 in fibroblasts, 28.9 in myoblasts and 22.3 in myotubes (Figure 3D, Table 2).

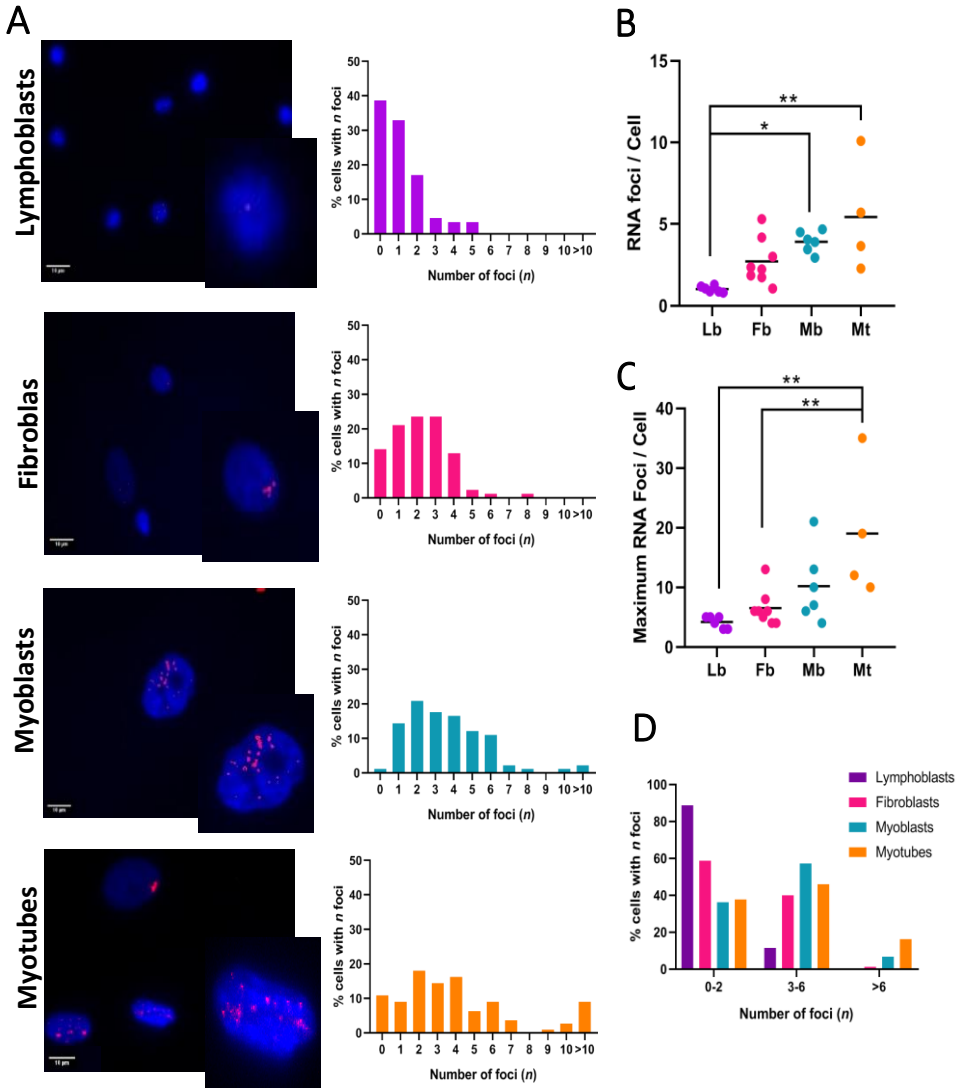

Figure 2. RNA foci accumulation differs between DM1 patient-derived cell types. A. Representative images of RNA foci (red) and DAPI (blue) staining in DM1 patient-derived lymphoblasts (Lb), fibroblasts (Fb), myoblasts (Mb) and myotubes (Mt). Scale bar: 10 µm. B. Average RNA foci. C. Maximum RNA foci. D. Percentage of cells with n foci. A minimum of 10 random cells were analyzed per cell type and patient: *n=6* for lymphoblasts, *n=8* for fibroblasts, *n=6* for myoblasts, *n=4* for myotubes. Age of onset of the disease in patients ranges from juvenile to late onset. Statistical significance was determined by one-way ANOVA.*$p \leq 0.05$ **$p \leq 0.01$

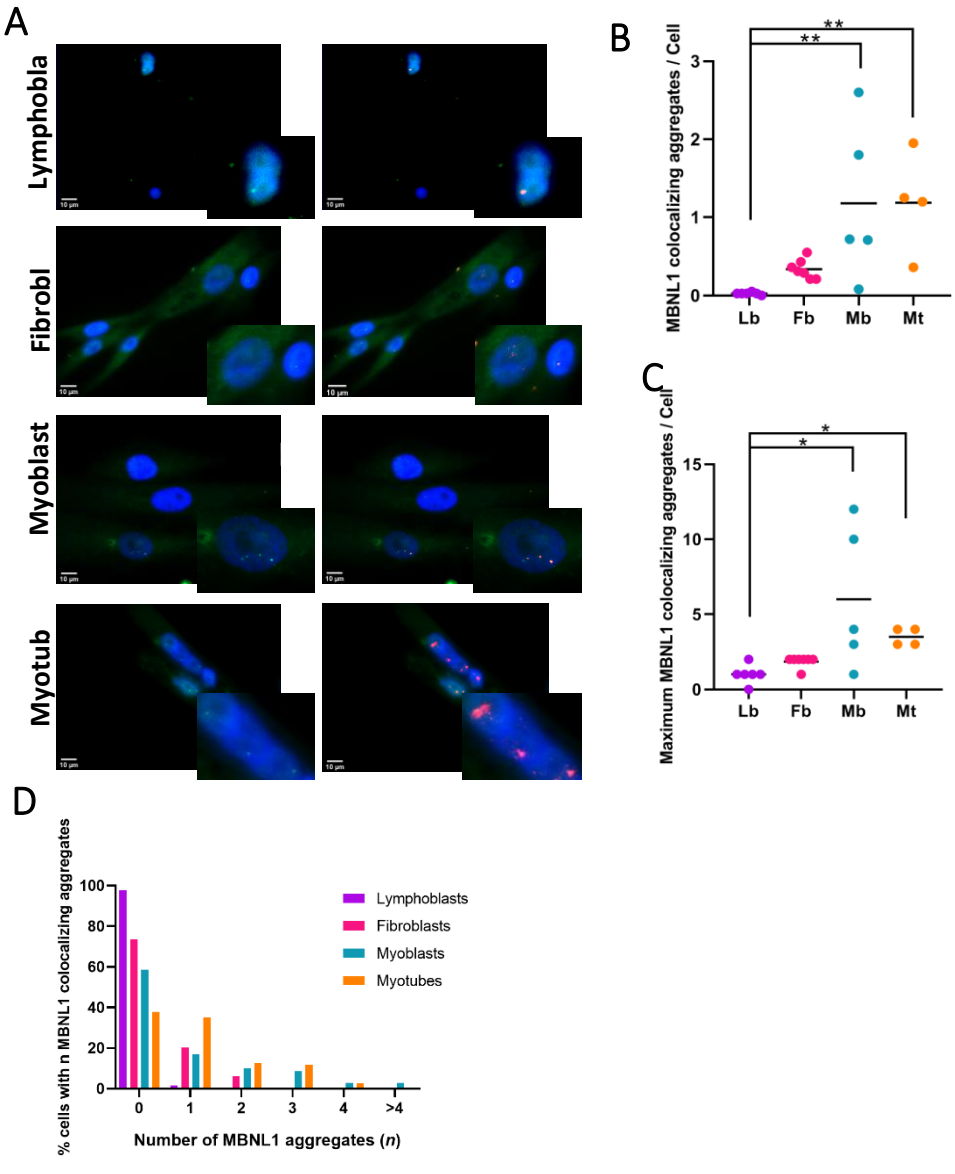

Figure 3. MBNL1 colocalizing aggregate number differs between DM1 patient-derived cell types. A. Representative images of MBNL1 aggregates foci (green) and DAPI (blue) staining in DM1 patient-derived lymphoblasts (Lb), fibroblasts (Fb), myoblasts (Mb) and myotubes (Mt). B. Average MBNL1 colocalizing aggregates. C. Maximum MBNL1 colocalizing aggregates. D. Percentage of cells with n MBNL1 colocalizing aggregates. A minimum of 10 random cells were analyzed per cell type and patient: *n=6* for lymphoblasts, *n=7* for fibroblasts, *n=5* for myoblasts, *n=4* for myotubes. Age of onset of the disease in patients ranges from juvenile to late onset. Statistical significance was determined by one-way ANOVA.*$p \leq 0.05$ **$p \leq 0.01$

Table 2. RNA foci parameters vary by DM1 patient-derived cell types.

Cell Type	Foci/cell average	Max. foci/cell	% of cells with foci	% of RNA foci with MBNL1 colocalization
Lymphoblasts	1.01 ± 0.19	4.17 ± 0.98	58.9 ± 9.2	3.77 ± 2.67
Fibroblasts	2.71 ± 1.40	6.50 ± 2.93	85.7 ± 14.7	14.7 ± 3.30
Myoblasts	3.92 ± 0.65	10.5 ± 5.96	99.1 ± 2.16	28.9 ± 25.6
Myotubes	5.44 ± 3.41	19.0 ±11.3	91.1 ± 15.0	22.3 ±6.96

A minimum of 10 random cells were analyzed per cell type and patient; *n=6* for lymphoblasts, *n=8* for fibroblasts (*n=7 for MBNL1)* , *n=6* for myoblasts (*n=5 for MBNL1)* , *n=4* for myotubes.

Single cell analysis reveals that RNA foci and DMPK expression does not correlate

To determine whether RNA foci number correlates with *DMPK* expression, we isolated single myoblasts from five of the DM1 patients of the study, quantified the RNA foci and determined the expression of *DMPK* at single cell level. We found differences in myoblast foci number both between and within patients, indicating the existence of heterogeneity in myoblast foci number. The number of RNA foci ranged from 0 to 7 and was heterogeneously distributed between patients (Fig4A-B, Table 3). Single cell *DMPK* expression analysis revealed a significantly lower expression in DM1 patients compared to controls (Fig. 4C). However, no correlation was found between the number of RNA foci and the level of *DMPK* expression per cell (Fig. 4D).

Table 3. DM1 patient's CTG expansion size and single muscle progenitor cell foci analysis.

PATIENT	FOCI ANALYSIS			
	% cells with foci	**Mean**	**Median**	**Range**
DM1-1	97,2%	2,3	2	0-6
DM1-2	98,6%	2,6	2	0-7
DM1-3	81%	1,4	1	0-4
DM1-4	97,4%	2,7	3	0-5
DM1-5	28,8%	0,6	0	0-7

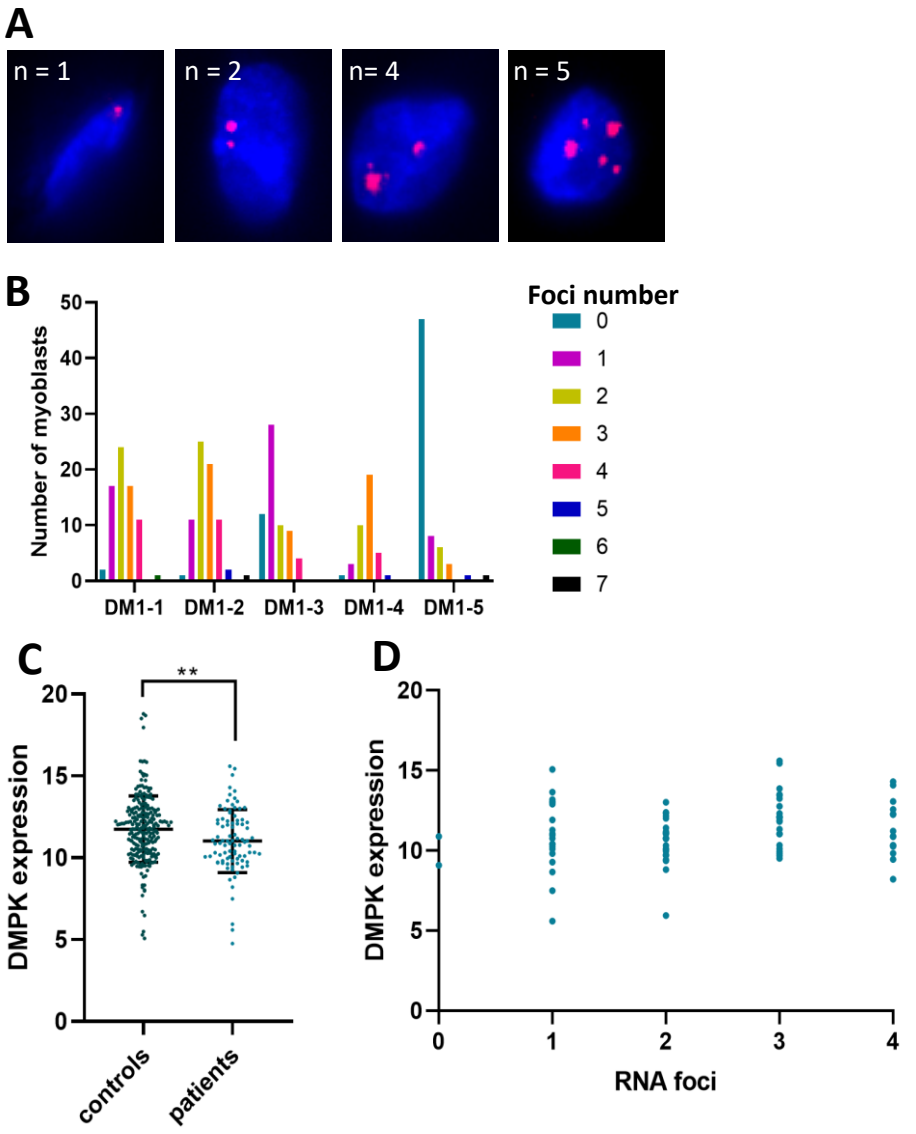

Figure 4. RNA foci number is heterogeneously distributed and DMPK expression is downregulated in DM1 patient's progenitor cells but there is no correlation between RNA foci number and DMPK expression. A. RNA foci staining in four myoblasts of the same patient. Foci staining is green and nuclei staining is blue. n = number of foci. The lighter stained foci are indicated by white triangles. B. Distribution of RNA foci per myoblast in every patient of this study. C. Comparison of the DMPK expression in muscle progenitor single cells from four patients and five controls. D. Correlation analysis between the DMPK expression levels and RNA foci number in the muscle progenitor cells of four DM1 patients. Statistical significance between two groups was determined by Kruskal-Wallis test and correlation was determined by Spearman rank correlation coefficient **p ≤ 0.01

Cells derived from DM1 patients with earlier onset of the disease show higher accumulation of RNA foci

Differences in RNA foci accumulation between DM1 patients of five different clinical subtypes were assessed in lymphoblasts. Results showed that there are significant differences among DM1 categories. Cells derived from congenital and childhood patients present a higher number of RNA foci than other categories, while late-onset cells show the lowest number of RNA foci. The RNA foci average per lymphoblastoids was 1.55 in congenital patients, 1.26 for childhood, 0.81 for juvenile, 0.75 for adult and 0.64 for late-onset patients (Table 4 and Figure 5B). The range of RNA foci per cell ranged from 0 to 6 in congenital patients; from 0 to 4 in childhood, juvenile and adult cases; and from 0 to 3 for late-onset patients (Table 4 and Figure 5A and 5C). Furthermore, cells from congenital patients showed the highest percentage of affected cells (i. e. cells presenting RNA foci), although there is no statistical significance. The percentage of lymphoblastoids with RNA foci was 75% in congenital patients, 65% in childhood, 56% in juvenile, 50% in adults and 45% in late-onset patients (Table 4 and Figure 5D).

Table 4. RNA foci parameters in DM1 patient-derived lymphoblastoids from all clinical subtypes. A

Category	Foci/cell average	Foci/cell max. Average	% average of cells with foci
Congenital	1.55 ± 0.41	4.33 ± 1.53	75 ± 13.23
Childhood	1.26 ± 0.24	3.75 ± 0.5	65 ± 17.8
Juvenile	0.81 ± 0.17	3 ± 0.82	56.25 ± 16.52
Adult	0.75± 0.41	2.80 ± 1.10	50 ± 14.14
Late-onset	0.64 ± 0.21	2.47 ± 0.58	45 ± 17.56

A minimum of 20 random cells were analysed per patient;
n=6 for controls, n=3 for congenital, n=4 for childhood, n=4 for juvenile, n=5 for adult, n=3 for late-onset. Data are given as mean ± SD.

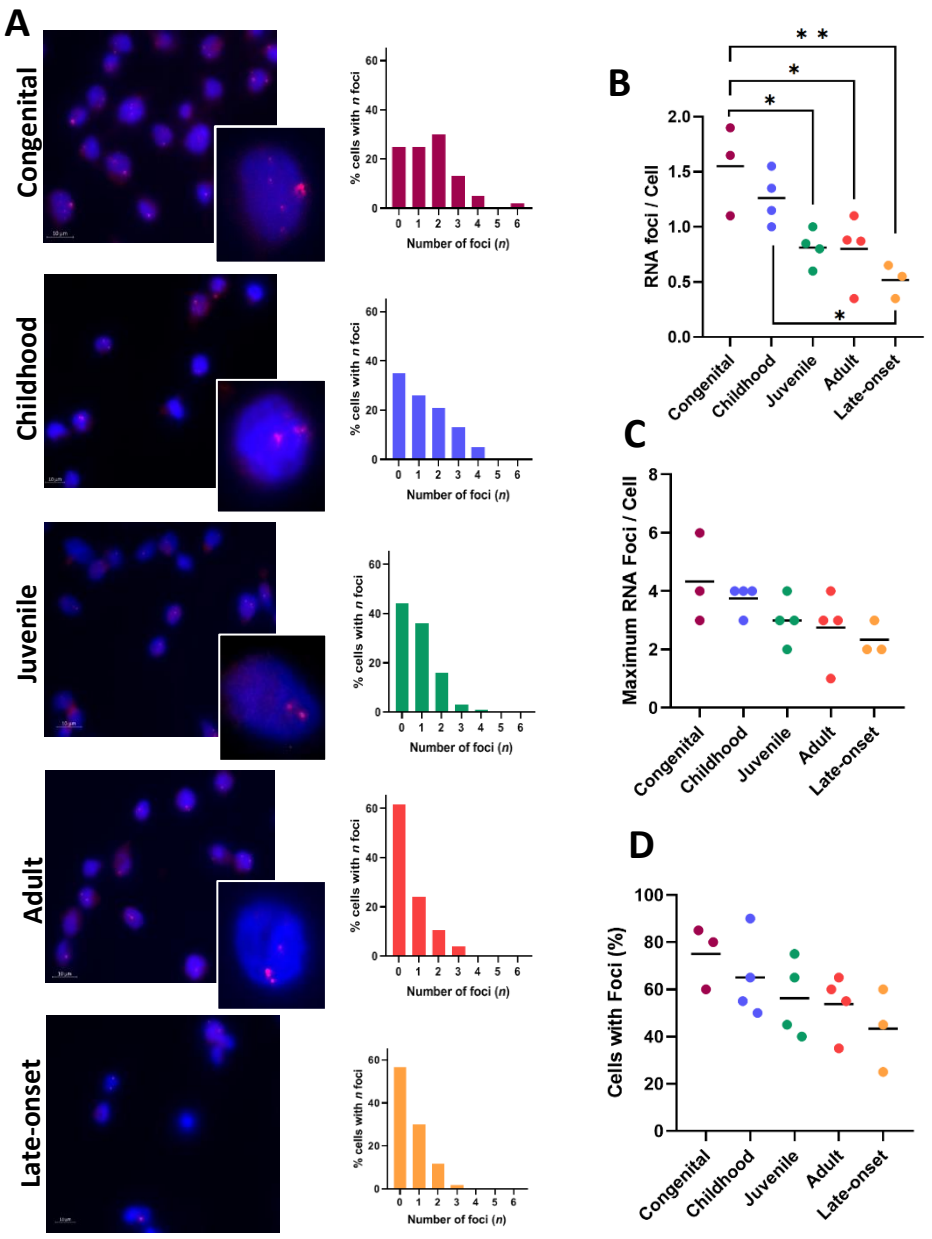

Figure 5. Lymphoblasts derived from DM1 patients with an earlier onset of the disease show higher accumulation of RNA foci. A. Left: Representative images of RNA foci (red) and nuclei (DAPI, blue) staining in lymphoblasts. Scale bar: 10 µm. Right: Distribution of cell percentage by number of RNA foci. B. Average of RNA foci per cell in lymphoblasts, C. Maximum RNA foci per cell, D. Percentage of cells containing RNA foci. A minimum of 20 random cells were analysed per individual; n=3 for congenital, n=4 for childhood, n=4 for juvenile, n=5 for adult, n=3 for late-onset. Statistical significance was determined by one-way ANOVA. *$p \leq 0.05$ **$p \leq 0.01$ ***$p \leq 0.005$ ****$p \leq 0.0001$

Discussion

Heterogeneity is a key factor in DM1 as symptoms can affect many tissues, are variable between patients and they can debut at any age. Studying this heterogeneity and how it affects the pathophysiology of the disease is essential to better understand the complexity of the disease and how candidate therapies could impact the patients. In our study, we analysed the molecular heterogeneity both between tissues and clinical subtypes and concluded that RNA foci accumulation is variable according to cell type and age of onset.

To analyse tissue heterogeneity, we obtained lymphoblastoids, skin fibroblasts, myoblasts and myotubes from eight different patients. We could observe that all four of them showed alterations at molecular level: RNA foci accumulation and MBNL1 sequestration, validating them as models to study DM1. However, we found differences in RNA foci and MBNL1 aggregates average between lymphoblasts and muscle cells. These differences could be influenced by the RNA expression levels of *DMPK* in each tissue. According to the Human Protein Atlas, normalized RNA expression levels of *DMPK* in skeletal muscle is 167.5, while in skin is 11.9 and in bone marrow 2.4. Other factor that could be affecting RNA foci in patients' accumulation is cell turnover, which is known to be higher in skin or blood compared to muscle[17]. These differences should be considered when choosing a DM1 cellular model to either study the pathophysiology or the potential effect of therapies.

To analyse DMPK expression and the possible correlation with RNA foci number we performed a single cell DMPK analysis. It revealed a decrease in *DMPK* levels in DM1 cells compared to control cells, which has been previously reported[18]. It has been hypothesized that this downregulation could be due to epigenetic changes surrounding the DMPK gene, which would be induced by the CTG repeats[19]. In this work, we used single cell technology to analyse both the *DMPK* levels and the number of RNA foci in single DM1 myoblasts. The analysis concluded that there is no correlation between the two factors. For future studies, it would be interesting to be able to distinguish between the expression of the mutant and wild-type RNA. This way we could decipher whether a higher expression of *DMPK* equals to greater accumulation of RNA foci or if there are other mechanisms or factors intervening.

To study age of onset heterogeneity at a molecular level, we obtained lymphoblasts samples from the 5 DM1 subgroups: congenital, infantile, juvenile, adult and late-onset. Although muscle samples would have been a better model, as it is one of the main affected tissues in DM1, we could not obtain children samples due to ethical reasons. The study revealed significant differences between categories, being the patients with an earlier age of onset the ones to accumulate more RNA foci. It has been described that there is an inverse correlation between the age of onset and the expansion size; the earlier the symptoms appear the larger the expansion and the more severe the symptoms are[3]. We hypothesise that the expansion size could be a factor influencing RNA foci accumulation, so that the larger the expansion the greater tendency to accumulate RNA foci.

References

1. Harper P. *Myotonic Dystrophy*. 3rd ed. London: WB Saunders; 2001.
2. Brook JD, McCurrach ME, Harley HG, et al. Molecular basis of myotonic dystrophy: expansion of a trinucleotide (CTG) repeat at the 3' end of a transcript encoding a protein kinase family member. *Cell*. 1992;68(4):799-808. doi:10.1016/0092-8674(92)90154-5
3. Bird TD. *Myotonic Dystrophy Type 1*.; 1993.
4. Lavedan C, Hofmann-Radvanyi H, Shelbourne P, et al. Myotonic dystrophy: size- and sex-dependent dynamics of CTG meiotic instability, and somatic mosaicism. *Am J Hum Genet*. 1993;52(5):875-883.
5. Ashizawa T, Dubel JR, Harati Y. Somatic instability of CTG repeat in myotonic dystrophy. *Neurology*. 1993;43(12):2674-2678. doi:10.1212/wnl.43.12.2674
6. Mahadevan M, Tsilfidis C, Sabourin L, et al. Myotonic dystrophy mutation: an unstable CTG repeat in the 3' untranslated region of the gene. *Science*. 1992;255(5049):1253-1255. doi:10.1126/science.1546325
7. Wong LJC, Ashizawa T, Monckton DG, et al. Somatic heterogeneity of the CTG repeat in myotonic-dystrophy is age and size-dependent. *Am J Hum Genet*. 1995;56:114-122. http://www.ncbi.nlm.nih.gov/pmc/articles/PMC1801291/

8. Taneja KL, McCurrach M, Schalling M, Housman D, Singer RH. Foci of trinucleotide repeat transcripts in nuclei of myotonic dystrophy cells and tissues. *Journal of Cell Biology*. 1995;128(6):995-1002. doi:10.1083/jcb.128.6.995

9. Dansithong W, Paul S, Comai L, Reddy S. MBNL1 is the primary determinant of focus formation and aberrant insulin receptor splicing in DM1. *J Biol Chem*. 2005;280(7):5773-5780. doi:10.1074/jbc.M410781200

10. De Antonio M, Dogan C, Hamroun D, et al. Unravelling the myotonic dystrophy type 1 clinical spectrum: A systematic registry-based study with implications for disease classification. *Rev Neurol (Paris)*. 2016;172(10):572-580. doi:10.1016/j.neurol.2016.08.003

11. Koehorst E, Núñez-Manchón J, Ballester-López A, et al. Characterization of RAN Translation and Antisense Transcription in Primary Cell Cultures of Patients with Myotonic Dystrophy Type 1. *J Clin Med*. 2021;10(23). doi:10.3390/jcm10235520

12. Miller SA, Dykes DD, Polesky HF. A simple salting out procedure for extracting DNA from human nucleated cells. *Nucleic Acids Res*. 1988;16(3):1215. doi:10.1093/nar/16.3.1215

13. Gomes-Pereira M, Bidichandani SI, Monckton DG. Analysis of unstable triplet repeats using small-pool polymerase chain reaction. *Methods Mol Biol*. 2004;277:61-76. doi:10.1385/1-59259-804-8:061

14. Monckton DG, Wong LJ, Ashizawa T, Caskey CT. Somatic mosaicism, germline expansions, germline reversions and intergenerational reductions in myotonic dystrophy males: small pool PCR analyses. *Hum Mol Genet*. 1995;4(1):1-8. doi:10.1093/hmg/4.1.1

15. Maeda M, Taft CS, Bush EW, et al. Identification, tissue-specific expression, and subcellular localization of the 80- and 71-kDa forms of myotonic dystrophy kinase protein. *J Biol Chem*. 1995;270(35):20246-20249. doi:10.1074/jbc.270.35.20246

16. Ståhlberg A, Kubista M. Technical aspects and recommendations for single-cell qPCR. *Mol Aspects Med*. 2018;59:28-35. doi:10.1016/j.mam.2017.07.004

17. Seim I, Ma S, Gladyshev VN. Gene expression signatures of human cell and tissue longevity. *NPJ Aging Mech Dis*. 2016;2:16014. doi:10.1038/npjamd.2016.14

18. Wang J, Pegoraro E, Menegazzo E, et al. Myotonic dystrophy: evidence for a possible dominant-negative RNA mutation. *Hum Mol Genet*. 1995;4(4):599-606. doi:10.1093/hmg/4.4.599

19. Brouwer JR, Huguet A, Nicole A, Munnich A, Gourdon G. Transcriptionally Repressive Chromatin Remodelling and CpG Methylation in the Presence of Expanded CTG-Repeats at the DM1 Locus. *J Nucleic Acids*. 2013;2013:567435. doi:10.1155/2013/567435

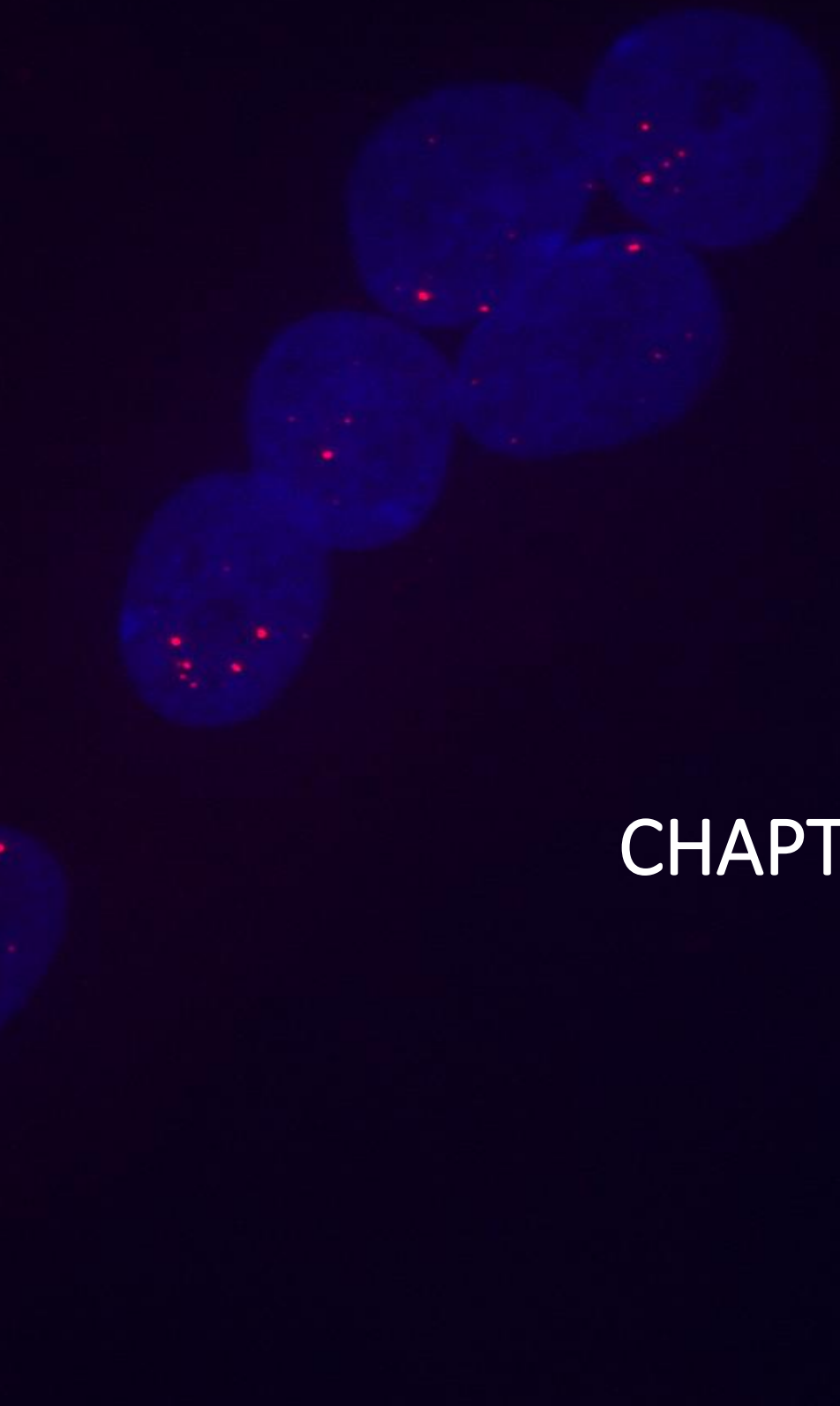

CHAPTER 2

AntimiR treatment corrects myotonic dystrophy primary cell defects across several CTG repeat expansions with a dual mechanism of action

Estefanía Cerro-Herreros[1,2,3], Judit Núñez-Manchón[4], Neia Naldaiz-Gastesi[5,6], Marc Carrascosa-Sàez[3], Andrea García-Rey[1,2], Diego Piqueras Losilla[3], Irene González-Martínez[1,2], Jorge Espinosa-Espinosa[1,2], Kevin Moreno[3], Javier Poyatos-García[7,8], Juan J Vilchez[7,8,9], Adolfo López de Munain[5,6,10,11], Mònica Suelves[4], Gisela Nogales-Gadea[4], Beatriz Llamusí[3] and Rubén Artero[1,2]

[1]Human Translational Genomics. University Research Institute for Biotechnology and Biomedicine (BIOTECMED), Universidad de Valencia, Valencia, Spain.
[2]INCLIVA Biomedical Research Institute, Valencia, Spain. Avenue Menéndez Pelayo 4 acc, 46010, Valencia, Spain.
[3]ARTHEx Biotech. Parque Científico de la Universidad de Valencia. Calle del Catedrático Agustín Escardino Benlloch, 9, 46980 Paterna, Valencia, Spain.
[4]Group of REsearch Neuromuscular of BAdalona (GRENBA), Institut d'Investigació en Ciències de la Salut Germans Trias i Pujol (IGTP), Campus Can Ruti, Universitat Autònoma de Barcelona, 08916 Badalona, Spain.
[5]Neuromuscular Diseases Group, Neurosciences Area, Biodonostia Health Research Institute, 20014 Donostia/San Sebastián, Spain.
[6]CIBERNED, Carlos III Institute, Spanish Ministry of Science & Innovation, Madrid, Spain.
[7]Neuromuscular and Ataxias Research Group, Health Research Institute Hospital La Fe (IIS La Fe), Valencia, Spain
[8] Centre for Biomedical Network Research on Rare Diseases (CIBERER); U763, CB06/05/0091, Madrid, Spain.
[9]Neuromuscular Referral Center, European Reference Network on Rare Neuromuscular Diseases (ERN EURO-NMD), Universitary and Polytechnic La Fe Hospital, Valencia, Spain.
[10] Department of Neurology, Donostialdea Integrated Health Organization, Osakidetza Basque Health Service, 20014 Donostia/San Sebastián, Spain.
[11] Department of Neurosciences, Faculty of Medicine and Nursery, University of the Basque Country UPV-EHU, 20014 Donostia/San Sebastián, Spain.

Corresponding author: Rubén Artero (ruben.artero@uv.es)

This chapter has been accepted for publication in Science Advances journal the 5th of September 2024.

Abstract

This study evaluated therapeutic antimiRs in primary myoblasts from myotonic dystrophy type 1 (DM1) patients. DM1 results from unstable CTG repeat expansions in the DMPK gene, leading to variable clinical manifestations by depleting Muscleblind-Like Splicing Regulator protein MBNL1. AntimiRs targeting natural repressors miR-23b and miR-218 boost MBNL1 expression but must be chemically optimized for a better pharmacological profile in humans. In untreated cells, miR-23b and miR-218 were upregulated, which correlated with CTG repeat size, supporting that active MBNL1 protein repression synergizes with the sequestration by CUG expansions in DMPK. AntimiR treatment improved RNA toxicity readouts and corrected regulated exon inclusions and myoblast defects such as fusion index and myotube area across CTG expansions. Unexpectedly, the treatment also reduced DMPK transcripts and ribonuclear foci. A leading antimiR reversed 68% of dysregulated genes. This study highlights the potential of antimiRs to treat various DM1 forms across a range of repeat sizes and genetic backgrounds by mitigating MBNL1 sequestration and enhancing protein synthesis.

Introduction

Myotonic dystrophy type 1 (DM1) is a rare neuromuscular disease caused by an expansion of a CTG microsatellite repeat in the 3' untranslated region (UTR) of the DM1 protein kinase (*DMPK*) gene[1]. The expansion size may reach thousands of CTG triplets in DM1 patients, compared to 5-37 in the general unaffected population. The disease has a prevalence of 1/3,000-1/8,000 individuals worldwide[2], making it the most common muscular dystrophy in adults. The length of the CTG tract in peripheral blood roughly correlates with disease severity, survival, and age of onset[3]. According to this, several clinical forms are described: congenital, infantile, juvenile, adult, and late-onset DM1[4]. A variable multisystem array of symptoms characterizes the disease due to the widespread ubiquitous expression of the *DMPK* gene, particularly cardiac conduction problems, skeletal muscle atrophy, and myotonia. Patient sex is also a modifying factor influencing DM1 phenotype[5].

DMPK transcripts containing expanded CUG triplets accumulate in the nucleus and induce toxicity by affecting RNA processing mechanisms and disturbing key cell signaling pathways[2,6]. A chief molecular event contributing to DM1 pathogenesis involves the expansion size-dependent sequestration of Muscleblind-like Splicing Regulator proteins in mutant *DMPK* transcripts, mainly MBNL1 in skeletal muscles, forming nuclear aggregates called foci[7]. MBNL1 sequestration affects the functional steady-state levels of the protein, depleting it from the nucleus and impairing its functions as a regulator of pre-mRNA alternative splicing and polyadenylation[8-10]. Stress responses triggered by the accumulation of toxic *DMPK* RNA in the cell nucleus also cause the activation of MBNL1 antagonists, such as CELF1[11], Staufen1[12], and hnRNPA1[13]. Together, these proteins function as developmental regulators, and their imbalance in DM1 causes abnormal persistence of fetal patterns of alternative splicing and other pre-mRNA processing defects in adult tissues. This pathological mechanism affects hundreds of genes in several tissues and organs, many of which have been directly connected to some pathological manifestations in DM1. For example, abnormal splicing of *cTNT*, *CLCN1*, and *INSR* have been respectively linked to cardiac conduction problems[14], myotonia[15], and insulin resistance[16].

The length of the CTG repeats changes over time in different cells and tissues[17], with a strong tendency towards generating expanded alleles[18]. In tissues relevant to DM1 pathology, much larger expansions are found in

skeletal muscles and the heart, compared to peripheral blood[19]. This phenomenon largely explains the age-dependent and variable nature of DM1 symptoms and has crucial implications for clinical management because the mutation size in a blood sample does not adequately predict the pathogenic load in other tissues[20], particularly muscle[21]. In addition, individual genetic background and non-CTG repeat interruptions are also known to impinge on the clinical presentation of the disease[22]. Thus, muscle cells directly isolated from a diverse cohort of patients constitute a valuable tool to validate novel DM1 therapies in the natural genetic context of the mutation[23].

Several therapeutical strategies are under development for DM1[24], including antisense oligonucleotides (AONs) designed to release sequestered MBNLs by either targeting *DMPK* transcripts for degradation or blocking the binding between both[25]. An alternative approach is using AONs to rescue the normal free levels of MBNL proteins because essential DM1 molecular alterations stem from the depletion of these proteins alone[25], which remain encoded in functional genes. From the three human MBNL paralogs, MBNL1 is mainly expressed in skeletal muscles and MBNL2 in the CNS, while MBNL3 performs functions associated with regeneration and aging[26-29]. MBNL1 overexpression is well tolerated and prevents typical DM1 alterations[30,31]. From a therapeutic perspective, this is a particularly favorable situation because MBNL1 protein depletion (and antagonist activity) can be compensated with enhanced endogenous expression[30-33], which is naturally repressed by miR-23b and miR-218 miRNAs[34]. Recently, miRNA-targeting AONs, so-called antimiRs, have been developed to block miR-23b and miR-218, increasing MBNL1 expression and correcting functional and histopathological DM1 alterations[34-36]. These AONs (antimiR-23b-V1 and antimiR-218-V1) were fully modified with 2'-O-Methyl (2'-OMe) chemistry, included several phosphorothioate (PS) linkages at each end, and were conjugated to cholesterol at the 3' end.

In the current study, we used eight DM1 primary myoblast cell lines and nine unaffected controls to test the effect of antimiR-23b-V1 and antimiR-218-V1, reported previously[34], together with a new generation of chemically modified antimiRs named antimiR-23b-V2 and antimiR-218-V2. V2 molecules incorporate a combination of 2'-OMe, 2'-O-Methoxyethyl (MOE), and locked nucleic acid (LNA) residues throughout their sequence, and furthermore, antimiR-23b-V2 and antimiR-218-V2 are conjugated with fatty acid to enhance their biodistribution[37]. The cells were transfected at two differentiation times to study multiple RNA toxicity readouts, finding that antimiRs enhance MBNL1

protein expression and reduce *DMPK* transcript levels. The results demonstrate that lead antimiR drugs rescue DM1 defects across multiple genetic backgrounds *in vitro* through a dual mechanism of action.

Materials and methods

Study design

This study aimed to evaluate the therapeutic potential of candidate drugs antimiR-23b-V1, antimiR-218-V1, antimiR-23b-V2, and antimiR-218-V2 in human DM1 primary myoblasts of Table 1, which includes diverse ages and repeat sizes, and both sexes. The investigation involved analysing DM1-related phenotypes such as fusion index, target miRNA levels, DMPK expression, ribonuclear foci number, MBNL1 nuclear foci and protein levels, and alternative splicing defects. Two differentiation time points (5 and 10 days) were evaluated. The concentrations used for antimiR-23b were 90 nM for immunocytochemistry (ICC) and fluorescent in situ hybridization (FISH) and 54 nM and 34 nM for protein and RNA analyses. The concentrations used for antimiR-218 were 366.7 nM for ICC and FISH studies and 220 nM and 138 nM for protein and RNA analyses. Myotubes for DNA, RNA, and protein analysis were collected as pellets, and coverslips were used for ICC and FISH assays at five and ten days after differentiation and treatment (Supp. Fig. S2). Additionally, we conducted a thorough assessment of the therapeutic potential of the antimiRs and examined the individual responses of each cell line to antimiR-23b-V2. Furthermore, an RNA-Seq experiment was carried out to investigate the impact of antimiR-23b-V2 on the transcriptome.

The sample sizes (n) are indicated in each figure, where each data point represents an individual cell line. Correlation analyses were performed to assess the degree of association between variables.

Sample donor characterization

A total of eight genetically confirmed DM1 patients and nine controls with no personal or family history of neuromuscular diseases were included in the study. The essential clinical characterization of healthy and DM1 primary myoblast line donors is shown in Table 1 and was compiled from pre-existing medical records from the indicated hospitals.

Primary myoblast isolation from muscle biopsy

Muscle biopsies were cleaned in a Ca^{2+}/Mg^{2+} containing Hank's balanced salt solution (HBSS; Thermo Fisher Scientific) supplemented with 1% of penicillin/streptomycin (P/S) and fungizone (amphotericin B; Thermo Fisher Scientific). Primary human myoblasts were isolated from the biopsied tissue by muscle explants and then purified by CD56 magnetic separation using CD56-coated microbeads (Miltenyi Biotec, Bergisch Gladbach, Germany) following the manufacturer's instructions.

Cell culture and transfection

Myoblasts were grown on 0.1% gelatin-coated flasks in a proliferation medium containing Dulbecco's Modified Eagle's Medium (DMEM) supplemented with 10% FBS, 22% M-199, 1x PSF, 1.74 µM insulin, 2 mM L-glutamine, 1.39 nM FGF and 0.135 mM EGF. When the cells reached 80-90% confluence, the proliferation medium was substituted by a differentiation medium containing DMEM supplemented with 2% FBS, 22% M-199, 1x PSF, 1.74 µM insulin, and 2 mM L-glutamine. At this point, cells were also transfected with antimiRs and Ribocellin (BioCellChallenge, #RC1000) was used as transfection reagent according to the manufacturer's instructions. The concentrations used for antimiRs-23b were 90 nM for immunocytochemistry (ICC) and FISH analyses, 54 nM and 34 nM for protein and RNA analyses on DM1 cell lines and 54 nM for protein and RNA analyses on control cell lines. The concentrations used for antimiRs-218 were 366.7 nM for ICC and FISH studies and 220 nM and 138 nM for protein and RNA analyses. Cell pellets for DNA, RNA, and protein extractions, and coverslips for ICC and FISH, were collected five and ten days after differentiation and treatment started. RNA and protein pellets from treated controls were collected only ten days after differentiation and treatment started.

AntimiR chemistry and synthesis

All miRNA inhibitors were obtained from Axolabs GmbH (Kulmbach, Germany). First, antagomirs antimiR-23b-V1 (5'-G*G*UAAUCCCUGGCAAUGU*G*A*U-3'-cholesterol) and antimiR-218-V1 (5'-A*C*AUGGUUAGAUCAAGCA*C*A*A-3'-cholesterol; * indicates phosphorothioate linkages) were prepared. Then, several rounds of optimization of length and modifications lead to the optimized antimiR-23b-V2 (16 nucleotides) and antimir-218-V2 (15 nucleotides) that contain an oleic acid moiety at the 3'-end and several modifications. AntimiR-23b-V2 contains 50% phosphorothioate linkages, 50% locked nucleic acid (LNA) residues, 30% 2'-O-methoxyethyl (MOE)-RNA and

20% 2'-O-methyl-RNA residues. AntimiR-218-V2 contains 66% phosphorothioate linkages, 53% LNA residues, and 47% MOE residues.

CTG expansion sizing

DNA samples were extracted using the QIAamp DNA mini kit (Qiagen, Hilden, Germany). To determine CTG expansion size, an *Eco*RI digestion, followed by a long PCR and subsequent electrophoresis and southern blot, was performed as described[78]. The modal allele of each patient, which corresponds to the densest CTG bands, was estimated through comparison against the molecular weight ladder (GeneRuler 1 kb Plus Ladder, Thermo Scientific, Waltham, USA) using GelAnalyzer 19.1 software.

***DMPK* expression quantification by RT-qPCR**

Total RNA was extracted using the miRNeasy Mini kit (Qiagen, #217004 and 79254), and 400 ng of RNA was converted to cDNA by random hexamer priming with SuperScript II (Invitrogen, #18064022), following the manufacturer's instructions. Subsequently, 0.2 ng cDNA was used with 5x HOT FIREPol® Probe qPCR Mix Plus (Solis BioDyne, #08-01-00001) and PrimeTime qPCR (IDT, sequences shown Supp. Table S1) probe assays for multiplex RT-qPCR on the QuantStudio 5 (Applied Biosystems; Foster City CA, USA). In the case of RNA isolated with Hot TRIzol from immortalized MyoD-inducible (doxycycline) DM1 fibroblasts[56], the protocol carried out was as described in Gagnon et al.[79]. Relative expression of *DMPK* was measured and normalized to GAPDH endogenous control, relative to transfection reagent control samples, using the $2^{-\Delta\Delta Ct}$ methodology.

Protein extraction and Jess Simple Western

For total protein extraction, primary DM1 and control myotubes were disrupted by mechanical homogenization with an insulin syringe in Pierce® RIPA buffer (Thermo Scientific, #89901) supplemented with protease and phosphatase inhibitor cocktails (Roche Applied Science, #11836153001 and #4906837001) and subsequently sonicated. Total protein concentration was measured using a BCA protein assay kit (Thermo Scientific Pierce, # 23225) and bovine serum albumin (BSA) as the protein standard.

The Jess Simple Western system was used to quantify MBNL1 protein from human primary myotubes, and measurements were normalized to total protein levels. Briefly, 1 µg of total protein from an individual experimental replicate (0.2 mg/ml) was separated in the Protein Normalization Assay

module (ProteinSimple, Bio-Techne, # AM_PN01) and used to detect MBNL1 using a mouse anti-Mbnl1 primary antibody (MB1a [4A8], 1:10, Developmental Studies Hybridoma Bank) and a goat HRP-conjugated anti-mouse IgG secondary antibody (ProteinSimple, Bio-Techne, # DM-002). Chemiluminescent detection was performed using luminol-S and peroxide, following the manufacturer's instructions (ProteinSimple, Bio-Techne, # DM-002). Normalization was done through total protein chemiluminescence analysis (ProteinSimple, Bio-Techne, # RP-001) using the Total Protein Detection module (ProteinSimple, Bio-Techne, # DM-TP01). Total MBNL1 levels were defined as the sum of the previously described MBNL1 42/43 (+ex5±ex7) and MBNL1 40/41 (-ex5±ex7) variants[44], normalized to total loaded protein. For the individual expression of each isoform, each form was separately analysed as MBNL1-42/43/loaded protein and MBNL1-42/43/loaded protein.

Fluorescence in situ hybridization (FISH) and MBNL1 immunocytochemistry (ICC)

Cells were fixed with 4% paraformaldehyde (PFA), washed, and permeabilized with 0.3% triton. For the ICC, cells were blocked (PBS-T with 1% BSA and 1% horse serum) and incubated with anti-Mbnl1 (MB1a(4A8), DSHB or MBNL1(3A4), Santacruz) at 1:200 overnight. The antibody was washed with PBS-T, and cells were incubated with biotinylated horse anti-mouse-IgG (Vector, #BA-9200) at 1:150 for 1 h at room temperature (r.t.). Elite ABC kit (VECTASTAIN, #PK-6100) was used for 30 min at r.t. to amplify the signal, followed by PBS-T washing and a two-hour incubation at r.t. with streptavidin-FITC (1:200, Vector). For FISH analysis, after permeabilization as indicated above, cells were washed and incubated with acetylation buffer (1.16% triethanolamine, 0.25% acetic anhydride) for 10 min at r.t. Upon pre hybridization in 2x SSC with 30% formamide, the cells were incubated with 1 µM Cy3-labelled (CAG)10 probe diluted 1:100 in hybridization buffer for 2 h at 37ºC[34]. Finally, the cells were washed and mounted in slides with Diamond Anti-Fade Mountant with DAPI (Thermo Fisher Scientific, #P36971). Images were taken with a Zeiss AxioObserver Z1 microscope with 63x objective. Analyses of MBNL1 quantification scale data, RNA nuclear foci, and MBNL1 nuclear foci per cell were performed using ZEN blue software. Nuclear MBNL1 fluorescence was visually quantified according to a previously defined MBNL1 quantification scale with values ranging from 0 to 3 that matched a gradient of

increasing MBNL1 signal. A value of 0 was defined as the complete absence of the MBNL1 signal, while 3 was the most intense signal found in control cell lines (Supp. Fig. S6).

Desmin Immunofluorescence

Cells were grown on coverslips and differentiated as described above. Cell lines B55, SP-12, and SP-6 were excluded from these experiments since they did not form clear myotubes on glass coverslips. After five or ten days of differentiation, cells were fixed with 4% PFA (Electron Microscopy Sciences) for 10 min at r.t. Then, they were washed in PBS and blocked and permeabilized with 0.3% Triton-X (Sigma-Aldrich) and 5% donkey serum in PBS (PBS-T) for one hour at r.t. Then, cells were incubated with the mouse anti-Desmin (Abcam clone D33, #ab8470) at 1:100 diluted in PBS-T overnight at 4°C. After several washes with PBS, samples were incubated with the corresponding secondary antibody diluted in PBS-T for one hour at r.t. Cells were washed with PBS and incubated for 2 min at r.t. with 1 µg/ml Hoechst solution (Thermo Fisher Scientific) for nuclear staining. Washed coverslips were then mounted on glass slides in a drop of fluorescence mounting medium. Samples were analysed by epifluorescence with a Zeiss Axio Cell Observer Microscope. The fusion index was defined as the percentage of nuclei within myotubes (>3 myonuclei) relative to the total number of nuclei in each condition. The average number of total nuclei per myotube was determined by counting over 250 nuclei from randomly chosen Desmin-positive cells (14 micrographs). For area measurement with Image J, the saturation of the green channel was initially increased by 35% to enhance quality and reduce noise. Subsequently, a threshold of 20, 255 was applied to create a mask for the green channel, precisely defining the area of myotubes. The total area of the image was then measured. Following this, the generated mask was selected, and the area within this selection was measured, thereby determining the area occupied by the myotubes. Finally, the area of the myotubes was divided by the total area, and the result was multiplied by 100 to express it as a percentage. Two independent transfection experiments were carried out. Quantification was performed using ImageJ software (NIH).

miRNA detection by RT-qPCR

Five ng of RNA from two individual experimental replicates were converted to cDNA using the miRCURY LNA RT kit (Qiagen #339340). Four µL of a cDNA dilution 1/60 were used in an RT-qPCR reaction with the miRCURY LNA SYBR Green PCR kit (Qiagen #339346) and Qiagen primers on the QuantStudio 5, according to the manufacturer's protocol. hsa-miR-218-5p (Qiagen, #YP00206034) and hsa-miR-23b-3p (Qiagen, #YP00204790) were detected and normalized to endogenous controls, RNU1A1 (Qiagen, #YP00203909) and U6 snRNA (Qiagen, #YP00203907), and the transfection reagent controls using a 2-ΔΔCt methodology.

Alternative splicing analysis

To analyse the alternative splicing, 2 µl of cDNA from two individual experimental replicates were used in a semiquantitative PCR reaction with GoTaq polymerase and Taq buffer (Promega, Madison, USA) and specific primers. For *MBNL1*, *KIF13A*, and *PPFIBP1*, the PCR amplicons were relatively weak, and a second PCR on the first products was performed with the same GoTaq polymerase and green Taq buffer. Primer sequences, exons analysed, and specific conditions of each PCR reaction are described in Supp. Table S2. PCR products were quantified using ImageJ software (NIH) and the percentage spliced-in (PSI) values for each splicing event of the selected genes was obtained to measure changes in splicing patterns. Delta PSI (ΔPSI) in splicing quantifies changes in alternative exon inclusion between conditions. Specifically, control and treated cells were compared to untreated cells, with the latter serving as the reference (change 0) (80). The overall ΔPSI was defined as the mean of the ΔPSI of *MBNL1* Ex5, *KIF13A* Ex32, *BIN1* Ex11, *SOS1* Ex25, and *PPFIBP1* Ex19.

RNA-seq analysis

Following the manufacturer's indications, libraries were prepared using TruSeq Stranded mRNA Library prep kit (Illumina). Libraries were sequenced using 150 base paired-end sequencing with the Illumina NovaSeq 6000 sequencer in the Centro Nacional de Análisis Genómico (CNAG-CRG), Barcelona. Around 50 million reads were obtained from each sample. A quality check eliminated any reads with a q value < 30, using TrimGalore (Version 0.6.6) software. All accepted reads were aligned to genome version GRCh38.p13 with STAR software (version 2.7.10a). Next, BAM results were analysed with RSEM (version v1.3.1) software to obtain transcripts per million (TPM) for each gene.

R package DESeq2 (version 1.36.0) was used to perform a differential gene expression (DGE) test. The threshold for DGE calls was an adjusted p-value < 0.05. We used a freely available online tool (http://nemates.org/MA/progs/representation.stats.html) to calculate the statistical significance of the overlap between groups of genes.

$$\%\, recovery = \frac{Mean\_treated\_genecount - Mean\_disease\_gene\_count}{Mean\_contol\_gene\_count - Mean\_disease\_gene\_count} X100$$

We categorized the recovery state of the genes according to the following scale: totally recovered genes (recovery % > 50 and < 150), partially recovered genes (recovery % > 0 and < 50), over recovered genes (recovery % > 150) and not recovered genes (recovery % < 0).

Statistical analyses

All statistical analyses were performed with Prism 8.2.1 (GraphPad). Results are presented as means ± S.E.M. An unpaired, two-tailed Student's t-test was used for comparisons between two groups. A two-way ANOVA test was performed to compare various groups and conditions, followed by Dunnett's post-test. Where data did not follow normality, Kruskal-Wallis's test was applied followed by Dunn's post-test. Differences were considered significant at $p < 0.05$. Details about the statistical analysis used for each quantification are described in the corresponding figure legend. Sample sizes (n) are included in each figure, where each data point represents an individual cell line. Correlation analyses were carried out to measure the degree of association between two variables. In each case, the most appropriate correlation type, Pearson's or Sperman's, was used and is indicated in the figure legends. Correlation values were interpreted as very high (0.9 to 1), high (0.7-0.9), moderate (0.5-0.7) or low (0.3-0.5).

Results

Cell characteristics and outcomes

Seven patients with adult-onset DM1 (five female, two male) and one with juvenile-onset DM1 (female) served as donors to derive the myoblast cell lines used in our study (Table 1). The length of the CTG repeat was determined in all cases using DNA from the cells, ranging from 117 to 1054 triplets. Information about repeat length from muscle tissue was available in two cases and closely matched the size observed *in vitro*: 726/736 and 835/788 (myoblasts/muscle). We also determined the CTG repeat length in blood at the time of biopsy collection. As expected, the number of triplets was lower compared to muscle tissue in all cell lines except MP-10-31.

Variability in the patient´s muscle function and disability were clearly shown by the battery of functional tests performed (Table 1), which included the 6-minute walking test (6MWT)[38], the muscle impairment rating scale (MIRS)[39], the modified Rankin Scale (mRS)[40], and the biceps Medical Research Council (MRC)[41]. Despite limited data availability and the qualitative nature of the variables (except 6MWT), we observed moderate positive correlations (R between 0.5 and 0.7; p-values<0.2) between CTG repeat length in muscle cells and scales of muscle impairment and patient disability (MIRS and mRS, respectively). In contrast, a negative correlation (R = -0.86) was observed between CTG repeat length and muscle strength, measured as the MRC score of the biceps (Supp. Fig. S1). Primary myoblasts from these patients were treated with antimiRs, differentiated, and evaluated for miR-23b and miR-218 levels, MBNL1 expression and subcellular distribution and nuclear foci, RNA foci, *DMPK* mRNA expression, myotube area and fusion index (Supp. Fig. S2).

Table 1. Characterization of DM1 and control cell donors that participated in this study. Muscle performance parameters, mutation size of DM1 patient donors used in the study, and muscle origin and age at sampling for both DM1 samples and controls.

ID	Sample type	Sex	Biopsy muscle	Age at sampling	Age of onset	CTG triplets in Myoblast /Muscle*	CTG triplets in Blood	6MWT[1] (m)	MIRS[2]	mRS[3]	Biceps MRC[4]	Cohort
SP3	DM1 (juvenile onset)	Female	Biceps brachialis	36	15	726/736*	445	348	4	2	4	A
SP6	DM1 (adult onset)	Female	Biceps brachialis	41	36	686	338	368	2	1	5	A
SP10	DM1 (adult onset)	Female	Biceps brachialis	39	27	835/788*	374	N.D.	4	4	4	A
SP12	DM1 (adult onset)	Male	Biceps brachialis	41	36	265	130	519	3	2	5	A
B55	DM1 (adult onset)	Female	Deltoid	47	30	1054	800	N.D.	4	3	4	B
MP-09-57	DM1 (adult onset)	Female	Intrinsic muscles of the hand or forearm	31	30	702	333	N.D.	2	N.D.	N.D.	C
MP-09-73	DM1 (adult onset)	Male	Intrinsic muscles of the hand or forearm	49	20	704	233	N.D.	2	N.D.	N.D.	C
MP-10-31	DM1 (adult onset)	Female	Biceps brachialis	34	15	117	1400	N.D.	3	N.D.	N.D.	C
C5	Control	Female	Intrinsic muscles of the hand or forearm	67	-	-	-	-	-	-	-	A
C7	Control	Female	Intrinsic muscles of the hand or forearm	66	-	-	-	-	-	-	-	A
C9	Control	Male	Intrinsic muscles of the hand or forearm	41	-	-	-	-	-	-	-	A
C10	Control	Male	Intrinsic muscles of the hand or forearm	26	-	-	-	-	-	-	-	A
C11	Control	Female	Intrinsic muscles of the hand or forearm	35	-	-	-	-	-	-	-	A
C12	Control	Male	Intrinsic muscles of the hand or forearm	73	-	-	-	-	-	-	-	A
B71	Control	Male	Medial calf	18	-	-	-	-	-	-	-	B
MP-35	Control	Male	Vastus lateralis	35	-	-	-	-	-	-	-	C
MP-49	Control	Female	Vastus lateralis	49	-	-	-	-	-	-	-	C

[1]The 6-minute walking test (6MWT) is an index of aerobic endurance capacity: distance in meters walked by a patient during six minutes (*38*). [2]Muscle impairment rating scale (MIRS): Assesses the degree of distal to proximal muscle involvement (*39*). [3]Modified Rankin Scale (mRS): an indicator of disability in patients (*40*). [4]Biceps Medical Research Council (MRC): scale indicative of muscle strength (*41*). N.D.: not determined; A: Germans Trias i Pujol Hospital, Barcelona, Catalonia (Spain); B: La Fe University and Polytechnic Hospital, Valencia, Valencian Community (Spain); C: Donostia University Hospital, San Sebastian, Bask Country (Spain).

miR-23b and miR-218, which get overexpressed during differentiation of DM1 myotubes, are detected reduced upon antimiR treatment

We analysed miR-23b and miR-218 levels in all primary myoblast cell lines as an indication of the expression of these miRNAs prior to antimiR treatment (Fig. 1A-B). At ten days of differentiation, the expression of miR-23 and miR-218 was ∼2.5-fold and five-fold higher in DM1 cells compared to control myoblasts, respectively ($p < 0.05$), a difference that was still not conspicuous by 5 days of differentiation. At both time points, we observed a marked variability in DM1 cells compared to controls. We wondered whether this higher dispersion could be attributed to phenotypic differences caused by the variability in CTG repeat length. In fact, in support of this possibility, we observed a significant correlation of CTG repeat length of DM1 myoblasts with miR-23b and miR-218 expression (Supp. Fig. S3). On the other hand, receptor operating curve (ROC) analysis revealed an area under the curve (AUC) of 82% for miR-23b and 89% for miR-218, indicating that levels of these miRNAs have the potential to predict CTG repeat size in patients accurately (Supp. Fig. S3).
Upon antimiR-23b-V1 treatment of DM1 myoblasts, we observed a significant 65-75% reduction in the detection of miR-23b at day ten of differentiation for both concentrations (34 and 54 nM). The detection on day five was already significantly lower using the 54 nM concentration, but not with the 34 nM dose (Fig. 1C). The miRNA antagonistic activity of antimiR-23b-V2 seems to be considerably stronger since 85-95% reduction of miRNA detection was observed at both time points, and it was significantly lower using the 34 nM dose. Regarding miR-218 AONs, antimiR-218-V1 and -V2 performed similarly across both differentiation time points (Fig. 1D). We observed reductions in the detection of miR-218 in the 30%-75% range, with trends of higher activities at 220 nM compared to 138 nM. Altogether, these results confirm robust reductions in the detected levels of target miRNAs in all cell lines. In addition, we observed a trend of increased efficacy of antimiR-23b-V2.

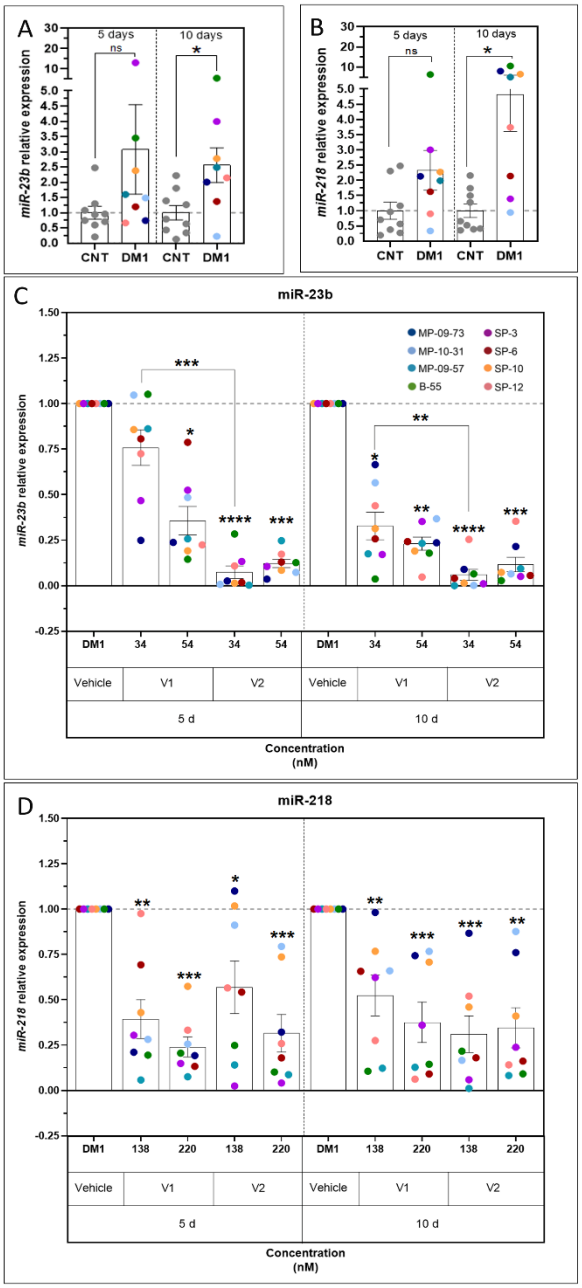

Figure 1. Expression of target miRNAs in DM1 cells and treatment modulation. The upper graphs show the quantification of (A) miR-23b and (B) miR-218 expression in control vs DM1 cells during differentiation. Unpaired t-test with Welch's correction. The bottom graphs show the quantification of (C) miR-23b and (D) miR218 expression upon antimiR treatment. Kruskal Wallis test *: p<0.05; **: p<0.01; ***: p<0.001; ****: p<0.0001 (Dunn's post-test). Each dot of a different colour denotes a different DM1 myoblast line. The asterisks above the bars denote

DM1 comparisons, while those above the boxes denote dose comparisons. The names of the lines are shown in the legend. Error bars represent the standard error of the mean (SEM).

MBNL1 levels, which get reduced during differentiation of DM1 myotubes, increase upon antimiR treatment

Alternative splicing of MBNL1 transcripts helps tailor protein function to actual cell necessities. The inclusion of exon 5 completes a bipartite nuclear localization signal. Consequently, abnormal inclusion of this exon is expected to enhance the potential of MBNL1 to be sequestered with nuclear CUG expansions so it can be used as an indicator of the pathogenic status of the cell. Importantly, as a result of its regulatory splicing activity, MBNL1 promotes the exclusion of its own exon 5[42,43].

MBNL1 protein levels were significantly lower in DM1 myotubes after ten days of differentiation compared to controls, with a trend already noticeable by day five (Fig. 2). This pattern was observed for total MBNL1 protein levels (Fig. 2A), MBNL1 42/43 kDa (+ex5±ex7) and MBNL1 40/41 kDa (-ex5±ex7) isoforms (Fig. 2BC). Total and isoform-specific MBNL1 levels were somewhat variable in both the control and DM1 cell cohorts. This was expected due to the combination of several factors such as muscle of origin, sex and age of donors, repeat expansion size, number of in vitro cell passages, and genetic background effects, in addition to the intrinsic experimental variability in all these determinations. Despite all these sources of variability, the average expression levels of total MBNL1 and isoforms 42/43 and 40/41 reached statistical significance. The biological relevance of these changes is reinforced by focusing on total MBNL1 levels, which reached statistical significance not because of lower dispersion of data (standard deviation is actually higher than at 5 days) but because of lower average amounts.

We observed a significant negative correlation between CTG repeat length of DM1 myoblasts and MBNL1 levels, both for total protein and each MBNL1 protein isoform individually (borderline for isoform 40/41 kDa; Fig. 2D-F). This coincides with the positive correlation between repeat length and miR-23 and miR-218 levels (Sup Fig. S3). The ratio between these isoforms changed during the differentiation of DM1 cells (Supp. Fig. S4). At day five of differentiation, we observed a ~60/40 ratio between high/low MW isoforms. By day ten, the ratio changed to ~70/30 in DM1 myotubes but remained ~60/40 in control cells, which is a difference consistent with observations reported by others[44].

Upon antimiR treatment, we observed a significant increase in total MBNL1 levels in both differentiation time points, using the higher doses of 54 nM and

220 nM for antimiRs against miR-23b and miR-218, respectively (Fig. 2G). Remarkably, we observed a four-fold increase in total MBNL levels using antimiR-23b-V2. In all cases, the derepression at these doses was significantly higher than at the lower doses of 34 nM and 138 nM, respectively. Both MBNL1 isoforms contributed to the total increase in protein levels (Supp. Fig. S5AB). AntimiRs brought about a solid dose-dependent upregulation of total MBNL1 levels, also detectable at the isoform level, in patient-derived primary myoblasts. Significantly, antimiR treatment had a similar effect on the isoform ratio at days five and ten of differentiation in DM1 cells, maintaining about 50-55% the percentage of MBNL1-42/43, but because untreated disease controls increased the percentage of this isoform from approximately 60% to 70% at days 5 and 10, respectively, the overall therapeutic activity of antimiRs (measured as skipping of ex5 in MBNL1, which is a splicing activity regulated by the protein itself), increased with differentiation time (Supp. Fig. S5C).

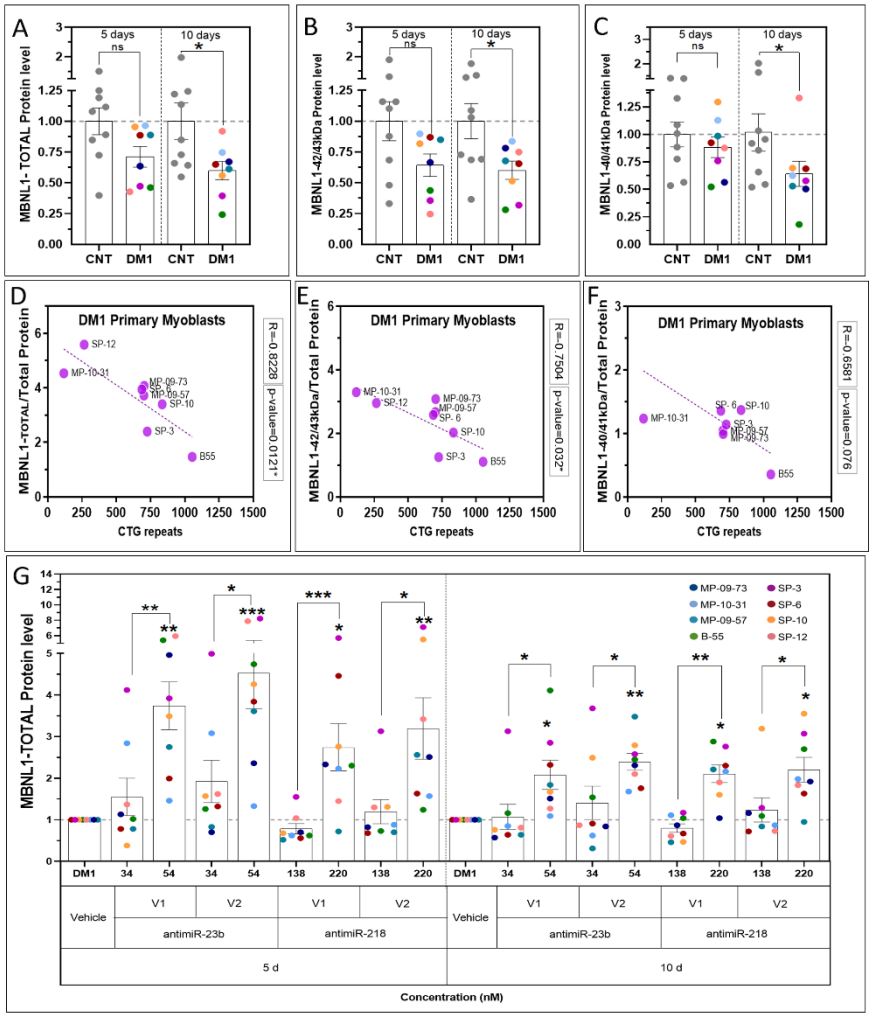

Figure 2. Expression of MBNL1 proteins in DM1 cells and modulation by antimiR treatments. (A-C) Quantification of MBNL1 protein levels in control vs DM1 cells during differentiation. MBNL1 total protein levels (A) and for each isoform independently: MBNL1 42/43 kDa (+ex5±ex7) variant (B) and MBNL1 40/41 kDa (-ex5±ex7) variant (C) relative to the control condition of the same differentiation time. Un-paired t-test. (D-F) Pearson correlation in untreated cells between MBNL1 protein levels normalized to the total protein and the number of CTG repetitions in DM1 myoblasts. CTG repeats vs. MBNL1 total protein levels (D), MBNL1 42/43 kDa (+ex5±ex7) variant (E), and MBNL1 40/41 kDa (-ex5±ex7) variant (F). The correlation R-value and p-value are shown in the graph for each correlation. (G) Quantification of MBNL1 upon antimiR treatment relative to the non-treated DM1 condition. The asterisks above the bars denote DM1 comparisons, while those above the boxes denote dose comparisons. Kruskal Wallis test *: p<0.05; **: p<0.01; ***: p<0.001; ****: p<0.0001 (Dunn's post-test). Each dot of a different color denotes an individual DM1 myoblast line (shown in the legend). Error bars represent the standard error of the mean (SEM).

The number of RNA and MBNL1 nuclear foci, and *DMPK* transcripts are reduced upon antimiR treatment

DM1 myotubes presented an average of 5-6 foci per nucleus and, as expected[45], control cells did not show any (Fig. 3A). AntimiR treatment at higher doses than in our previous reports[34] reduced the average number of foci in DM1 cells (Fig. 3B). These reductions were significant for both versions of antimiR-23b and differentiation time points. AntimiR-218-V1 and -V2 also reduced the number of foci in both time points, but a statistically significant difference was reached only after ten days of differentiation. DM1 cells also presented an average of 1.7-2.0 MBNL1 nuclear foci (Fig. 3C) and a reduced presence of the protein as a diffused free-form in the nucleus (Fig. 3E), both indicative of functional sequestration of the protein. Both parameters were partially corrected upon antimiR treatment (Fig. 3DF), especially at the ten-day differentiation time point. As previously reported by others[46], we also detect more *DMPK* than MBNL1 nuclear foci in our primary myoblast cohort. While several technical issues could impinge on this result, particularly higher sensitivity of RNA than protein detection because of lower background in the first than in the second case, it is also possible that expanded CUG transcripts go through several transient molecular stages inside the nucleus and show different protein binding capabilities. Representative images used for foci and MBNL1 quantification for all cell lines are shown in Supp. Fig. S6, which also includes the use of an anti-human MBNL1 antibody to discard potential issues with the specific anti-mouse Mbnl1 epitope detected by MB1a(4A8).

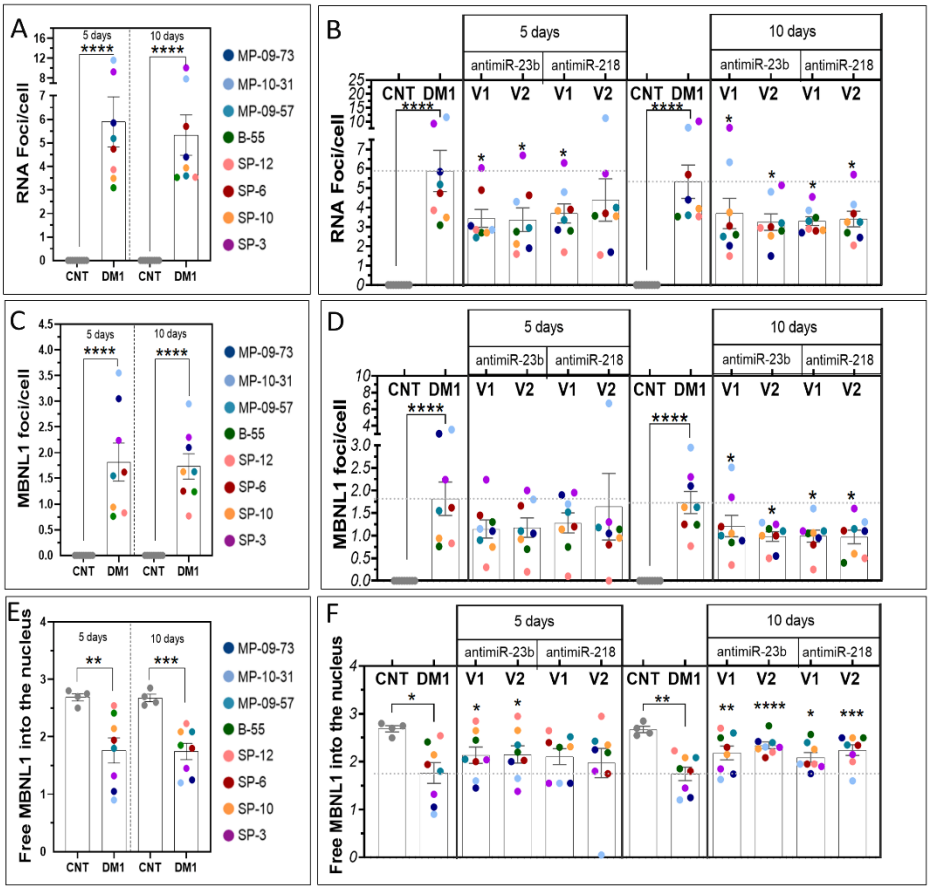

Figure 3. Effect on foci number and cellular distribution of MBNL1. Number of (A) RNA nuclear foci per cell, (C) MBNL1 nuclear foci, and (E) MBNL1 free form in the nucleus in control vs DM1 cells during differentiation. Mann Whitney test and Unpaired t-test with Welch's correction. Additionally, the figure shows their responses to the indicated antimiR treatments (B, D, F). Kruskal Wallis test and Two-way ANOVA *: p<0.05; **: p<0.01; ***: p<0.001; ****: p<0.0001 (Dunn's post-test and Dunnett's post-test). Each dot of a different color denotes an individual DM1 myoblast line (shown in the legend). Error bars represent the standard error of the mean (SEM).

At this point, we wondered about the reason behind the antimiR-mediated reduction of RNA and MBNL1 protein nuclear foci number. We analysed *DMPK* expression in control and DM1 myoblasts to answer this question. We observed around 50% of normal *DMPK* expression in DM1 vs control cells after five days of differentiation, which went further down to 30% at the ten days

timepoint (Fig. 4A). Our observation is in line with previous studies showing lower expression of *DMPK* expanded alleles[47,48] but *DMPK* relative expression only showed a trend towards correlating with CTG repeat size (Fig. 4B). AntimiR treatment induced a further reduction of *DMPK* levels in DM1 cells, particularly at the ten days timepoint, of up to ~25% (Fig. 4C). These results were reproduced with antimiR-23b-V1 and antimiR-23-V2 in immortalized DM1 muscle cells using a hot trizol protocol to ensure complete extractability of mutant *DMPK* transcripts (Supplementary Figure 7A) and are consistent with previously published observations with the antimiR-218-V1 using the same cell line[36]. Notably, cell lines that first reduced *DMPK* expression (at 5 days of differentiation) were those with a larger number of repeats, such as B55, MP-09-57, and MP-09-73, while lines showing a delayed response (at 10 days of differentiation) were those with smaller repeat sizes, such as MP-10-31 or SP-12. This suggests that the kinetics of *DMPK* degradation in response to antimiRs may depend on cellular cues, particularly repeat expansion size, but does not rule out that differences in basal *DMPK* gene expression or cellular compensation mechanisms among the cell lines used may also contribute to some cell lines responding earlier than others. Altogether, these data indicate that antimiR treatment successfully contributed to increasing the functional free-form levels of MBNL1 by increasing the protein expression and reducing the number of *DMPK* transcripts contributing to its sequestration.

When we analysed these parameters' relationship with each cell line's disease load, we did not observe a significant correlation between the number of RNA or MBNL1 nuclear foci with CTG repeat length (Supp. Fig. S7BC), which is consistent with the lack of relationship already observed between *DMPK* levels and repeat size (Fig. 4B). While to the extent of our knowledge, a correlation between foci number and disease severity has not been reported in the literature, we do detect a significant negative correlation between total MBNL1 protein and repeat expansion size (Figure 2D). Finally, we did observe a modest significant correlation between MBNL1 protein levels and the MBNL1 free into the nucleus, indicating a direct relationship between the increase of the protein and its availability as free form (Supp. Fig. S7D). In sum, antimiRs rescue characteristic DM1 cellular alterations.

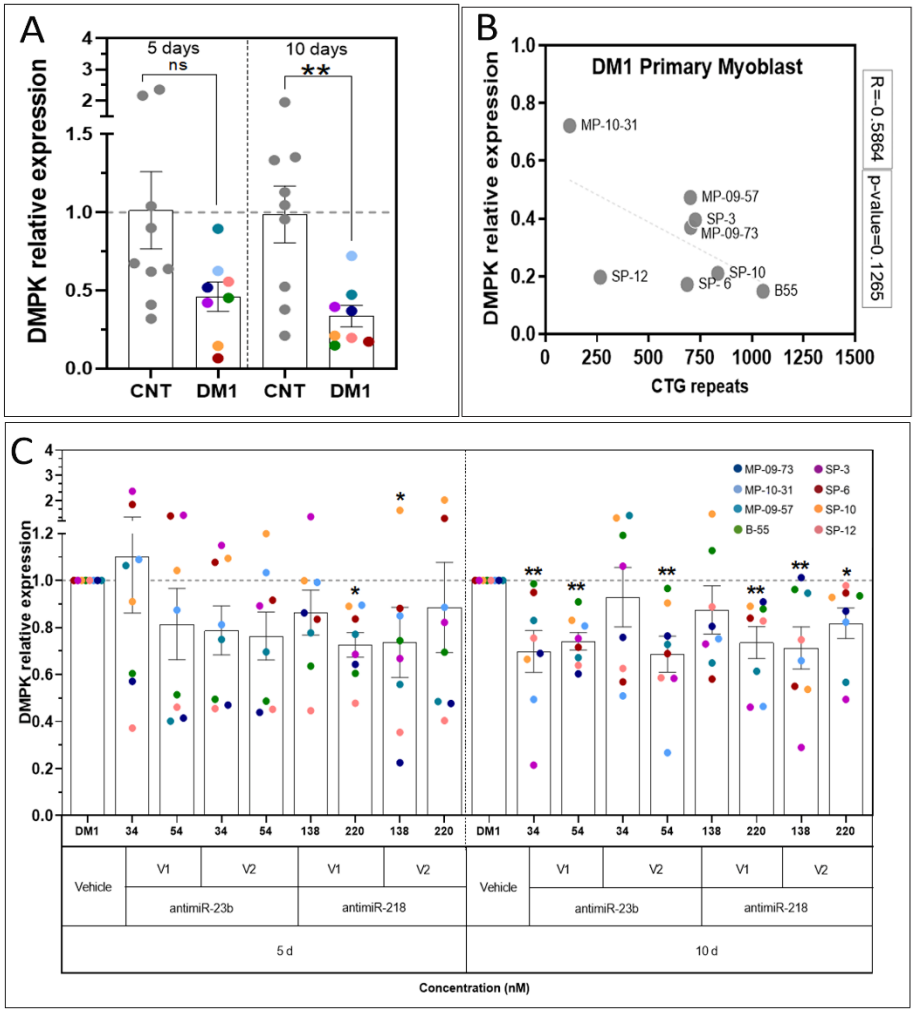

Figure 4. Expression of DMPK mRNA in DM1 cells and treatment modulation. (A) Quantification of DMPK expression in control vs DM1 cells during differentiation. Mann Whitney test and Un-paired t-test with Welch's correction. (B) Pearson correlation between DMPK expression levels and CTG repeat sizes in the cell lines. The correlation R-value and p-value are shown in the graph for each correlation (C) Quantification of DMPK expression upon antimiR treatments. Kruskal Wallis test *: p<0.05; **: p<0.01; ***: p<0.001; ****: p<0.0001 (Dunn's post-test). Each dot of a different color denotes an individual DM1 myoblast line (shown in the legend). Error bars represent the standard error of the mean (SEM).

Correction of aberrant splicing in DM1 myoblasts

Next, we evaluated antimiRs on DM1 splicing defects at day 10 of differentiation because they generally show higher anti-DM1 disease activity than on day five, and phenotypes are more clearly shown. With this purpose, we selected for validation by semiquantitative RT-PCR experiments a panel of 5 genes whose splicing has been previously reported to be altered in DM1 skeletal muscle[49]: *MBNL1* exon 5, *KIF13A* exon 26, *BIN1* exon 11, *SOS1* exon 21, and *PPFIBP1* exon 19 (Supp. Fig S8A). The quantification of exon inclusion from these genes revealed an ample window and significant difference between DM1 and control cells (Fig. 5A).

The splicing of *MBNL1* exon 5, *KIF13A* exon 26, *BIN1* exon 11, and *SOS1* exon 21 has been directly linked with a lack of MBNL1 activity in previous studies[11, 50-52]. In addition, they correlate with force dorsiflexion in DM1 patients[50]. Notably, aberrant splicing of *BIN1*, a gene with crucial roles for muscle function[53], positively correlated with the patients' MIRS scale (Supp. Fig S8B; p-value=0.0815). In contrast, *PPFIBP1* exon 19 is not MBNL1-dependent[54], but it is also implicated in DM1 pathology, and its aberrant splicing can be rescued by the biguanide metformin, a drug that promotes corrective effects on several splicing defects associated with DM1[55]. We included this exon to verify whether antimiR treatment could contribute to its rescue independently of MBNL1 (e.g., through the downregulation of *DMPK*).

Upon antimiR treatment, we observed an improved percentage of exon spliced-in ($\Delta PSI = PSI_{disease} - PSI_{treated}$), which was statistically significant for most alternative exons (Fig. 5B). In the case of BIN1 exon 11, a significant correction was only reached with the higher doses of the antimiRs. For the rest of the alternative exons, both doses were effective. When looking at the overall ΔPSI that combined all exons analysed (Fig. 5C), we observed a significant ∼50% shift from the DM1 splicing pattern towards the control pattern for all antimiRs and doses used. ΔPSI values for each exon and treatment and gel images used for the quantification are depicted in Supp. Fig. S9. We observed a moderate correlation of global ΔPSI scores with total MBNL1 protein levels (Fig. 5D, p=0.0005, R=0.59) and a low to moderate correlation for free MBNL1 form (Fig. 5E, p=0.0411, R=0.37), supporting a relationship between splicing correction and increased expression of total MBNL1 in cells treated with the antimiRs.

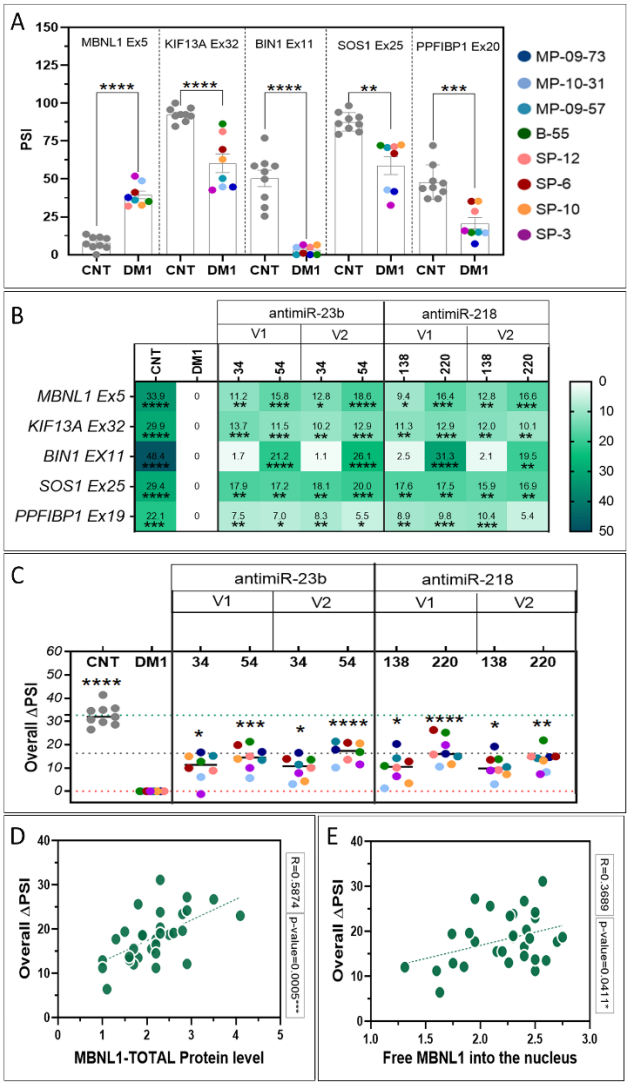

Figure 5. Correction of DM1 splicing alterations. (A) Characterization of the percentage of spliced-in (PSI) in control vs DM1 cells for a selection of transcript exons. Unpaired t-test and Mann-Whitney test. (B) Heatmap of the effect of antimiR treatment on the delta percentage of spliced-in (ΔPSI) of the indicated genes/exons. The numbers within the cells indicate the percentage changes in alternative exon inclusion between control and treated cells compared to untreated cells, which serve as the reference (change 0). The shading in the cells indicates the magnitude of the percentage change, with darker shades representing larger changes compared to the reference condition. (C) Overall correction of the ΔPSI per cell line. Kruskal Wallis test *: p<0.05; **: p<0.01; ***: p<0.001; ****: p<0.0001 (Dunn's post-test). Each dot of a different color denotes an individual DM1 myoblast line (shown in the legend). Error bars represent the standard error of the mean (SEM). Pearson correlation between overall ΔPSI and total MBNL1 (D) and free form levels (E) in treated myotubes with the antimiRs. The correlation R-value and p-value are shown in the graph for each correlation.

The correlation between overall ΔPSR scores and total MBNL1 protein levels was analysed separately for miR-23b and miR-218 inhibition. The study found that samples using miR-23b-V1 and V2 anti-miR-23b showed a higher correlation compared to those using miR-218-V1 and V2 anti-miR-218 (Supp. Fig. S9FG).

We observed ~50% overall ΔPSI correction, with better rescues at the higher doses in MBNL1-dependent exons, consistent with the increased MBNL1 levels observed. Although all cell lines generally responded to treatment, 10-31 and SP-3 yielded somewhat lower splicing correction. Altogether, these results are consistent with the notion that only a moderate increase in MBNL1 is sufficient to achieve a therapeutic benefit and that antimiR treatment efficiently corrects downstream molecular DM1 alterations.

Functional rescue of myotubes area and fusion index

In previous studies, DM1 myoblasts have been shown to display defective differentiation compared to control cells, as determined by lower myotube area and fusion index[56,57]. We analysed both parameters in our DM1 primary myotubes and observed a strong reduction at days five and ten of differentiation (Fig. 6AB). CTG repeat length only roughly correlated with decreased myotube area and fusion index (Supp. Fig. S10AB). Representative images used for these quantifications are depicted in Supp. Fig. S11A. We observed a negative correlation trend between the MIRS scale and myotube area (Supp. Fig. S10C), but no correlation with the fusion index (Supp. Fig. S10D). We had previously shown that miR-218 blockage alleviates fusion index upon differentiation of immortalized myoblasts[36] and miR-23b inhibition improved myotube area in a bioengineered in vitro 3D model of DM1[58]. AntimiR treatment improved both parameters in primary DM1 cells (Fig. 6CD). In fact, antimiR-23b-V2 managed to increase myotube area already at day five of differentiation and further improved this parameter by day ten (Fig. 6C). Both antimiR-23b versions rescued the fusion index at the day ten differentiation time point (Fig. 6D). It is worth noting that in 2D cultures, the fusion index showed a significant correlation with myotube area ($p < 0.0001$, Supp. Fig. S10E) in treated cells. Representative images of DM1 cells used for myotube area and fusion index quantification upon antimiR treatment are depicted in Supp. Fig. S11B. These data support an improved ability for treated DM1 myoblasts with different genetic backgrounds and CTG expansions to differentiate into myotubes.

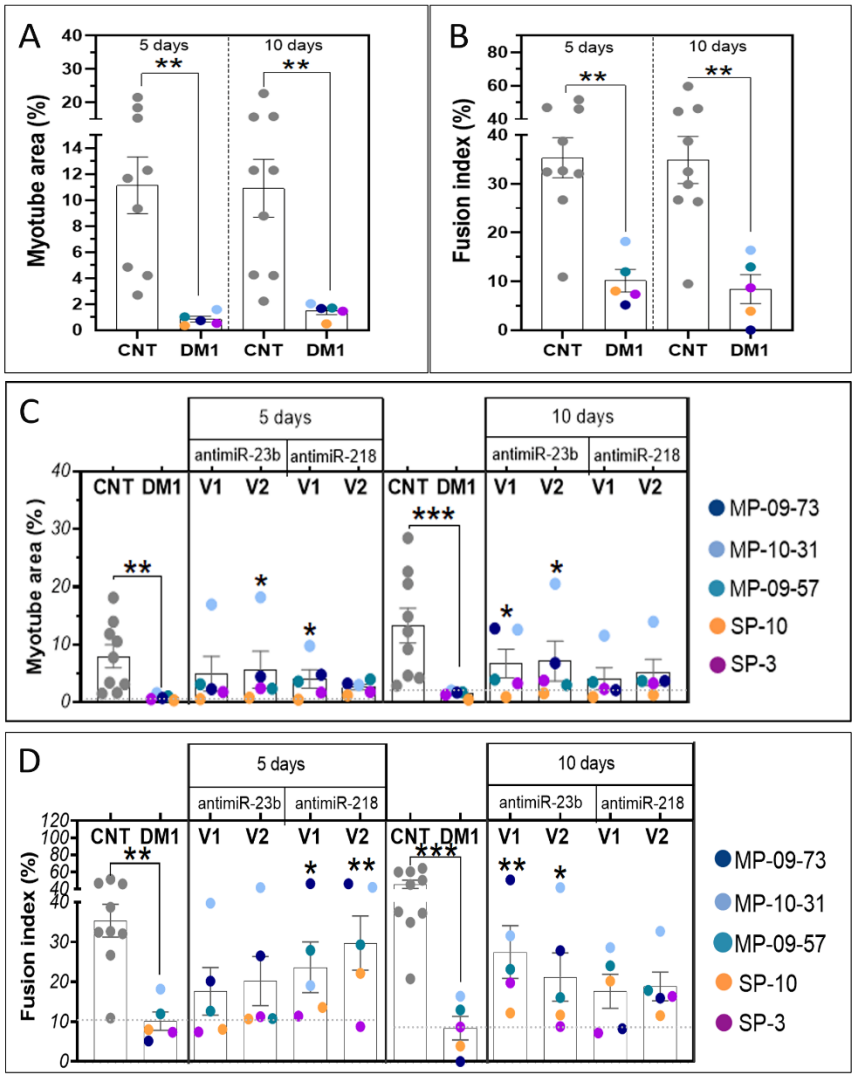

Figure 6. Quantification of myotube area and fusion index in DM1 cells and treatment effect. Myotube area (A) and fusion index (B) quantifications are shown in control vs DM1 cells during differentiation. Unpaired t-test with Welch's correction. Rescue of myotube area (C) and fusion index (D) upon treatment with the indicated antimiRs and conditions. Kruskal Wallis test and Two-way ANOVA *: p<0.05; **: p<0.01; ***: p<0.001; ****: p<0.0001 (Dunn's post-test and Dunnett's post-test). Each dot of a different color denotes an individual DM1 myoblast line (shown in the legend).

Integrated evaluation of the antimiR's therapeutic potential

To rank the preclinical potential of the antimiRs tested in this study, we evaluated the overall performance of the tested antimiRs. The four candidates were plotted in a spider graph comparing the degree of change (compared to control cells) in the five most important parameters previously evaluated: MBNL1 protein increase, RNA foci reduction, MBNL1 nuclear foci reduction, splicing recovery, and myotube differentiation recovery (Fig. 7A). This analysis suggested the selection of antimiR-23b-V2 as the lead candidate for further evaluation, since it most consistently ranked at the top of these parameters, giving the largest area in the spider plot.

Focusing on antimiR-23b-V2, Fig. 7C shows not only the mean of DM1-derived myoblast lines more than doubled total MBNL1 levels compared to untreated but, importantly, that every single cell line responded to the antimiR despite unrelated genetic backgrounds and expansion sizes, which is indicative of a highly reliable *in vitro* effect. However, antimiR-23b-V2 potential to increase MBNL1 protein levels did not correlate significantly with CTG repeat size (Fig. 7B). Reduction of *DMPK* transcript levels followed a different behaviour (Fig. 7DE) since three lines slightly increased *DMPK* mRNA levels with antimiR-23b-V2 while five reduced it, and lines with shorter expansions responded stronger reducing *DMPK*. AntimiR-23b-V2 effect on overall splicing rescue was also remarkable since all lines responded to the treatment despite the fact that the antimiR activity in this parameter did not correlate with repeat size (Fig. 7FG). Finally, the myotube area showed a significant repeat size-dependent rescue, and all individual lines improved (Fig. 7HI). Other parameters, such as MBNL1 quantification scale or fusion index, also revealed a general response by individual cell lines but did not seem to depend on CTG repeat number except for the fusion index response that was higher the lower the repeat size (Supp. Fig. S12).

A significant controversy in the DM1 field involves the possibility that delayed differentiation issues could explain gene expression changes compared with control cells. Indeed, while some studies describe normal myogenesis and increased apoptosis in primary DM1 muscle cells[59], others have reported myogenic defects in DM1 cell models[60]. To address this possibility, we have quantified miR-23b, MBNL1, and *DMPK* in healthy and DM1 cell lines before and at differentiation days 5 and 10, finding that compared to health controls,

none of the gene expression changes can be explained as a delayed differentiation issue (Supp Fig. 13A-C). Reduced MBNL1 levels during myogenesis in the presence of the expanded DM1 repeats were also consistent with previous reports[44]. Also, of interest is whether the repressive activity of miR-23b is active in a normal background or requires higher-than-normal miRNA levels. Indeed, Supp Fig. 13DE shows that antimiR-23b-V2 can robustly antagonize miR-23b in a normal background, likely because of lower starting levels compared to DM1 and that this translates into upregulated levels of MBNL1 protein as similarly observed in DM1 cells.

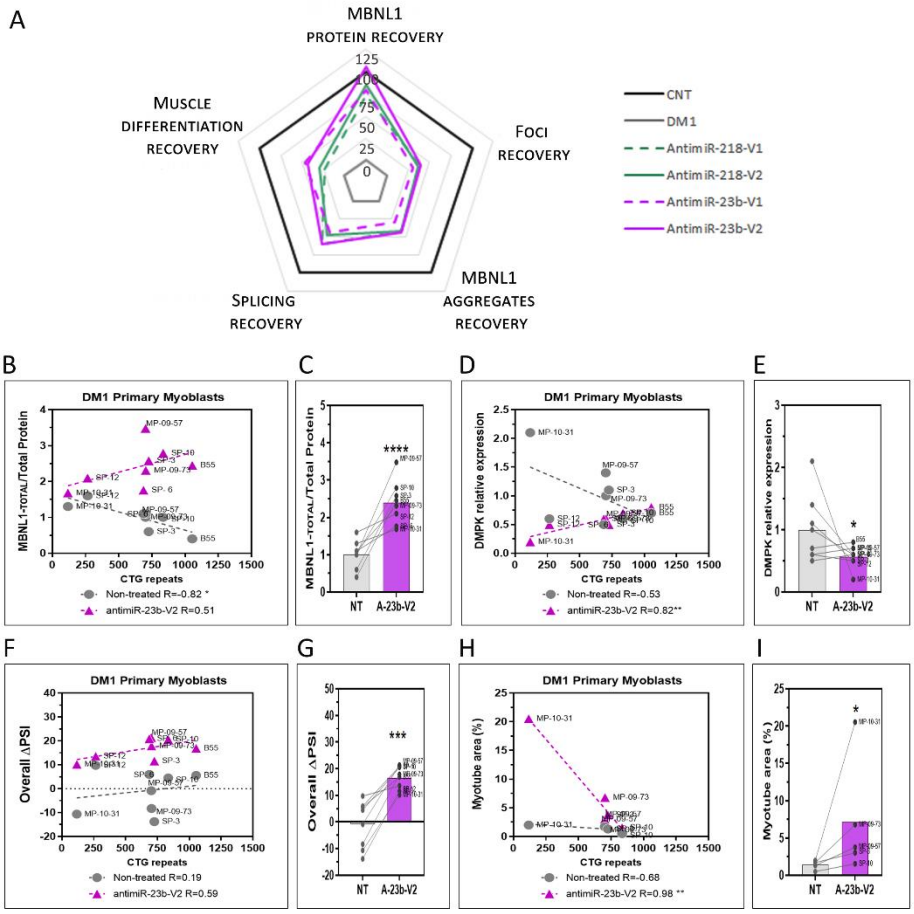

Figure 7. Integrated evaluation of the antimiR's therapeutic potential. (A) Spider plot depicting the most relevant DM1 molecular readouts for each antimiR candidate. (B-H) Comparison of untreated DM1 myotubes with antimiR-23b-V2-treated DM1 myotubes, including the Pearson correlation with CTG repeat number, for the following parameters: (B-C) MBNL1 protein levels, (D-E) DMPK transcript levels, (F-G) overall ΔPSI, and (H-I) myotube area. Unpaired t-test and

Mann-Whitney test. *: p<0.05; **: p<0.01; ***: p<0.001; ****: p<0.0001. The correlation R-values are shown in the corresponding graphs.

RNA-Seq analysis of primary cells treated with antimiR-23b-V2

Next, we performed RNA-Seq experiments to test the effect on the transcriptome of our leading antimiR molecule. The depth of RNAseq datasets was insufficient for a transcriptome-wide assessment, but this was already partially addressed by directly measuring five MBNL1-regulated alternative exons. We first analysed the RNA samples of control vs. DM1 myotubes at day ten of differentiation to identify disease-related genes (DRGs). This analysis revealed a total of 109 genes commonly dysregulated in all cell lines, 44 of which were downregulated and 65 upregulated (Fig. 8A). *TAF11L12*, *PRAMEF11*, *THBS4*, *MYH14,* and *AOC1* were the five most downregulated genes, while *PRAME*, *THSD7B*, *SEMA3D*, *SNAP25,* and *CDH6* displayed the highest overexpression. To validate the clinical relevance of the detected DRGs, we crossed the list of 109 genes with publicly available RNA-Seq data comparing tibialis muscle samples of DM1 patients with controls (Fig. 8B). We observed a significant overlap of 29 genes (p = 0.01), proving that over 25% of the DRGs detected *in vitro* are also deregulated in patient muscle biopsies. Then, we analysed the change in the transcriptome of DM1 cells upon antimiR-23b-V2 treatment (Fig. 8C), detecting 42 and 44 genes significantly downregulated and upregulated, respectively. The $\log_2$ fold change ($\log_2$FC) magnitude of downregulated genes (mean log2FC of ~ -0.55) was low (i.e., close to untreated cells levels), while that of upregulated genes was much more apparent (mean $\log_2$FC of ~ 3.8), where *HOXC12*, *THBS4*, *ZFP57*, *MYH14*, and *RPL29* pseudogene ranked among the top-five. It is worth noting that antagomiR-23b-v2 was capable of increasing the expression of the MYH14 gene, which had previously been reported to be decreased in DM1[61]. From the list of genes with expression changes upon antimiR-23b-V2 treatment, we calculated how many shifted towards the expression observed in control cells (Fig. 8D). We observed that the expression of 69% of the DRGs was partially or completely corrected by antimiR treatment. Finally, we estimated the overall expression change of the DRGs upon antimiR-23b-V2 treatment for each cell line, finding that all primary myotubes improved gene expression upon treatment (Fig. 8E), thus reinforcing the reliability of the therapeutic effect in genetically diverse DM1 cells. Finally, it is noteworthy that the largest changes in DRGs expression between untreated and antimiR-23V-2 treated cells were

found at the transcriptome level in cell lines with longer CTG repeats, like B55, showing a moderate correlation (Fig. 8F).

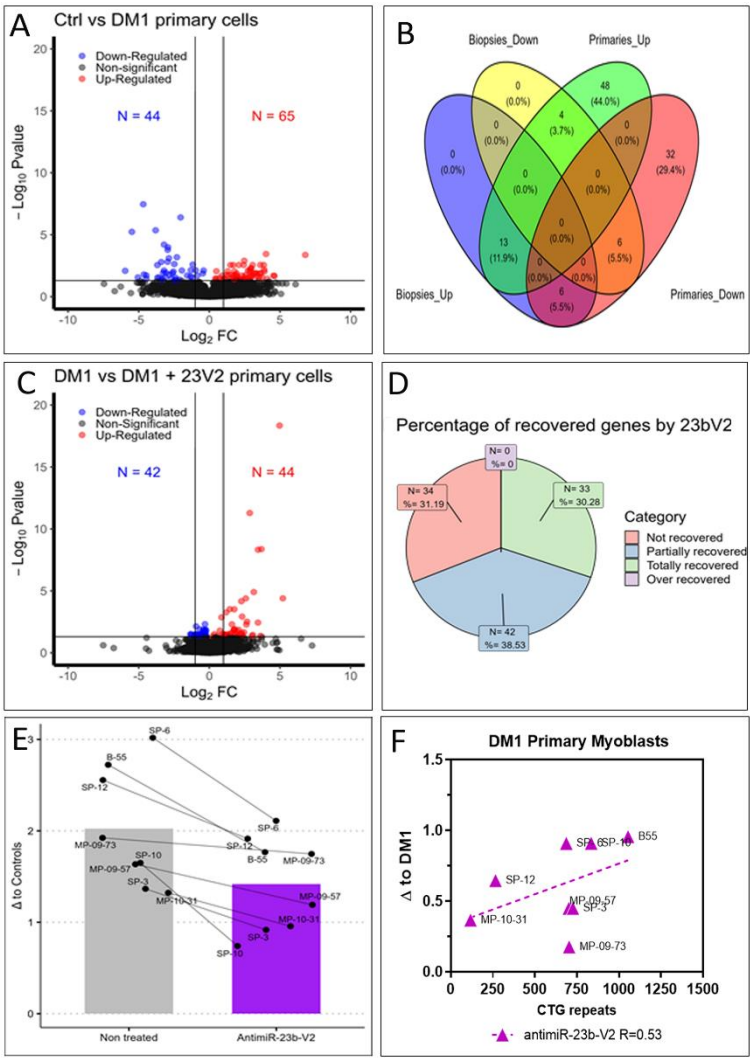

Figure 8. RNA-Seq analysis of primary myotubes after antimiR-23b-V2 treatment. (A) Volcano plot comparing the expression signature of untreated DM1 cells to control myotubes. (B) Overlap of disease-related genes (DRGs) found in the primary myotubes in vitro and genes dysregulated in the tibialis muscle of DM1 patients. (C) Volcano plot depicting the expression changes of DM1 cells upon antimiR23bV2 treatment. (D) Distribution of DRGs according to their change in expression upon antimiR23bV2, taking as reference the levels observed in control cells. (E) Average changes in DRG expression before and after antimiR-23b-V2 treatment (solid bars) and per cell line (connected dots) to highlight individual behaviors. (F) Linear regression between the overall change in DRG expression relative to DM1 and the number of CTG repeats

in myotubes treated with antimiR-23b-V2. The correlation R values are displayed in the corresponding graphs.

Discussion

Our study in DM1 human-derived mature myotubes revealed that the most critical disease-associated molecular alterations could be reversed by blocking miR-23b and miR-218, two miRNAs that are natural repressors of MBNL1(34). Transfection with antimiRs upregulated this protein, alleviating main DM1 hallmarks such as foci number and *DMPK* expression, alternative missplicing, myotube area, and fusion index. Furthermore, as determined by RNA-Seq, antimiR-23b-V2 reversed a substantial percentage of the common abnormal expression patterns observed in primary DM1 cells. All these molecular and cellular phenotypes have been previously confirmed in cell models of disease by independent studies[56,62-68]. Notably, total MBNL1 levels moderately correlated with splicing correction upon antimiR treatment (Fig. 5D, E), consistent with a causal relationship.

Since DM1 is a highly heterogeneous disease, with variable degrees of clinical manifestations depending on CTG repeat size, our study using a diverse range of primary cells proves that antimiR treatment may successfully treat a broad spectrum of DM1 patients. Also, based on these results, we selected antimiR-23b-V2 for future preclinical development.

Previously, we reported that miR-218 was upregulated in HSALR mice, DM1 cells, and muscle biopsies[36]. In the present study, we extended these observations to primary mature myotubes. By ten days in the differentiation medium, we found both miR-23b and miR-218 significantly upregulated, consistent with the observed lowered amounts of total MBNL1 detected in untreated cells. Furthermore, estimated CTG repeat length in the cell lines significantly correlated with both miRNA levels, suggesting a shared pathological activation mechanism. Importantly, from a therapeutic perspective, the fact that miR-218 and miR-23b are overexpressed in DM1 allows for a wider reduction window before reaching possible unwanted effects due to their complete inhibition. In this regard, it is worth noting that loss of the miR-23b/27b/24-1 cluster impairs glucose tolerance in mice, noticeable after a high-fat diet induction[69]. Thus, the combination of a higher-

than-normal expression level of the therapeutic target miR-23b and lack of severe phenotypes, even with the complete removal of the miRNA in mice, makes it unlikely that a human antimiR-23b treatment may lead to significant detrimental effects as a DM1 therapy.

Prompted by the observation that antimiRs noticeably reduced ribonuclear foci in treated cells (Fig 3B), we also quantified *DMPK* mRNA levels and found significant reductions (Fig. 4C). Compared to reports from actual clinical trials[70], this approximately 30% reduction in DMPK transcript levels in treated primary myoblasts is expected to have a clinically meaningful impact since smaller percentages of reduction from baseline (25%) already achieved a mean splicing correction of 13% across a panel of 22 genes and patients experienced a mean benefit of 3.8 s in myotonia after six months of administration. On top of this, antimiRs are expected to directly affect MBNL1 and 2 protein synthesis because of lowered amounts of repressive miR-23b and miR-218. Even though our RT-qPCR assay cannot distinguish between normal and mutant *DMPK* transcripts, the fact that both the number of RNA and MBNL1 nuclear foci were strongly reduced suggests that at least a significant portion of expanded transcripts were reduced by antimiR treatment. In support of this hypothesis, non-expanded *DMPK* mRNAs are naturally exported to the cytoplasm and do not colocalize in the foci with MBNL1 proteins[7]. Notably, independent studies reported the same phenomenon upon treatment with molecules not directly targeting *DMPK*[71,72] but failed to explain it mechanistically. Correcting abnormal MBNL1 exon 5 inclusion by antimiR treatment is expected to promote cytoplasmic MBNL1 levels (MBNL1 40/41)[42,73,74], which is consistent with the confirmed change in the ratio between MBNL1 40/41 and MBNL1 42/43 in treated cells (Supp S5C). Since it has been previously shown that MBNL1 is the primary determinant of focus formation[63], by lowering the relative amount of MBNL1 in the nucleus, we hypothesize that foci may destabilize and originate the observed reduction of *DMPK* mRNA levels. In conclusion, because a direct interaction by the antimiRs with the *DMPK* RNA is unlikely due to minimal complementarity and MBNL1 has been shown to promote foci formation[63] and stability of nuclear *DMPK*[75], we hypothesize that the subcellular distribution of MBNL1 protein isoforms contributes to the destabilization of mutant DMPK mRNA, ultimately leading to the reduction of ribonuclear foci. Several other potential mechanisms, however, are also possible, such as an indirect effect through other RNA-binding proteins involved in nuclear RNA stability and/or transport

or DMPK-binding miRNAs, such as those proposed in[76] as potential binders to CUG repeat expansions. Also, DMPK transcript reduction may explain why we observed correction of PPFIBP1 exon 19 inclusion because this missplicing was reported altered in DM1 but independently of MBNL1 function[54,55]. Thus, any reduction in disease-causing *DMPK* levels is expected to rescue PPFIBP1 splicing regardless of MBNL1 expression.

How antimiR molecules may reduce miRNA levels is a controversial issue as high-affinity antimiR chemistry has been shown to sequester the targeted miRNA in a heteroduplex, while lower affinity oligonucleotides seem to promote miRNA degradation[77]. However, the reduction in the levels may also be impacted by competence between primer and antimiR annealing to the miRNA to be detected. Thus, reduction in the miRNA levels may be real or apparent, but in all cases, it is functionally relevant because the inability to amplify also confirms functional blockade. When comparing the ability of antimiRs against miR-23b or miR-218 to increase MBNL1 and reverse DM1-associated features, we obtained different results depending on the target. Based on previous experiments[34], we estimated that targeting miR-23b requires lower doses than those used for miR-218 to achieve comparable levels of MBNL1 upregulation. In this study, we confirmed that lower doses (34 nM and 54 nM vs. 138 nM and 220 nM) are sufficient to achieve therapeutic benefit in vitro using miR-23b- vs. miR-218-targeting antimiRs, respectively. Compared to the previous versions (V1), our second-generation antimiRs (V2) incorporated PS backbone in the entire sequence, with a combination of 2'-OMe, MOE, and LNA residues, and were conjugated to a fatty acid instead of cholesterol. Additionally, a side-by-side graphical comparison of desirable molecular and cellular rescues in DM1 reveals that V2 versions of antimiR-23b and -218 were superior to their V1 counterparts (Fig. 7A), used at the same concentration, in terms of the degree of MBNL1 upregulation, correction of alternative splicing, reduction of RNA and MBNL1 nuclear foci, and muscle differentiation markers (myotube area and fusion index). Overall, the improvement of antimiR-23b-V2 over antimiR-23b-V1 was greater than for the antimiR-218 counterparts.

The molecular response to antimiR-23b-V2 depended on CTG repeat sizes, and cell lines with small expansions showed significantly more pronounced DMPK mRNA reduction than those with longer repeats, while an inverse correlation was also significant for myotube area recovery. The reason why cell lines bearing small expansions reduced *DMPK* levels better than others may stem

from the fact that they show higher basal MBNL1 levels compared to other DM1 lines (non-treated condition in Fig. 7B). Hence, as expected, cell lines with long repeats may require a higher increase in MBNL1 levels to get rid of *DMPK*, whereas cell lines with shorter repeats seem already closer to normal amounts, seemingly protective of *DMPK* accumulation. AntimiR-23b-V2's ability to enhance total MBNL1 levels and rescue splicing moderately (R=0.82, and 0.59, respectively) correlated with CTG repeat size (Fig. 7B, F).

Transcriptomics data analyses confirmed that treatment with antimiR-23b-V2 reversed the characteristic expression signature of DRGs that were dysregulated in primary DM1 myoblasts. These DM1-associated in vitro changes were representative (25%, p=0.01) of gene expression alterations already reported in muscle biopsies (tibialis) of DM1 patients[49], which is indicative of their therapeutic predictive power. Notably, individual analyses confirmed that all cell lines reduced the amount of dysregulated DRG upon antimiR-23b-V2 treatment, even with moderate increases in MBNL1 levels (~2-3-fold increases for all lines, Fig. 2G).

We propose a new model for the mechanism of action of antimiRs (Supplementary Figure S14) in which the combined effect of blocking upregulated miR-23b or miR-218 will derepress MBNL1 and other direct targets of these miRNAs, and reduce DMPK transcript levels, leading to a synergistic correction of DM1 spliceopathy and related functional alterations. This poses a significant step forward in the preclinical validation of antimiRs together with previously demonstrated efficacy in vivo[34-36]. To conclude, our study with antimiRs in a cohort of primary DM1 cell lines revealed that these molecules have therapeutic potential across unrelated genetic backgrounds. The approach works in cells with a wide range of repeats (range 117 to 1054), so it could be beneficial for treating multiple clinical forms of the disease.

Supplementary material

Supplementary Table S1. PrimeTime qPCR primers sequence.

GAPDH qPCR primers	GAPDH Probe 5'	5'/MAXN/-GCCTGGTCACCAGGGCTGCT-/3BHQ_1/3'
	GAPDH Primer F	5'-TGATGGCAACAATATCCACTTTACC-3'
	GAPDH Primer R	5'-CAACGGATTTGGTCGTATTGG-3'
DMPK qPCR primers	DMPK Probe	5'/56-FAM/AGGCCATCCGCACGGACAACC/3IAbRQSp/3'
	DMPK Primer F	5'- AGCCTGAGCCGGGAGATG-3'
	DMPK Primer R	5'- GCGTAGTTGACTGGCGAAGTT-3'

Supplementary Table S2. Primer sequences, exons analysed, and specific conditions of alternative splicing analysis

			PCR 1		PCR 2	
Event	**Forward Primer**	**Reverse Primer**	**Annealing T (°C)**	**Cycles**	**Annealing T (°C)**	**Cycles**
MBNL1 exon 5	CCAATACCAGGTCAACCAGGC	AGTGTTAAAGACTGCGGTGGC	55	30	55	30
KIF13A exon 32	TCCTGTCAGTATCCATCGGCT	TGAGTGCATCTGACCACCTCT	65	30	65	28
BIN1 exon 11	AGAACCTCAATGATGTGCTGG	TCGTGTTGACTCTGATCTCGG	63	30	-	-
SOS1 exon 25	GTTAACACCTCCGCCTGCTTC	AGGGACAGGCACTTCATCAGT	60	30	-	-
PPFIBP1 exon 19	GTCAGATCTTCCTTTGGCCGG	CCAGCCAGATCTAGGTGCTCT	65	30	65	28

.

SUPPLEMENTARY FIGURE S1

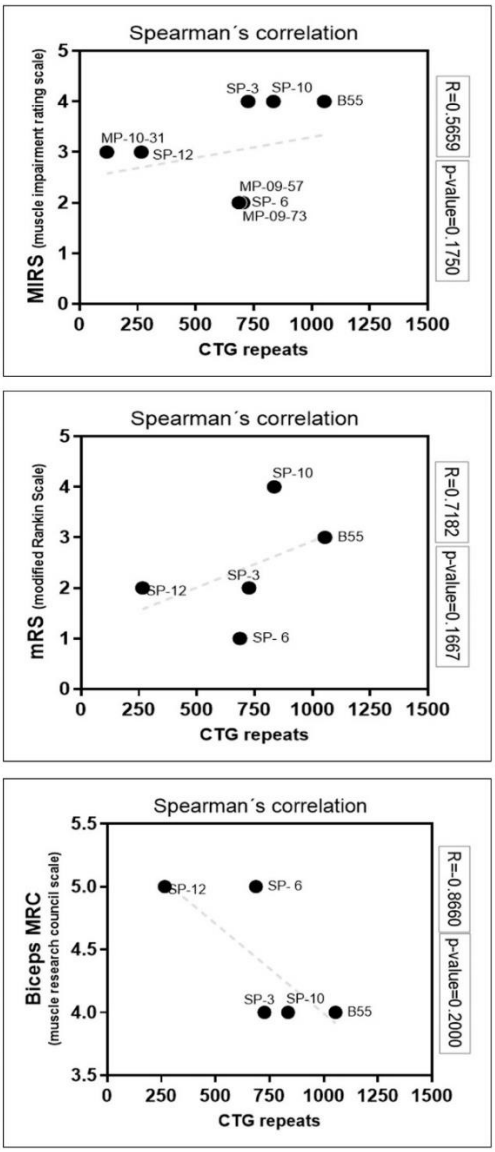

Supplementary Figure S1: Pearson or Spearman correlation between the number of CTG repeats in untreated myoblasts and muscle impairment rating scale (MIRS), modified Rankin scale (mRS), and Medical Research Council (MRC) biceps. The correlation R-value and p-value are shown in the graph for each correlation.

SUPPLEMENTARY FIGURE S2

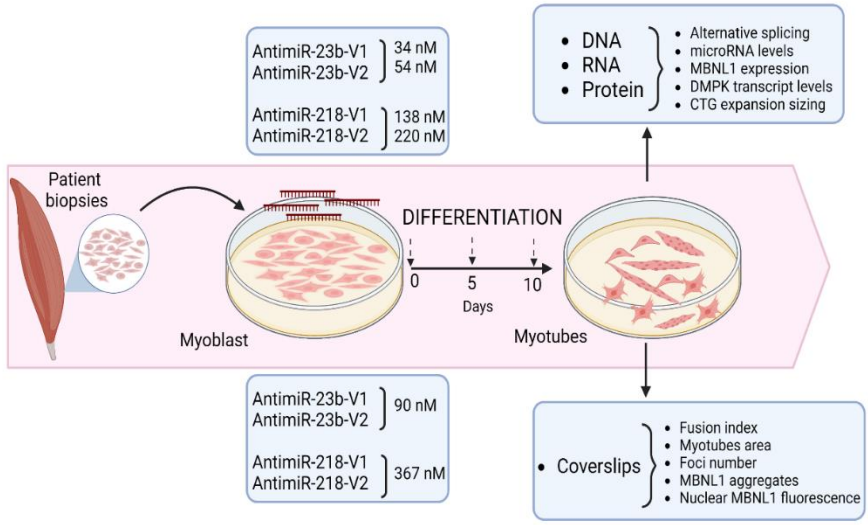

Supplementary Figure S2: Experimental design for evaluating the therapeutic potential of antimiRs in human DM1 primary myoblasts. Schematic representation of the experimental design used to assess the therapeutic potential of four candidate antimiRs (antimiR-23b-V1, antimiR-218-V1, antimiR-23b-V2, and antimiR-218-V2) in human DM1 primary myoblasts. The evaluation analyzed various DM1-related phenotypes, including fusion index, miRNA levels, DMPK expression, RNA foci number, MBNL1 nuclear foci, protein levels, and alternative splicing defects. Two differentiation time points (5 and 10 days) were considered for assessing the effects of the antimiRs. Concentrations of antimiR-23b used for ICC and FISH analyses (90 nM) and for protein and RNA analyses (54 nM and 34 nM) are indicated. Concentrations of antimiR-218 used for ICC and FISH studies (366.7 nM) and for protein and RNA analyses (220 nM and 138 nM) are also included. Myotubes were collected as pellets for DNA, RNA, and protein analysis, and fixed on coverslips for ICC and FISH assays at five and ten days after differentiation and treatment.

SUPPLEMENTARY FIGURE S3

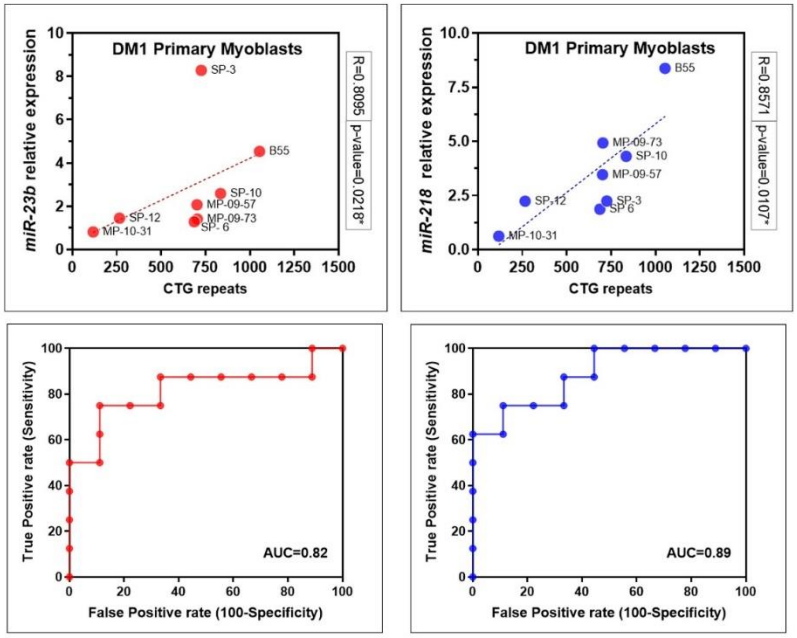

Supplementary Figure S3: Pearson or Spearman correlation between microRNA expression (miR-23b and miR-218) and the number of CTG repeats in untreated myoblast. The correlation (R-value) and p-values are shown in the graphs. The top two panels illustrate the correlation between miR-23b and miR-218 levels and the number of CTG repeats in myoblasts, highlighting their potential as predictors of DM1 disease. The area under the curve (AUC) analyses for miRNA levels provide additional insights into their diagnostic utility, with AUC values between 0.8-0.9 considered to have good predictive value.

SUPPLEMENTARY FIGURE S4

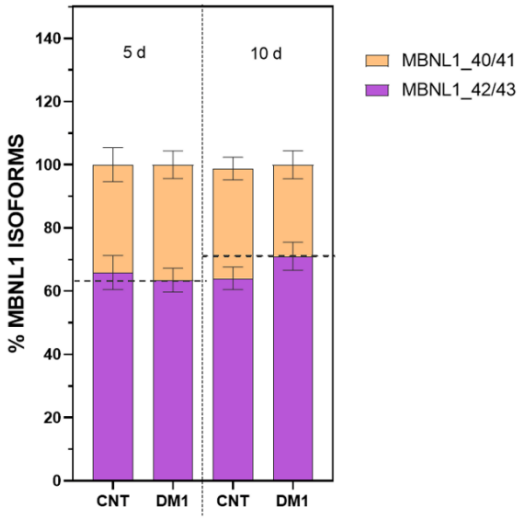

Supplementary Figure S4: Changes in the ratio of high MW/low MW MBNL1 isoforms during DM1 cell differentiation. Jess Simple Western was used to analyze the MBNL1 42/43 kDa, or high MW (+ex5±ex7) variant, and MBNL1 40/41 kDa, or low MW (-ex5±ex7) variant, in DM1 and control cells during differentiation. Error bars represent the standard error of the mean (SEM).

SUPPLEMENTARY FIGURE S5

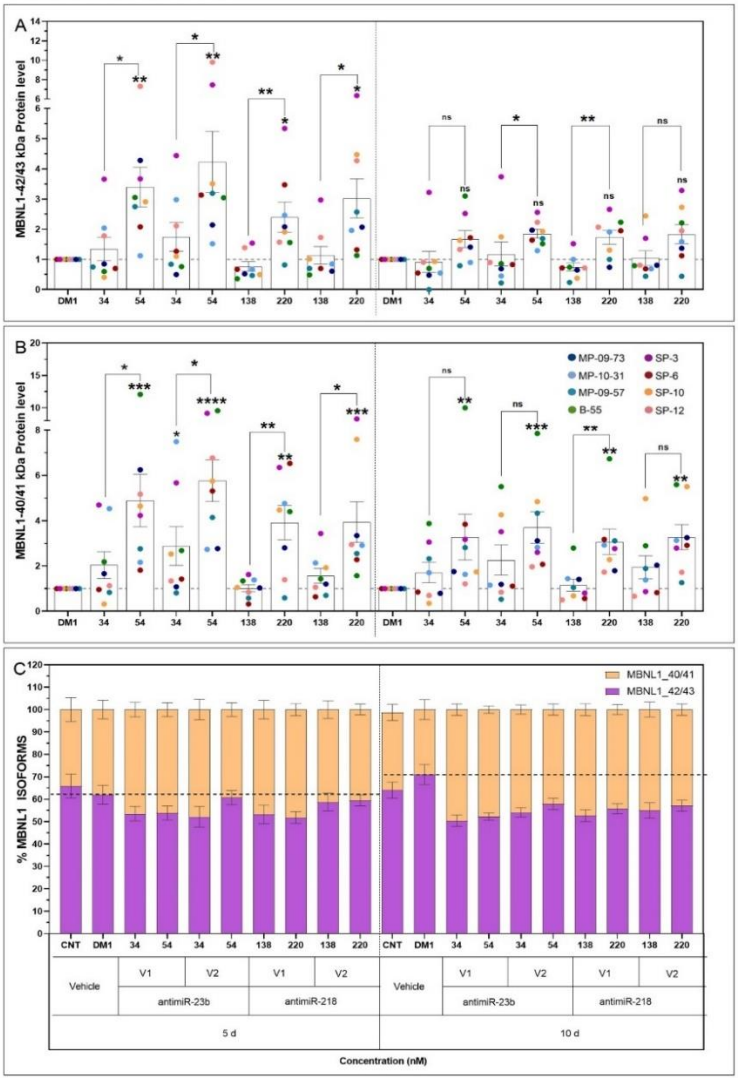

Supplementary Figure S5: Simple Western Jess system was used to quantitate the 42/43 kDa (high MW, +ex5±ex7) and the 40/41 kDa (low MW, -ex5±ex7) MBNL1 protein variants in antimiR-treated DM1 myoblasts compared to untreated DM1 cells. (A-B). Both high MW (A) and low MW (B) MBNL1 isoforms contributed to the increased total protein levels. The highest doses of antimiRs were the most effective in increasing MBNL1 levels. Kruskal Wallis test *: $p<0.05$; **: $p<0.01$; ***: $p<0.001$; ****: $p<0.0001$ (Dunn's post-test). The asterisks above the bars denote comparisons to untreated DM1 myotubes, while those above the boxes denote dose comparisons. Each dot of a different color denotes an individual DM1 myoblast line (shown in the legend). (C). Changes in the ratio of high/MW/low MW MBNL1 after treatment with the antimir for 5 and 10 days. Treatment with antimiRs restored the abnormal isoform ratio observed in DM1 cells at day 10 of differentiation. Error bars represent the standard error of the mean (SEM).

SUPPLEMENTARY FIGURE S6

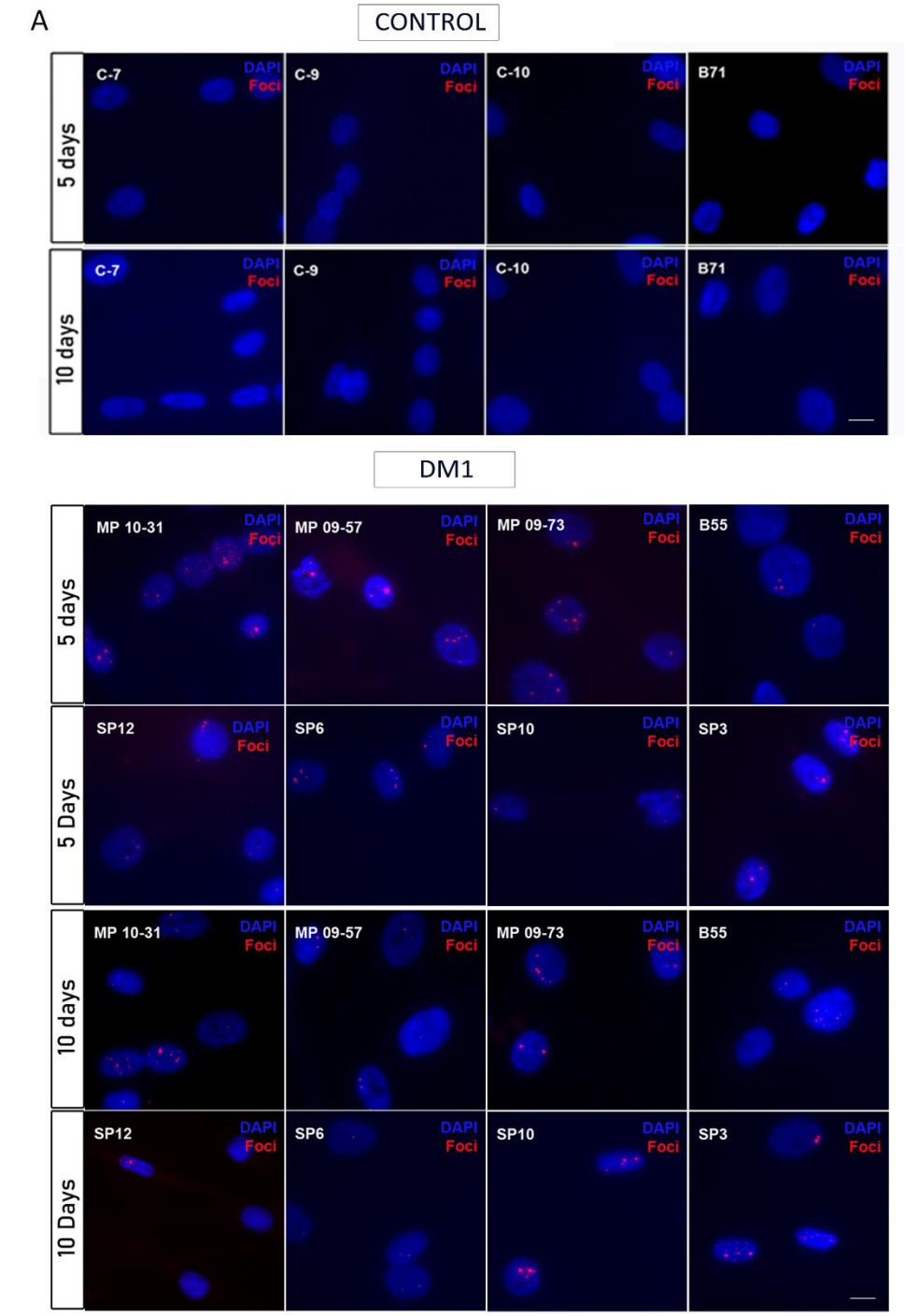

SUPPLEMENTARY FIGURE S6 (CONTINUATION)

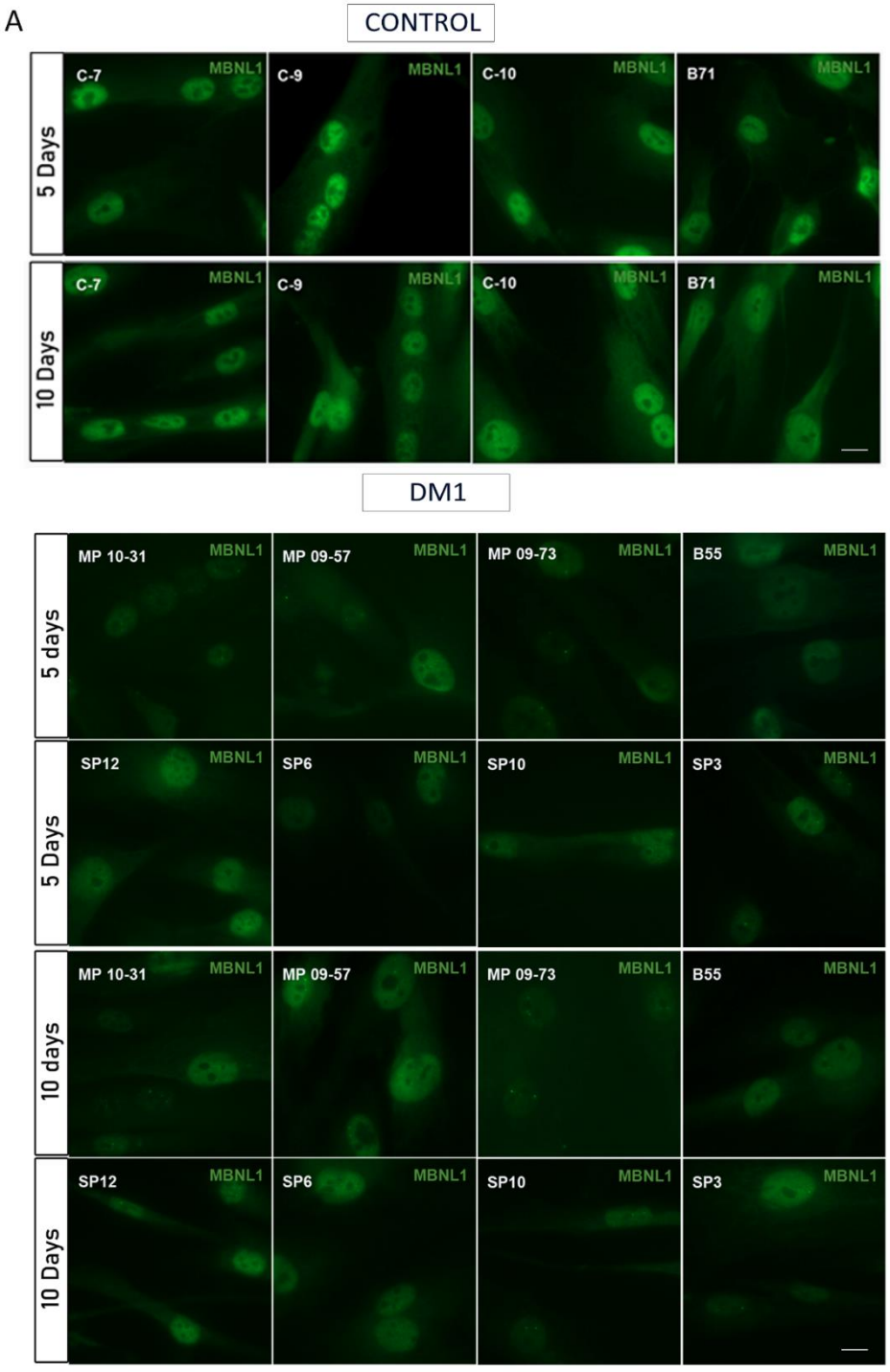

SUPPLEMENTARY FIGURE S6 (CONTINUATION)

B

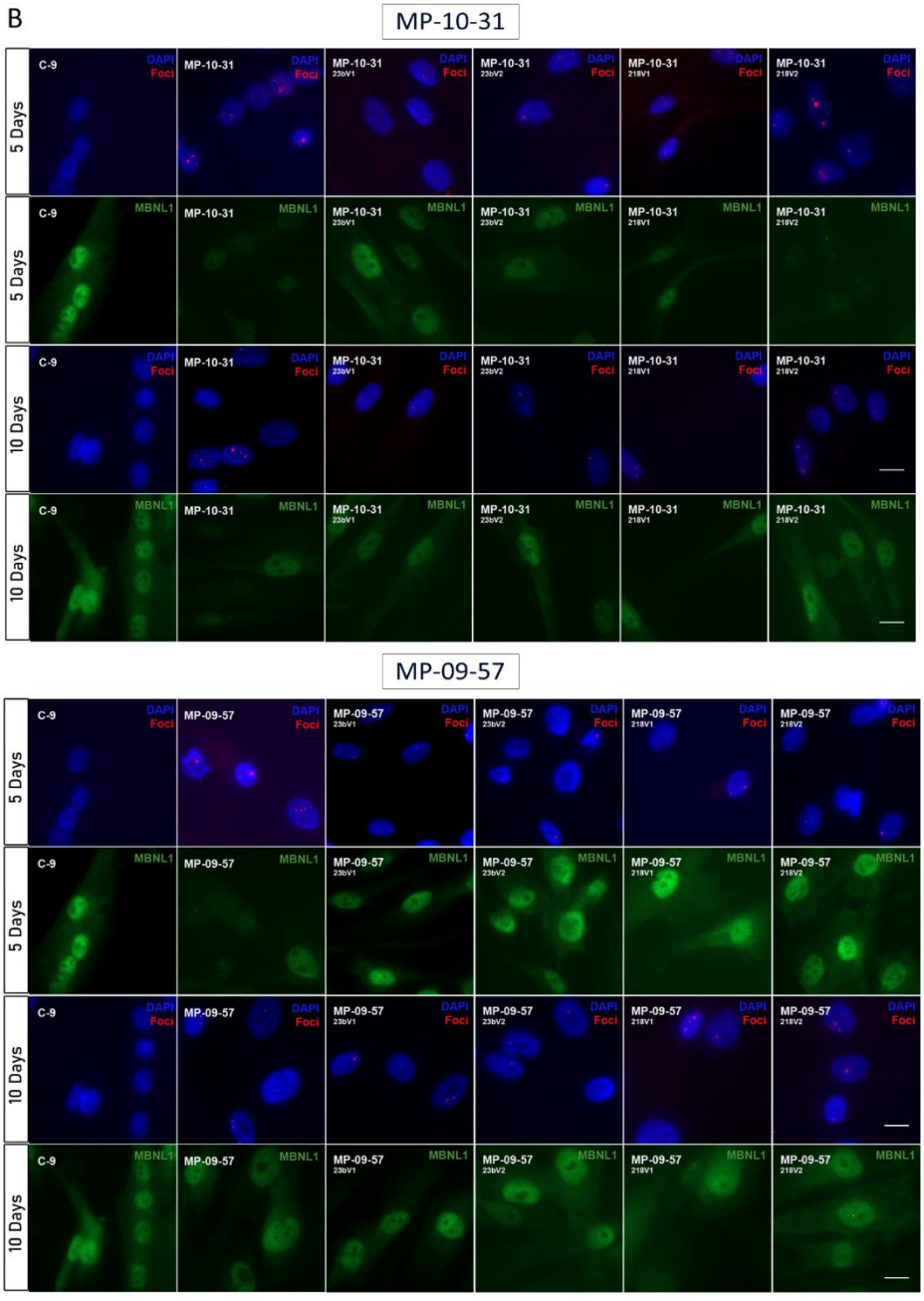

SUPPLEMENTARY FIGURE S6 (CONTINUATION)

B

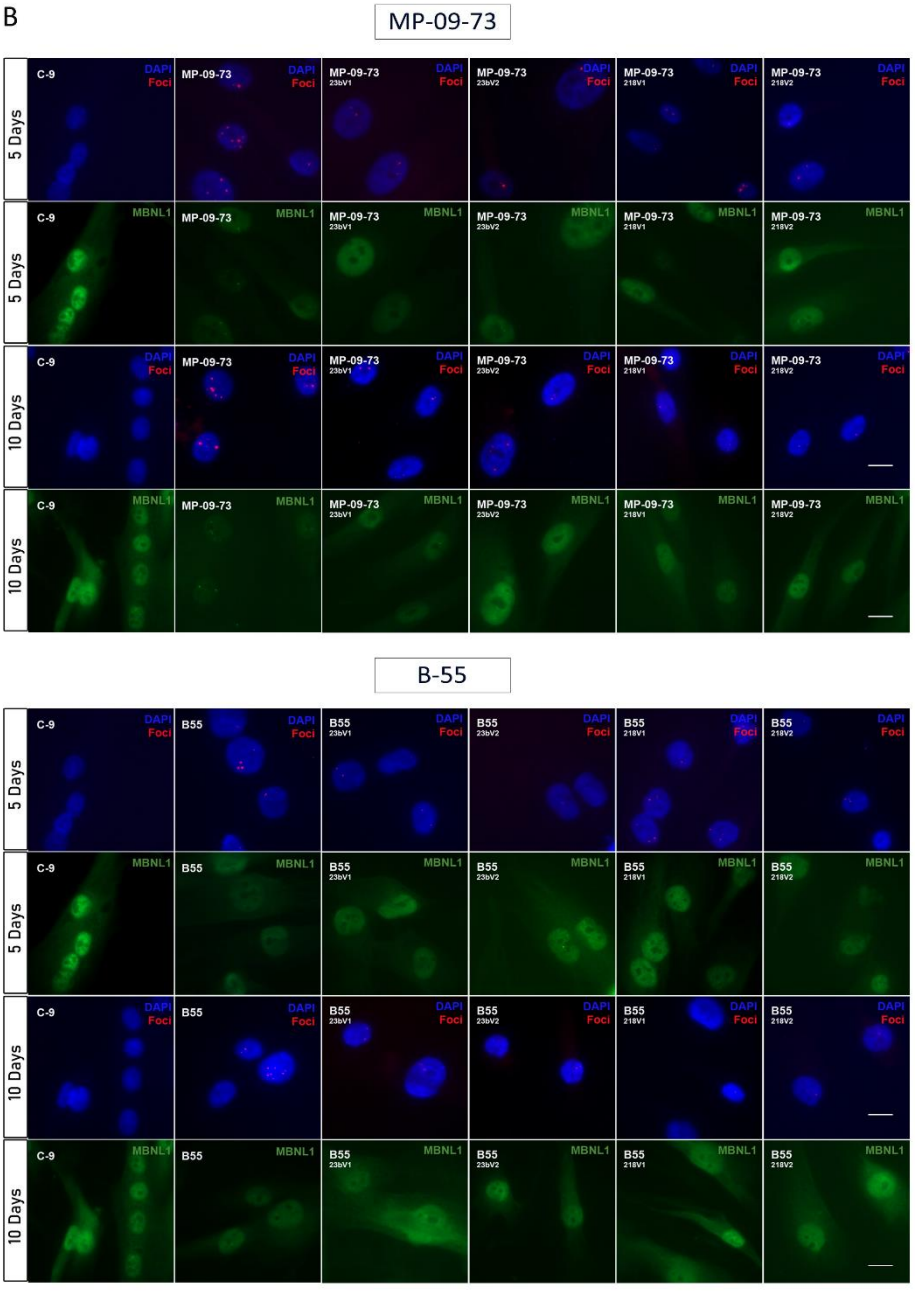

SUPPLEMENTARY FIGURE S6 (CONTINUATION)

B

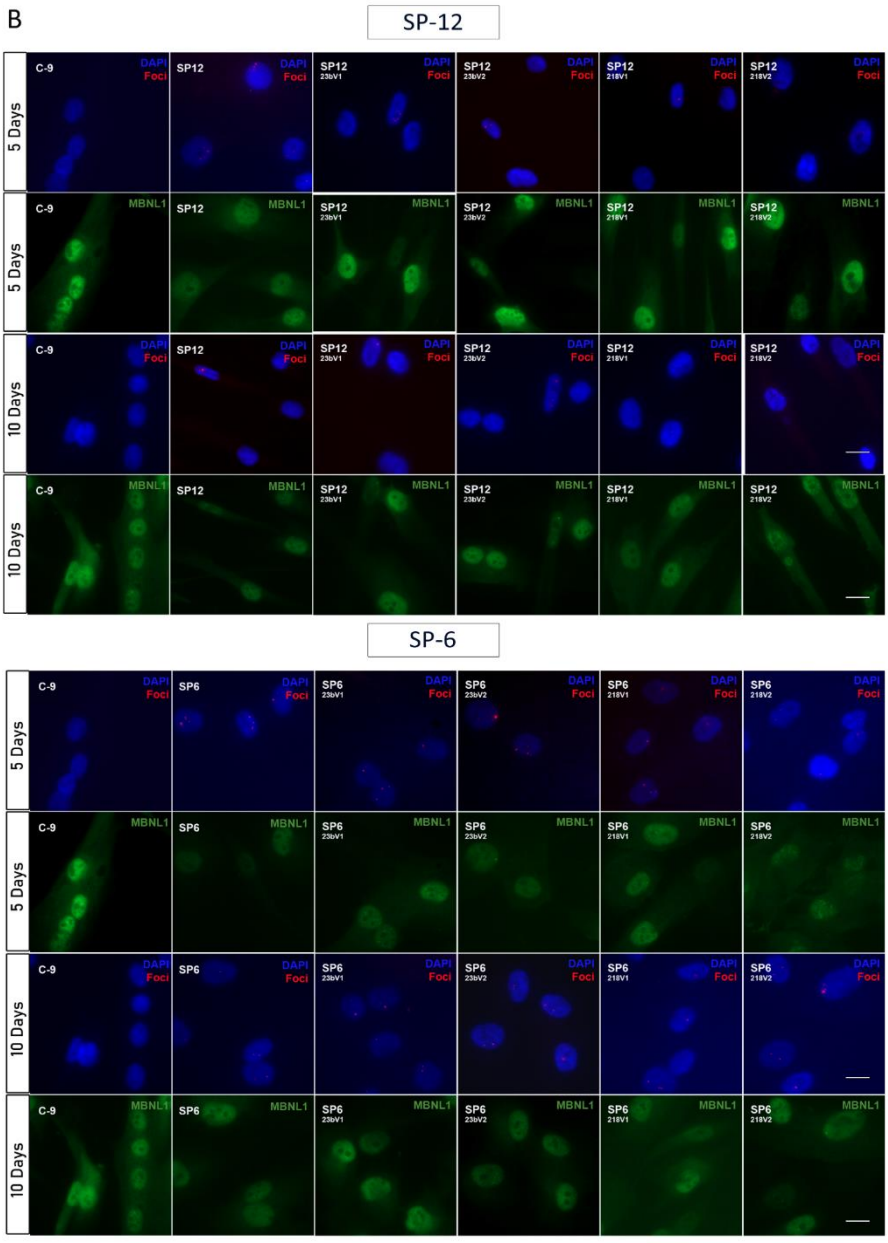

SUPPLEMENTARY FIGURE S6 (CONTINUATION)

B

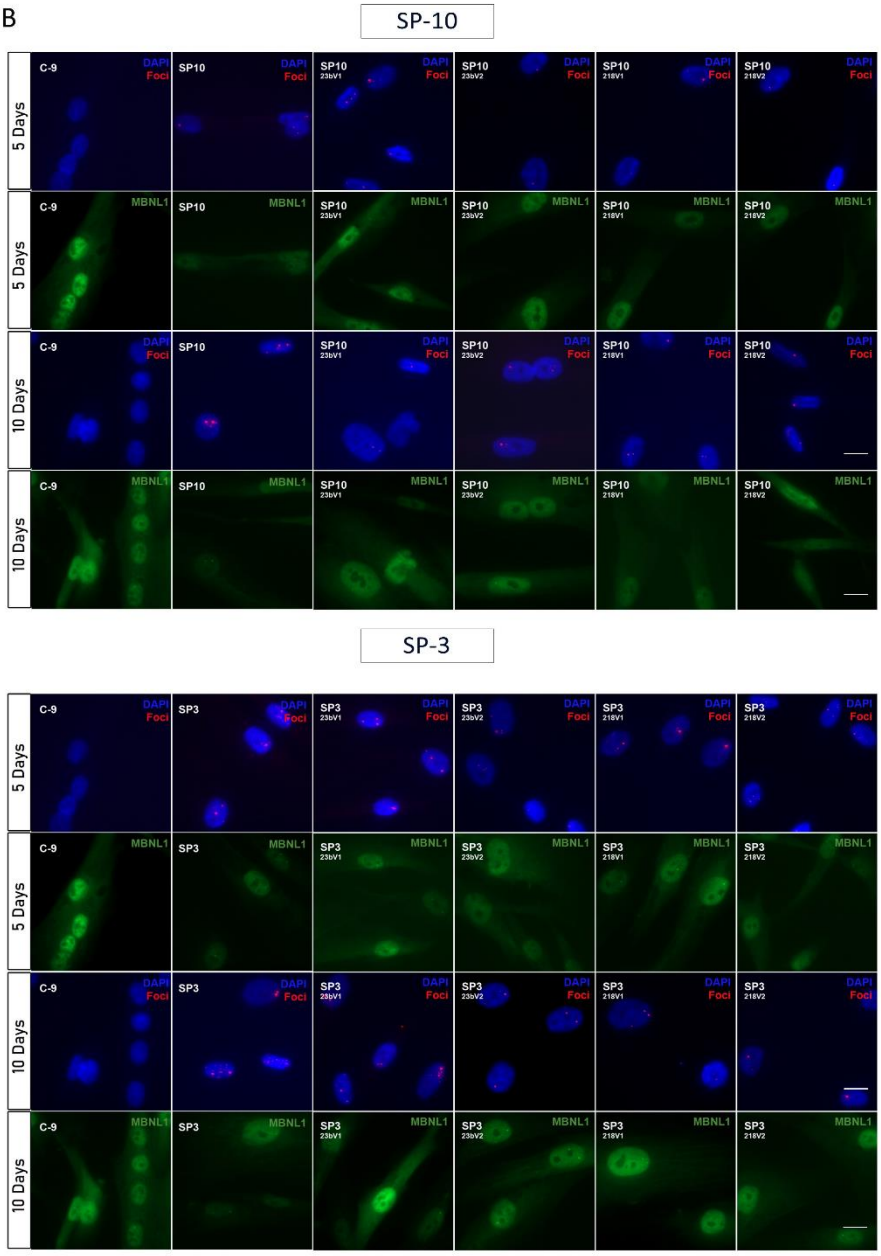

SUPPLEMENTARY FIGURE S6 (CONTINUATION)

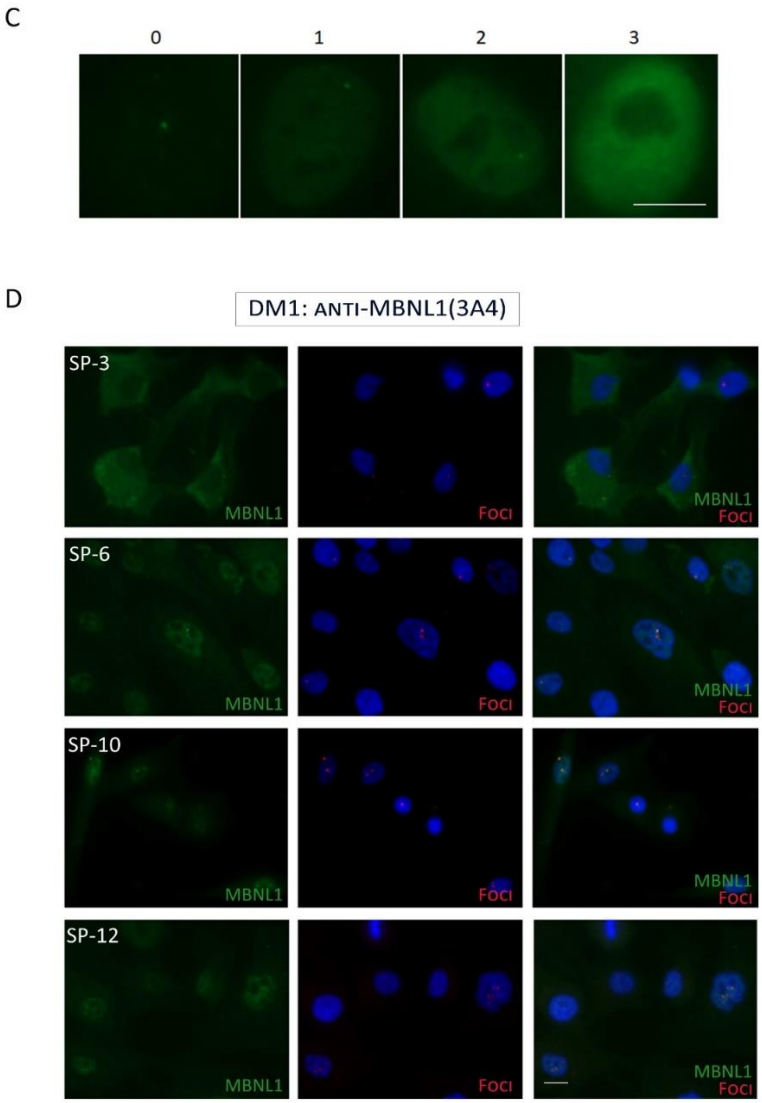

Supplementary Figure S6: Representative confocal images of untreated healthy control myotubes (C7, C9, C10, and B71) and DM1 myotubes (MP-10-31, MP-09-57, MP-09-73, B55, SP12, SP6, S10, and SP3) after 5 or 10 days of differentiation (A), or DM1 myoblasts treated with the antimiRs in the same conditions (B). Representative confocal images of nuclear MBNL1 fluorescence according to a pre-designed MBNL1 quantification scale, ranging from 0 to 3, corresponding to an increasing gradient of MBNL1 nuclear signal (C). Representative confocal images of DM1 myotubes (SP12, SP6, S10, and SP3) after 5 days of differentiation with anti-MBNL1 antibody (3A4) (D). Myotubes were immunostained with anti-MBNL1 (MB1a(4A8) (A-C) or MBNL1(3A4) (D), green) for detection of the protein or in situ hybridized with a Cy3-labelled CAG probe (red) for detecting ribonuclear foci. Nuclei were contrasted with DAPI (blue). The

type of treatment, differentiation time, and cell lines are indicated in the images. Scale bar = 20 µm.

SUPPLEMENTARY FIGURE S7

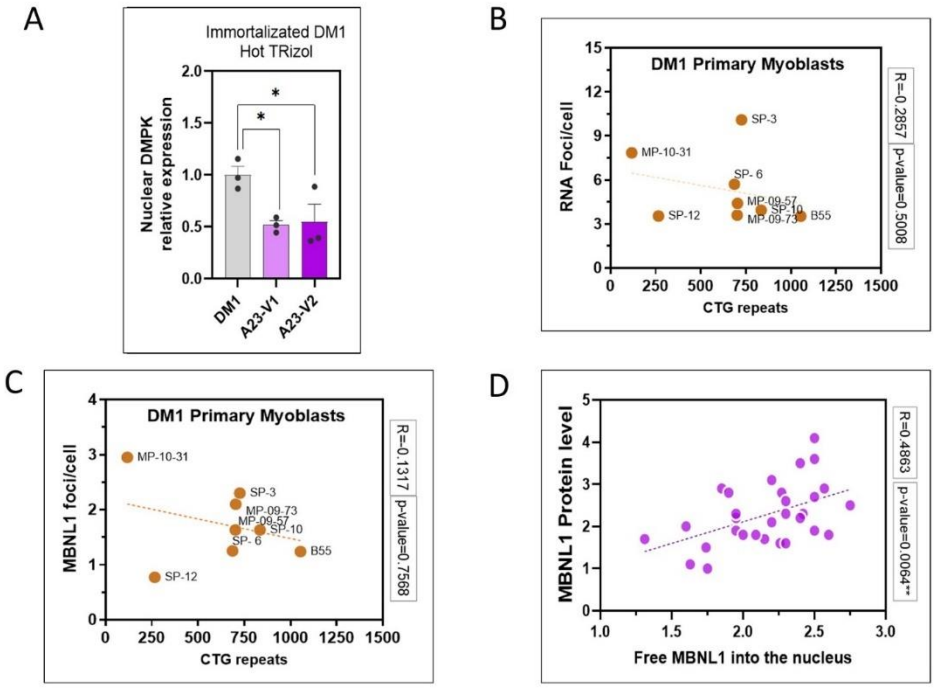

Supplementary Figure S7: Bar graph representation showing the quantification of the DMPK transcripts relative to GAPDH from RNA isolated from the nuclear fraction of immortalized DM1 myotubes treated with anti-miR-23b-V1 and V2 using Trizol extraction (A). Pearson correlation between the number of CTG repeats in myoblast cell lines and the number of (B) RNA nuclear foci per cell and (C) MBNL1 nuclear foci in untreated cells. (D) Correlation between MBNL1 protein levels and MBNL1 free form in the nucleus in cells treated with antimiRs for 10 days. The correlation R-value and p-value are shown for each graph.

SUPPLEMENTARY FIGURE S8

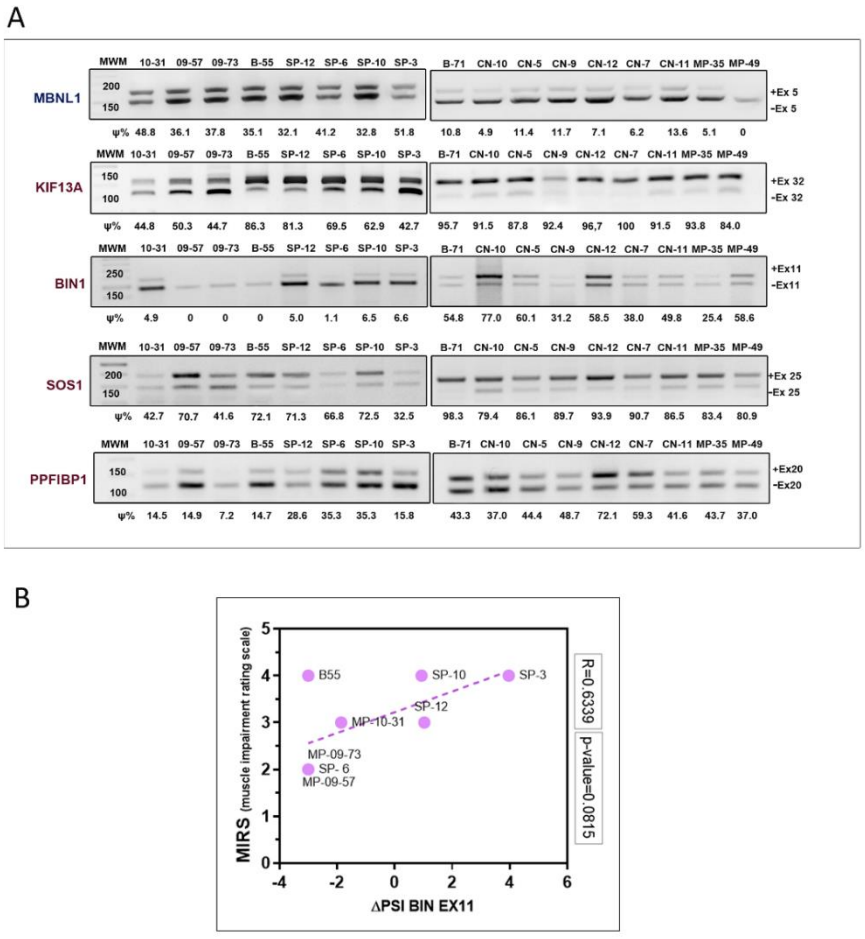

Supplementary Figure S8: Representative gels of semiquantitative RT-PCR are shown to illustrate alternative splicing patterns from MBNL1 exon 5, KIF13A exon 26, BIN1 exon 11, SOS1 exon 25, and PPFIBP1 exon 19 transcripts in CNT and DM1 myotubes. The Delta percentage Spliced In (ΔPSI) from two independent experiments is shown underneath each lane. (B) Pearson correlation between BIN1 splicing in DM1 myotubes and the MIRS scale of DM1 patients from which the myotubes were derived. The correlation R-value and p-value are shown.

SUPPLEMENTARY FIGURE S9

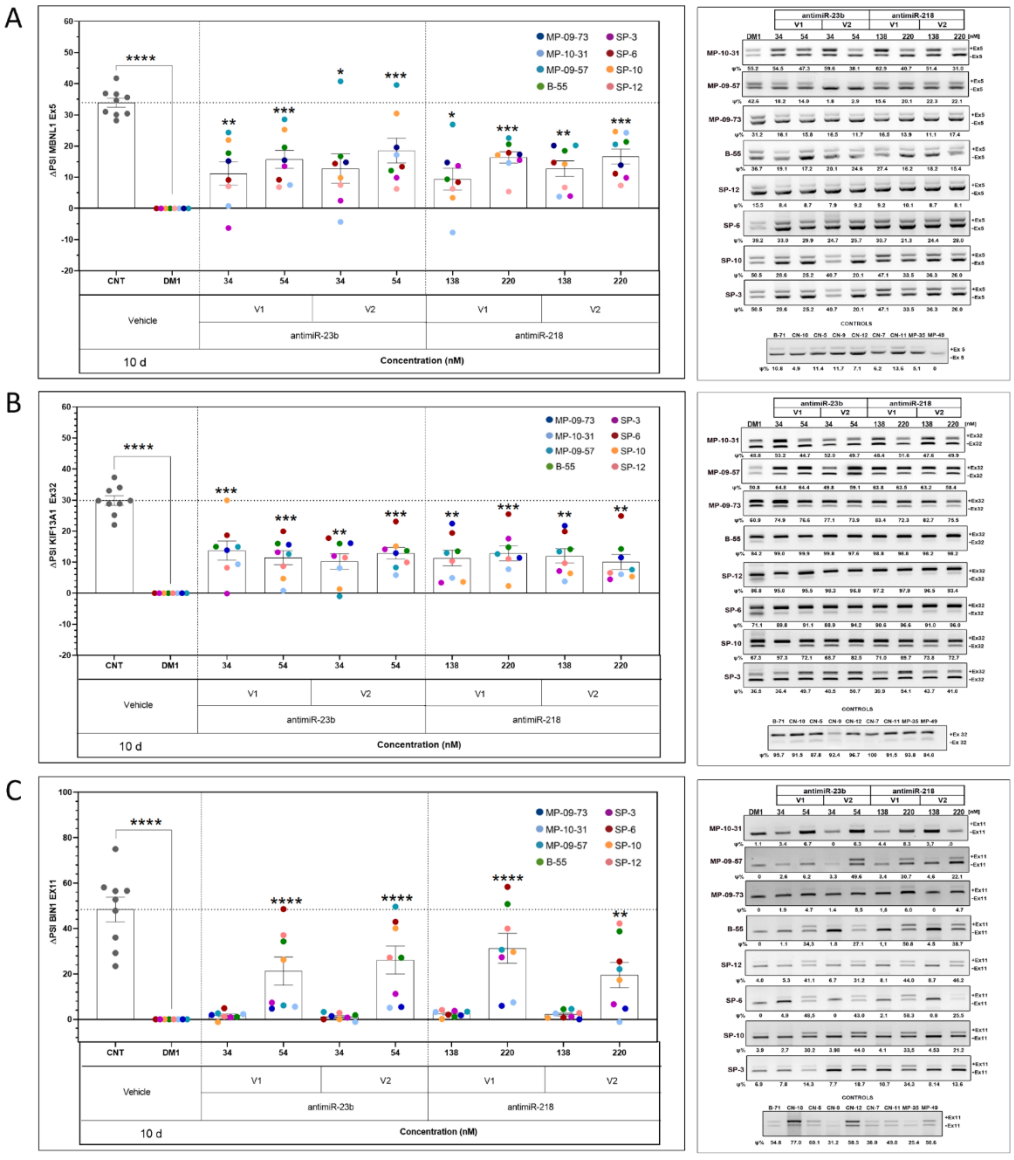

SUPPLEMENTARY FIGURE S9 (CONTINUATION)

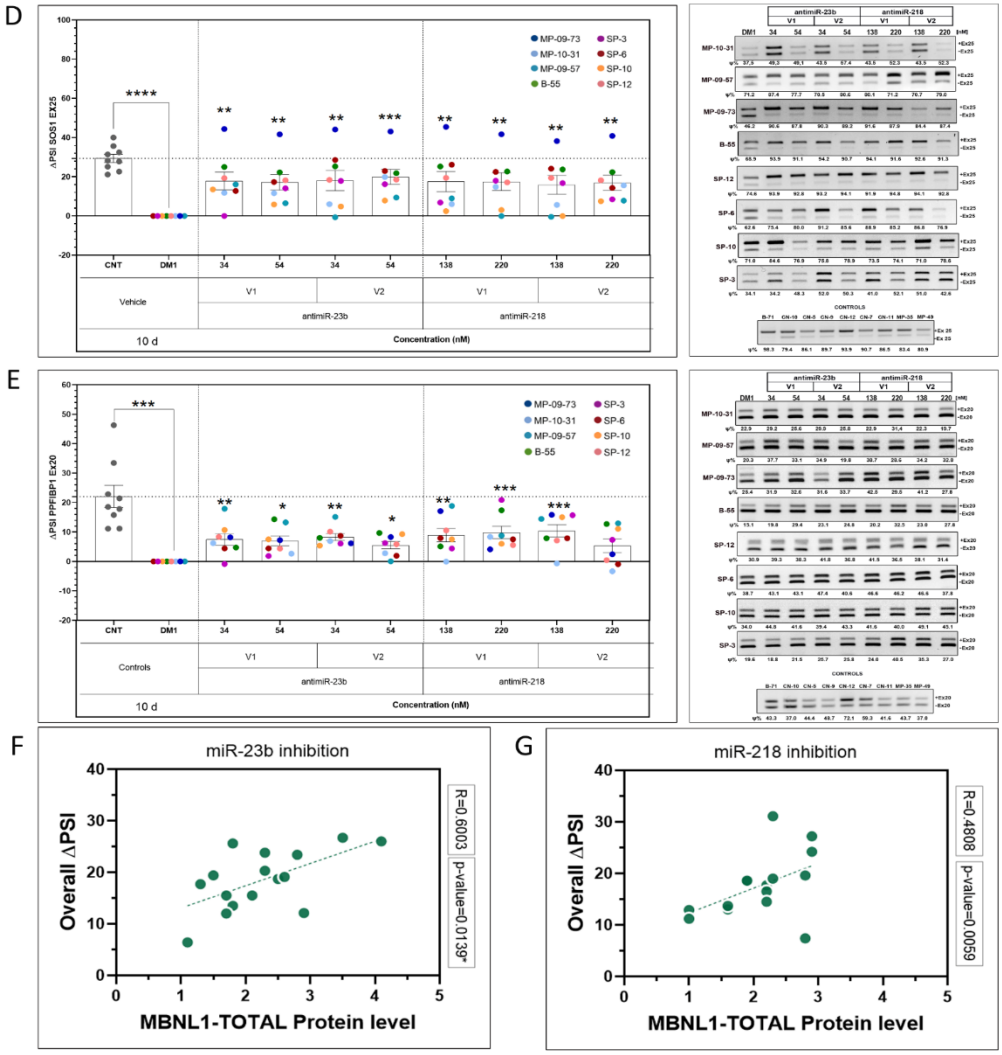

Supplementary Figure S9: The alternative splicing patterns of MBNL1 exon 5 (A), KIF13A exon 26 (B), BIN1 exon 11 (C), SOS1 exon 25 (D), and PPFIBP1 exon 19 (E) transcripts were analyzed using ΔPSI values for each exon and treatment. Representative images of semiquantitative RT-PCR are shown. Each dot of a different color denotes an individual DM1 myoblast cell line. The names of the lines are shown in the legend. The correlation between overall ΔPSR scores and total MBNL1 protein levels was separately analyzed for miR-23b (F) and miR-218 inhibition (G). The correlation R-value and p-value are shown in the graphs. Kruskal Wallis test *: p<0.05; **: p<0.01; ***: p<0.001; ****: p<0.0001 (Dunn's post-test). Error bars represent the standard error of the mean (SEM).

SUPPLEMENTARY FIGURE S10

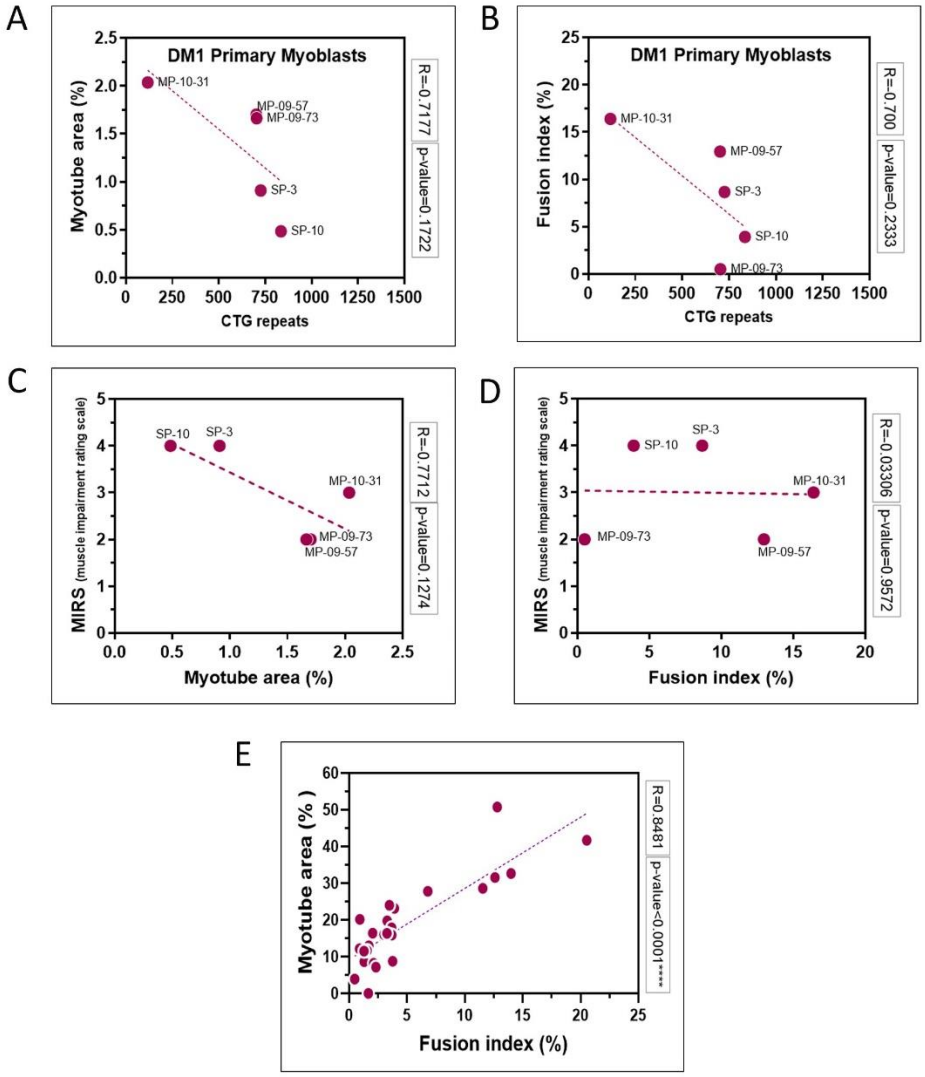

Supplementary Figure S10: Pearson and Spearman correlation analyses of myotube area (A) and fusion index (B) with myoblast repeat size. Pearson correlation analysis between myotube area (C), fusion index (D), and MIRS scale in untreated DM1 myotubes. Pearson correlation between myotube area and fusion index in antimiR-treated myotubes at 10 days of differentiation (E). The correlation R-value and p-value are shown in the graphs.

SUPPLEMENTARY FIGURE S11

A

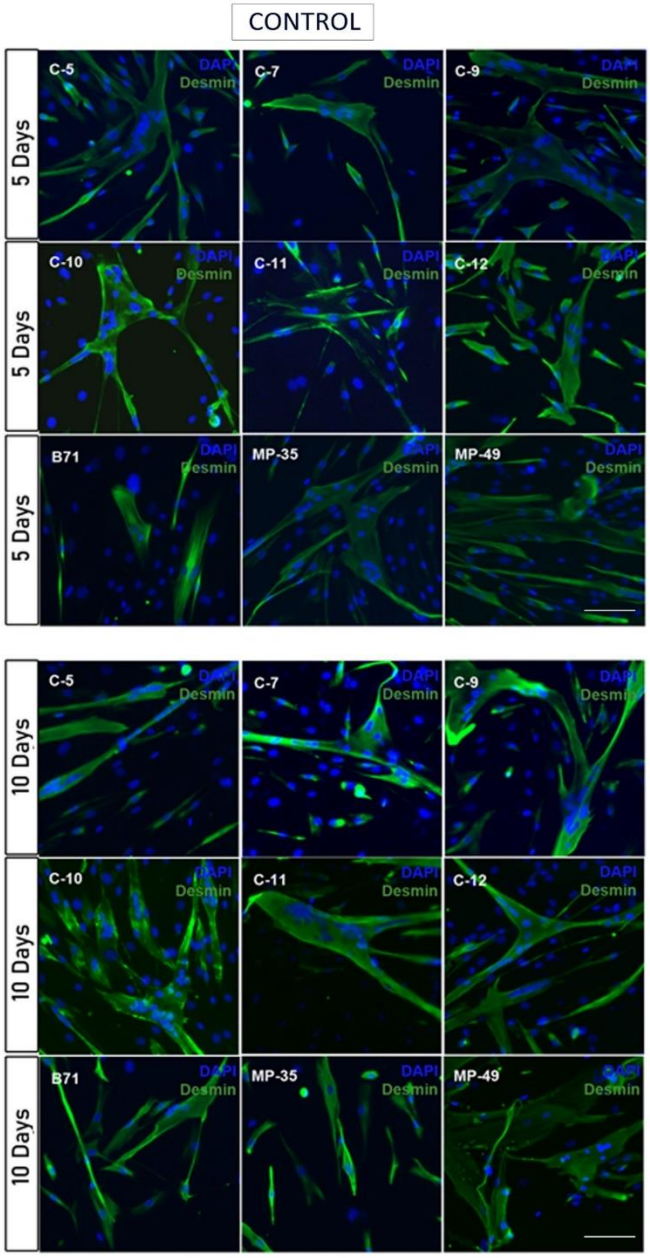

SUPPLEMENTARY FIGURE S11 (CONTINUATION)

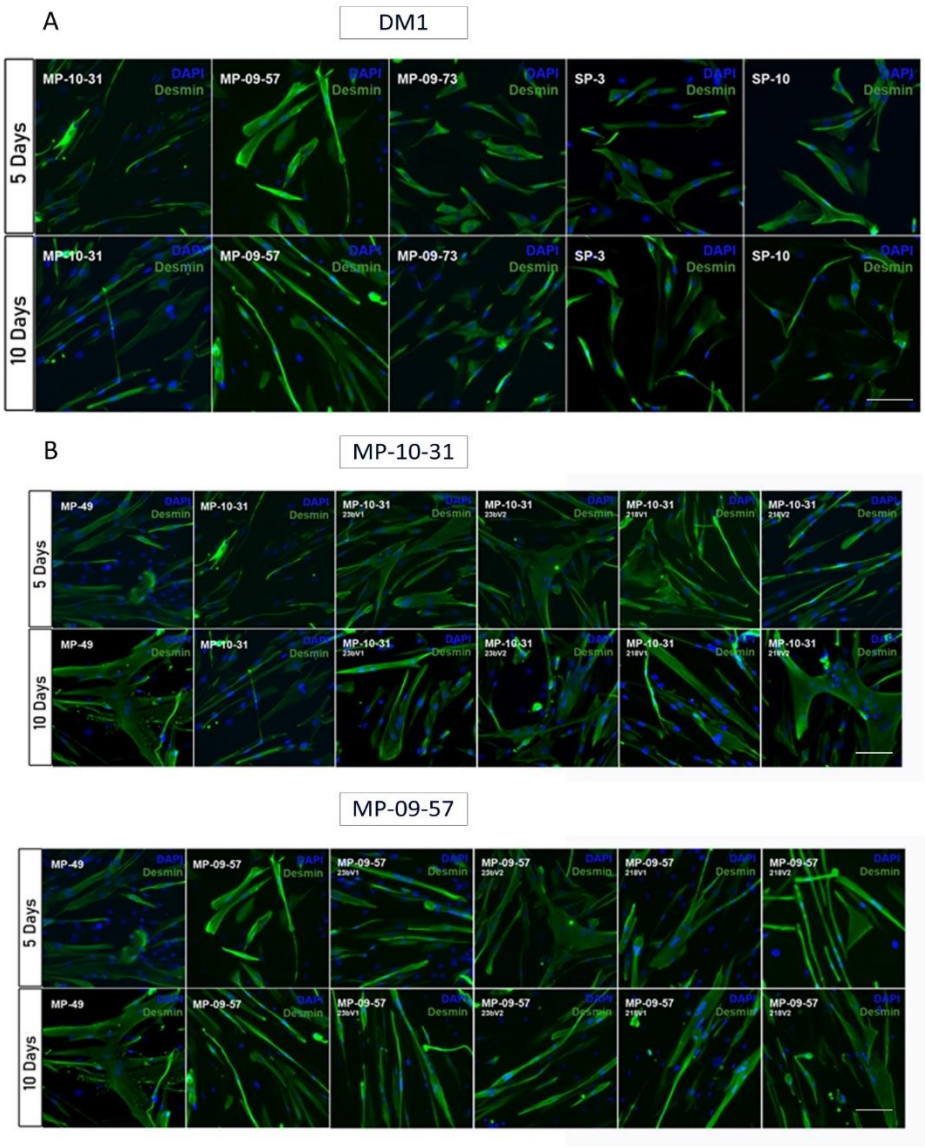

SUPPLEMENTARY FIGURE S11 (CONTINUATION)

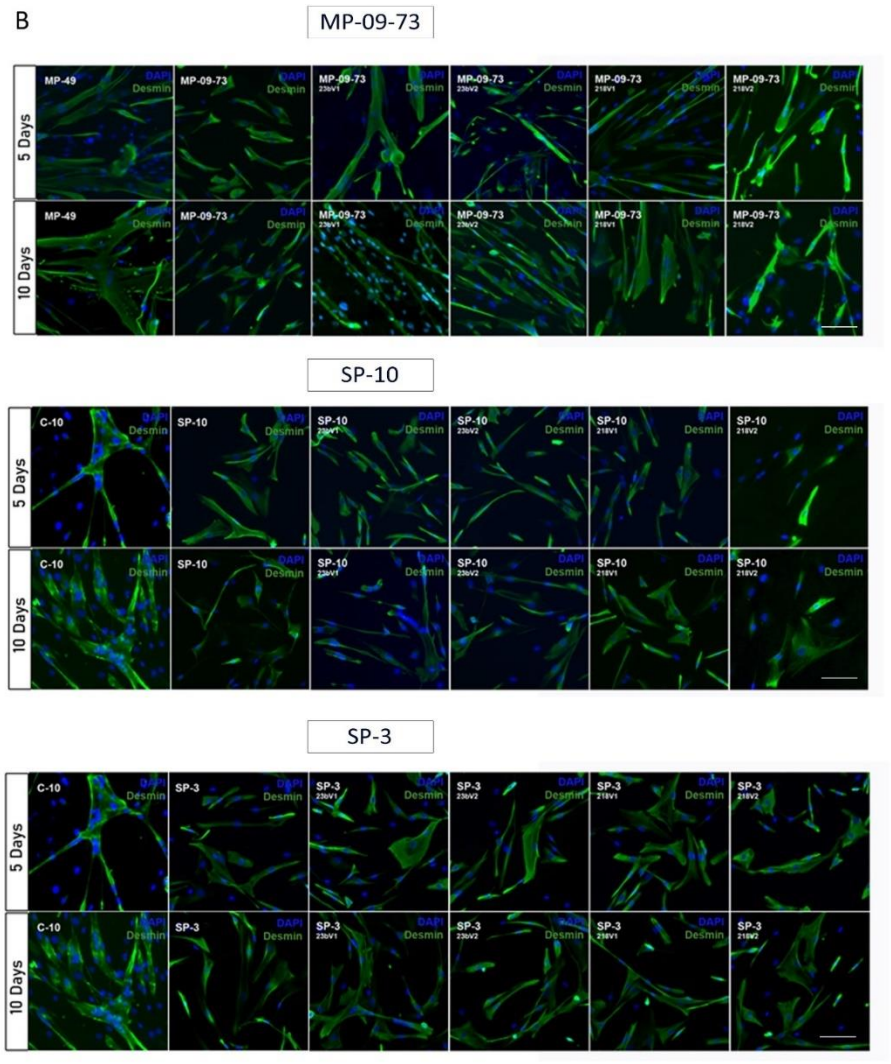

Supplementary Figure S11: Representative confocal images of healthy control myotubes (C5, C7, C9, C10, C11, C12, B71, MP-35, MP-49) and DM1 myotubes (MP-10-31, MP-09-57, MP-09-73, S3, and S10) at 5 and 10 days of differentiation (A) and DM1 myotubes treated with the indicated antimiRs in the same conditions (B). Myotubes were immunostained with anti-Desmin (green) to detect desmin, a class-III intermediate filament protein widely used as a marker of myogenic cells. The type of treatment, differentiation time, and cell lines are indicated in the images. Scale bar = 100 µm.

.

SUPPLEMENTARY FIGURE S12

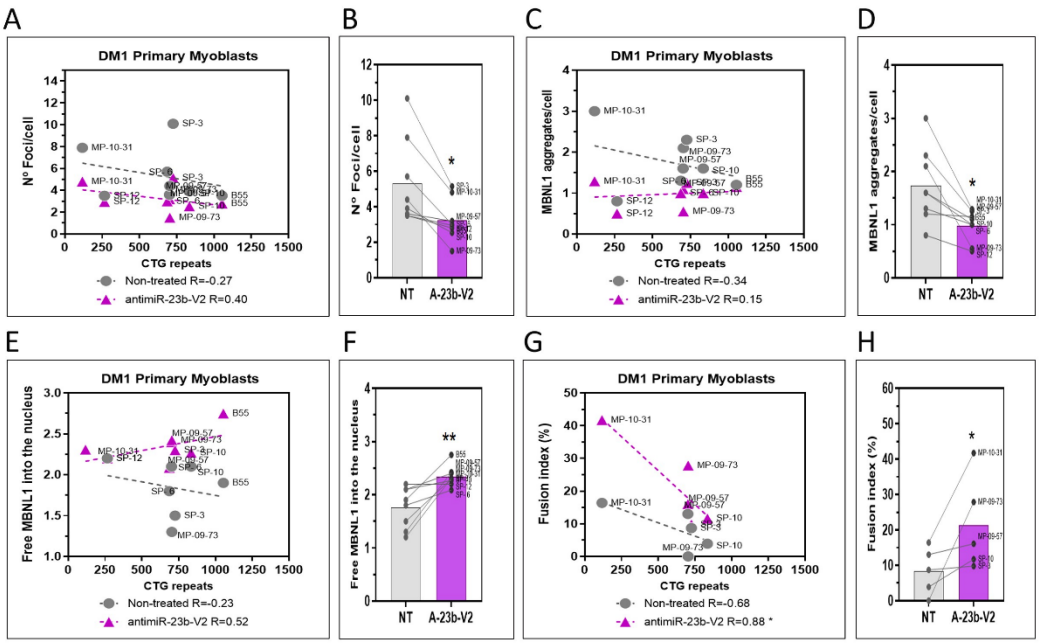

Supplementary Figure S12: Integrated evaluation of the antimiR's therapeutic potential for all DM1 myotube lines. (A-H) Comparison of untreated myotubes with antimiR-23b-V2-treated cells, including the Pearson correlation with CTG repeat number (A, C, E, G), or fold change (B, D, F, H) for the following parameters: (A, B) Number of RNA foci per cell, (C, D) MBNL1 nuclear foci, (E, F) MBNL1 free form in the nucleus, and (G, H) fusion index. The correlation R-values are shown in the corresponding graphs. Un-paired t-test with Welch's correction *: $p<0.05$; **: $p<0.01$; ***: $p<0.001$; ****: $p<0.0001$.

SUPPLEMENTARY FIGURE S13

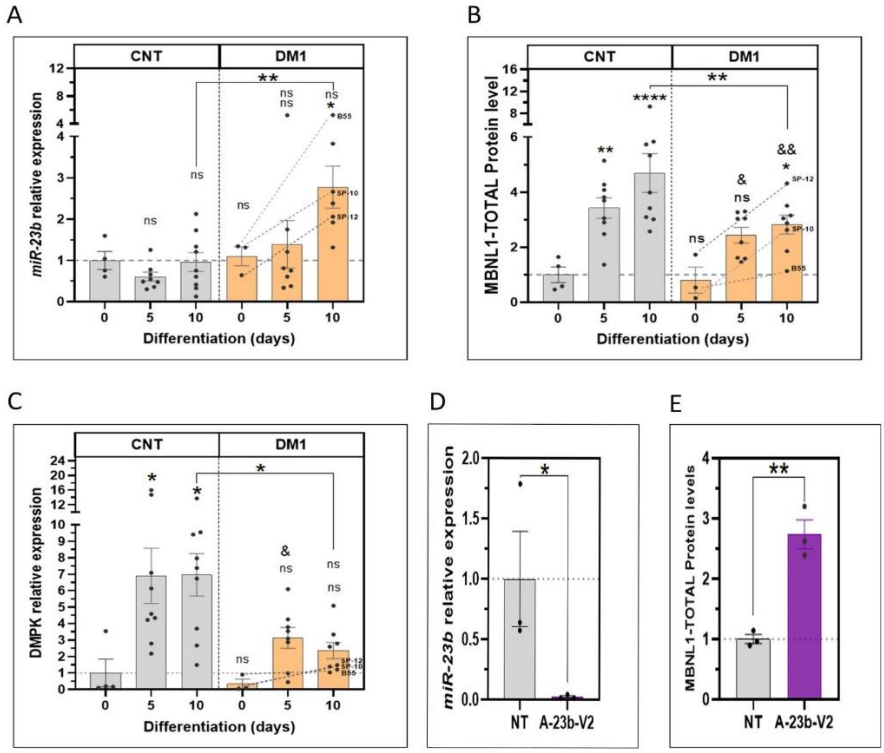

Supplementary Figure S13: Impact of differentiation time on control and DM1 primary cell lines on the relative miR-23b expression (A), MBNL1 total protein levels (B) and DMPK expression (C). Notably, at time 0, only the available cell lines were utilized (C12, C9, C11, MP-35M, MP-B55, SP12 and SP10). Kruskal Wallis test */&: p<0.05 (Dunn's post-test). The first set of symbols above compares all conditions to undifferentiated control cells (0 days). The second set of symbols above DM1 bars compares undifferentiated DM1 myoblasts to 5- and 10-day time points. Symbols above boxes compare control and DM1 cells at the same differentiation time points. Comparison between untreated healthy myotubes MP-35 and those treated with antimiR-23b-V2 after 10 days of differentiation for the following parameters: miR-23b expression (D) and total MBNL1 protein levels (E). Unpaired t-test: *: p<0.05. Each point represents an individual line of DM1 myoblasts. Error bars indicate the standard error of the mean (SEM).

SUPPLEMENTARY FIGURE S14

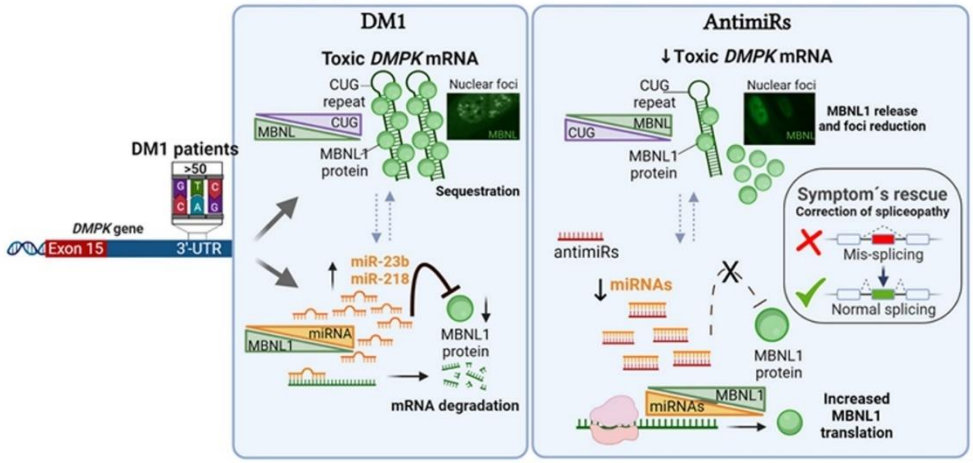

Supplementary Figure S14: Model of antimiR's dual mechanism of action. DM1 originates from CTG expansions in the 3'-UTR of the DMPK gene. (DM1 box) mutant DMPK transcripts generate double-stranded CUG RNA structures that sequester MBNL1 proteins and upregulate expression of miR-23b and miR-218, which further reinforce MBNL1 functional depletion by reducing protein translation. (AntimiR box). AntimiRs against miR-23b or miR-218 release excessive inhibition on MBNL1 translation and reduce DMPK levels and foci, thus contributing to a reduction in protein sequestration. The combined effect of lower sequestration and higher MBNL1 translation rescues molecular (mis-splicing) and cellular DM1 phenotypes.

References

1. J. D. Brook, M. E. McCurrach, H. G. Harley, A. J. Buckler, D. Church, H. Aburatani, K. Hunter, V. P. Stanton, J. P. Thirion, T. Hudson, et al, Molecular basis of myotonic dystrophy: expansion of a trinucleotide (CTG) repeat at the 3' end of a transcript encoding a protein kinase family member. *Cell* **68**, 799–808 (1992).

2. T. Ashizawa, C. Gagnon, W. J. Groh, L. Gutmann, N. E. Johnson, G. Meola, R. Moxley, S. Pandya, M. T. Rogers, E. Simpson, N. Angeard, G. Bassez, K. N. Berggren, D. Bhakta, M. Bozzali, A. Broderick, J. L. B. Byrne, C. Campbell, E. Cup, J. W. Day, E. De Mattia, D. Duboc, T. Duong, K. Eichinger, A. B. Ekstrom, B. van Engelen, B. Esparis, B. Eymard, M. Ferschl, S. M. Gadalla, B. Gallais, T. Goodglick, C. Heatwole, J. Hilbert, V. Holland, M. Kierkegaard, W. J. Koopman, K. Lane, D. Maas, A. Mankodi, K. D. Mathews, D. G. Monckton, D. Moser, S. Nazarian, L. Nguyen, P. Nopoulos, R. Petty, J. Phetteplace, J. Puymirat, S. Raman, L. Richer, E. Roma, J. Sampson, V. Sansone, B. Schoser, L. Sterling, J. Statland, S. H. Subramony, C. Tian, C. Trujillo, G. Tomaselli, C. Turner, S. Venance, A. Verma, M. White, S. Winblad, Consensus-based care recommendations for adults with myotonic dystrophy type 1. *Neurol Clin Pract* **8**, 507–520 (2018).

3. W. J. Groh, M. R. Groh, C. Shen, D. G. Monckton, C. L. Bodkin, R. M. Pascuzzi, Survival and CTG repeat expansion in adults with myotonic dystrophy type 1. *Muscle Nerve* **43**, 648–51 (2011).

4. M. De Antonio, C. Dogan, D. Hamroun, M. Mati, S. Zerrouki, B. Eymard, S. Katsahian, G. Bassez, Unravelling the myotonic dystrophy type 1 clinical spectrum: A systematic registry-based study with implications for disease classification. *Rev Neurol (Paris)* **172**, 572–580 (2016).

5. C. Dogan, M. De Antonio, D. Hamroun, H. Varet, M. Fabbro, F. Rougier, K. Amarof, M. C. Arne Bes, A. L. Bedat-Millet, A. Behin, R. Bellance, F. Bouhour, C. Boutte, F. Boyer, E. Campana-Salort, F. Chapon, P. Cintas, C. Desnuelle, R. Deschamps, V. Drouin-Garraud, X. Ferrer, H. Gervais-Bernard, K. Ghorab, P. Laforet, A. Magot, L. Magy, D. Menard, M. C. Minot, A. Nadaj-Pakleza, S. Pellieux, Y. Pereon, M. Preudhomme, J. Pouget, S. Sacconi, G. Sole, T. Stojkovich, V. Tiffreau, A. Urtizberea, C. Vial, F. Zagnoli, G. Caranhac, C. Bourlier, G. Riviere, A. Geille, R. K. Gherardi, B. Eymard, J. Puymirat, S. Katsahian, G. Bassez, Gender as a Modifying Factor Influencing Myotonic Dystrophy Type 1 Phenotype Severity and Mortality: A Nationwide Multiple Databases Cross-Sectional Observational Study. *PLoS One* **11**, e0148264 (2016).

6. L. L. Ozimski, M. Sabater-Arcis, A. Bargiela, R. Artero, The hallmarks of myotonic dystrophy type 1 muscle dysfunction. *Biol Rev Camb Philos Soc* **96**, 716–730 (2021).

7. I. Holt, S. Mittal, D. Furling, G. S. Butler-Browne, J. D. Brook, G. E. Morris, Defective mRNA in myotonic dystrophy accumulates at the periphery of nuclear splicing speckles. *Genes Cells* **12**, 1035–48 (2007).

8. E. S. Goers, J. Purcell, R. B. Voelker, D. P. Gates, J. A. Berglund, MBNL1 binds GC motifs embedded in pyrimidines to regulate alternative splicing. *Nucleic Acids Res* **38**, 2467–84 (2010).

9. R. Batra, K. Charizanis, M. Manchanda, A. Mohan, M. Li, D. J. Finn, M. Goodwin, C. Zhang, K. Sobczak, C. A. Thornton, M. S. Swanson, Loss of MBNL leads to disruption of developmentally regulated alternative polyadenylation in RNA-mediated disease. *Mol Cell* **56**, 311–322 (2014).

10. X. Lin, J. W. Miller, A. Mankodi, R. N. Kanadia, Y. Yuan, R. T. Moxley, M. S. Swanson, C. A. Thornton, Failure of MBNL1-dependent post-natal splicing transitions in myotonic dystrophy. *Hum Mol Genet* **15**, 2087–97 (2006).

11. N. M. Kuyumcu-Martinez, G. S. Wang, T. A. Cooper, Increased steady-state levels of CUGBP1 in myotonic dystrophy 1 are due to PKC-mediated hyperphosphorylation. *Mol Cell* **28**, 68–78 (2007).

12. A. Ravel-Chapuis, G. Bélanger, R. S. Yadava, M. S. Mahadevan, L. DesGroseillers, J. Côté, B. J. Jasmin, The RNA-binding protein Staufen1 is increased in DM1 skeletal muscle and promotes alternative pre-mRNA splicing. *J Cell Biol* **196**, 699–712 (2012).

13. M. Li, Y. Zhuang, R. Batra, J. D. Thomas, M. Li, C. A. Nutter, M. M. Scotti, H. A. Carter, Z. J. Wang, X. S. Huang, C. Q. Pu, M. S. Swanson, W. Xie, HNRNPA1-induced spliceopathy in a transgenic mouse model of myotonic dystrophy. *Proc Natl Acad Sci U S A* **117**, 5472–5477 (2020).

14. F. Freyermuth, F. Rau, Y. Kokunai, T. Linke, C. Sellier, M. Nakamori, Y. Kino, L. Arandel, A. Jollet, C. Thibault, M. Philipps, S. Vicaire, B. Jost, B. Udd, J. W. Day, D. Duboc, K. Wahbi, T. Matsumura, H. Fujimura, H. Mochizuki, F. Deryckere, T. Kimura, N. Nukina, S. Ishiura, V. Lacroix, A. Campan-Fournier, V. Navratil, E. Chautard, D. Auboeuf, M. Horie, K. Imoto, K.-Y. Lee, M. S. Swanson, A. L. de Munain, S. Inada, H. Itoh, K. Nakazawa, T. Ashihara, E. Wang, T. Zimmer, D. Furling, M. P. Takahashi, N. Charlet-Berguerand, Splicing misregulation of SCN5A contributes to cardiac-conduction delay and heart arrhythmia in myotonic dystrophy. *Nat Commun* **7**, 11067 (2016).

15. T. M. Wheeler, J. D. Lueck, M. S. Swanson, R. T. Dirksen, C. A. Thornton, Correction of ClC-1 splicing eliminates chloride channelopathy and myotonia in mouse models of myotonic dystrophy. *J Clin Invest* **117**, 3952–3957 (2007).

16. R. S. Savkur, A. V. Philips, T. A. Cooper, Aberrant regulation of insulin receptor alternative splicing is associated with insulin resistance in myotonic dystrophy. *Nat Genet* **29**, 40–47 (2001).

17. D. Savić Pavićević, J. Miladinović, M. Brkušanin, S. Šviković, S. Djurica, G. Brajušković, S. Romac, Molecular genetics and genetic testing in myotonic dystrophy type 1. *Biomed Res Int* **2013**, 391821 (2013).

18. F. Morales, J. M. Couto, C. F. Higham, G. Hogg, P. Cuenca, C. Braida, R. H. Wilson, B. Adam, G. del Valle, R. Brian, M. Sittenfeld, T. Ashizawa, A. Wilcox, D. E. Wilcox, D. G. Monckton, Somatic instability of the expanded CTG triplet repeat in myotonic dystrophy type 1 is a heritable quantitative trait and modifier of disease severity. *Hum Mol Genet* **21**, 3558–67 (2012).

19. T. Ashizawa, J. R. Dubel, Y. Harati, Somatic instability of CTG repeat in myotonic dystrophy. *Neurology* **43**, 2674–8 (1993).

20. C. A. Thornton, K. Johnson, R. T. Moxley, Myotonic dystrophy patients have larger CTG expansions in skeletal muscle than in leukocytes. *Ann Neurol* **35**, 104–7 (1994).

21. M. Zatz, M. R. Passos-Bueno, A. Cerqueira, S. K. Marie, M. Vainzof, R. C. Pavanello, Analysis of the CTG repeat in skeletal muscle of young and adult myotonic dystrophy patients: when does the expansion occur? *Hum Mol Genet* **4**, 401–6 (1995).

22. S. Peric, J. Pesovic, D. Savic-Pavicevic, V. Rakocevic Stojanovic, G. Meola, Molecular and Clinical Implications of Variant Repeats in Myotonic Dystrophy Type 1. *Int J Mol Sci* **23**, 354 (2021).

23. M. Matloka, A. F. Klein, F. Rau, D. Furling, Cells of Matter-In Vitro Models for Myotonic Dystrophy. *Front Neurol* **9**, 361 (2018).

24. M. Pascual-Gilabert, R. Artero, A. López-Castel, The myotonic dystrophy type 1 drug development pipeline: 2022 edition. *Drug Discov Today* **28**, 103489 (2023).

25. S. J. Overby, E. Cerro-Herreros, B. Llamusi, R. Artero, RNA-mediated therapies in myotonic dystrophy. *Drug Discov Today* **23**, 2013–2022 (2018).

26. P. Konieczny, E. Stepniak-Konieczna, K. Sobczak, MBNL proteins and their target RNAs, interaction and splicing regulation. *Nucleic Acids Res* **42**, 10873–87 (2014).

27. K. Charizanis, K. Y. Lee, R. Batra, M. Goodwin, C. Zhang, Y. Yuan, L. Shiue, M. Cline, M. M. Scotti, G. Xia, A. Kumar, T. Ashizawa, H. B. Clark, T. Kimura, M. P. Takahashi, H. Fujimura, K. Jinnai, H. Yoshikawa, M. Gomes-Pereira, G. Gourdon, N. Sakai, S. Nishino, T. C. Foster, M. Ares, R. B. Darnell, M. S. Swanson, Muscleblind-like 2-mediated alternative splicing in the developing brain and dysregulation in myotonic dystrophy. *Neuron* **75**, 437–50 (2012).

28. M. G. Poulos, R. Batra, M. Li, Y. Yuan, C. Zhang, R. B. Darnell, M. S. Swanson, Progressive impairment of muscle regeneration in muscleblind-like 3 isoform knockout mice. *Hum Mol Genet* **22**, 3547–58 (2013).

29. J. Choi, D. M. Dixon, W. Dansithong, W. F. Abdallah, K. P. Roos, M. C. Jordan, B. Trac, H. S. Lee, L. Comai, S. Reddy, Muscleblind-like 3 deficit results in a spectrum of age-associated pathologies observed in myotonic dystrophy. *Sci Rep* **6**, 30999 (2016).

30. C. M. Chamberlain, L. P. Ranum, Mouse model of muscleblind-like 1 overexpression: skeletal muscle effects and therapeutic promise. *Hum Mol Genet* **21**, 4645–54 (2012).

31. K. Y. Song, X. M. Guo, H. Q. Wang, L. Zhang, S. Y. Huang, Y. C. Huo, G. Zhang, J. Z. Feng, R. R. Zhang, Y. Ma, Q. Z. Hu, X. Y. Qin, MBNL1 reverses the proliferation defect of skeletal muscle satellite cells in myotonic dystrophy type 1 by inhibiting autophagy via the mTOR pathway. *Cell Death Dis* **11**, 545 (2020).

32. R. N. Kanadia, J. Shin, Y. Yuan, S. G. Beattie, T. M. Wheeler, C. A. Thornton, M. S. Swanson, Reversal of RNA missplicing and myotonia after muscleblind overexpression in a mouse poly(CUG) model for myotonic dystrophy. *Proc Natl Acad Sci U S A* **103**, 11748–53 (2006).

33. G. Chen, A. Masuda, H. Konishi, B. Ohkawara, M. Ito, M. Kinoshita, H. Kiyama, T. Matsuura, K. Ohno, Phenylbutazone induces expression of MBNL1 and suppresses formation of MBNL1-CUG RNA foci in a mouse model of myotonic dystrophy. *Sci Rep* **6**, 25317 (2016).

34. E. Cerro-Herreros, M. Sabater-Arcis, J. M. Fernandez-Costa, N. Moreno, M. Perez-Alonso, B. Llamusi, R. Artero, miR-23b and miR-218 silencing increase Muscleblind-like expression and alleviate myotonic dystrophy phenotypes in mammalian models. *Nat Commun* **9**, 2482 (2018).

35. E. Cerro-Herreros, I. González-Martínez, N. Moreno-Cervera, S. Overby, M. Pérez-Alonso, B. Llamusí, R. Artero, Therapeutic Potential of AntagomiR-23b for Treating Myotonic Dystrophy. *Mol Ther Nucleic Acids* **21**, 837–849 (2020).

36. E. Cerro-Herreros, I. González-Martínez, N. Moreno, J. Espinosa-Espinosa, J. M. Fernández-Costa, A. Colom-Rodrigo, S. J. Overby, D. Seoane-Miraz, J. Poyatos-García, J. J. Vilchez, A. López de Munain, M. A. Varela, M. J. Wood, M. Pérez-Alonso, B. Llamusí, R. Artero, Preclinical characterization of antagomiR-218 as a potential treatment for myotonic dystrophy. *Mol Ther Nucleic Acids* **26**, 174–191 (2021).

37. S. Benizri, A. Gissot, A. Martin, B. Vialet, M. W. Grinstaff, P. Barthélémy, Bioconjugated Oligonucleotides: Recent Developments and Therapeutic Applications. *Bioconjug Chem* **30**, 366–383 (2019).

38. R. J. Butland, J. Pang, E. R. Gross, A. A. Woodcock, D. M. Geddes, Two-, six-, and 12-minute walking tests in respiratory disease. *Br Med J (Clin Res Ed)* **284**, 1607–8 (1982).

39. J. Mathieu, H. Boivin, D. Meunier, M. Gaudreault, P. Bégin, Assessment of a disease-specific muscular impairment rating scale in myotonic dystrophy. *Neurology* **56**, 336–40 (2001).

40. J. C. van Swieten, P. J. Koudstaal, M. C. Visser, H. J. Schouten, J. van Gijn, Interobserver agreement for the assessment of handicap in stroke patients. *Stroke* **19**, 604–7 (1988).

41. A. Compston, Aids to the investigation of peripheral nerve injuries. Medical Research Council: Nerve Injuries Research Committee. His Majesty's Stationery Office: 1942; pp. 48 (iii) and 74 figures and 7 diagrams; with aids to the examination of the peripheral nervous system. By Michael O'Brien for the Guarantors of Brain. Saunders Elsevier: 2010; pp. [8] 64 and 94 Figures. *Brain* **133**, 2838–44 (2010).

42. H. Tran, N. Gourrier, C. Lemercier-Neuillet, C.-M. Dhaenens, A. Vautrin, F. J. Fernandez-Gomez, L. Arandel, C. Carpentier, H. Obriot, S. Eddarkaoui, L. Delattre, E. Van Brussels, I. Holt, G. E. Morris, B. Sablonnière, L. Buée, N. Charlet-Berguerand, S. Schraen-Maschke, D. Furling, I. Behm-Ansmant, C. Branlant, M.-L. Caillet-Boudin, N. Sergeant, Analysis of Exonic Regions Involved in Nuclear Localization, Splicing Activity, and Dimerization of Muscleblind-like-1 Isoforms. *J Biol Chem* **286**, 16435–16446 (2011).

43. G. Dp, C. La, B. Ja, Autoregulated splicing of muscleblind-like 1 (MBNL1) Pre-mRNA. *The Journal of biological chemistry* **286** (2011).

44. L. M. André, R. T. P. van Cruchten, M. Willemse, D. G. Wansink, (CTG)n repeat-mediated dysregulation of MBNL1 and MBNL2 expression during myogenesis in DM1 occurs already at the myoblast stage. *PLoS One* **14**, e0217317 (2019).

45. A. Ballester-Lopez, J. Núñez-Manchón, E. Koehorst, I. Linares-Pardo, M. Almendrote, G. Lucente, N. Guanyabens, M. Lopez-Osias, A. Suárez-Mesa, S. A. Hanick, J. Chojnacki, A. Lucia, G. Pintos-Morell, J. Coll-Cantí, A. Martínez-Piñeiro, A. Ramos-Fransi, G. Nogales-Gadea, Three-dimensional imaging in myotonic dystrophy type 1: Linking molecular alterations with disease phenotype. *Neurol Genet* **6**, e484 (2020).

46. N. El Boujnouni, M. L. van der Bent, M. Willemse, P. A. C. 't Hoen, R. Brock, D. G. Wansink, Block or degrade? Balancing on- and off-target effects of antisense strategies against transcripts with expanded triplet repeats in DM1. *Mol Ther Nucleic Acids* **32**, 622–636 (2023).

47. S. Salvatori, M. Fanin, C. P. Trevisan, S. Furlan, S. Reddy, J. I. Nagy, C. Angelini, Decreased expression of DMPK: correlation with CTG repeat expansion and fibre type composition in myotonic dystrophy type 1. *Neurol Sci* **26**, 235–42 (2005).

48. A. Gudde, I. D. G. van Kessel, L. M. André, B. Wieringa, D. G. Wansink, Trinucleotide-repeat expanded and normal DMPK transcripts contain unusually long poly(A) tails despite differential nuclear residence. *Biochim Biophys Acta Gene Regul Mech* **1860**, 740–749 (2017).

49. E. T. Wang, D. Treacy, K. Eichinger, A. Struck, J. Estabrook, H. Olafson, T. T. Wang, K. Bhatt, T. Westbrook, S. Sedehizadeh, A. Ward, J. Day, D. Brook, J. A. Berglund, T. Cooper, D. Housman, C. Thornton, C. Burge, Transcriptome alterations in myotonic dystrophy skeletal muscle and heart. *Hum Mol Genet* **28**, 1312–1321 (2019).

50. M. Nakamori, K. Sobczak, A. Puwanant, S. Welle, K. Eichinger, S. Pandya, J. Dekdebrun, C. R. Heatwole, M. P. McDermott, T. Chen, M. Cline, R. Tawil, R. J.

Osborne, T. M. Wheeler, M. S. Swanson, R. T. Moxley, C. A. Thornton, Splicing biomarkers of disease severity in myotonic dystrophy. *Ann Neurol* **74**, 862–72 (2013).

51. D. P. Gates, L. A. Coonrod, J. A. Berglund, Autoregulated splicing of muscleblind-like 1 (MBNL1) Pre-mRNA. *J Biol Chem* **286**, 34224–33 (2011).

52. C. Fugier, A. F. Klein, C. Hammer, S. Vassilopoulos, Y. Ivarsson, A. Toussaint, V. Tosch, A. Vignaud, A. Ferry, N. Messaddeq, Y. Kokunai, R. Tsuburaya, P. de la Grange, D. Dembele, V. Francois, G. Precigout, C. Boulade-Ladame, M. C. Hummel, A. Lopez de Munain, N. Sergeant, A. Laquerrière, C. Thibault, F. Deryckere, D. Auboeuf, L. Garcia, P. Zimmermann, B. Udd, B. Schoser, M. P. Takahashi, I. Nishino, G. Bassez, J. Laporte, D. Furling, N. Charlet-Berguerand, Misregulated alternative splicing of BIN1 is associated with T tubule alterations and muscle weakness in myotonic dystrophy. *Nat Med* **17**, 720–5 (2011).

53. I. Prokic, B. S. Cowling, C. Kutchukian, C. Kretz, H. Tasfaout, V. Gache, J. Hergueux, O. Wendling, A. Ferry, A. Toussaint, C. Gavriilidis, V. Nattarayan, C. Koch, J. Lainé, R. Combe, L. Tiret, V. Jacquemond, F. Pilot-Storck, J. Laporte, Differential physiological roles for BIN1 isoforms in skeletal muscle development, function and regeneration. *Dis Model Mech* **13** (2020).

54. M. Koshelev, S. Sarma, R. E. Price, X. H. Wehrens, T. A. Cooper, Heart-specific overexpression of CUGBP1 reproduces functional and molecular abnormalities of myotonic dystrophy type 1. *Hum Mol Genet* **19**, 1066–75 (2010).

55. D. Laustriat, J. Gide, L. Barrault, E. Chautard, C. Benoit, D. Auboeuf, A. Boland, C. Battail, F. Artiguenave, J. F. Deleuze, P. Bénit, P. Rustin, S. Franc, G. Charpentier, D. Furling, G. Bassez, X. Nissan, C. Martinat, M. Peschanski, S. Baghdoyan, In Vitro and In Vivo Modulation of Alternative Splicing by the Biguanide Metformin. *Mol Ther Nucleic Acids* **4**, e262 (2015).

56. L. Arandel, M. Polay Espinoza, M. Matloka, A. Bazinet, D. De Dea Diniz, N. Naouar, F. Rau, A. Jollet, F. Edom-Vovard, K. Mamchaoui, M. Tarnopolsky, J. Puymirat, C. Battail, A. Boland, J. F. Deleuze, V. Mouly, A. F. Klein, D. Furling, Immortalized human myotonic dystrophy muscle cell lines to assess therapeutic compounds. *Dis Model Mech* **10**, 487–497 (2017).

57. M. Sabater-Arcis, A. Bargiela, N. Moreno, J. Poyatos-Garcia, J. J. Vilchez, R. Artero, Musashi-2 contributes to myotonic dystrophy muscle dysfunction by promoting excessive autophagy through miR-7 biogenesis repression. *Mol Ther Nucleic Acids* **25**, 652–667 (2021).

58. X. Fernández-Garibay, M. A. Ortega, E. Cerro-Herreros, J. Comelles, E. Martínez, R. Artero, J. M. Fernández-Costa, J. Ramón-Azcón, Bioengineeredin vitro3D model of myotonic dystrophy type 1 human skeletal muscle. *Biofabrication* **13** (2021).

59. E. Loro, F. Rinaldi, A. Malena, E. Masiero, G. Novelli, C. Angelini, V. Romeo, M. Sandri, A. Botta, L. Vergani, Normal myogenesis and increased apoptosis in myotonic dystrophy type-1 muscle cells. *Cell Death Differ* **17**, 1315–1324 (2010).

60. J. D. Amack, M. S. Mahadevan, Myogenic defects in myotonic dystrophy. *Dev Biol* **265**, 294–301 (2004).

61. F. Rinaldi, C. Terracciano, V. Pisani, R. Massa, E. Loro, L. Vergani, S. Di Girolamo, C. Angelini, G. Gourdon, G. Novelli, A. Botta, Aberrant splicing and expression of the non muscle myosin heavy-chain gene MYH14 in DM1 muscle tissues. *Neurobiology of Disease* **45**, 264–271 (2012).

62. D. Furling, L. Coiffier, V. Mouly, J. P. Barbet, J. L. St Guily, K. Taneja, G. Gourdon, C. Junien, G. S. Butler-Browne, Defective satellite cells in congenital myotonic dystrophy. *Hum Mol Genet* **10**, 2079–87 (2001).

63. W. Dansithong, S. Paul, L. Comai, S. Reddy, MBNL1 is the primary determinant of focus formation and aberrant insulin receptor splicing in DM1. *J Biol Chem* **280**, 5773–80 (2005).

64. A. Bigot, A. F. Klein, E. Gasnier, V. Jacquemin, P. Ravassard, G. Butler-Browne, V. Mouly, D. Furling, Large CTG repeats trigger p16-dependent premature senescence in myotonic dystrophy type 1 muscle precursor cells. *The American journal of pathology* **174**, 1435–1442 (2009).

65. V. François, A. F. Klein, C. Beley, A. Jollet, C. Lemercier, L. Garcia, D. Furling, Selective silencing of mutated mRNAs in DM1 by using modified hU7-snRNAs. *Nat Struct Mol Biol* **18**, 85–7 (2011).

66. A. Botta, A. Malena, E. Loro, G. Del Moro, M. Suman, B. Pantic, G. Szabadkai, L. Vergani, Altered Ca2+ homeostasis and endoplasmic reticulum stress in myotonic dystrophy type 1 muscle cells. *Genes* **4**, 275–292 (2013).

67. M. Sabater-Arcis, A. Bargiela, D. Furling, R. Artero, miR-7 Restores Phenotypes in Myotonic Dystrophy Muscle Cells by Repressing Hyperactivated Autophagy. *Mol Ther Nucleic Acids* **19**, 278–292 (2020).

68. V. Todorow, S. Hintze, A. R. W. Kerr, A. Hehr, B. Schoser, P. Meinke, Transcriptome Analysis in a Primary Human Muscle Cell Differentiation Model for Myotonic Dystrophy Type 1. *Int J Mol Sci* **22** (2021).

69. Y.-H. Jiang, Y.-Y. Man, Y. Liu, C.-J. Yin, J.-L. Li, H.-C. Shi, H. Zhao, S.-G. Zhao, Loss of miR-23b/27b/24-1 Cluster Impairs Glucose Tolerance via Glycolysis Pathway in Mice. *Int J Mol Sci* **22**, 550 (2021).

70. Dyne Therapeutics Announces Positive Initial Clinical Data from ACHIEVE Trial in DM1 Patients and DELIVER Trial in DMD Patients Demonstrating Promise of the FORCE™ Platform in Developing Therapeutics for Rare Muscle Diseases | Dyne Therapeutics, Inc. https://investors.dyne-tx.com/news-releases/news-release-details/dyne-therapeutics-announces-positive-initial-clinical-data/.

71. K. Jones, C. Wei, P. Iakova, E. Bugiardini, C. Schneider-Gold, G. Meola, J. Woodgett, J. Killian, N. A. Timchenko, L. T. Timchenko, GSK3β mediates muscle pathology in myotonic dystrophy. *J Clin Invest* **122**, 4461–72 (2012).

72. L. Witherspoon, S. O'Reilly, J. Hadwen, N. Tasnim, A. MacKenzie, F. Farooq, Sodium Channel Inhibitors Reduce DMPK mRNA and Protein. *Clin Transl Sci* **8**, 298–304 (2015).

73. Y. Kino, C. Washizu, M. Kurosawa, Y. Oma, N. Hattori, S. Ishiura, N. Nukina, Nuclear localization of MBNL1: splicing-mediated autoregulation and repression of repeat-derived aberrant proteins. *Hum Mol Genet* **24**, 740–56 (2015).

74. F. Terenzi, A. N. Ladd, Conserved developmental alternative splicing of muscleblind-like (MBNL) transcripts regulates MBNL localization and activity. *RNA Biol* **7**, 43–55 (2010).

75. X. Xing, R. Markus, T. Ghosh, S. Buxton, D. J. Nieves, M. Wojciechowska, J. D. Brook, Regulation of Toxic RNA Foci and Mutant DMPK Transcripts: Role of MBNL Proteins and RNA Decay Pathways. bioRxiv [Preprint] (2023). https://doi.org/10.1101/2023.09.28.559487.

76. E. Koscianska, T. M. Witkos, E. Kozlowska, M. Wojciechowska, W. J. Krzyzosiak, Cooperation meets competition in microRNA-mediated DMPK transcript regulation. *Nucleic Acids Res* **43**, 9500–9518 (2015).

77. J. Stenvang, A. Petri, M. Lindow, S. Obad, S. Kauppinen, Inhibition of microRNA function by antimiR oligonucleotides. *Silence* **3**, 1 (2012).

78. E. Koehorst, J. Núñez-Manchón, A. Ballester-López, M. Almendrote, G. Lucente, A. Arbex, J. Chojnacki, R. P. Vázquez-Manrique, A. P. Gómez-Escribano, G. Pintos-Morell, J. Coll-Cantí, A. Ramos-Fransi, A. Martínez-Piñeiro, M. Suelves, G. Nogales-Gadea, Characterization of RAN Translation and Antisense Transcription in Primary Cell Cultures of Patients with Myotonic Dystrophy Type 1. *J Clin Med* **10** (2021).

79. K. T. Gagnon, L. Li, B. A. Janowski, D. R. Corey, Analysis of nuclear RNA interference in human cells by subcellular fractionation and Argonaute loading. *Nat Protoc* **9**, 2045–2060 (2014).

80. K.-T. Lin, A. R. Krainer, PSI-Sigma: a comprehensive splicing-detection method for short-read and long-read RNA-seq analysis. *Bioinformatics* **35**, 5048–5054 (2019).

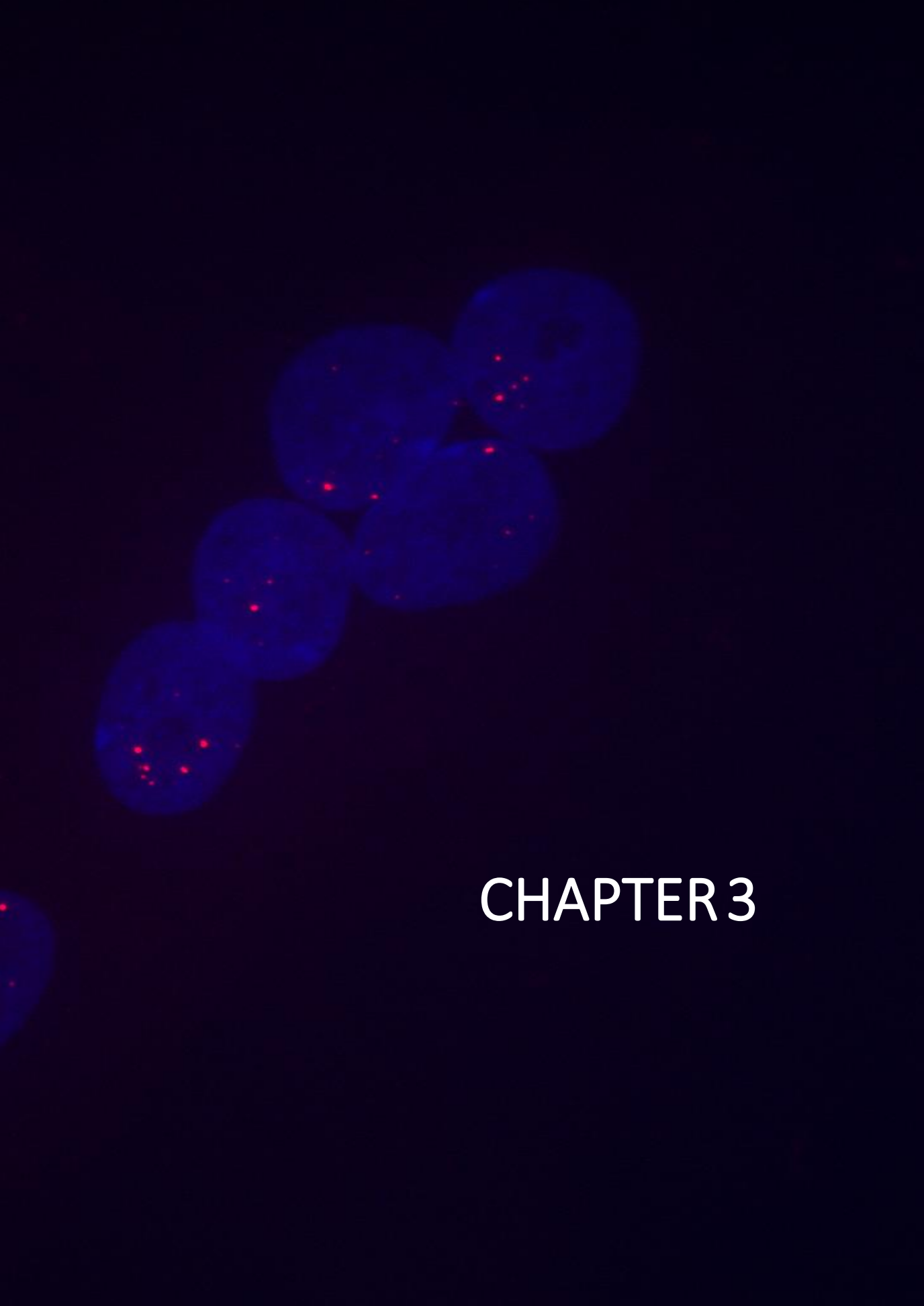

CHAPTER 3

Immortalized human myotonic dystrophy type 1 muscle cell lines to address patient heterogeneity

Judit Núñez-Manchón[1], Júlia Capó[1], Alicia Martínez-Piñeiro[1,2], Eduard Juanola[1,2], Jovan Pesovic[3], Laura Mosqueira-Martín[4], Klaudia González-Imaz[4], Pau Maestre-Mora[1], Renato Odria[1], Dusanka Savic-Pavicevic[3], Ainara Vallejo-Illarramendi[4], Kamel Mamchaoui[5], Anne Bigot[5], Vincent Mouly[5], Mònica Suelves[1*], Gisela Nogales-Gadea[1*]

[1]Grup de REcerca Neuromuscular de BAdalona (GRENBA), Institut d'Investigació en Ciències de la Salut Germans Trias i Pujol (IGTP), Campus Can Ruti, Universitat Autònoma de Barcelona, 08916 Badalona, Spain.

[2]Neuromuscular Pathology Unit, Neurology Service, Neuroscience Department, Hospital Universitari Germans Trias i Pujol, 08916 Badalona, Spain.

[3]University of Belgrade - Faculty of Biology, Center for Human Molecular Genetics, Belgrade, Serbia

[4]Group of Neurosciences, Department of Pediatrics, UPV/EHU, Hospital Universitario Donostia - IIS Biodonostia, 20014 San Sebastian, Spain

[5] Sorbonne Université, Inserm, Institut de Myologie, Centre de Recherche en Myologie, F-75013 Paris, France.

*Equally contributed

Corresponding author: Gisela Nogales-Gadea, Grup de REcerca Neuromuscular de Badalona (GRENBA), Institut d'Investigació en Ciències de la Salut Germans Trias i Pujol. Ctra. de Can Ruti. Camí de les Escoles, s/n 08916 Badalona (Barcelona), Spain. Tel.: +34 93 4978684; e-mail address: gnogales@igtp.cat ORCID: 0000-0002-7414-212X

This chapter was published in iScience journal the 21st of June 2024. A copy of the manuscript can be found in Appendix 1.

Abstract

Historically, cellular models have been used as a tool to study myotonic dystrophy type 1 (DM1) and the validation of therapies in said pathology. However, there is a need for in vitro models that represent the clinical heterogeneity observed in DM1 patients lacking in classical models. In this study, we immortalized three DM1 muscle lines derived from patients with different DM1 subtypes and clinical backgrounds, and characterized them at the genetic, epigenetic, and molecular levels. All three cell lines display DM1 hallmarks, such as accumulation of RNA foci, MBNL1 sequestration, splicing alterations, and reduced fusion. In addition, alterations in early myogenic markers, myotube diameter and CTCF1 DNA methylation were also found in DM1 cells. Notably, the new lines show a high level of heterogeneity in both the size of the CTG expansion and the aforementioned molecular alterations. Importantly, these immortalized cells also responded to previously tested therapeutics. Altogether, our results show that these three human DM1 cellular models are suitable to study the pathophysiological heterogeneity of DM1 and to test future therapeutic options.

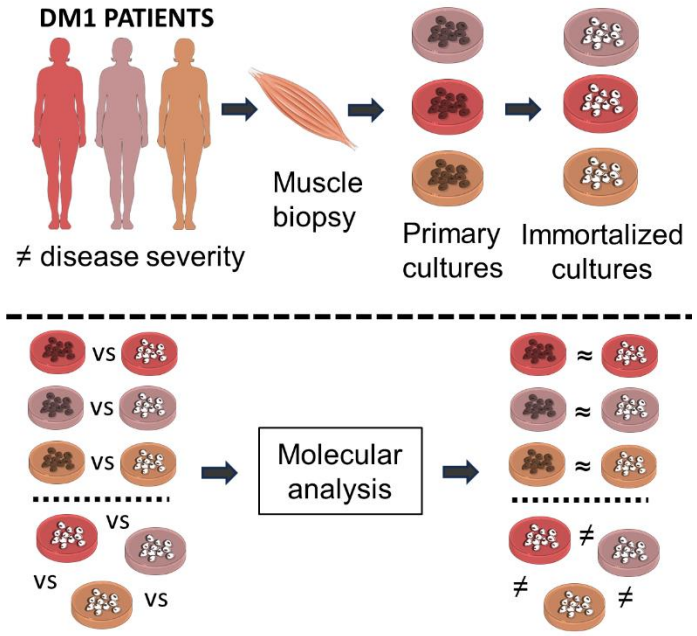

Introduction

Myotonic dystrophy type 1 (DM1) is an autosomal dominant multisystemic disease caused by a CTG expansion in the 3' untranslated region of the myotonic dystrophy protein kinase (*DMPK*) gene. It is the most prevalent muscular dystrophy in adults affecting 1 in 8000. It causes a variety of symptoms that include, but are not limited to: muscle weakness, myotonia, cardiac defects, respiratory failure, endocrine alterations such as diabetes, and cognitive impairment. The presence of these symptoms and their severity differs between patients. They can appear at any age and there is an earlier onset of clinical manifestations in successive generations, which is known as genetic anticipation. According to the age of onset, DM1 patients can be classified as congenital, childhood, juvenile, adult or late-onset. An earlier age of onset is associated with a greater disease severity and higher CTG expansion sizes[1].

The CTG expansion length varies in the range between 50 and thousands of repeats[2] and it has a high degree of instability biased towards expansions in germline and somatic cells. Therefore, the size of the CTG repeat increases over generations in affected pedigrees and through a patients' life[3–5]. Moreover, DM1 patients present somatic mosaicism in CTG expansion length between different tissues and cell types[6,7]. Altogether, this results in patients presenting heterogeneity at the genetic level, which makes it extremely challenging to determine a precise expansion size for each patient[8]. Currently, CTG expansion size can be determined by small pool PCR which allows researchers to analyse trinucleotide repeat instability[9] in a quantitative manner, detecting common and low abundant CTG sizes in a pool of cells. This technique allows characterization of the CTG expansion dynamics of this highly unstable repeat expansion.

Epigenetics may have a role in DM1, as the CTG expansion overlaps with a 3.5 kb CpG island[10–13]. The *DMPK* gene is in chromosome 19q surrounded by the *DMWD* (upstream) and *SIX5* (downstream) genes. The *DMPK* locus contains several CpG islands, including the CTCF1 and CTCF2 regions, which are surrounding the CTG expansion. In the case of CTCF1, aberrant methylation patterns have been described by other labs and by ours. For example, DM1 muscle and muscle derived DM1 cells show CTCF1 hypermethylation compared to controls; while blood samples from congenital cases show CTCF1 hypermethylation compared to controls and adult DM1 cases[12,14,15]. However,

it is not clear how hypermethylation of this CpG island contributes to the pathogenesis of the disease, although it has been reported that *DMPK* and the surrounding genes (*DMWD* and *SIX5*) are downregulated in DM1[16,17].

It has been demonstrated that RNA gain of function[18,19] is the main molecular pathology mechanism in DM1. *DMPK* transcripts containing the CTG expansion accumulate,[20] form hairpin structures[21] and agglomerate in the nucleus. These agglomerations receive the name of RNA foci, whose quantity varies between cells, and patient tissues[20]. We and others have found correlation between RNA foci formation and CTG expansion size, and RNA foci formation and age of onset[22,23]. It is known that foci can bind to important cellular proteins, such as the splicing regulator, muscleblind-like 1 (MBNL1)[24]. MBNL1 sequestration and downregulation causes the aberrant splicing of several genes, including insulin receptor (*INSR*)[25], sarcoplasmic reticulum Ca(2+)-ATPase 1 (*ATP2A1*)[26], LIM Domain Binding 3 (*LDB3*)[27], dystrophin (*DMD*)[28], bridging Integrator 1 (*BIN1*)[29], and *MBNL1* (which regulates its own splicing)[30]. Some splicing alterations are tightly connected with some of the symptoms that DM1 patients present: *INSR* is associated with insulin resistance[31], *BIN1* with muscle weakness[32], *LDB3* with sudden cardiac death[33] and *ATP2A1* and *DMD* with muscle regeneration[34,35].

Cellular DM1 models have proven to be a valuable tool for studying the molecular aspects of diseases and for evaluating the efficacy of potential treatments[36,37]. Nowadays, different cellular models have been developed for studying DM1, each with their own pros and cons[38]. Among them, we have cell lines with artificial expressions of exogenous CTG repeats and patient derived cell lines[39]. Cells artificially expressing CTGs, even though they reproduce the hallmarks of the disease[25,39], lack the genetic context of the *DMPK* gene, including its regulation by the gene promoter and the expression alterations of adjacent genes (*DMWD* and *SIX5*). This inconvenience is overcome in the patient derived cell lines, which can be either primary or immortalized cells. Primary cells are obtained from patient biopsies. The most frequently used are skin fibroblasts, because they are easier to obtain, and myoblasts, as muscle is one of the main affected tissues in DM1, which can fuse into myotubes. However, primary cultures have limitations in the number and type of experiments that can be performed because they have a reduced number of divisions, and it is ethically controversial to take biopsies from DM1 patients. Since skin biopsies are more accessible, skin fibroblasts can be transdifferentiated into myoblasts by *MYOD1* transduction[31]. However, it has been shown that the transdifferentiation does not lead to full muscle cell

reprogramming[40]. Another strategy consists in the reprogramming of patient cells into iPSCs[41]. This approach offers the advantage of differentiating iPSCs into any type of cell, including those located in tissues where biopsies are not feasible, such as cardiomyocytes or neurons which are also affected in DM1[42]. The downsides of iPSCs include a highly unstable CTG repeat during reprogramming, incomplete cell maturation, and high maintenance cost. To resolve these problems, immortalized muscle patient cells were developed by inserting lentiviral vectors expressing the catalytic subunit of human telomerase (*TERT*), cyclin-dependent kinase 4 (*CDK4*), and cyclin D1 (*CCND1*)[38]. With these changes, cells can divide an unlimited number of times, thus diminishing the need to perform muscle biopsies and allowing the execution of experiments that need a high cell number. Nonetheless, it still needs to be proven that the insertion of these transgenes does not produce alterations in cellular behaviour[43]. To date, there are only three reports in which four myoblast patient derived cell lines have been generated[44–46].

In this work we have immortalized and characterized three DM1 muscle cell lines from adult DM1 patients that belonged to the juvenile, adult and late onset DM1 subtypes. These patients were clinically heterogeneous in their symptomatology, which is demonstrated by their muscle, heart, and lung pathologies. The immortalized muscle cell models were also heterogeneous in their molecular alterations, but they presented similar alterations to the parental cells from which they were derived. Notably, antisense oligonucleotide treatment rescued a substantial portion of the molecular alterations in these models. In conclusion, the three models generated are adequate models to address the heterogeneity in DM1 and to analyse genetic, epigenetic, transcriptomic and proteomic alterations, cellular functions, and response to therapies in a more diverse way.

Material and methods

Sample collection and patient characterization

This study was approved by the Ethics Committee of the University Hospital Germans Trias i Pujol and was performed in accordance with the Declaration of Helsinki for Human Research. Written informed consent was obtained from all participants. Three genetically confirmed DM1 patients with different clinical features aged 36, 39 and 42 were selected to perform the immortalization of biopsy-derived primary myoblasts. The biopsies from the patients were obtained from left biceps. Two different types of controls,

obtained from different individuals, were used: primary controls, whose biopsies were obtained from intrinsic hand muscles and immortalized controls that were obtained from healthy individuals quadriceps (AB678, AB1079) and paravertebral muscles (KM1412). Clinical information of DM1 patients was obtained from medical records.

Cell culture and immortalization

Primary myoblasts were isolated from muscle biopsy explants on culture plates treated with human plasma and gelatin 1.5% and then purified by CD56 magnetic separation according to manufacturer's instructions (Miltenyi Biotec; Bergisch Gladbach). Primary myoblasts were grown on 0.1% gelatin-coated flasks in proliferation medium containing Dulbecco's Modified Eagle's Medium (DMEM) supplemented with 10% FBS, 22% M-199, PSF 1x, 10 µg/ml insulin, L-glutamine 2 mM, 25 ng/ml FGF and 5 ng/ml EGF. At 80-90% confluence proliferation medium was substituted by differentiation medium containing DMEM supplemented with 2% FBS, 22% M-199, PSF 1x, 10 µg/ml insulin and L-glutamine 2 mM. For immortalization, 50.000 primary myoblasts were transduced with hTERT and Cdk4 lentiviral vectors with a MOI of 3 in the presence of 4 µg/ml of polybrene (Sigma-Aldrich) overnight. 48h after, transduced cell cultures were selected with puromycin (1 µg/ml, LifeTechnologies) for 6 days and neomycin (0.1 mg/ml, Life Technologies) for 10 days. Cells were then seeded at clonal density (2 cells per cm2) for 10 days. Selected individual myogenic clones were isolated from each population, using glass cylinders, and their proliferation and differentiation capacities were evaluated. We selected clones which were able to proliferate and to differentiate correctly (we tested their ability to differentiate into myotubes, using immunostaining with MF20 antibody, which recognizes all skeletal-muscle myosin heavy chains (MyHCs). We removed the non-myogenic clones[83]. Immortalized myoblasts were grown on uncoated flasks in proliferation medium containing DMEM supplemented with 16% M-199, 20% FBS, Gentamycin 50 µg/ml, fetuin 25 µg/ml, hEGF 5 ng/ml, bFGF 0,5 ng/ml, Insulin 5 µg/ml and dexamethasone 0,2 µg/ml. For differentiation experiments cells were grown in 1:100 matrigel matrix (Corning) coated surfaces until 80-90% confluence. Proliferation medium was substituted by differentiation medium containing DMEM supplemented with 10 µg/ml of insulin and 50 µg/ml Gentamycin. Both primary and immortalized myoblasts were differentiated into myotubes for 5 or 9 days, depending on the experiment. Pellets for RNA and DNA analysis were collected and coverslips for FISH and ICC were fixed with 4% PFA and permeabilized with 0.3% triton. We

performed a STR variant analysis of 16 loci for cell authentication purposes. Mycoplasma test was performed both before and after the immortalization and it turned out negative for all the cell lines.

CTG expansion sizing

DNA from the primary and immortalized myotube cultures was extracted using the PureLink Genomic DNA Mini Kit (Invitrogen) according to the manufacturer's instructions. To determine CTG expansion size we performed a small-pool PCR from EcoRI digested DNA followed by Southern blotting. The PCR was performed with 5 ng of digested DNA, using Expand™ Long Template PCR System (Roche) and primers 102 (5'-GAACGGGGCTCGAAGGGTCCTTGTAGC-3') and 101 (5'-CTTCCCAGGCCTGCAGTTTGCCCATC-3'). The conditions of the PCR were divided in four steps: 1) 3' at 96°C. 2) 30'' at 65°C followed by 3' at 68°C and 30'' at 95°C for 10 cycles. 3) 30'' at 65°C followed by 3' at 68°C, which increase the duration 30'' each cycle and 30'' at 95°C for 15 cycles. 4) 1' at 65°C and 8' at 68°C. PCR products were run in an agarose gel (Serva) ON at 4°C and transferred into a nylon membrane. The membrane is cross-linked and incubated with a DIG-labelled $(CAG)_7$ LNA probe at 65ºC for 2 hours. The membrane is finally developed using anti-DIG alkaline phosphatase and CDP-star (Roche) according to the manufacturer's instructions. The progenital and modal alleles of each culture were estimated through comparison against the molecular weight ladder GeneRuler 1Kb (ThermoScientific) using GelAnalyzer 19.1 software. The progenital allele length was estimated as the 10^{th} percentile of allele frequency distribution. The modal allele length was determined as the most frequent allele. The level of somatic instability was calculated by subtracting the 10^{th} percentile from the 90^{th} percentile.

DNA Methylation analysis

DNA was bisulphite converted using the EZ DNA Methylation Gold kit (Zymo Research), according to the manufacturer's protocol. Bisulphite-converted DNA was amplified by nested PCR for the CTCF1 region (located upstream of the CTG repeat in the *DMPK* gene) with the TaKaRa Taq DNA polymerase (TaKaRa Bio Inc.). For the first PCR, 50 ng of bisulphite-converted DNA were used, while for the second PCR 3 µl of the first PCR product were used. Primers sequences were the following: CTCF1 F1 5'-TGTYGTYGTTTTGGGTTGTATTG-3', CTCF1 R1 5'-TTCCYGACTACAAAAACCCTTYG-3', CTCF1 F2 5'-GTTGTATTGGGTTGGTGGTTTA-3', CTCF1 R2 5'-CTACAAAAACCCTTYGAACCC-3'. PCR conditions for both amplifications were: 5 min of initial denaturation at 94

°C, 40 cycles of 30 s denaturation at 94 °C, 30 s annealing at 57 °C, and 30 s of extension at 72 °C and a final extension of 5 min at 72 °C. Amplicons were purified using Illustra™ ExoProStar 1-Step (Merck), according to the manufacturer's instructions. Purified products were sequenced using the BigDye Terminator v3.1 cycle sequencing kit (Thermo Fisher Scientific), following the manufacturer's guidelines. Sequencing products were run on an ABI Prism 3130 Genetic Analyzer (Applied Biosystems) and were analysed with Chromas software version 2.6.6. The data obtained was represented with the Methylation Plotter web tool[84].

Expression analysis by qPCR

RNA was extracted from 5 days differentiated myotubes using PureLink RNA Mini Kit (Invitrogen) according to the manufacturer's instructions. 500ng of RNA was retrotranscribed using SuperScript IV reverse transcriptase (Thermo Fisher Scientific). cDNA was amplified by qPCR in a LightCycler 480 using the Lightcycler 480 SYBR Green I Master (Roche). The primers used are listed in Supplementary table 1. Amplification consisted of 40 cycles with the following conditions: 10 seconds at 95 °C for denaturation, 10 seconds at 65 °C for annealing and 15 seconds at 72 °C for extension. Results were analyzed with the LightCycler 480 software.

Impedance measurements

Real-time impedance measurements were used for addressing myogenic behaviour of control and DM1 immortalized human myoblasts, by using the Maestro Edge equipment with the impedance module (Axion BioSystems). Prior to cell seeding, Cytoview Z 96-well plates (Axion BioSystems) were overlaid with 100 µL of culture media and placed into the Maestro Edge to record baseline readings of the background impedance without cells. Afterwards, myoblasts were seeded on the plates at 20,000 cells per well and left 1 hour at room temperature to ensure homogeneous distribution of cells. Impedance was measured every minute at 41.5 kHz for the entire duration of cell culture, by the exposure of cells to small electrical currents delivered by electrodes on the plate surface. Cells were kept at 37 °C and 5% CO2 inside the Maestro Edge throughout the experiment for impedance recording. Impedance data (resistance in ohms) was obtained with the AxIS Z software. Cells were grown in Skeletal Muscle Cell growth medium (SGM, PeloBiotech) and differentiated. First in basic differentiation media (bDM) and then in complete differentiation media (cDM), which includes different growth factors

and extracellular matrix proteins to promote high myotube maturation (Toral-Ojeda et al., 2018, Lasa-Elgarresta et al., 2022).

Jess Western blot

RIPA lysis buffer (50mM Tris-HCl pH 7.2, NaCl 0.9%, NP40 1%, EGTA 1mM, EDTA 1mM) with proteinase and phosphatase inhibitor cocktails (Thermo Fisher Scientific) and Cell-permeable inhibitor of calpain I, calpain II, cathepsin B and cathepsin L (Merck) was used to extract proteins. A Bovine Serum Albumin (BSA) concentration curve was used to quantify protein. Reagents and equipment for Jess Western blotting were all purchased from Protein Simple. Cell lysates were diluted at a final concentration of 0.5ug/ul with 0.1X sample buffer. 5X Fluorescent Master Mix was added to each sample at a 4:1 ratio (final concentrations of 1% (v/v) SDS and 40 mM DTT) and samples were incubated at 95 °C for 5 min. 3 microliters of each sample were loaded into the cartridge. Subsequent rows of the plate were filled with blocking buffer (antibody diluent 2), primary and secondary antibody solutions, chemiluminescence reagents, and wash buffer according to the manufacturer's instructions. Previously optimized primary antibodies were diluted in antibody diluent at different ratios (1:10 MyoD Antibody (C-20): sc-304, 1:10 sc-12732 - myogenin (F5D), 1:10 Myf-5 (C-20): sc-302), followed by HRP-conjugated secondary antibodies. Finally, the plate was spun down for 5 min at 1000xg. Plates and capillaries were loaded into a Jess machine, and assays were carried out using the standard 12- to 230-kDa or 66-440kDa separation range protocol. Compass reports data as spectra of chemiluminescence signals versus apparent MW by assigning ladder peaks to capillary positions. Peak area calculations were performed using the Gaussian method.

Fluorescence in situ hybridization (FISH) and immunocytochemistry (ICC)

ICC was performed on fixed and permeabilized cell coverslips. They were blocked (PBS triton 0,1% with 1% BSA and 1% horse serum) and incubated with anti-MBNL1 (1:200, MB1a(4A8), DSHB) or anti-desmin (1:50, D33, Abcam) overnight at 4 °C. Next, the coverslips were washed with PBS-T and cells were then incubated with biotinylated horse anti-mouse-IgG (1:150, Vector) for 1 hour at RT. Elite ABC kit (VECTASTAIN) was used for 30' at RT to amplify the signal, followed by some PBS-T washes and a 2-hour incubation at RT with streptavidin-FITC (1:200, Vector). In the anti-MBNL1 incubated cells we subsequently performed FISH. For that, the cells were washed and incubated with acetylation buffer (1.16% triethanolamine, 0.25% acetic anhydride) for 10

m at RT. After pre-hybridization (SSC2X, 30% formamide) the cells were incubated with 1 µM Cy3-labelled (CAG)10 probe diluted 1:100 in hybridization buffer (40% formamide, 2x SSC, 0,2% BSA, dextransulfate 100mg/ml, vanadyl 2Mm, tRNA 1ug/ml, herring sperm 1mg/ml) for 2 hours at 37 °C. Finally, the coverslips were washed and mounted in slides with Diamond Anti-Fade mounting medium with DAPI (Thermo Fisher Scientific). Images were taken with Zeiss AxioObserver Z1 microscope at 63x and analysed with ZEN blue software and Image J.

Splicing analysis

Total RNA from primary and immortalized myotube cultures was extracted with the PureLink RNA Mini Kit (Invitrogen) according to the manufacturer's instructions. 500 ng of RNA was retrotranscribed to cDNA using SuperScript IV Reverse Transcriptase (Invitrogen) according to the manufacturer's protocol. One microliter of cDNA was used for the subsequent PCRs to analyse splicing alterations. Primers and PCR conditions are described in Supplementary table 2.

Treatment

To study treatment effect in the immortalized cell lines, we differentiated both primary and immortalized myoblasts into myotubes. On differentiation day 7 we added an antisense oligonucleotide (ASO), targeting the expansion repeat, for 48 hours. The ASO used was a BNA^{NC} gapmer with the sequence AGCagcagcagCAG (Bio-Synthesis) in which capital letters mean BNA^{NC} modifications. The ASO concentration used was 30 nM.[48] Transfection was performed in differentiation media containing 0.2% lipofectamine 2000 (Thermo Fisher Scientific) and 25% Opti-Mem (Gibco).

Statistical analysis

Statistical analysis was performed with GraphPad Prism 8 software. Normality was determined with ShapiroWilk test. T-test or Mann-Whitney test were used for two-group comparison analysis while one-way ANOVA with Dunn's post-test or Kruskal-Wallis test was used for comparison analysis between the three cell lines. *$p \leq 0.05$, **$p \leq 0.01$, ***$p \leq 0.001$, ****$p \leq 0.0001$.

Results

Immortalization of muscle cells derived from DM1 patients with clinical heterogeneity

In this study, we have immortalized myoblasts from 3 patients with DM1 showing different clinical manifestations and degrees of disability (Table 1). An STR variant analysis of 16 locus was performed for line authentication purposes and it confirmed that the immortalized and primary cell lines of each patient shared the same alleles (Table 2). The samples came from three female patients, ranging in age from 36 to 46 at the moment of sampling. Their ages of onset were 15, 27 and 42, placing them in the juvenile, adult and late onset DM1 subtypes, respectively. Muscular involvement was determined with the Medical Research Council (MCR) scale in both proximal and distal muscles. Patients JCC-DM1 and ADE-DM1 had moderate muscle involvement; they had an MRC score of 4 for proximal muscles and an MRC score of 3 for distal muscles. In contrast, GPM-DM1 had mild involvement with an MRC score of 5 for proximal muscles and an MRC score of 4 for distal muscles. Cardiac involvement was mild in patients JCC-DM1 and GPM1-DM1, while in ADE-DM1 it was severe. This patient needed a pacemaker after suffering several bouts of syncope and after being diagnosed with an elongated HV interval. Respiratory involvement was mild in ADE-DM1 who had a forced vital capacity (FVC) of 65%, moderate in JCC-DM1 who had an FVC of 58% and severe in GPM-DM1 who had a FVC of 50% and required mechanical ventilation. Finally, to determine their level of functionality, we used the modified Rankin scale (mRS), which determines DM1 patient's degree of disability and dependence in daily activities. GPM-DM1 had a mRS of 1, implying she did not present significant disability and was able to carry out usual activities. JCC-DM1 had a mRS of 2, implying she suffered a slight disability and even though she could live unassisted, she could not perform all the activities she performed previous to the onset of the disease. ADE-DM1 had a mRS of 4; implying she had a moderately severe disability and wasn't able to attend bodily functions or walk without assistance. Globally, ADE-DM1 was the most affected patient as she suffered from severe cardiac and functional involvement, as well as moderate muscular involvement. She is followed by JCC-DM1 in severity, who had moderate functional, muscular and respiratory involvement. Lastly, GPM-DM1 had mild involvement in all the parameters studied, except for respiratory function which was severely affected.

Table 1: General data and clinical characterization of the DM1 patients and controls.

SAMPLE	TYPE OF SAMPLE	AGE AT SAMPLING	GENDER	AGE OF ONSET	MUSCLE INVOLVEMENT	CARDIAC INVOLVEMENT	RESPIRATORY INVOLVEMENT	mRS	TYPE OF CELLS DERIVED
JCC-DM1	Patient	36	F	15	moderate	mild	moderate	2	Primary and immortalized
GPM-DM1	Patient	46	F	42	mild	mild	severe	1	Primary and immortalized
ADE-DM1	Patient	39	F	27	moderate	severe	mild	4	Primary and immortalized
C7	Control	66	F						Primary
C9	Control	41	M						Primary
C10	Control	26	M						Primary
AB678	Control	53	M						Immortalized
AB1079	Control	38	M						Immortalized
KM1421	Control	13	F						Immortalized

mRS: Modified Rankin Scale

Table 2: STR profiling of the patients from which the cells were isolated and immortalized.

Locus	Chromosome location	JCC-DM1	GPM-DM1	ADE-DM1
D8S1179	8	13	10, 14	12, 14
D21S11	21q11.2-21-22	31, 32.2	29, 32.2	30, 33.2
D7S820	7q11.21-22	8, 10	10, 11	10
CSF1PO	5q33.3-34	10, 11	10, 12	11, 13
D3S1358	3p	17, 18	17	16, 17
TH01	11p15.5	6	6	8, 9.3
D13S317	13q22-31	8, 10	11	11
D16S539	16q24-qter	12, 13	12	11
D2S1338	2q35-37.1	17, 19	19, 23	17
D19S433	19q12-13.1	13, 15	12, 13	14, 15
vWA	12p12-pter	14, 16	15, 18	16, 18
TPOX	2p23-2per	9, 11	8, 12	8
D18S51	16q21.3	12, 15	12, 14	14, 15
AMELOGENIN	X: p22.1-22.3 Y: p11.2	X	X	X
D5S818	5q21-31	11, 13	10, 12	11
FGA	4q28	20, 21	25, 26	21, 25

A high level of CTG repeats instability characterized all studied DM1 cell lines

CTG expansion was measured in primary and immortalized cell lines from the three DM1 patients by small pool PCR, which revealed highly heterogeneous CTG expansion patterns within each patient. We created density plots with the

results and calculated the estimated progenitor allele (ePAL), the size of the two main expanded populations, and the expansion instability observed in each cell line (Fig. 1A and Fig. 1B). Primary GPM-DM1 cells had an ePAL of 435 CTGs and showed two expanded main populations with 581 CTGs and 1028 CTGs, while in the immortalized cells the ePAL was 280 CTGs and the two most abundant populations had 379 and 863 CTGs, respectively. Primary JCC-DM1 cells had an ePAL of 663 CTGs and the average sizes of the two main expansion populations were 875 CTGs and 1950 CTG, while the ePAL in the immortalized cells was 654 CTGs, and the two main populations had a size of 953 CTGs and 2080 CTGs. Primary ADE-DM1 cells had an ePAL of 578 CTGs, and the highest expansion sizes of the most abundant populations (1505 CTG and 3075 CTG), while the immortalized cells, had an ePAL of 700 CTGs, and the two most abundant populations had a size of 1224 CTGs and 2301 CTGs. When analysing the expansion instability, GPM-DM1 had the lowest levels both in the primary and the immortalized cell lines, followed by JCC-DM1 and then ADE-DM1 (Fig.1B). All immortalized cell lines had some increase in expansion instability, which was between 6 and 25% of that observed in the parental cell lines, but the expansion instability pattern closely resembled the parental after the immortalization process. Interestingly, the larger the size of the most abundant CTG expansion and the greater degree of instability, the more severely affected the patient was. However, maybe due to small sample size, no significant correlation was found.

A

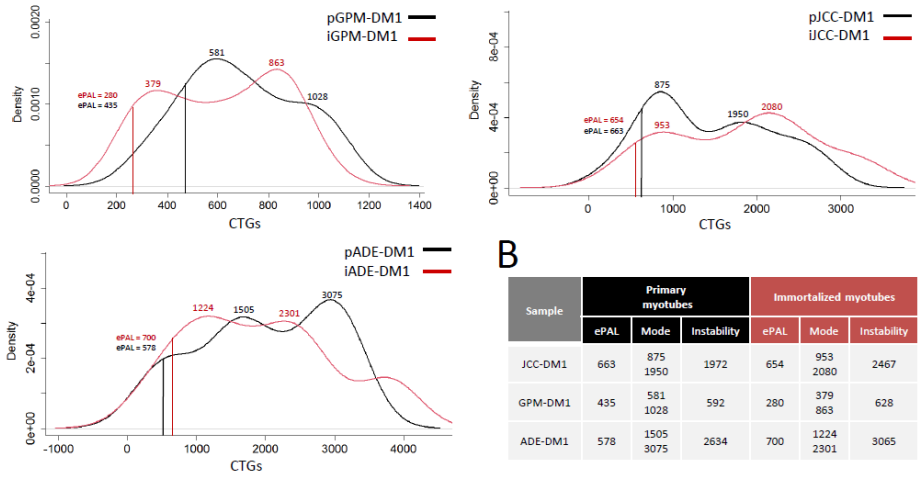

B

Sample	Primary myotubes			Immortalized myotubes		
	ePAL	Mode	Instability	ePAL	Mode	Instability
JCC-DM1	663	875 1950	1972	654	953 2080	2467
GPM-DM1	435	581 1028	592	280	379 863	628
ADE-DM1	578	1505 3075	2634	700	1224 2301	3065

Figure 1. CTG instability is similar between primary and immortalized DM1 cells lines. A. Density plots showing the distribution of the CTG alleles detected in both the primary (black) and immortalized (red) myotubes derived from the three patients participating in the study. We

measured between 41 and 105 alleles per sample. B. CTG expansion ePAL, mode and instability in primary and immortalized myotubes of the three DM1 patients participating in the study. The progenital allele length was estimated as the 10th percentile of allele frequency distribution. The modal allele length was determined as the most frequent allele. The level of somatic instability was calculated by subtracting the 10th percentile from the 90th percentile. “p” and “i” before cell line name mean primary and immortalized, respectively.

CTCF1 Methylation level is increased in the DM1 immortalized cell lines when compared with immortalized control cell lines as observed in primary cell lines

We analysed DNA methylation levels of the CTCF1 region, which is located upstream of the CTG expansion in the DMPK gene (Fig. 2A), in myoblasts and in 5 days differentiated myotubes derived from the primary and immortalized cell lines, in both controls and DM1 patients. There were significant differences in the level of methylation between controls and patients; while controls did not show methylation in the analysed CpG sites of the CTCF1 region, DM1 patients showed increased levels of methylation, both in myoblasts and in myotubes, in most of the CpG sites (Fig. 2B). Moreover, we observed a significant increase in the methylation level in immortalized myoblasts compared to primary ones (Fig. 2C). In the case of myotubes, a tendency ($p = 0.06$) was observed. No consistent differences were detected between patients regarding the methylation level of the CTCF1 site (Supplemental Fig. 1). To determine whether the methylation status of this region could change the expression level of neighbouring genes, we analysed the expression of DMWD, DMPK, and SIX5 in immortalized myotubes from controls (iCtrls) and DM1 patients (iDM1). Although significance was not reached due to dispersion in control cell values, all patient cell values were below any of the control values for the three genes (Fig. 2D). More data would be needed to confirm the downregulation of DMWD, DMPK and SIX5, which could be a consequence of the hypermethylation in the CTCF1 region in DM1 muscle cells compared to controls.

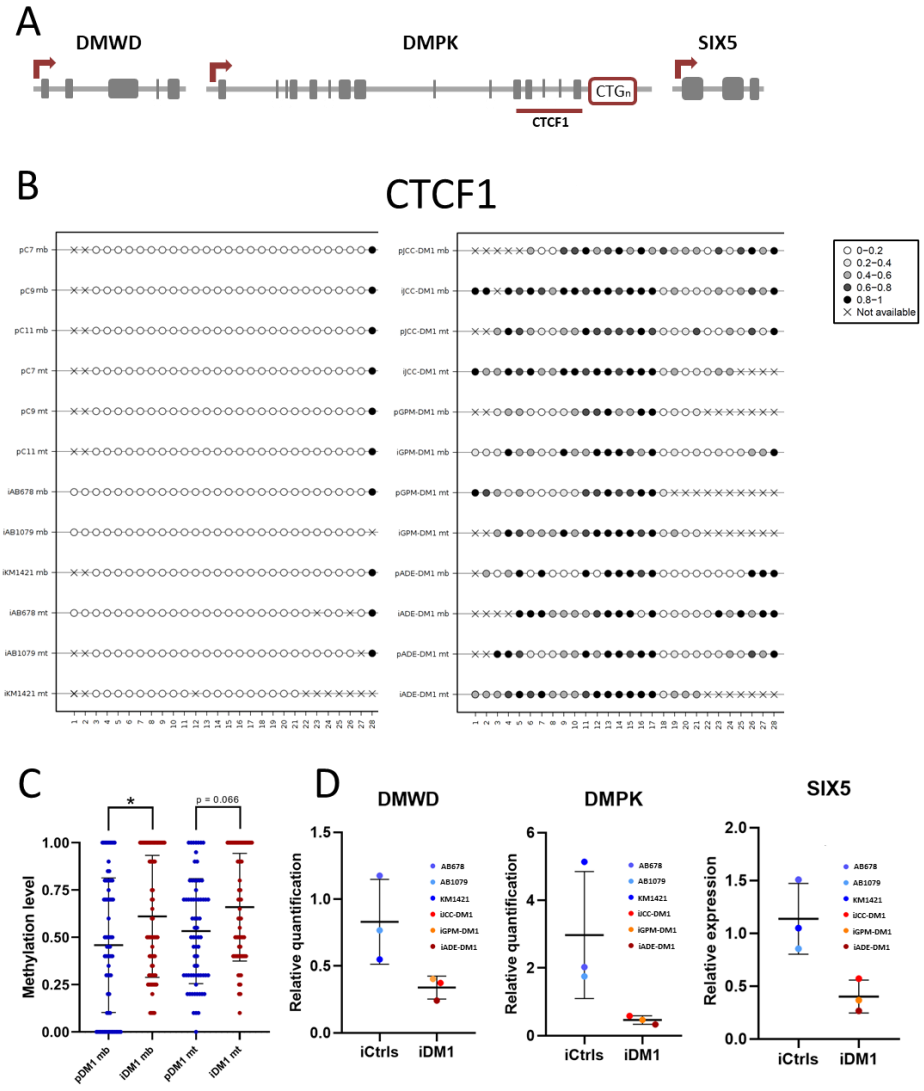

Figure 2. DNA methylation levels in CTCF1 is increased in immortalized cell lines when compared to primary cell lines. A. Schematic representation of the genomic DMPK locus. B. Methylation plotter showing the methylation status of the CTCF1 region. Each circle represents a CpG dinucleotide. The level of methylation is represented by the grey gradient. C. Graphical representation of the methylation levels in DM1 immortalized and primary myoblasts and myotubes. D. Relative expression of DMWD, DMPK and SIX5 genes at 5 days of differentiation. HPRT was used as housekeeping gene to normalize the data. All data are expressed as mean ± SEM. "p" and "i" before cell line name mean primary and immortalized, respectively. "mb" refers to myoblasts and "mt" to myotubes. Means were compared using unpaired two-tail Mann-Whitney test.

DM1 myoblasts show higher cell proliferation and reduction of early myogenic markers

We next sought to characterize the myogenic process in immortalized DM1 myoblasts by using real-time impedance analysis. Figure 3A shows the average real-time impedance curves of control (blue) and DM1 (red) myoblast samples throughout the myogenic process. Initially, all cultures increased their impedance values, which was indicative of myoblast adhesion, spreading, and proliferation, until they reached confluence, which resulted in achieving their maximum impedance values. Notably, at this step DM1 myoblasts showed a significant increase in impedance at 24 and 48 hours after seeding, which was indicative of a higher adhesion, spreading, and proliferation levels in comparison to the control cells (Fig. 3B). After switching to differentiation medium, a decrease in resistance was observed in both, control and DM1 cells, at 2 days post differentiation (dpd), due to cell reorganisation prior to muscle differentiation/fusion, being this decrease higher in DM1 cells (Fig. 3C). To address whether myogenic process could be altered in DM1 cells, we analysed the levels of the myogenic regulatory factors Myf5, MyoD and myogenin, in time course experiments by Jess Western blots. Myf5 is expressed during stem cell activation and myoblasts proliferation; MyoD is expressed during myoblast proliferation, commitment to differentiation and myotube fussion; and myogenin is expressed during myotube fussion and maturation into myofiber[47]. As shown in Figure 3D, Myf5 levels were significantly reduced in DM1 cells at 0,2,3 dpd, meanwhile MyoD was also significantly reduced at 3 dpd. No differences were found for Myogenin levels. In conclusion, DM1 cells show alterations in early myogenic markers My5 and MyoD.

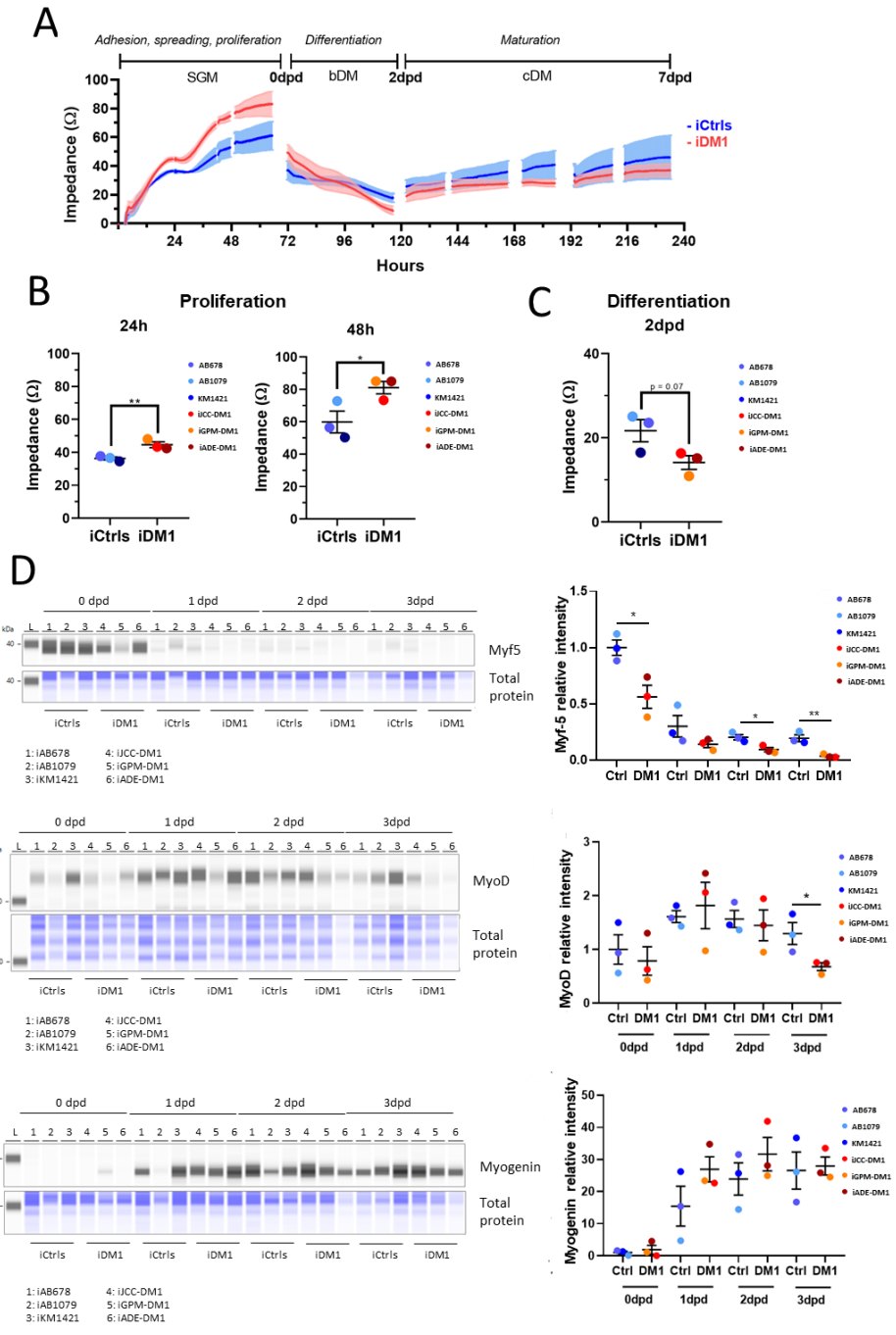

Figure 3. DM1 myoblasts show higher cell proliferation and reduced levels of early myogenic markers. A. Real-time impedance curves of human iCtrl (blue) and iDM1 (red) myoblasts during culture in proliferation medium (SGM) and differentiation media (bDM and cDM). B.

Proliferation of iCtrl (blue) and iDM1 (red) myoblasts was analysed at 24 and 48 hours after seeding. C. Differentiation of iCtrl and iDM1 myoblasts was analysed after 2 days in differentiation medium bDM (2dpd). D. Jess Western blot analysis of Myf5, MyoD and Myogenin in iCtrl and iDM1 3 differentiating myoblasts at 4 different time-points: 0, 1, 2 and 3 (dpd. Values are represented over Ctrl 0 dpd. Data information: n=3 for iCtrl and iDM1. Dpd: days post differentiation. All data are expressed as mean ± SEM. A-B-C. Dots indicate mean values of individual samples from 10 replicates. Means were compared using unpaired two-tail Student's t test. *p ≤ 0.05, **p ≤ 0.01. "i" mean immortalized cell line.

DM1 immortalized cells maintain a reduced fusion index as observed in their parental lines

Next, we investigated the fusion capacity of immortalized DM1 myotubes at 5 days of differentiation by desmin staining (Fig. 4A). As shown in Figure 4B, the fusion index was significantly reduced in both primary and immortalized DM1 myotubes compared to the corresponding controls. We also observed that immortalized cells, both control and DM1, showed a higher fusion index than the parental cell lines (Fig. 4B). When studied individually, we found significant differences in the fusion index between the three immortalized control cell lines and the three immortalized DM1 cell lines (Fig. 4C). Moreover, we found differences in nuclei distribution in the myotubes (Fig. 4D). We found a significant difference between patients and controls in the number of myotubes with more than three nuclei. Immortalized patients myotubes with two nuclei were more abundant than immortalized controls with two nuclei, reaching statistical significance. The number of myotubes with more than three nuclei was significantly higher in controls than in patients both in primary and immortalized cell lines (Fig. 4D). Furthermore, the diameter of DM1 myotubes was dramatically reduced compared to the control ones (Fig. 4E). When analysing individually the cell lines, differences in myotube diameter were found in all cell lines (Fig. 4F). iGPM-DM1 was the cell line that had the smallest myotube diameter size when compared to the other cell lines. Altogether, the results demonstrate that the immortalized DM1 cell lines also show reduced muscle fusion capacity.

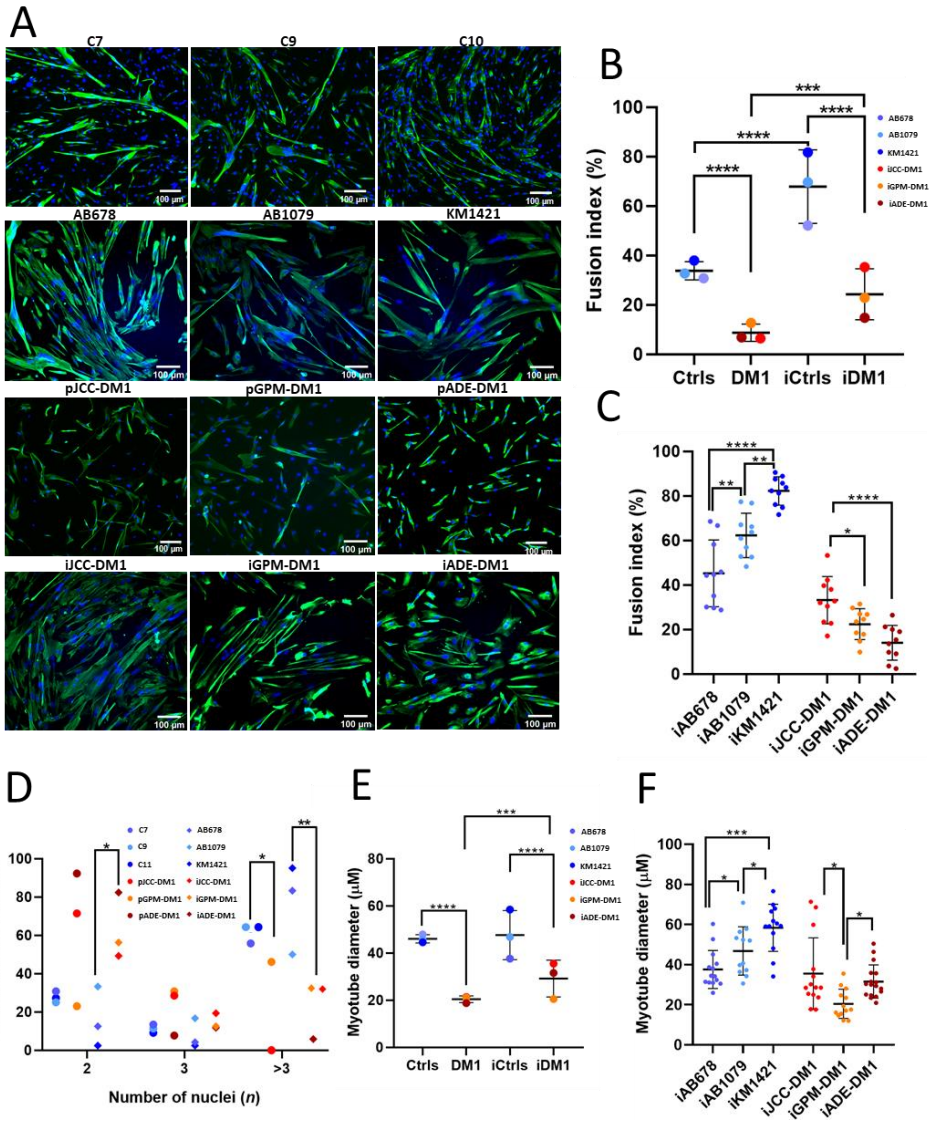

Figure 4. DM1 primary and immortalized myotubes present a lower fusion index compared to controls. A. Desmin (green) and nuclei (blue) immunofluorescence analysis performed in 5 days differentiated primary and immortalized DM1 or control myotubes. B. Fusion index (% of nuclei in desmin positive myotubes with 2 or more nuclei) in primary and immortalized 5 days differentiated DM1 or control myotubes. C. Fusion index (% of nuclei in desmin positive myotubes with 2 or more nuclei) in individualized immortalized 5 days differentiated DM1 or control myotubes D. Percentage of 5 days differentiated primary and immortalized myotubes containing 2, 3, >3 nuclei. E. Myotube diameter (calculated using the maximum diameter value of desmin positive myotubes with 2 or more nuclei) in primary and immortalized 5 days differentiated DM1 or control myotubes. F. Myotube diameter in individualized immortalized 5 days differentiated DM1 or control myotubes. All data are expressed as mean ± SEM. In figures

B and C, dots indicate mean values of 5 individual analysed images. In figures B and D at least 350 nuclei/cell line were analysed. In figure C at least 850 nuclei/cell line were analysed. In figures E and F at least 20 myotubes/cell line were analysed. Means were compared using unpaired two-tail t-test. *p ≤ 0.05, ****p ≤ 0.0001. “p” and “i” before cell line name mean primary and immortalized, respectively.

DM1 immortalized myotubes maintain patient-derived heterogeneity and have equal or greater RNA foci and MBNL1 co-localization than their primary myotubes

First, we checked for the presence of nuclear RNA foci in 5 days differentiated myotubes. Primary and immortalized control cells did not show RNA foci as expected (Supplemental Fig. 1), whereas primary DM1 myotubes showed variable numbers in the percentage of cells carrying RNA foci and in the number of RNA foci per cell (Fig. 5A-B). Notably, this patient-derived heterogeneity with respect to the accumulation of RNA foci was greatest in immortalized DM1 cells. Interestingly, the JCC-DM1 and ADE-DM1 immortalized myotubes, which are the cells carrying the longest CTG expansions and derived from the most affected patients, showed not only a significantly higher number of RNA foci per cell compared to GPM-ADE (Fig. 5D), but also the highest proportion of cells carrying more than 10 foci per cell (Table 3).

It is well known that staining with an anti-MBNL1 antibody shows the presence of MBNL-1 aggregates, which co-localize with RNA foci only in DM1 cells. This aggregation of MBNL1 leads to a decrease in cytoplasmic and nuclear fluorescence of MBNL1 compared to that of control cells (Fig. 5A). As we observed with RNA foci, primary DM1 cells had a variable number of co-localized aggregates. Immortalized JCC-DM1 and ADE-DM1 myotubes showed a significantly higher mean number of MBNL1 aggregates, as well as a high percentage of cells with more than 10 MBNL1 aggregates when compared to primary cell lines (Fig. 5D and Table 3). Altogether, these results indicate that these DM1 immortalized cell lines also show the cell heterogeneity associated with DM1 tissues.

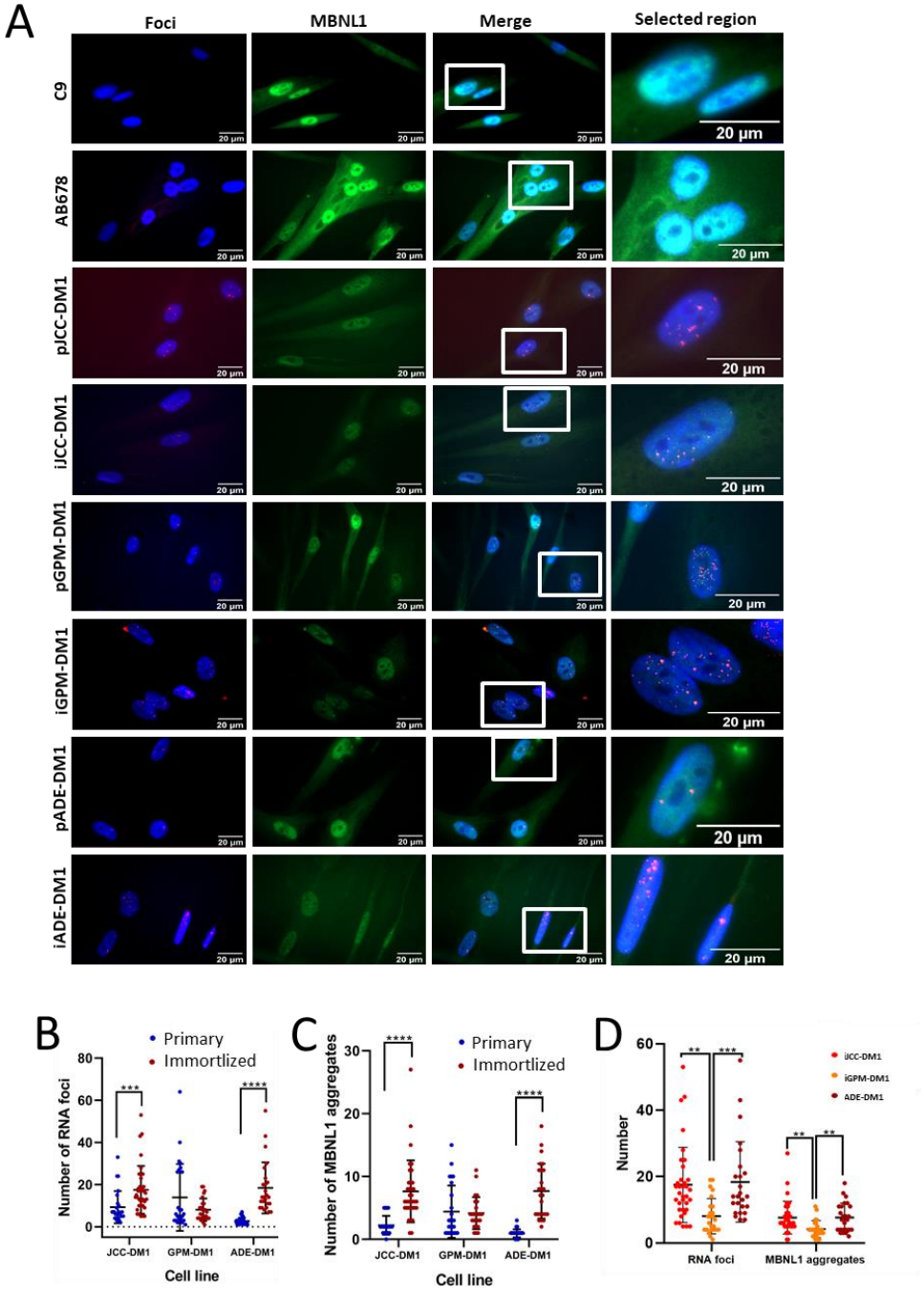

Figure 5. DM1 immortalized myotubes present equal or higher amount of RNA foci and MBNL1 aggregates than the original primary culture. A. Foci (red), MBNL1 (green) and nuclei (blue) immunofluorescence analysis performed in 5 days differentiated primary and immortalized DM1 myotubes. B. Number of RNA foci/nucleus in primary and immortalized 5 days

differentiated DM1 myotubes C. MBNL1 aggregates/nucleus in primary and immortalized 5 days differentiated DM1 myotubes. D. Comparison of the number of RNA foci/nucleus and MBNL1 aggregates/nucleus between the three immortalized DM1 cell lines. All data are expressed as mean ± SEM. Between 25 and 35 DM1 nuclei and between 20 and 25 control nuclei were analysed per cell line. "p" and "i" before cell line name mean primary and immortalized, respectively. Means were compared using unpaired two-tail Mann-Whitney test. ***p ≤ 0.001, ****p ≤ 0.0001.

Table 3: Detailed data of the RNA foci and MBNL1 aggregates found in 5 days differentiated primary and immortalized myotubes.

Cell line	Foci avg.	RANGE OF RNA FOCI (% of cells)						MBNL1 avg.	RANGE OF MBNL1 AGGREGATES (% of cells)					
		0	1-5	6-10	11-15	16-20	>20		0	1-5	6-10	11-15	16-20	>20
pJCC-DM1	9,28	0	32	44	8	4	12	2,24	4	96	0	0	0	0
iJCC-DM1	17,51	0	8,6	20	22,9	25,7	22,9	7,63	0	34,3	45,7	14,3	2,85	2,85
pGPM-DM1	13,88	0	48	20	0	0	32	4,4	0	72	20	8	0	0
iGPM-DM1	8,08	0	44	28	12	16	0	4,16	0	76	20	4	0	0
pADE-DM1	2,69	0	91,4	8,6	0	0	0	0,94	20	80	0	0	0	0
iADE-DM1	18,40	0	0	24%	36	12	28	7,68	0	40	28	28	4	0

"p" and "i" before cell line name mean primary and immortalized, respectively.

DM1 immortalized myotubes showed the same pathological splicing alterations than their primary myotubes

Next, we analysed splicing alterations in immortalized DM1 myotubes. We addressed the splicing pattern of transcripts previously described as altered in DM1 patients (BIN1 (exon 11), MBNL1 (exon 5), LDB3 (exon 11), INSR (exon 11), DMD (exon 78), and ATP2A1 (exon 22)). As shown in Figure 6A, DM1 primary myotubes have significantly different BIN1 and LDB3 splicing patterns, while a p-value of 0.08 was observed in ATP2A1 splicing. The same results were obtained when analysing immortalized DM1 myotubes and comparing them with control cells (Fig. 6B). Moreover, we found a splicing alteration in KIF13A gene that was heterogeneously expressed among DM1 immortalized myotubes (Fig. 7A). IJCC-DM1 myotubes had a significantly higher exon 32 inclusion than iGPM-DM1 myotubes (Fig. 7B), as it can be observed in the agarose gels (Fig. 7C). These results indicate that immortalized DM1 myotubes maintain the splicing defects that characterise this disease, although they can show heterogeneity in the levels of splicing alteration.

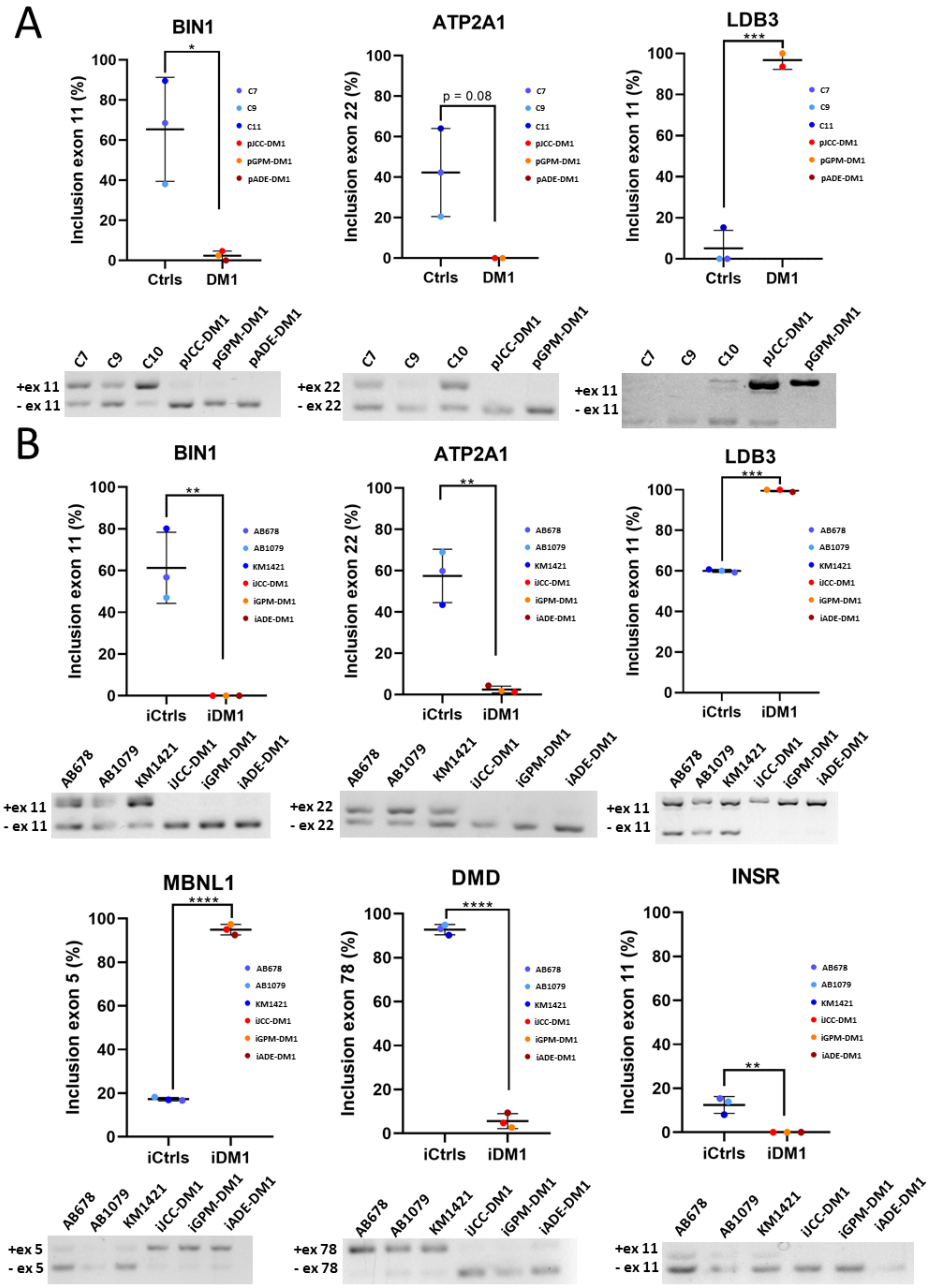

Figure 6. Immortalized DM1 myotubes maintain the splicing defects that characterize DM1 primary myotubes. A. Exon inclusion analysis of BIN1, LDB3 and ATP2A1 in primary control and DM1 5 days differentiated myotubes. B. Exon inclusion analysis of BIN1, MBNL1, LDB3, INSR, DMD and ATP2A1 in immortalized control and DM1 5 days differentiated myotubes. All data are expressed as mean ± SEM. 3 DM1 samples and 3 control samples were analysed in each splicing

both in primary and immortalized samples, except for ATP2A1 and LDB3 in primary samples where 2 DM1 samples and 3 controls were analysed. Means were compared using unpaired two-tail t-test. *p ≤ 0.05, **p ≤ 0.01, ***p ≤ 0.001, ****p ≤ 0.0001. “p” and “i” before cell line name mean primary and immortalized, respectively.

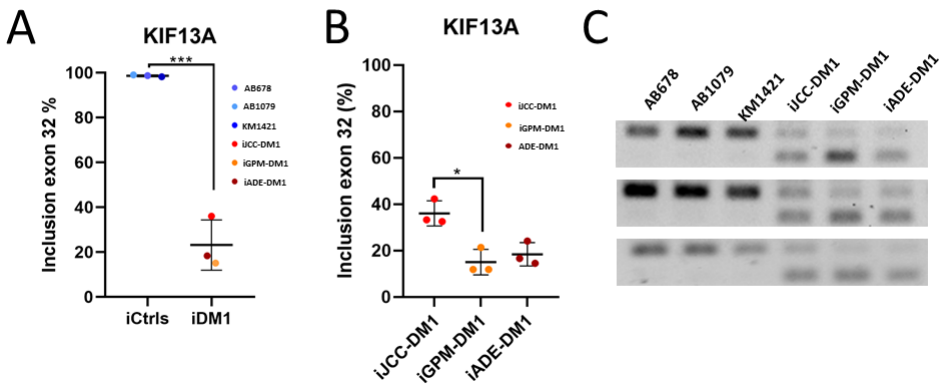

Figure 7. KIF13A splicing defect is heterogeneously expressed among immortalized cell lines. A. Exon inclusion analysis of KIF13A in immortalized control and DM1 5 days differentiated myotubes. B. Exon inclusion analysis of KIF13A in immortalized 5 days differentiated myotubes derived from the three DM1 cell lines. C. Gel analysis of KIF13A splicing analysis in control and patient DM1 myotubes. All data are expressed as mean ± SEM. n = 3 for each cell line. Means in A were compared using unpaired two-tail t-test and in B with ANOVA. *p ≤ 0.05, ***p ≤ 0.001. “i” before cell line name means immortalized.

Antisense oligonucleotide treatment is equally efficient in DM1 immortalized cell lines as in their original parental lines

To test whether these immortalised cell lines would be suitable for testing DM1 treatments, we treated the cells with an ASO targeting the CTG expansion[48], previously used in our laboratory (unpublished data). We measured the effect of treatment by analysing the number of RNA foci and colocalising aggregates of MBNL1 (Fig. 8A and Supplemental Figure 3). Importantly, we observed a significant reduction in both the number of RNA foci (Fig. 8B) and the MBNL1 colocalising aggregates (Fig. 8C) in all immortalised DM1 cell lines. These reductions were also observed in two of the primary cell lines, JCC-DM1 and GPM-DM1, but not in ADE-DM1. Notably, the MBNL-1 colocalising aggregates decrease was associated in some cases with an increase in the fluorescence signal of MBNL1 in the nucleus. To test whether the RNA foci reduction caused splicing restoration we studied the effect of the ASO treatment in the usual DM1 splicing alterations. Notably, we found a significant reduction in MBNL1 exon 5 splicing alteration. (Fig. 8D).

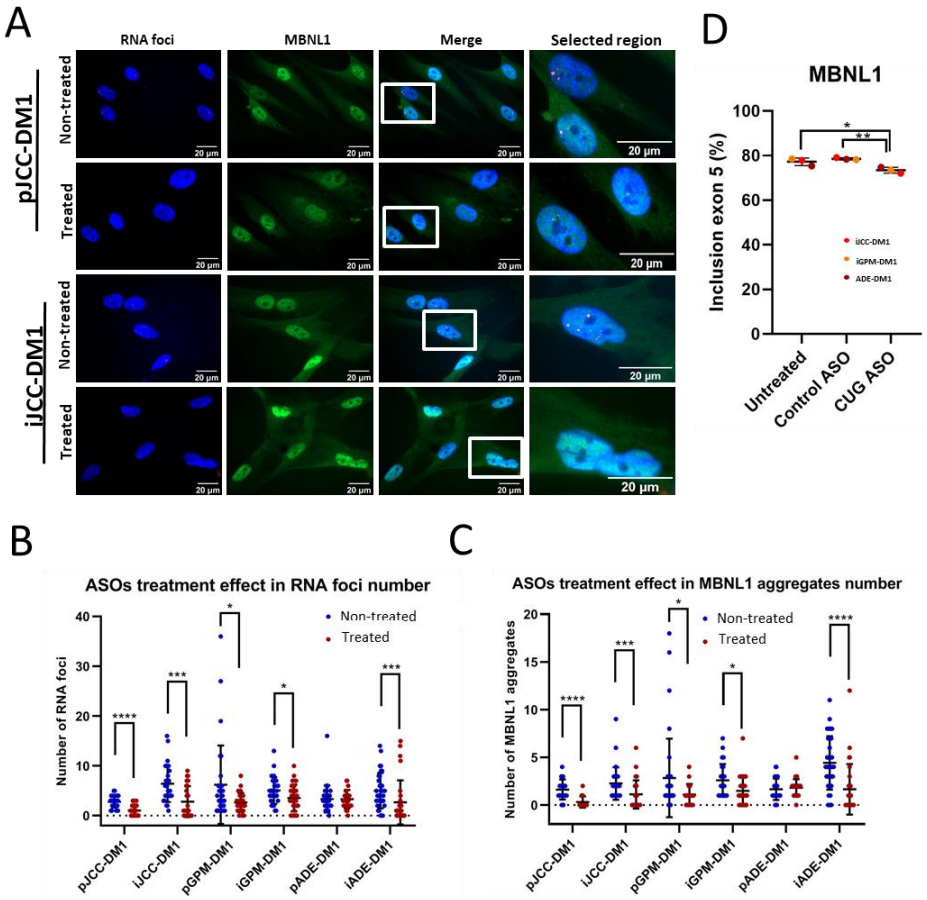

Figure 8. Immortalized DM1 myotubes respond to treatment in a similar way to primary DM1 myotubes. A. Foci (red), MBNL1 (green) and nuclei (blue) immunofluorescence analysis performed in 9 days differentiated primary and immortalized DM1 myotubes. Rows 1 and 3 correspond to non-treated cells while rows 2 and 4 correspond to 48 hours ASO-treated cells. B. Number of RNA foci/nucleus in primary and immortalized 48 hours ASO-treated or non-treated 9 days differentiated DM1 myotubes. C. Number of MBNL1 aggregates/nucleus in primary and immortalized 48 hours ASO-treated or non-treated 9 days differentiated DM1 myotubes. D. MBNL1 splicing analysis in immortalized 48 hours ASO-treated, control-treated or non-treated 9 days differentiated myotubes. All data are expressed as mean ± SEM. For each cell line in figures B and C, it was analysed between 29 and 43 DM1 nuclei. In figure D, 3 DM1 samples were analysed for each condition. "p" and "i" before cell line name mean primary and immortalized, respectively. Means were compared using unpaired two-tail Mann-Whitney test. *p ≤ 0.05, ***p ≤ 0.001, ****p ≤ 0.0001.

Discussion

Heterogenicity in molecular, clinical, and functional parameters in DM1 is often not represented in the cellular models used to study this disease. The need to generate cellular models that mimic the reported patient differences is increasing, especially with the current development of therapies, and with the necessities to understand pathophysiological mechanisms of DM1. To have more robust results, it is important to work with cell cultures derived from DM1 muscle biopsies, which can show patient heterogeneity and preserve their natural genomic context. However, the accessibility and availability of muscle biopsies from DM1 patients is very limited, and primary muscle cultures show a reduced proliferative capacity after few passages. In this study we have generated three immortalized human muscle cell lines derived from three different subtypes of DM1 patients (juvenile, adult, late-onset). The genetic, epigenetic, and molecular characterization of these cellular models have shown that all three present the hallmarks of the disease and importantly, they are heterogeneous both from a clinical and molecular point of view.

Given the high instability of the CTG repeat in DM1, we performed SP-PCR to better characterize the genetic expansion variability in our cellular models. Our results revealed high heterogeneity in CTG expansion, with two of the patient-derived cells (ADE-DM1 and JCC-DM1) showing higher ePAL (above 500) and higher instability (above 1900) than the other cell line (GPM-DM1, below 500 and 700, respectively). In addition, the patient-derived muscle cell line with the highest instability (ADE-DM1) was the one whose most abundant populations had the largest CTG expansions and interestingly, corresponded with the most severely affected patient, both from the cardiac and functional points of view. In contrast, the patients with less instability (JCC-DM1 and GPM-DM1) were the mildest affected patients, both cardiacally and functionally. Somatic instability of the CTG expansion has been previously described to be a contributor of disease severity[49], yet the major contributor of the severity is the ePAL. In this case, the highest ePAL was also found in the immortalized cells of the patient with the highest disease severity (ADE-DM1). However, the primary cells derived from this same patient did not have the highest ePAL, in fact JCC-DM1 had the highest one of the primary cells. These differences between primary and immortalized cells must be derived from the

clonal selection that takes place during the immortalization process, in which the CTG expansion tends to expand, but can also contract.

It is indeed remarkable, that clonal cells originating from a single CTG expansion end up having a very similar instability to the primary cells they derived from. It has been hypothesized that individual specific differences, as well as environmental or genetic factors, may contribute to somatic instability[49]. Although 40% of the variance has been reported to be attributed to genetic factors, our results indicate that the contribution of the genetic factors should be above 75% (since only between 6 and 25% variation in instability was found between parental and immortalized cell models). In addition, it is likely that part of the instability was not detected in our study, since measuring these CTG expansions was challenging, and muscle, unlike other tissue such as blood, has larger CTG expansions that are difficult to detect by SP-PCR[50–52]. Deep genomic sequencing techniques[53,54] would probably give more accurate and precise information regarding the larger CTG fragments in muscle and the instability of CTG expansion in DM1 samples.

The CTG expansion overlaps with a 3.5 kb CpG island flanked by two CTCF binding sites, named CTCF1 and CTCF2. We and others have reported changes in the DNA methylation pattern of the CTCF1 region in blood samples from DM1[10–12]. In addition, our group also demonstrated that the CTCF1 region was methylated in a tissue-specific manner only in DM1 muscle biopsies (and not in skin or blood from the same patients), as well as in primary DM1 muscle cells, whereas tissues from unaffected individuals were completely unmethylated[12]. Importantly, the DM1 immortalized muscle cells showed the previously reported CTCF1 hypermethylation in both myoblasts (muscle progenitor cells) and myotubes (mature muscle cells), indicating that the DNA methylation alterations were conserved. However, we observed a significant difference in the methylation levels between primary and immortalized cell lines. Immortalized cell lines methylation levels were increased compared to the primary ones. This can be explained by the observation that cellular models, especially immortalized cell lines that have been in culture for a substantial amount of time (since they are originated from a single cellular clone), can increase DNA methylation levels[55,56] and/or because of the purity of cell cultures. The presence of a small portion of fibroblasts in the primary cultures, which have an unmethylated CTCF1 region, can have an impact in these CTCF1 methylation studies. DNA methylation is considered a repressive

epigenetic mark that plays a role in gene silencing[57–59]. Although we did not find a significant reduction of DMPK, SIX5, DMWD in our study, probably due to a small sample, it has been previously reported a decrease in the expression of these genes in DM1[60–62]. This reduction could be suggesting that DNA hypermethylation in the CTCF1 region could alter transcriptional activity in DM1 muscle samples, which could affect muscle functions. Notably, *SIX5* is abundantly expressed in muscle, heart, brain, and eyes, which are tissues that are affected in DM1. It is homologous to the Drosophila eye development gene sine oculis and it has been proven that *SIX5* deficient mice develop cataracts, as observed in DM1 patients[63]. The *DMWD* gene is abundantly expressed in the brain and testis[64], although its function is still not clear. However, very recently a quadruple mutant mouse was generated in which expression of *SIX5, DMWD, DMPK* and *MBNL1* were reduced, and these mice recapitulate many important manifestations in congenital DM1, suggesting that changes in gene expression in genes at the *DMPK* locus may modulate disease severity[65].

The immortalized DM1 cellular models showed an increased proliferation rate when compared with immortalized control models. An advantage in growth and proliferation has already been described in immortalized DM1 lymphocyte cell lines[66]. This effect has been termed “mitotic drive” and it explains why the CTG region tends to expand. Khajavi and colleagues demonstrated that immortalized lymphocytes carrying longer CTG expansions had a growing advantage due to increased Ras, Erk1, and Erk2 activity and decreased $p21^{WAFI}$ activity. However, once DM1 immortalized muscle cell models stop growing and are stimulated to differentiate, they start having alterations[44]. In our immortalized cellular models, DM1 immortalized cells showed a decrease in the impedance during the myotube fusion process, reduced levels of early myogenic markers, a diminished fusion capacity with smaller myotubes, and lower nuclei number per myotube. Some of these alterations have also been found in primary muscle derived cells and have been linked to abnormalities in the temporal expression of differentiation regulators, myogenic progression markers, and alternative splicing patterns before and immediately after the onset of differentiation[67]. These alterations are intrinsically linked to the CTG expansion, since excision of the expanded repeat reverts all these abnormalities[67]. However, some influence may also come from the environment, since studies in 3D models with immortalized cells demonstrated that these differentiation deficiencies were attenuated[68] when

a better niche for differentiation was utilized. Moreover, when comparing primary and immortalized myotubes, we observed an increase in the fusion index in immortalized cell lines, both in controls and DM1. As discussed with the methylation pattern in CTCF1, it is likely that this difference is due to the greater purity of immortalized cultures compared to primary ones. Regarding heterogeneity in the fusion index between cell lines, we found differences between both immortalized controls and patients; meaning that other factors may contribute to the fusion capacity.

Analysis of the molecular hallmarks of the disease revealed heterogeneous alterations in the accumulation of RNA foci and in the sequestration of MBNL1 in our immortalized cell models. Importantly, we have observed that the higher the CTG instability, the higher the average RNA foci per cell. ADE-DM1, had an instability of 3068 CTGs, and had a mean of 18,40 foci per nucleus; JCC-DM1 had an instability of 2467 CTGs and a mean of 17,51 foci per nucleus, and GPM-DM1 had an instability of 828 CTGs and an average of 8,08 foci per nucleus. A direct association between CTG size and foci number in muscle cells has been reported before by our group[23]. We hypothesize that although the CTG size would determine the number of RNA foci at the single cell level, the instability of the CTG repeat in the cells of a certain tissue, would determine the mean of the RNA foci in this particular tissue[18,24,30].

MBNL1 sequestration was also dependant on the RNA foci average. So, the higher RNA foci/ cell, the more MBNL1 aggregates/cell colocalizing with those foci. Again, ADE-DM1 is the cell line carrying more MBNL1 aggregates (7,68 per myotube), followed by JCC-DM1 (7,63 aggregates per myotube), and finally, GPM-DM1 (carrying 4,16 aggregates per myotube). So, it is clear that there is a relationship between CTG expansion, *DMPK* pathological transcript accumulation, and MBNL1 trapping. Heterogeneity in RNA foci accumulation and MBNL1 sequestration can be modified by different experimental conditions. A lower number of RNA foci was observed in the immortalized patients cell lines with 9 differentiation days, when compared to 5 differentiation days. We hypothesize that the heterogeneity could be due to the higher mortality rate observed after 9 days of differentiation, which may difficult the detection of RNA foci.

Splicing alterations were also found in our cellular models. We observed alterations in the splicing of *ATP2A1* and *SERCA1*, which is observed only in

mature skeletal muscle cells and is sometimes hard to detect in patient primary cultures[34,69] and in patient derived iPSCs that are differentiated to myotubes[70]. Our cell models showed alterations in *BIN1, ATP2A1, MBNL1, LDB3, INSR*, *DMD* and *KIF13A*, which have previously been found altered in DM1 muscle cell models[44]. We found heterogenicity in the alterations of *KIF13A* with JCC-DM1 having significantly less alterations than GPM-DM1. *KIF13* codes for a gene involved in the positioning of endosomes[71]. It is likely that heterogenicity is present in other splicing alterations, but more global transcriptomic studies would be needed to further determine this heterogenicity.

The generation of specific therapies[72] targeting either the gene through CRISPR-Cas9[73–75], the foci[76,77], or the increase in MBNL1 availability[78,79] would make these cells an attractive cellular model in which the heterogenous defects are present in different proportions, which can be quantified after treatments. Notably, the three models showed a significant reduction of RNA foci and MBNL1 aggregates after being treated with an ASO directed against the CTG expansion[48]. Moreover, a significant recovery of the *MBNL1* splicing alteration was observed. Overall, these models would allow treatments to be tested on a larger and more heterogeneous sample than was previously possible.

Prior to this publication, only four DM1 immortalized muscle cellular models have been developed by different research groups (Table 4)[44,45]. These cellular models have been a powerful tool used to discover knowledge, develop therapeutic strategies, and overcome the challenges presented by artificial, primary or transdifferentiated disease models. However, heterogenicity in molecular, clinical, and functional parameters was not represented even though it is a hallmark of the disease.

In this paper, we have presented three immortalized muscle cell models for the study of DM1. We have demonstrated that these immortalized cell models behave similarly to the parental cells from which they derive. However, they are heterogenous, and harbour different molecular alterations that are linked to the presentation of different clinical symptoms in patients. These models will offer new possibilities to understand DM1 from a more diverse point of view. The cells will serve as a tool to study and quantify the degree of certain molecular alterations, and to assess the efficacy of different therapies in a

context of different molecular alterations in different genetic backgrounds. Overall, we have generated three cellular models for DM1 that we expect will contribute to the better understanding of this pathology from a more diverse point of view.

Table 4: Comparative table of the characterization of the immortalized DM1 myoblasts/myotubes models available

CELL LINE	AGE OF ONSET /CLINICAL SUBTYPE	DISEASE PROGRESSION AT SAMPLING	CTG EXPANSION	EPIGENETICS	RNA FOCI NUMBER	MBNL1 AGGREGATES	SPLICING	DIFFERENTIATION STUDIES	TREATMENT ASSESSMENT	PUBLICATION
JCC-DM1	15	✓	✓	✓	✓	✓	✓	✓	✓	Núñez-Manchón et.al. 2023
GPM-DM1	42	✓	✓	✓	✓	✓	✓	✓	✓	Núñez-Manchón et.al. 2023
ADE-DM1	27	✓	✓	✓	✓	✓	✓	✓	✓	Núñez-Manchón et.al. 2023
DM1	Infantile	NA	✓	NA	✓	✓	✓	✓	✓	Arandel et.al. 2017[44]
DM#1	NA	NA	✓	NA	✓	NA	✓	✓	✓	Pantic et.al. 2016[45]
DM#2	NA	NA	✓	NA	✓	NA	✓	✓	✓	Pantic et.al 2016[45]
DM1	Congenital	NA	✓	NA	NA	NA	NA	NA	NA	Bigot et.al. 2009 [46]

NA: not available

Supplemental information

Supplementary table 1. Primers used for qPCR. Related to Material and Methods

PCRs Transcript	Forward primer	Reverse primer	Fragment size (bp)
SIX5	AGGTCAGCAACTGGTTCAAG	ACTCGTCCTCAGTCGTGG	108
DMWD	GCTCTATTTCTACCCAGGCTG	TGAAATCGTGGCAGGTGG	113
DMPK	GCCCAGGACAAGTACGTG	CTTCATCTTCACTACCGCTACC	150
HPRT	TGAAATCGTGGCAGGTGG	ACAGAGGGCTACAATGTGATG	115

Supplementary table 2. Primers and conditions used for splicing analysis. Related to the STAR Methods

PCRs Transcript	Forward primer	Reverse primer	Annealing Tª	Cycles	Fragment sizes (bp)	Reference
BIN1 (exon 11)	AGAACCTCAATGATGTGCTGG	TCGTGTTGACTCTGATCTCGG	58	28	208-163	Fugier et al. 2011[32]
MBNL1 (exon 7)	GCCCAATACCAGGTCAACCA	GGCCTCTTTGGTAATGGGGG	58	35	101-155	Ketley et al. 2020[80]
LDB3 (exon 11)	GCAAGACCCTGATGAAGAAGCTC	GACAGAAGGCCGGATGCTG	61	28	352-163	François et.al 2011[81]
INSR (exon 11)	CCAAAGACAGACTCTCAGAT	AACATCGCCAAGGGACCTGC	60	35	131-167	Savkur et al. 2011[31]
DMD (exon 78)	TTAGAGGAGGTGATGGAGCA	GATACTAAGGACTCCATCGC	58	28	148-116	Rau et. Al. 2015[28]
ATP2A1 (exon 22)	CTCATGGTCCTCAAGATCTCAC	AGCTCTGCCTGAAGATGTGTCAC	58	35	161-203	Wang et al. 2018[82]
KIF13A (exon 32)	TCCTGTCAGTATCCATCGGCT	TGAGTGCATCTGACCACCTCT	65	30	156-117	-

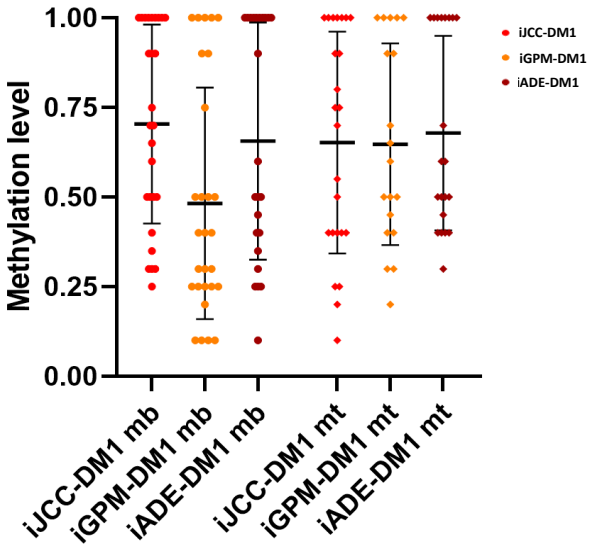

Supplementary Figure 1. Methylation levels did not differ between the three DM1 cell lines except for iJCC-DM1 vs iGPM-DM1 immortalized myoblasts. Related to Figure 2. "i" before cell line name means immortalized. "mb" and "mt" after cell line name mean myoblasts and myotubes, respectively. For each patient there are between 19 and 28 single measurements.

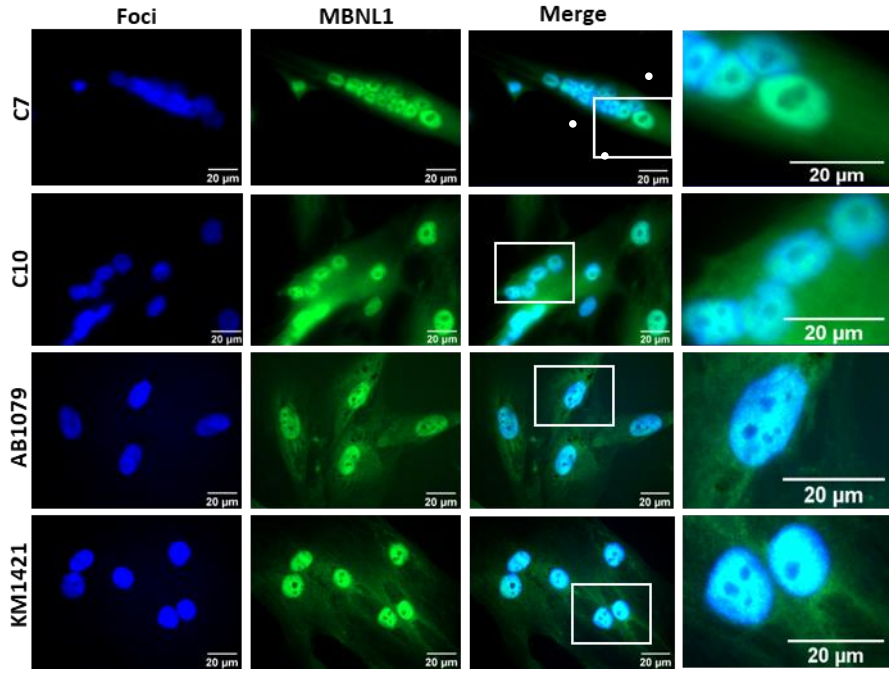

Supplementary Figure 2. Immortalized control myotubes do not show neither RNA foci or MBNL1 aggregates. Related to Figure 5 Foci (red), MBNL1 (green) and nuclei (blue) immunofluorescence analysis performed in 5 days differentiated primary and immortalized control myotubes.

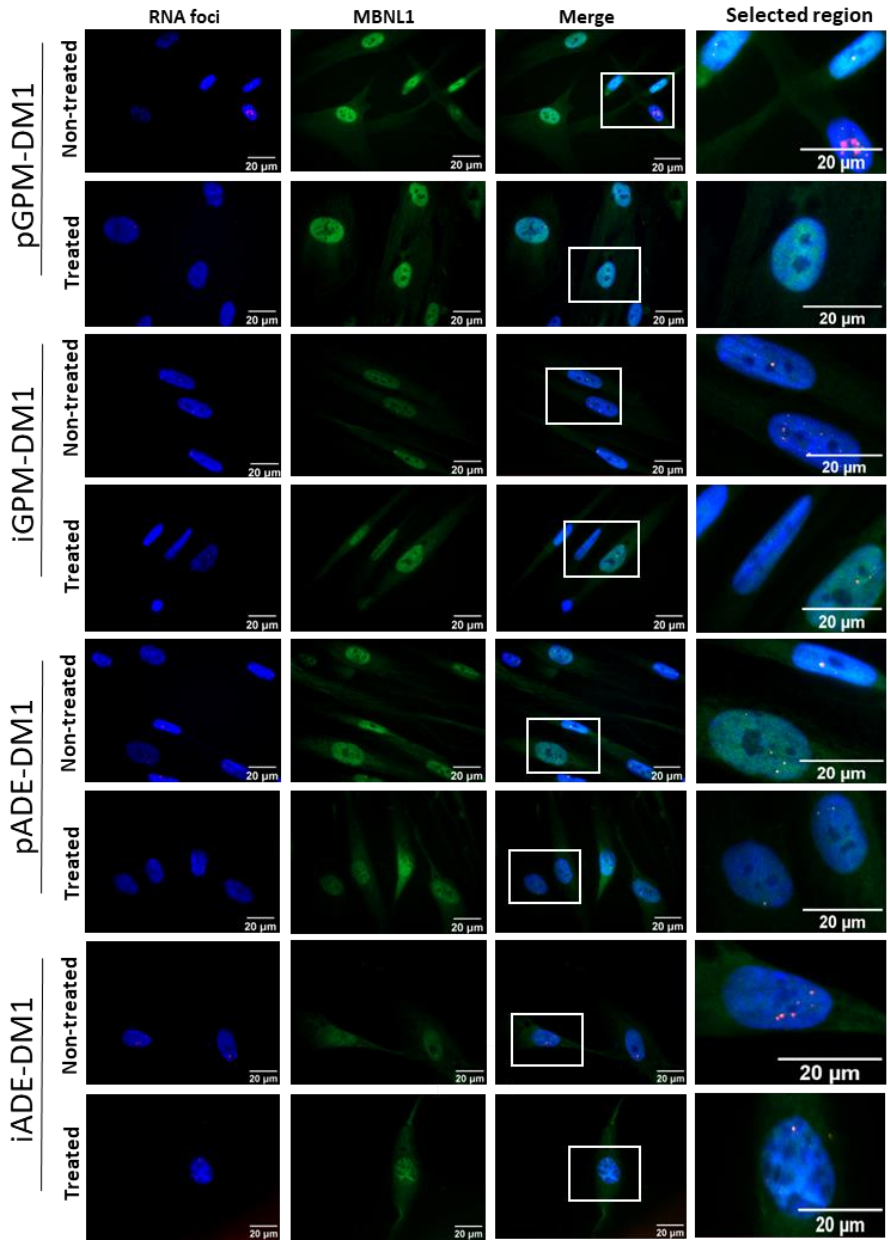

Supplementary Figure 3. Immortalized DM1 myotubes respond to treatment in a similar way to primary DM1 myotubes. Related to Figure 8. Foci (red), MBNL1 (green) and nuclei (blue) immunofluorescence analysis performed in 5 days differentiated primary and immortalized DM1 myotubes. "p" and "i" before cell line name mean primary and immortalized, respectively.

References

1. Bird, T. (1999). Myotonic Dystrophy Type 1. GeneReviews.
2. Brook, J.D., McCurrach, M.E., Harley, H.G., Buckler, A.J., Church, D., Aburatani, H., Hunter, K., Stanton, V.P., Thirion, J.P., Hudson, T., et al. (1992). Molecular basis of myotonic dystrophy: Expansion of a trinucleotide (CTG) repeat at the 3′ end of a transcript encoding a protein kinase family member. Cell *68*, 799–808. 10.1016/0092-8674(92)90154-5.
3. Ashizawa, T., Anvret, M., Baiget, M., Barcelo, J.M., Brunner, H., Cobo, # A M, Dallapiccola, B., Fenwick, R.G., Grandell, " ′ U, Harley, H., et al. (1994). Characteristics of Intergenerational Contractions of the CTG Repeat in Myotonic Dystrophy.
4. Martorell, L., Martinez, J.M., Carey, N., Johnson, K., and Baiget, M. (1995). Comparison of CTG repeat length expansion and clinical progression of myotonic dystrophy over a five year period. J. Med. Genet. *32*, 593–596. 10.1136/jmg.32.8.593.
5. Wong, L.J.C., Ashizawa, T., Monckton, D.G., Caskey, C.T., Richards, C.S., A, B, C, and D (1995). Somatic heterogeneity of the CTG repeat in myotonic-dystrophy is age and size-dependent. Am. J. Hum. Genet. *56*, 114–122.
6. Ballester-Lopez, A., Koehorst, E., Linares-Pardo, I., Núñez-Manchón, J., Almendrote, M., Lucente, G., Arbex, A., Alonso, C.P., Lucia, A., Monckton, D.G., et al. (2020). Preliminary findings on ctg expansion determination in different tissues from patients with myotonic dystrophy type 1. Genes (Basel). *11*, 1–8. 10.3390/genes11111321.
7. Kinoshita, M., Takahashi, R., Hasegawa, T., Komori, T., Nagasawa, R., Hirose, K., and Tanabe, H. (1996). (CTG)n expansions in various tissues from a myotonic dystrophy patient. Muscle and Nerve *19*, 240–242. 10.1002/(SICI)1097-4598(199602)19:2<240::AID-MUS21>3.0.CO;2-X.
8. Ballester-Lopez, A., Linares-Pardo, I., Koehorst, E., Núñez-Manchón, J., Pintos-Morell, G., Coll-Cantí, J., Almendrote, M., Lucente, G., Arbex, A., Magaña, J.J., et al. (2020). The need for establishing a universal CTG sizing method in myotonic dystrophy type 1. Genes (Basel). *11*, 1–9. 10.3390/genes11070757.
9. Gomes-Pereira, M., Bidichandani, S.I., and Monckton, D.G. (2004). Analysis of unstable triplet repeats using small-pool polymerase chain reaction. Methods Mol. Biol. *277*, 61–76. 10.1385/1-59259-804-8:061.
10. Barbé, L., Lanni, S., López-Castel, A., Franck, S., Spits, C., Keymolen, K.,

Seneca, S., Tomé, S., Miron, I., Letourneau, J., et al. (2017). CpG Methylation, a Parent-of-Origin Effect for Maternal-Biased Transmission of Congenital Myotonic Dystrophy. Am. J. Hum. Genet. *100*, 488–505. 10.1016/j.ajhg.2017.01.033.

11. Morales, F., Corrales, E., Zhang, B., Vásquez, M., Santamaría-Ulloa, C., Quesada, H., Sirito, M., Estecio, M.R., Monckton, D.G., and Krahe, R. (2021). Myotonic dystrophy type 1 (DM1) clinical sub-types and CTCF site methylation status flanking the CTG expansion are mutant allele length-dependent. Hum. Mol. Genet. 10.1093/HMG/DDAB243.

12. Koehorst, E., Odria, R., Capó, J., Núñez-Manchón, J., Arbex, A., Almendrote, M., Linares-Pardo, I., Benito, D.N. De, Saez, V., Nascimento, A., et al. (2022). An Integrative Analysis of DNA Methylation Pattern in Myotonic Dystrophy Type 1 Samples Reveals a Distinct DNA Methylation Profile between Tissues and a Novel Muscle-Associated Epigenetic Dysregulation. Biomedicines *10*. 10.3390/BIOMEDICINES10061372.

13. Boucher, C.A., King, S.K., Carey, N., Krahe, R., Winchester, C.L., Rahman, S., Creavin, T., Mehji, P., Bailey, M.E.S., Chartier, F.L., et al. (1995). A novel homeodomain-encoding gene is associated with a large CpG island interrupted by the myotonic dystrophy unstable (CTG)n repeat. Hum. Mol. Genet. *4*, 1919–1925. 10.1093/HMG/4.10.1919.

14. Barbé, L., Lanni, S., López-Castel, A., Franck, S., Spits, C., Keymolen, K., Seneca, S., Tomé, S., Miron, I., Letourneau, J., et al. (2017). CpG Methylation, a Parent-of-Origin Effect for Maternal-Biased Transmission of Congenital Myotonic Dystrophy. Am. J. Hum. Genet. *100*, 488–505. 10.1016/j.ajhg.2017.01.033.

15. Morales, F., Corrales, E., Zhang, B., Vásquez, M., Santamaría-Ulloa, C., Quesada, H., Sirito, M., Estecio, M.R., Monckton, D.G., and Krahe, R. (2022). Myotonic dystrophy type 1 (DM1) clinical subtypes and CTCF site methylation status flanking the CTG expansion are mutant allele length-dependent. Hum. Mol. Genet. *31*, 262–274. 10.1093/hmg/ddab243.

16. Inukai, A., Doyu, M., Kato, T., Liang, Y., Kuru, S., Yamamoto, M., Kobayashi, Y., and Sobue, G. (2000). Reduced expression of DMAHP/SIX5 gene in myotonic dystrophy muscle. Muscle and Nerve *23*, 1421–1426. 10.1002/1097-4598(200009)23:9<1421::AID-MUS14>3.0.CO;2-Y.

17. Alwazzan, M., Newman, E., Hamshere, M.G., and Brook, J.D. (1999). Myotonic dystrophy is associated with a reduced level of RNA from

the DMWD allele adjacent to the expanded repeat. Hum. Mol. Genet. *8*, 1491–1497. 10.1093/hmg/8.8.1491.

18. Kanadia, R.N., Johnstone, K.A., Mankodi, A., Lungu, C., Thornton, C.A., Esson, D., Timmers, A.M., Hauswirth, W.W., and Swanson, M.S. (2003). A Muscleblind Knockout Model for Myotonic Dystrophy. Science (80-.). *302*, 1978–1980. 10.1126/science.1088583.

19. AMI MANKODI, ERIC LOGIGIAN, LINDA CALLAHAN, CAROLYN MCCLAIN, ROBERT WHITE, DON HENDERSON, MATT KRYM, A.C.A.T. (2000). Myotonic Dystrophy in Transgenic Mice Expressing an Expanded CUG Repeat. Science (80-.). *289*, 1769/1772. 10.1126/science.289.5485.176.

20. Taneja, K.L., McCurrach, M., Schalling, M., Housman, D., and Singer, R.H. (1995). Foci of trinucleotide repeat transcripts in nuclei of myotonic dystrophy cells and tissues. J. Cell Biol. *128*, 995–1002. 10.1083/jcb.128.6.995.

21. Michalowski, S., Miller, J.W., Urbinati, C.R., Paliouras, M., Swanson, M.S., and Griffith, J. (1999). Visualization of double-stranded RNAs from the myotonic dystrophy protein kinase gene and interactions with CUG-binding protein. Nucleic Acids Res. *27*, 3534–3542. 10.1093/nar/27.17.3534.

22. Botta, A., Rinaldi, F., Catalli, C., Vergani, L., Bonifazi, E., Romeo, V., Loro, E., Viola, A., Angelini, C., and Novelli, G. (2008). The CTG repeat expansion size correlates with the splicing defects observed in muscles from myotonic dystrophy type 1 patients. J. Med. Genet. *45*, 639–646. 10.1136/JMG.2008.058909.

23. Ballester-Lopez, A., Núñez-Manchón, J., Koehorst, E., Linares-Pardo, I., Almendrote, M., Lucente, G., Guanyabens, N., Lopez-Osias, M., Suárez-Mesa, A., Hanick, S.A., et al. (2020). Three-dimensional imaging in myotonic dystrophy type 1: Linking molecular alterations with disease phenotype. Neurol. Genet. *6*. 10.1212/NXG.0000000000000484.

24. Miller, J.W., Urbinati, C.R., Teng-Umnuay, P., Stenberg, M.G., Byrne, B.J., Thornton, C.A., and Swanson, M.S. (2000). Recruitment of human muscleblind proteins to (CUG)(n) expansions associated with myotonic dystrophy. EMBO J. *19*, 4439–4448. 10.1093/emboj/19.17.4439.

25. Ho, T.H., Charlet-B, N., Poulos, M.G., Singh, G., Swanson, M.S., and Cooper, T.A. (2004). Muscleblind proteins regulate alternative splicing. EMBO J. *23*, 3103–3112. 10.1038/sj.emboj.7600300.

26. Hino, S.I., Kondo, S., Sekiya, H., Saito, A., Kanemoto, S., Murakami, T., Chihara, K., Aoki, Y., Nakamori, M., Takahashi, M.P., et al. (2007). Molecular mechanisms responsible for aberrant splicing of SERCA1 in myotonic dystrophy type 1. Hum. Mol. Genet. *16*, 2834–2843. 10.1093/hmg/ddm239.

27. Yamashita, Y., Matsuura, T., Kurosaki, T., Amakusa, Y., Kinoshita, M., Ibi, T., Sahashi, K., and Ohno, K. (2014). LDB3 splicing abnormalities are specific to skeletal muscles of patients with myotonic dystrophy type 1 and alter its PKC binding affinity. Neurobiol. Dis. *69*, 200–205. 10.1016/j.nbd.2014.05.026.

28. Rau, F., Lainé, J., Ramanoudjame, L., Ferry, A., Arandel, L., Delalande, O., Jollet, A., Dingli, F., Lee, K.Y., Peccate, C., et al. (2015). Abnormal splicing switch of DMD's penultimate exon compromises muscle fibre maintenance in myotonic dystrophy. Nat. Commun. *6*. 10.1038/ncomms8205.

29. Fugier, C., Klein, A.F., Hammer, C., Vassilopoulos, S., Ivarsson, Y., Toussaint, A., Tosch, V., Vignaud, A., Ferry, A., Messaddeq, N., et al. (2011). Misregulated alternative splicing of BIN1 is associated with T tubule alterations and muscle weakness in myotonic dystrophy. Nat. Med. *17*, 720–725. 10.1038/NM.2374.

30. Lin, X., Miller, J.W., Mankodi, A., Kanadia, R.N., Yuan, Y., Moxley, R.T., Swanson, M.S., and Thornton, C.A. (2006). Failure of MBNL1-dependent post-natal splicing transitions in myotonic dystrophy. Hum. Mol. Genet. *15*, 2087–2097. 10.1093/hmg/ddl132.

31. Savkur, R.S., Philips, A. V., and Cooper, T.A. (2001). Aberrant regulation of insulin receptor alternative splicing is associated with insulin resistance in myotonic dystrophy. Nat. Genet. *29*, 40–47. 10.1038/ng704.

32. Fugier, C., Klein, A.F., Hammer, C., Vassilopoulos, S., Ivarsson, Y., Toussaint, A., Tosch, V., Vignaud, A., Ferry, A., Messaddeq, N., et al. (2011). Misregulated alternative splicing of BIN1 is associated with T tubule alterations and muscle weakness in myotonic dystrophy. Nat. Med. *17*, 720–725. 10.1038/nm.2374.

33. Yamamoto, T., Miura, A., Itoh, K., Takeshima, Y., and Nishio, H. (2019). RNA sequencing reveals abnormal LDB3 splicing in sudden cardiac death. Forensic Sci. Int. *302*, 109906. 10.1016/j.forsciint.2019.109906.

34. Kimura, T., Nakamori, M., Lueck, J.D., Pouliquin, P., Aoike, F., Fujimura, H., Dirksen, R.T., Takahashi, M.P., Dulhunty, A.F., and Sakoda, S. (2005). Altered mRNA splicing of the skeletal muscle ryanodine receptor and sarcoplasmic/endoplasmic reticulum Ca2+-ATPase in myotonic

dystrophy type 1. Hum. Mol. Genet. *14*, 2189–2200. 10.1093/hmg/ddi223.

35. Rau, F., Lainé, J., Ramanoudjame, L., Ferry, A., Arandel, L., Delalande, O., Jollet, A., Dingli, F., Lee, K.Y., Peccate, C., et al. (2015). Abnormal splicing switch of DMD's penultimate exon compromises muscle fibre maintenance in myotonic dystrophy. Nat. Commun. *6*. 10.1038/ncomms8205.

36. Lee, J.E., Bennett, C.F., and Cooper, T.A. (2012). RNase H-mediated degradation of toxic RNA in myotonic dystrophy type 1. Proc. Natl. Acad. Sci. U. S. A. *109*, 4221–4226. 10.1073/pnas.1117019109.

37. Wojtkowiak-Szlachcic, A., Taylor, K., Stepniak-Konieczna, E., Sznajder, L.J., Mykowska, A., Sroka, J., Thornton, C.A., and Sobczak, K. (2015). Short antisense-locked nucleic acids (all-LNAs) correct alternative splicing abnormalities in myotonic dystrophy. Nucleic Acids Res. *43*, 3318–3331. 10.1093/nar/gkv163.

38. Matloka, M., Klein, A.F., Rau, F., and Furling, D. (2018). Cells of matter-In vitro models for myotonic dystrophy. Front. Neurol. *9*, 1–9. 10.3389/fneur.2018.00361.

39. Philips, A. V., Timchenko, L.T., and Cooper, T.A. (1998). Disruption of splicing regulated by a CUG-binding protein in myotonic dystrophy. Science (80-.). *280*, 737–741. 10.1126/science.280.5364.737.

40. Manandhar, D., Song, L., Kabadi, A., Kwon, J.B., Edsall, L.E., Ehrlich, M., Tsumagari, K., Gersbach, C.A., Crawford, G.E., and Gordân, R. (2017). Incomplete MyoD-induced transdifferentiation is associated with chromatin remodeling deficiencies. Nucleic Acids Res. *45*, 11684–11699. 10.1093/nar/gkx773.

41. Spitalieri, P., Talarico, R. V., Caioli, S., Murdocca, M., Serafino, A., Girasole, M., Dinarelli, S., Longo, G., Pucci, S., Botta, A., et al. (2018). Modelling the pathogenesis of Myotonic Dystrophy type 1 cardiac phenotype through human iPSC-derived cardiomyocytes. J. Mol. Cell. Cardiol. *118*, 95–109. 10.1016/j.yjmcc.2018.03.012.

42. Ueki, J., Nakamori, M., Nakamura, M., Nishikawa, M., Yoshida, Y., Tanaka, A., Morizane, A., Kamon, M., Araki, T., Takahashi, M.P., et al. (2017). Myotonic dystrophy type 1 patient-derived iPSCs for the investigation of CTG repeat instability. Sci. Rep. *7*, 1–7. 10.1038/srep42522.

43. Maqsood, M.I., Matin, M.M., Bahrami, A.R., and Ghasroldasht, M.M. (2013). Immortality of cell lines: Challenges and advantages of establishment. Cell Biol. Int. *37*, 1038–1045. 10.1002/cbin.10137.

44. Arandel, L., Espinoza, M.P., Matloka, M., Bazinet, A., De Dea Diniz, D., Naouar, N., Rau, F., Jollet, A., Edom-Vovard, F., Mamchaoui, K., et al. (2017). Immortalized human myotonic dystrophy muscle cell lines to assess therapeutic compounds. DMM Dis. Model. Mech. *10*, 487–497. 10.1242/dmm.027367.

45. Pantic, B., Borgia, D., Giunco, S., Malena, A., Kiyono, T., Salvatori, S., De Rossi, A., Giardina, E., Sangiuolo, F., Pegoraro, E., et al. (2016). Reliable and versatile immortal muscle cell models from healthy and myotonic dystrophy type 1 primary human myoblasts. Exp. Cell Res. *342*, 39–51. 10.1016/j.yexcr.2016.02.013.

46. Bigot, A., Klein, A.F., Gasnier, E., Jacquemin, V., Ravassard, P., Butler-Browne, G., Mouly, V., and Furling, D. (2009). Large CTG repeats trigger p16-dependent premature senescence in myotonic dystrophy type 1 muscle precursor cells. Am. J. Pathol. *174*, 1435–1442. 10.2353/ajpath.2009.080560.

47. Romagnoli, C., and Brandi, M.L. (2021). Muscle Physiopathology in Parathyroid Hormone Disorders. Front. Med. *8*, 1–7. 10.3389/fmed.2021.764346.

48. Manning, K.S., Rao, A.N., Castro, M., and Cooper, T.A. (2017). BNANC Gapmers Revert Splicing and Reduce RNA Foci with Low Toxicity in Myotonic Dystrophy Cells. ACS Chem. Biol. *12*, 2503–2509. 10.1021/ACSCHEMBIO.7B00416/SUPPL_FILE/CB7B00416_SI_001.PDF.

49. Morales, F., Couto, J.M., Higham, C.F., Hogg, G., Cuenca, P., Braida, C., Wilson, R.H., Adam, B., del Valle, G., Brian, R., et al. (2012). Somatic instability of the expanded CTG triplet repeat in myotonic dystrophy type 1 is a heritable quantitative trait and modifier of disease severity. Hum. Mol. Genet. *21*, 3558–3567. 10.1093/hmg/dds185.

50. Cumming, S.A., Jimenez-Moreno, C., Okkersen, K., Wenninger, S., Daidj, F., Hogarth, F., Littleford, R., Gorman, G., Bassez, G., Schoser, B., et al. (2019). Genetic determinants of disease severity in the myotonic dystrophy type 1 OPTIMISTIC cohort. Neurology *93*, e995–e1009. 10.1212/WNL.0000000000008056.

51. Pešović, J., Perić, S., Brkušanin, M., Brajušković, G., Rakoč Ević - Stojanović, V., and Savić-Pavić Ević, D. (2018). Repeat Interruptions Modify Age at Onset in Myotonic Dystrophy Type 1 by Stabilizing DMPK Expansions in Somatic Cells. Front. Genet. *9*, 1–14. 10.3389/FGENE.2018.00601.

52. Ballester-Lopez, A., Koehorst, E., Linares-Pardo, I., Núñez-Manchón, J., Almendrote, M., Lucente, G., Arbex, A., Alonso, C.P., Lucia, A., Monckton, D.G., et al. (2020). Preliminary Findings on CTG Expansion

Determination in Different Tissues from Patients with Myotonic Dystrophy Type 1. Genes (Basel). *11*, 1–8. 10.3390/GENES11111321.

53. Tsai, Y.C., de Pontual, L., Heiner, C., Stojkovic, T., Furling, D., Bassez, G., Gourdon, G., and Tomé, S. (2022). Identification of a CCG-Enriched Expanded Allele in Patients with Myotonic Dystrophy Type 1 Using Amplification-Free Long-Read Sequencing. J. Mol. Diagn. *24*, 1143–1154. 10.1016/J.JMOLDX.2022.08.003.

54. Rasmussen, A., Hildonen, M., Vissing, J., Duno, M., Tümer, Z., and Birkedal, U. (2022). High Resolution Analysis of DMPK Hypermethylation and Repeat Interruptions in Myotonic Dystrophy Type 1. Genes (Basel). *13*. 10.3390/GENES13060970.

55. Jones, P.A., Wolkowicz, M.J., Rideout, W.M., Gonzales, F.A., Marziasz, C.M., Coetzee, G.A., and Tapscott, S.J. (1990). De novo methylation of the MyoD1 CpG island during the establishment of immortal cell lines. Proc Natl Acad Sci U S A. *87*. 10.1073/pnas.87.16.6117.

56. Antequera, F., and J Boyes, A.B. (1990). High levels of de novo methylation and altered chromatin structure at CpG islands in cell lines. Cell *62*. 10.1016/0092-8674(90)90015-7.

57. Jones, P.A. (2012). Functions of DNA methylation: islands, start sites, gene bodies and beyond. Nat. Rev. Genet. *13*, 484–492. 10.1038/NRG3230.

58. Carrió, E., Díez-Villanueva, A., Lois, S., Mallona, I., Cases, I., Forn, M., Peinado, M.A., and Suelves, M. (2015). Deconstruction of DNA methylation patterns during myogenesis reveals specific epigenetic events in the establishment of the skeletal muscle lineage. Stem Cells *33*, 2025–2036. 10.1002/STEM.1998.

59. Reik, W. (2007). Stability and flexibility of epigenetic gene regulation in mammalian development. Nature *447*, 425–432. 10.1038/NATURE05918.

60. Fu, Y.H., Friedman, D.L., Richards, S., Pearlman, J.A., Gibbs, R.A., Pizzuti, A., Ashizawa, T., Perryman, M.B., Scarlato, G., Fenwick, R.G., et al. (1993). Decreased expression of myotonin-protein kinase messenger RNA and protein in adult form of myotonic dystrophy. Science *260*, 235–238. 10.1126/SCIENCE.8469976.

61. T R Klesert, A D Otten, T D Bird, S.J.T. (1997). Trinucleotide repeat expansion at the myotonic dystrophy locus reduces expression of DMAHP. Nat Genet. *16*. 10.1038/ng0897-402.

62. M Alwazzan, E Newman, M G Hamshere, J.D.B. (1999). Myotonic dystrophy is associated with a reduced level of RNA from the DMWD

allele adjacent to the expanded repeat. Hum Mol Genet *8*. 10.1093/hmg/8.8.1491.

63. Klesert, T.R., Cho, D.H., Clark, J.I., Maylie, J., Adelman, J., Snider, L., Yuen, E.C., Soriano, P., and Tapscott, S.J. (2000). Mice deficient in Six5 develop cataracts: implications for myotonic dystrophy. Nat. Genet. *25*, 105–109. 10.1038/75490.

64. Westerlaken, J.H.A.M., Van Der Zee, C.E.E.M., Peters, W., and Wieringa, B. (2003). The DMWD protein from the myotonic dystrophy (DM1) gene region is developmentally regulated and is present most prominently in synapse-dense brain areas. Brain Res. *971*, 116–127. 10.1016/S0006-8993(03)02430-2.

65. Yin, Q., Wang, H., Li, N., Ding, Y., Xie, Z., Jin, L., Li, Y., Wang, Q., Liu, X., Xu, L., et al. (2020). Dosage effect of multiple genes accounts for multisystem disorder of myotonic dystrophy type 1. Cell Res. *30*, 133–145. 10.1038/S41422-019-0264-2.

66. Khajavi, M., Tari, A.M., Patel, N.B., Tsuji, K., Siwak, D.R., Meistrich, M.L., Terry, N.H., and Ashizawa, T. (2001). “Mitotic drive” of expanded CTG repeats in myotonic dystrophy type 1 (DM1). Hum Mol Genet *10*, 855-863. 10.1093/hmg/10.8.855.

67. André, L.M., van Cruchten, R.T.P., Willemse, M., Bezstarosti, K., Demmers, J.A.A., van Agtmaal, E.L., Wansink, D.G., and Wieringa, B. (2019). Recovery in the myogenic program of congenital myotonic dystrophy myoblasts after excision of the expanded (CTG)n repeat. Int. J. Mol. Sci. *20*. 10.3390/ijms20225685.

68. Fernández-Garibay, X., Ortega, M.A., Cerro-Herreros, E., Comelles, J., Martínez, E., Artero, R., Fernández-Costa, J.M., and Ramón-Azcón, J. (2021). Bioengineered in vitro 3D model of myotonic dystrophy type 1 human skeletal muscle. Biofabrication *13*. 10.1088/1758-5090/abf6ae.

69. Guglielmi, V., Vattemi, G., Gualandi, F., Voermans, N.C., Marini, M., Scotton, C., Pegoraro, E., Oosterhof, A., Kósa, M., Zádor, E., et al. (2013). SERCA1 protein expression in muscle of patients with Brody disease and Brody syndrome and in cultured human muscle fibers. Mol. Genet. Metab. *110*, 162–169. 10.1016/j.ymgme.2013.07.015.

70. Kawada, R., Jonouchi, T., Kagita, A., Sato, M., Hotta, A., and Sakurai, H. (2023). Establishment of quantitative and consistent in vitro skeletal muscle pathological models of myotonic dystrophy type 1 using patient-derived iPSCs. Sci. Rep. *13*, 1–17. 10.1038/s41598-022-26614-z.

71. Masayuki Nakamori, Krzysztof Sobczak, Araya Puwanant, Steve Welle, Katy Eichinger, Shree Pandya, Jeannne Dekdebrun, Chad R Heatwole, Michael P McDermott, Tian Chen, Melissa Cline, Rabi Tawil, Robert J Osborne, Thurman M Wheeler, Maurice S Swanson, Richard, C.A.T. (2013). Splicing biomarkers of disease severity in myotonic dystrophy. Ann Neurol . *74*. 10.1002/ana.23992.

72. Pascual-Gilabert, M., Artero, R., and López-Castel, A. (2023). The myotonic dystrophy type 1 drug development pipeline: 2022 edition. Drug Discov. Today *28*, 103489. 10.1016/j.drudis.2023.103489.

73. Batra, R., Nelles, D.A., Roth, D.M., Krach, F., Nutter, C.A., Tadokoro, T., Thomas, J.D., Sznajder, Ł.J., Blue, S.M., Gutierrez, H.L., et al. (2021). The sustained expression of Cas9 targeting toxic RNAs reverses disease phenotypes in mouse models of myotonic dystrophy type 1. Nat. Biomed. Eng. *5*, 157–168. 10.1038/s41551-020-00607-7.

74. Lo Scrudato, M., Poulard, K., Sourd, C., Tomé, S., Klein, A.F., Corre, G., Huguet, A., Furling, D., Gourdon, G., and Buj-Bello, A. (2019). Genome Editing of Expanded CTG Repeats within the Human DMPK Gene Reduces Nuclear RNA Foci in the Muscle of DM1 Mice. Mol. Ther. *27*, 1372–1388. 10.1016/j.ymthe.2019.05.021.

75. Raaijmakers, R.H.L., Ripken, L., Ausems, C.R.M., and Wansink, D.G. (2019). CRISPR/Cas Applications in Myotonic Dystrophy: Expanding Opportunities. Int. J. Mol. Sci. *20*. 10.3390/IJMS20153689.

76. Hu, N., Antoury, L., Baran, T.M., Mitra, S., Bennett, C.F., Rigo, F., Foster, T.H., and Wheeler, T.M. (2018). Non-invasive monitoring of alternative splicing outcomes to identify candidate therapies for myotonic dystrophy type 1. Nat. Commun. *9*. 10.1038/s41467-018-07517-y.

77. Hsieh, W.C., Bahal, R., Thadke, S.A., Bhatt, K., Sobczak, K., Thornton, C., and Ly, D.H. (2018). Design of a “mini” Nucleic Acid Probe for Cooperative Binding of an RNA-Repeated Transcript Associated with Myotonic Dystrophy Type 1. Biochemistry *57*, 907–911. 10.1021/acs.biochem.7b01239.

78. Arandel, L., Matloka, M., Klein, A.F., Rau, F., Sureau, A., Ney, M., Cordier, A., Kondili, M., Polay-Espinoza, M., Naouar, N., et al. (2022). Reversal of RNA toxicity in myotonic dystrophy via a decoy RNA-binding protein with high affinity for expanded CUG repeats. Nat. Biomed. Eng. *6*, 207–220. 10.1038/s41551-021-00838-2.

79. Cerro-Herreros, E., González-Martínez, I., Moreno-Cervera, N., Overby, S., Pérez-Alonso, M., Llamusí, B., and Artero, R. (2020). Therapeutic Potential of AntagomiR-23b for Treating Myotonic Dystrophy. Mol. Ther. Nucleic Acids *21*, 837–849. 10.1016/J.OMTN.2020.07.021.

80. Ketley, A., Chen, C.Z., Li, X., Arya, S., Robinson, T.E., Granados-Riveron, J., Udosen, I., Morris, G.E., Holt, I., Furling, D., et al. (2014). High-content screening identifies small molecules that remove nuclear foci, affect MBNL distribution and CELF1 protein levels via a PKC-independent pathway in myotonic dystrophy cell lines. Hum. Mol. Genet. *23*, 1551–1562. 10.1093/HMG/DDT542.

81. François, V., Klein, A.F., Beley, C., Jollet, A., Lemercier, C., Garcia, L., and Furling, D. (2010). Selective silencing of mutated mRNAs in DM1 by using modified hU7-snRNAs. Nat. Struct. Mol. Biol. 2010 181 *18*, 85–87. 10.1038/nsmb.1958.

82. Wang, Y., Hao, L., Wang, H., Santostefano, K., Thapa, A., Cleary, J., Li, H., Guo, X., Terada, N., Ashizawa, T., et al. (2018). Therapeutic Genome Editing for Myotonic Dystrophy Type 1 Using CRISPR/Cas9. Mol. Ther. *26*, 2617. 10.1016/J.YMTHE.2018.09.003.

83. Mamchaoui, K., Trollet, C., Bigot, A., Negroni, E., Chaouch, S., Wolff, A., Kandalla, P.K., Marie, S., Di Santo, J., St Guily, J.L., et al. (2011). Immortalized pathological human myoblasts: towards a universal tool for the study of neuromuscular disorders. Skelet. Muscle *1*. 10.1186/2044-5040-1-34.

84. Mallona, I., Díez-Villanueva, A., and Peinado, M.A. (2014). Methylation plotter: a web tool for dynamic visualization of DNA methylation data. Source Code Biol. Med. *9*. 10.1186/1751-0473-9-11.

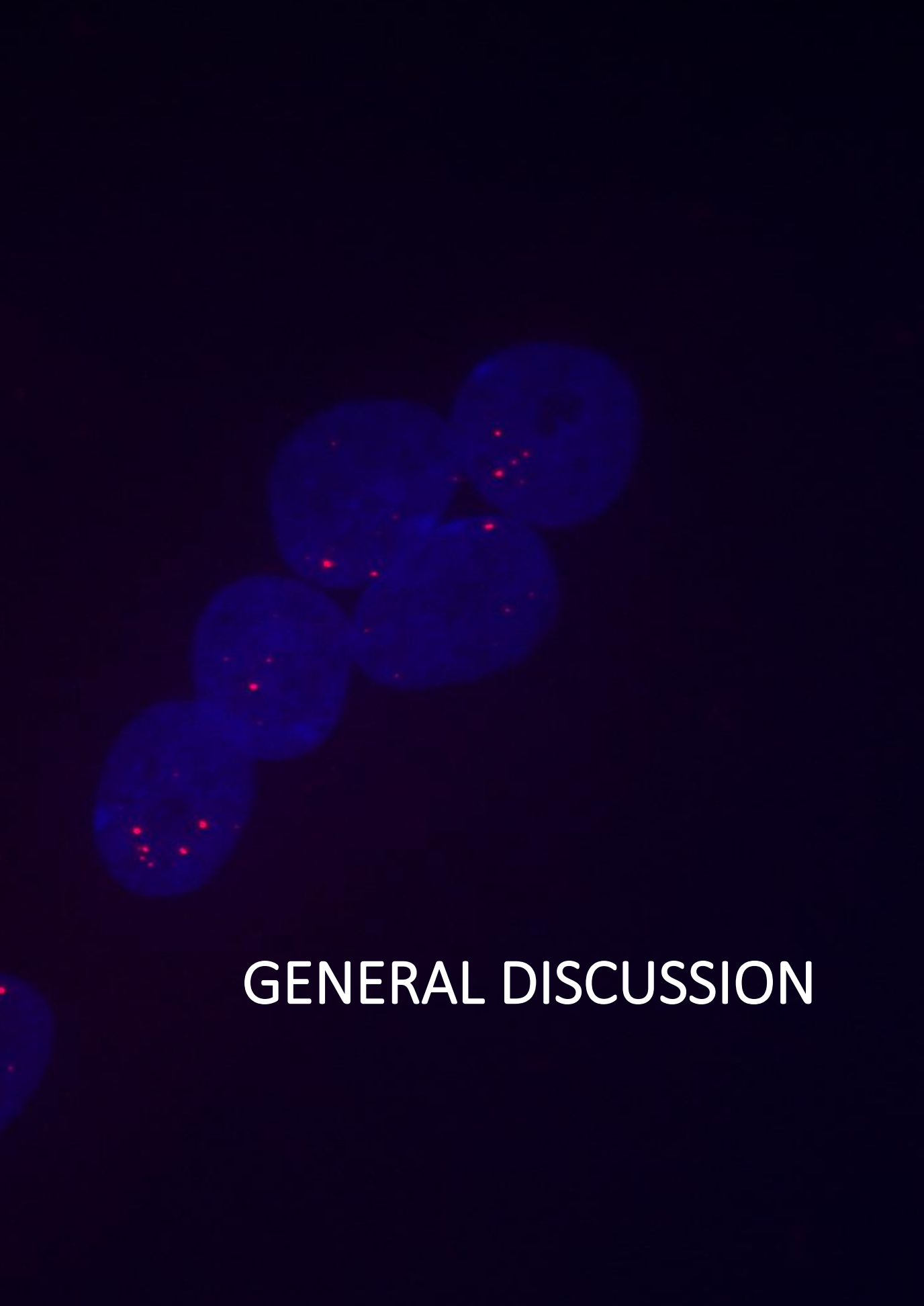

GENERAL DISCUSSION

Heterogeneity is a key factor in DM1, which is observed both clinically and genetically. The organs or systems affected, and the severity of the symptoms can vary significantly between patients. This clinical heterogeneity is partially caused by the CTG repeat expansions instability, which leads to both inter and intraindividual expansion size variability. Clinical and genetic heterogeneity are likely to produce molecular pathophysiology variability and could influence in the degree of efficacy of treatments. For these reasons, DM1 models that reproduce said variability, are a valuable tool in DM1 studies. In this thesis, heterogeneity has been approached from different points of view and results strengthen the need to take into account heterogeneity in DM1 studies.

One of the main molecular hallmarks of DM1, RNA foci accumulation is variable according to cell type and age of onset

DM1 is a multisystemic disease, however, not all organs and tissues are equally affected. Actually, it is known that CTG expansion size is variable in the same patient depending on the tissue or cell type analysed, but no studies had been performed to analyse the molecular alterations in different cell types from a single patient. Moreover, DM1 is a disease that can appear at any age, and despite it is know that the earlier it appears, the more severe the symptom are, it has not been studied the impact of the age of onset at a molecular level. In this study it is analysed the molecular heterogeneity in DM1 samples derived from different cell types and DM1 subtypes.

The study of four different cell types (lymphoblasts, fibroblasts, myoblasts and myotubes) revealed that despite all of them had RNA foci accumulation in the nucleus and MBNL1 aggregates colocalizing with the RNA foci, there were significant differences between lymphoblasts and muscle cells. These differences may be caused by differences in *DMPK* expression levels, which according to the Human Protein Atlas are more than 10 times higher in muscle compared to skin and bone marrow. However, our single-cell study showed no correlation between *DMPK* levels and RNA foci number meaning that there are possibly other contributors. Another contributing factor could be cell turnover, which is known to be lower in muscle than skin and blood, which could benefit the accumulation of RNA foci in muscle cells[135]. These differences highlight the

importance of choosing an appropriate cell model according to the objective of the study.

The study of RNA foci in lymphoblasts samples from the 5 DM1 subtypes (congenital, infantile, juvenile, adult and late-onset) showed significant differences between the subtypes. A higher number of RNA foci was found in the patients of the subtypes with an earlier age of onset. It is known that an earlier age of onset correlates with a larger expansion, which could mean that another factor influencing RNA foci number would be the CTG expansion size[1]. The differences between categories observed in one of the main molecular hallmarks of DM1 emphasize the heterogeneity of the disease and how it is important to consider that therapies may have a different efficacy depending on the patient.

The most relevant disease-associated DM1 molecular alterations are reversed by blocking miR-23b and miR-218 in DM1 human-derived mature myotubes with unrelated genetic backgrounds

Recently, antimiRs, which target and block MBNL1 repressors miR-23b and miR-218 have been developed as potentials treatments to DM1[126,128,129]. Its positive effect had been tested in in vitro and in vivo models; however, it had not been assessed in a range of cell lines that represented the heterogeneity of the disease. In this study, a range of heterogeneous DM1 primary muscle cells were used to test the effect of antimiR-23b-V1 and antimiR-218-V1, reported previously [124dyne], together with a new generation of chemically modified antimiRs named antimiR-23b-V2 and antimiR-218-V2. Results show that the drugs significantly reduce the DM1 associated molecular alterations across a genetically heterogeneous DM1 sample. Moreover, in this study it is discovered that the antimiRs do not only enhance MBNL1 expression, but also reduce *DMPK* transcript levels.

In the study, it was observed a significant upregulation of miR-23b and miR-218 in ten days differentiated DM1 myotubes, which was consistent with the observed lowered amounts of total MBNL1. Moreover, estimated CTG repeat length in the cell lines correlated with both miRNA levels, suggesting a shared pathological activation mechanism. The upregulation of miR-218 and miR-23b

in DM1 is relevant from a therapeutical point of view because it allows for a wider reduction window before possibly reaching undesirable effects.

The treatment with antimiRs, even though it is not directly targeting DMPK, was found to reduce the number of RNA foci in the nucleus of DM1 cells. Prompted by this observation, *DMPK* expression levels were also quantified and it was found an approximate 30% significant reduction. This reduction is expected to have a clinical benefit in patients, as a smaller reduction observed with another drug in a clinical trial significantly improved splicing deregulation and myotonia (ACHIEVE Trial). It is hypothesized that the treatment's correction of the abnormal DM1 exon 5 inclusion in MBNL1 gene may be responsible of the decrease in DMPK RNA foci. The abnormal exon 5 including isoforms, MBNL1 42/43 are mostly expressed in the nucleus, while the exon 5 excluding isoforms, MBNL1 40/41 are mostly expressed in the cytoplasm. Considering that it is known that nuclear MBNL1 promotes foci formation and stabilization, it is proposed that a reduction of the aberrant nuclear splicing isoforms, would minimize RNA foci formation and stabilization[136,137].

Even though all antimiRs showed a positive effect, different results were obtained depending on the target and the chemical version. Versions V1 of the antimiRs had 2'-O-Methyl (2'-OMe) chemistry, included several phosphorothioate (PS) linkages at each end, and were conjugated to cholesterol at the 3' end. Versions V2 of the antimiRs had a combination of 2'-OMe, 2'-O-Methoxyethyl (MOE), and locked nucleic acid (LNA) residues throughout their sequence, and were conjugated to a fatty acid instead of a cholesterol to enhance their biodistribution[138]. It was observed that targeting miR-23b required lower doses than targeting miR-218 to achieve comparable levels of MBNL1 upregulation. Moreover, it was observed that the V2 antimiRs improvement was greater than the V1 antimiRs improvement

AntimiR-23b-V2 treatment effect depended on CTG repeat sizes, as cell lines with small expansions showed significantly more pronounced *DMPK* mRNA reduction than those with longer repeats. Furthermore, DM1 cell lines with shorter CTG expansions showed higher basal MBNL1 levels compared to the other DM1 lines, suggesting that cell lines with long repeats may require a higher increase in MBNL1 levels to reduce *DMPK* expression.

Overall, results suggest that the antimiRs tested in this study may have a combined mechanism of action in which MBNL1 and other direct targets of

the miRNAs 23b and 218 are derepressed and in which *DMPK* transcripts levels are reduced. This combined mechanism corrects DM1 aberrant splicing and other functional DM1 alterations. In conclusion, the study reveals that antimiRs 23b and 218 have therapeutical potential across heterogeneous genetic backgrounds, meaning that they could be useful for treating multiple clinical forms of the disease. Finally, and based on this study results, antimir-23b-V2 was selected for preclinical development.

The development of three immortalized DM1 muscle cell lines, which reproduce the main molecular hallmarks of the disease, will be useful to study DM1's pathophysiology and treatment efficacy in different genetic and molecular contexts

Clinical, genetic and molecular heterogenicity in DM1 is often not represented in the cellular models used to study the disease. Cellular models that mimic patient's heterogeneity may be key to better understand the molecular mechanisms of DM1 and to assess therapeutical effect of therapies that are under development. Even though, primary cells from the most affected tissues may be the most reliable cellular models to study DM1, limitations in its accessibility and proliferation opened the need to find alternatives such as immortalized cell models. We have generated three immortalized human muscle cell lines derived from three different subtypes of DM1 patients (juvenile, adult, late-onset) who show different clinical characteristics.

The study revealed that the generated DM1 cellular models show the genetic, epigenetic and molecular hallmarks of the disease and are suitable to study potential treatments. Moreover, it showed that there is heterogeneity between the three cell lines DM1 studied alterations.

From a genetic point of view, it was studied the ePAL, the most abundant population and the instability of the CTG expansion. Somatic instability of the CTG expansion has been previously described to be a contributor of disease severity[139], yet the major genetic contributor of the severity is usually the ePAL. It was found that there was genetic variability in the CTG expansion size and instability between the three patient's samples. In our sample, the most severely affected patient was the one with the largest most abundant population and with the greatest instability in both primary and immortalized

cells, but it was the one with the largest ePAL just in immortalized cells. The differences between primary and immortalized cultures could be due the clonal selection that takes place during the immortalization process.

From an epigenetic point of view, it was studied the methylation pattern of CTCF1, a region upstream the CTG repeat, which flanks one of the ends of a 3.5 kb CpG island that overlaps with the expansion. It has been previously demonstrated that the CTCF1 region was methylated in a tissue-specific manner in DM1 muscle biopsies and in primary DM1 muscle cells, whereas tissues and cells from unaffected individuals were completely unmethylated[45]. In this study, the DM1 immortalized muscle cells showed the previously reported CTCF1 hypermethylation in both myoblasts and myotubes meaning that the DNA methylation alterations were preserved. However, we observed a significant increase in the methylation levels in immortalized cell lines methylation levels compared to the primary ones. This could be explained either by the fact that immortalized cell lines are in culture for a prolongated time (they derive from a single clone) which is known to increase DNA methylation levels[140,141] and/or because of the purity of cell cultures. DNA methylation is considered a repressive epigenetic mark that plays a role in gene silencing[142–144]. Although it was not found a significant reduction of DMPK and its surrounding genes SIX5 and DMWD in the study, probably due to a small sample, it has been previously reported a decrease in the expression of these genes in DM1[145–147]. In fact, a quadruple mutant mouse model in which expression of SIX5, DMWD, DMPK and MBNL1 were reduced, reproduced the most typical manifestations in congenital DM1, which suggests that changes in DMPK, SIX5 and DMWD expression, which could be partially regulated by CTCF1 methylation levels, modulate DM1 severity[148].

From a molecular point of view, it was studied RNA foci accumulation, MBNL1 sequestration and splicing alterations. It was revealed a heterogeneous accumulation of RNA foci and sequestration of MBNL1 in the immortalized cell models. Indeed, it was observed that the higher the CTG instability, the higher the average RNA foci and MBNL1 aggregates per cell. These results match with a previous study that reported a direct association between CTG size and foci number in muscle cells[149]. The study also showed that the immortalized models had the splicing alterations that characterize DM1 in *BIN1, ATP2A1, MBNL1, LDB3, INSR*, *DMD* and *KIF13A* trancripts[150]. Moreover, it was found

that there were significant differences in the missplicing levels of KIF13A between the DM1 cell lines.

From a therapeutic point of view, in this study it was demonstrated that the immortalized DM1 models, equally to what is observed in primary DM1 models, showed a reduction in RNA foci and MBNL1 aggregates and a significant recovery of *MBNL1* splicing after being treated with an ASO that targeted the CTG expansion[151].

Overall, results reveal that the immortalized DM1 cellular models reproduce the main genetic, epigenetic and molecular hallmarks present in the primary models and that are a suitable model to study therapies under development. Moreover, the results show heterogeneity between the three cell lines which will allow to study the disease pathophysiology and to test candidate treatments in a larger and more diverse sample than was previously available.

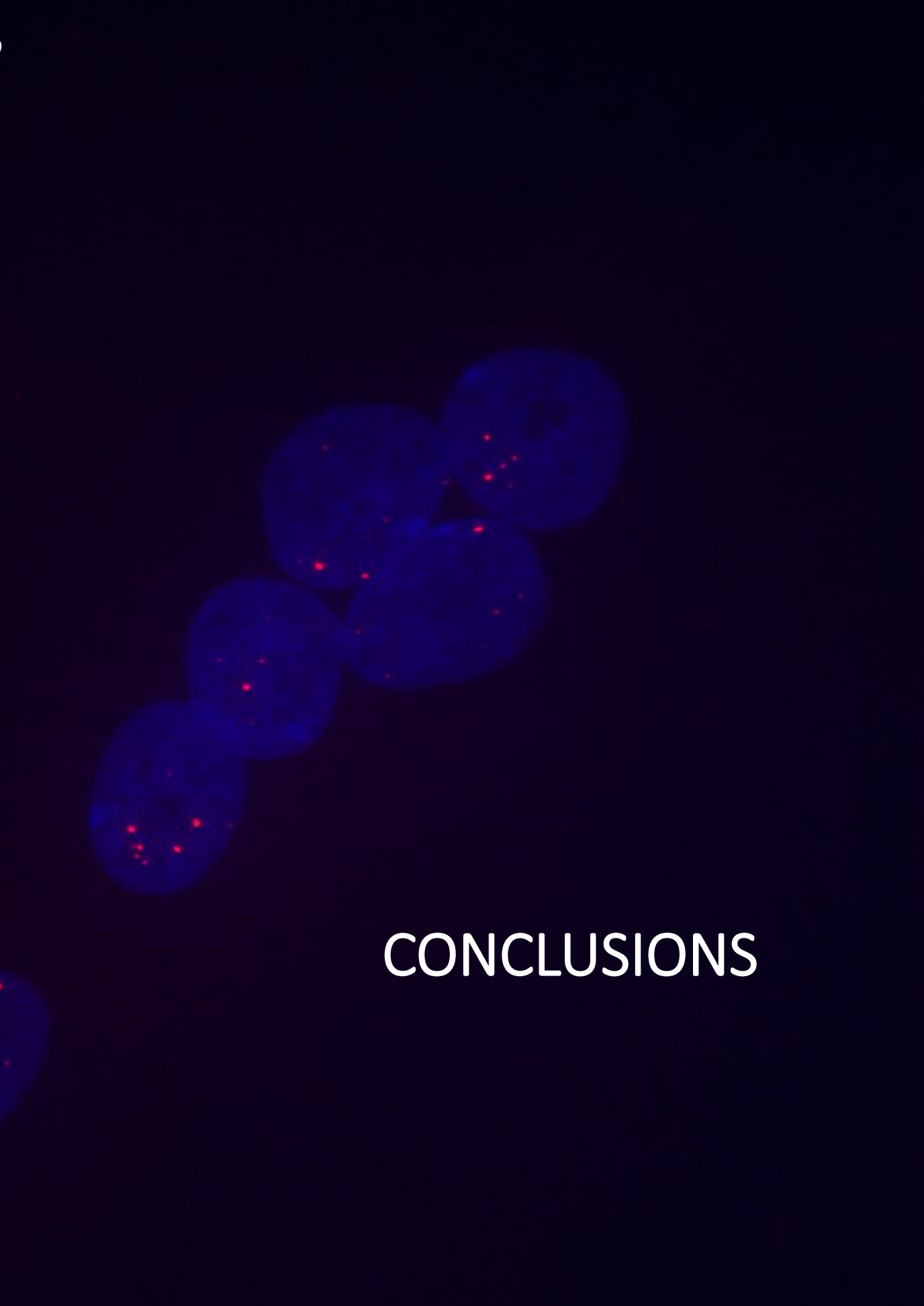

CONCLUSIONS

The main conclusion of this doctoral thesis is that heterogeneity is a key factor in DM1, which should be taken into account when studying the pathophysiology or the efficacy of a new therapeutical compound.

Chapter 1

- Lymphoblast, fibroblast, myoblast and myotube cells derived from patients are good models to study DM1, since they show alterations in two of the main hallmarks of the disease, RNA foci accumulation and MBNL1 sequestration.

- The differences in RNA foci formation and MBNL1 sequestration, due to the cell type model and due to the patient age of onset, should be kept in mind when selecting DM1 models for scientific studies.

- Number of RNA foci in patient derived myoblasts does not correlate with *DMPK* expression levels, indicating that single cell RNA foci accumulation is dependent on other factors.

Chapter 2

- AntimiRs 23b and 218 significantly ameliorate DM1-associated molecular alterations in primary myotubes with heterogeneous genetic background, indicating that these therapies in development could be of use for a broad group of DM1 patients.

- Our results suggest that antimiR-23b and antimir-218 have a combined mechanism of action by both upregulating its direct target, MBNL1, and reducing *DMPK* transcripts levels.

- The chemical improvements of antimiR-23b-V2 showed better results in reversing the molecular alterations in DM1 than V1 and the two versions of antimiR-218, Furthermore antimiR-23b achieved these results at lower doses than antimiR-218. Based on these results, antimiR-23b-V2 has been selected for further clinical studies.

Chapter 3

- The three immortalized DM1 muscle cell lines generated reproduce the main genetic, epigenetic and molecular hallmarks present in the primary DM1 models and in DM1, and are a suitable tool to study further the disease and to test therapies under development.

- The presence of molecular heterogeneity, which characterizes DM1, among the three generated muscle cell lines, will allow studies of disease pathophysiology and testing of treatments, in a larger and more diverse sample than previously available.

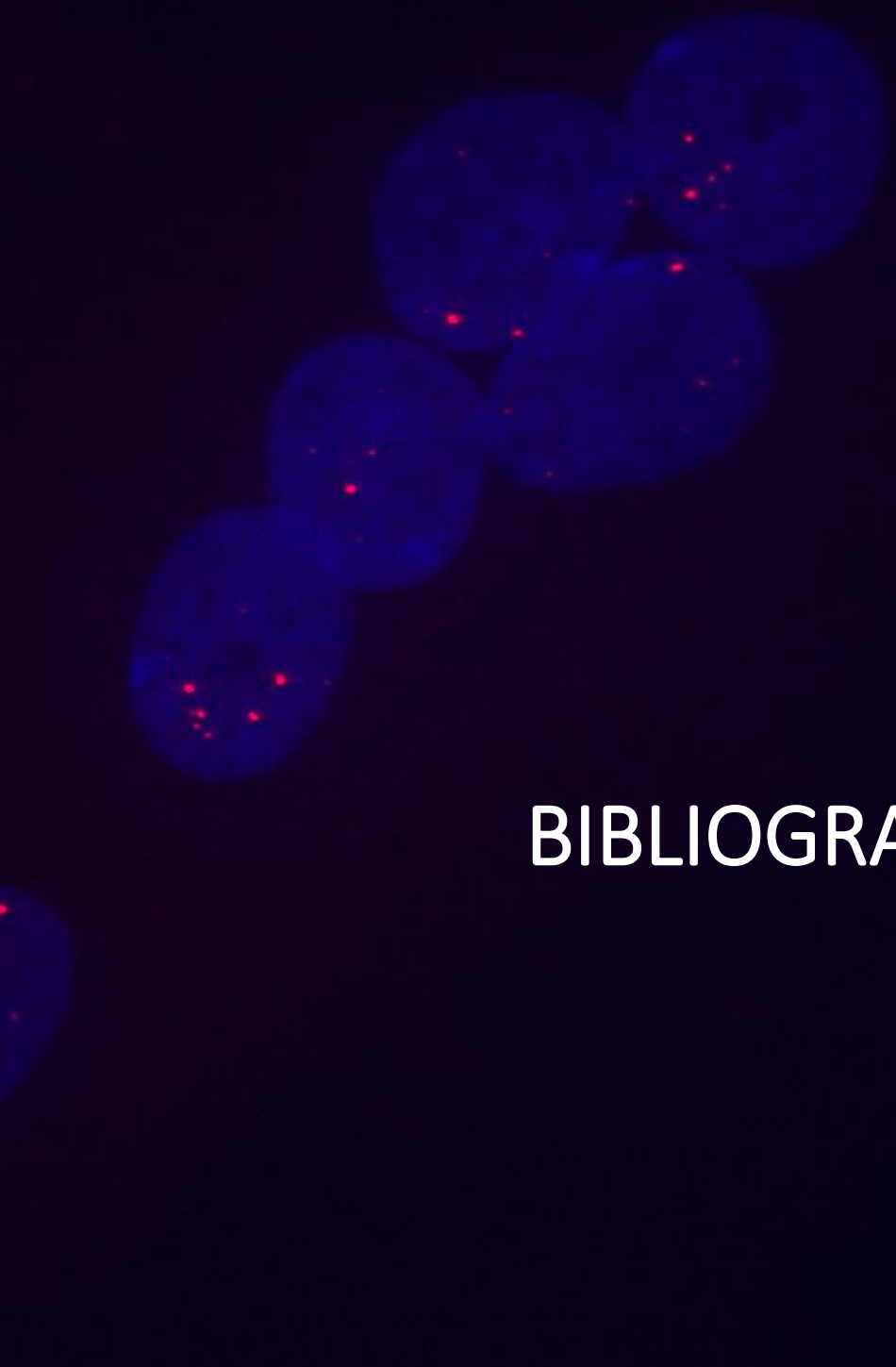

BIBLIOGRAPHY

1. Bird TD. *Myotonic Dystrophy Type 1*.; 1993.

2. Brook JD, McCurrach ME, Harley HG, et al. Molecular basis of myotonic dystrophy: expansion of a trinucleotide (CTG) repeat at the 3' end of a transcript encoding a protein kinase family member. *Cell*. 1992;68(4):799-808. doi:10.1016/0092-8674(92)90154-5

3. Mishra SK, Singh S, Lee B, Khosa S, Moheb N, Tandon VA. "Dystrophia Myotonica" and the Legacy of Hans Gustav Wilhelm Steinert. *Ann Indian Acad Neurol*. 2018;21(2):116-118. doi:10.4103/aian.AIAN_182_17

4. Johnson NE, Butterfield RJ, Mayne K, et al. Population-Based Prevalence of Myotonic Dystrophy Type 1 Using Genetic Analysis of Statewide Blood Screening Program. *Neurology*. 2021;96(7):e1045-e1053. doi:10.1212/WNL.0000000000011425

5. Ashizawa T, Gagnon C, Groh WJ, et al. Consensus-based care recommendations for adults with myotonic dystrophy type 1. *Neurol Clin Pract*. 2018;8(6):507-520. doi:10.1212/CPJ.0000000000000531

6. Liao Q, Zhang Y, He J, Huang K. Global Prevalence of Myotonic Dystrophy: An Updated Systematic Review and Meta-Analysis. *Neuroepidemiology*. 2022;56(3):163-173. doi:10.1159/000524734

7. De Antonio M, Dogan C, Hamroun D, et al. Unravelling the myotonic dystrophy type 1 clinical spectrum: A systematic registry-based study with implications for disease classification. *Rev Neurol (Paris)*. 2016;172(10):572-580. doi:10.1016/j.neurol.2016.08.003

8. Campbell C, Levin S, Siu VM, Venance S, Jacob P. Congenital myotonic dystrophy: Canadian population-based surveillance study. *J Pediatr*. 2013;163(1):120-5.e1-3. doi:10.1016/j.jpeds.2012.12.070

9. Echenne B, Bassez G. Congenital and infantile myotonic dystrophy. *Handb Clin Neurol*. 2013;113:1387-1393. doi:10.1016/B978-0-444-59565-2.00009-5

10. Echenne B, Rideau A, Roubertie A, Sébire G, Rivier F, Lemieux B. Myotonic dystrophy type I in childhood Long-term evolution in patients surviving the neonatal period. *Eur J Paediatr Neurol*. 2008;12(3):210-223. doi:10.1016/j.ejpn.2007.07.014

11. Ho G, Cardamone M, Farrar M. Congenital and childhood myotonic dystrophy: Current aspects of disease and future directions. *World J Clin Pediatr*. 2015;4(4):66. doi:10.5409/wjcp.v4.i4.66

12. Meola G, Cardani R. Myotonic dystrophies: An update on clinical aspects, genetic, pathology, and molecular pathomechanisms. *Biochim Biophys Acta Mol Basis Dis*. 2015;1852(4):594-606. doi:10.1016/j.bbadis.2014.05.019

13. de Die-Smulders CE, Höweler CJ, Thijs C, et al. Age and causes of death in adult-onset myotonic dystrophy. *Brain*. 1998;121 (Pt 8):1557-1563. doi:10.1093/brain/121.8.1557

14. Bellini M, Biagi S, Stasi C, et al. Gastrointestinal manifestations in myotonic muscular dystrophy. *World J Gastroenterol*. 2006;12(12):1821-1828. doi:10.3748/wjg.v12.i12.1821

15. Antonini G, Soscia F, Giubilei F, et al. Health-related quality of life in myotonic dystrophy type 1 and its relationship with cognitive and emotional functioning. *J Rehabil Med*. 2006;38(3):181-185. doi:10.1080/16501970500477967

16. Turner C, Hilton-Jones D. The myotonic dystrophies: diagnosis and management. *J Neurol Neurosurg Psychiatry*. 2010;81(4):358-367. doi:10.1136/jnnp.2008.158261

17. Redman JB, Fenwick RG, Fu YH, Pizzuti A, Caskey CT. Relationship between parental trinucleotide GCT repeat length and severity of myotonic dystrophy in offspring. *JAMA*. 1993;269(15):1960-1965.

18. Hunter A, Tsilfidis C, Mettler G, et al. The correlation of age of onset with CTG trinucleotide repeat amplification in myotonic dystrophy. *J Med Genet*. 1992;29(11):774-779. doi:10.1136/jmg.29.11.774

19. Harper PS, Harley HG, Reardon W, Shaw DJ. Anticipation in myotonic dystrophy: new light on an old problem. *Am J Hum Genet*. 1992;51(1):10-16.

20. Morales F, Vásquez M, Cuenca P, et al. Parental age effects, but no evidence for an intrauterine effect in the transmission of myotonic dystrophy type 1. *Eur J Hum Genet*. 2015;23(5):646-653. doi:10.1038/ejhg.2014.138

21. Brunner HG, Brüggenwirth HT, Nillesen W, et al. Influence of sex of the transmitting parent as well as of parental allele size on the CTG expansion in myotonic dystrophy (DM). *Am J Hum Genet*. 1993;53(5):1016-1023.

22. Lagrue E, Dogan C, De Antonio M, et al. A large multicenter study of pediatric myotonic dystrophy type 1 for evidence-based management. *Neurology*. 2019;92(8):e852-e865. doi:10.1212/WNL.0000000000006948

23. Dogan C, De Antonio M, Hamroun D, et al. Gender as a Modifying Factor Influencing Myotonic Dystrophy Type 1 Phenotype Severity and Mortality: A Nationwide Multiple Databases Cross-Sectional Observational Study. *PLoS One*. 2016;11(2):e0148264. doi:10.1371/journal.pone.0148264

24. Redman JB. Relationship Between Parental Trinucleotide GCT Repeat Length and Severity of Myotonic Dystrophy in Offspring. *JAMA: The Journal of the American Medical Association*. 1993;269(15):1960. doi:10.1001/jama.1993.03500150072029

25. Jansen G, Willems P, Coerwinkel M, et al. Gonosomal mosaicism in myotonic dystrophy patients: involvement of mitotic events in (CTG)n repeat variation and selection against extreme expansion in sperm. *Am J Hum Genet*. 1994;54(4):575-585.

26. Dogan C, De Antonio M, Hamroun D, et al. Gender as a Modifying Factor Influencing Myotonic Dystrophy Type 1 Phenotype Severity and Mortality: A Nationwide Multiple Databases Cross-Sectional Observational Study. *PLoS One*. 2016;11(2):e0148264. doi:10.1371/journal.pone.0148264

27. Ashizawa T, Anvret M, Baiget M, et al. Characteristics of intergenerational contractions of the CTG repeat in myotonic dystrophy. *Am J Hum Genet*. 1994;54(3):414-423.

28. Harley HG, Rundle SA, MacMillan JC, et al. Size of the unstable CTG repeat sequence in relation to phenotype and parental transmission in myotonic dystrophy. *Am J Hum Genet*. 1993;52(6):1164-1174.

29. Morales F, Couto JM, Higham CF, et al. Somatic instability of the expanded CTG triplet repeat in myotonic dystrophy type 1 is a heritable quantitative trait and modifier of disease severity. *Hum Mol Genet*. 2012;21(16):3558-3567. doi:10.1093/hmg/dds185

30. Monckton DG, Wong LJ, Ashizawa T, Caskey CT. Somatic mosaicism, germline expansions, germline reversions and intergenerational reductions in myotonic dystrophy males: small pool PCR analyses. *Hum Mol Genet*. 1995;4(1):1-8. doi:10.1093/hmg/4.1.1

31. Cheng S, Barceló JM, Korneluk RG. Characterization of large CTG repeat expansions in myotonic dystrophy alleles using PCR. *Hum Mutat*. 1996;7(4):304-310. doi:10.1002/(SICI)1098-1004(1996)7:4<304::AID-HUMU3>3.0.CO;2-8

32. Thornton CA, Johnson K, Moxley RT. Myotonic dystrophy patients have larger CTG expansions in skeletal muscle than in leukocytes. *Ann Neurol*. 1994;35(1):104-107. doi:10.1002/ana.410350116

33. Anvret M, Ahlberg G, Grandell U, Hedberg B, Johnson K, Edström L. Larger expansions of the CTG repeat in muscle compared to lymphocytes from patients with myotonic dystrophy. *Hum Mol Genet*. 1993;2(9):1397-1400. doi:10.1093/hmg/2.9.1397

34. Peterlin B, Logar N, Zidar J. CTG repeat analysis in lymphocytes, muscles and fibroblasts in patients with myotonic dystrophy. *Pflugers Arch*. 1996;431(6 Suppl 2):R199-200. doi:10.1007/BF02346337

35. Martorell L, Martinez JM, Carey N, Johnson K, Baiget M. Comparison of CTG repeat length expansion and clinical progression of myotonic dystrophy over a five year period. *J Med Genet*. 1995;32(8):593-596. doi:10.1136/jmg.32.8.593

36. Pešović J, Perić S, Brkušanin M, Brajušković G, Rakoč Ević -Stojanović V, Savić-Pavić Ević D. Repeat Interruptions Modify Age at Onset in Myotonic Dystrophy Type 1 by Stabilizing DMPK Expansions in Somatic Cells. *Front Genet*. 2018;9:1-14. doi:10.3389/FGENE.2018.00601

37. Musova Z, Mazanec R, Krepelova A, et al. Highly unstable sequence interruptions of the CTG repeat in the myotonic dystrophy gene. *Am J Med Genet A*. 2009;149A(7):1365-1374. doi:10.1002/ajmg.a.32987

38. Braida C, Stefanatos RKA, Adam B, et al. Variant CCG and GGC repeats within the CTG expansion dramatically modify mutational dynamics and likely contribute toward unusual symptoms in some myotonic dystrophy type 1 patients. *Hum Mol Genet*. 2010;19(8):1399-1412. doi:10.1093/hmg/ddq015

39. Botta A, Rossi G, Marcaurelio M, et al. Identification and characterization of 5' CCG interruptions in complex DMPK expanded alleles. *Eur J Hum Genet*. 2017;25(2):257-261. doi:10.1038/ejhg.2016.148

40. Pešović J, Perić S, Brkušanin M, Brajušković G, Rakočević-Stojanović V, Savić-Pavićević D. Molecular genetic and clinical characterization of myotonic dystrophy type 1 patients carrying variant repeats within DMPK expansions. *Neurogenetics*. 2017;18(4):207-218. doi:10.1007/s10048-017-0523-7

41. Cumming SA, Hamilton MJ, Robb Y, et al. De novo repeat interruptions are associated with reduced somatic instability and mild or absent clinical

features in myotonic dystrophy type 1. *Eur J Hum Genet*. 2018;26(11):1635-1647. doi:10.1038/s41431-018-0156-9

42. Tomé S, Dandelot E, Dogan C, et al. Unusual association of a unique CAG interruption in 5' of DM1 CTG repeats with intergenerational contractions and low somatic mosaicism. *Hum Mutat*. 2018;39(7):970-982. doi:10.1002/humu.23531

43. Ballester-Lopez A, Koehorst E, Almendrote M, et al. A DM1 family with interruptions associated with atypical symptoms and late onset but not with a milder phenotype. *Hum Mutat*. 2020;41(2):420-431. doi:10.1002/humu.23932

44. Moore LD, Le T, Fan G. DNA Methylation and Its Basic Function. *Neuropsychopharmacology*. 2013;38(1):23-38. doi:10.1038/npp.2012.112

45. Filippova GN, Thienes CP, Penn BH, et al. CTCF-binding sites flank CTG/CAG repeats and form a methylation-sensitive insulator at the DM1 locus. *Nat Genet*. 2001;28(4):335-343. doi:10.1038/ng570

46. Koehorst E, Odria R, Capó J, et al. An Integrative Analysis of DNA Methylation Pattern in Myotonic Dystrophy Type 1 Samples Reveals a Distinct DNA Methylation Profile between Tissues and a Novel Muscle-Associated Epigenetic Dysregulation. *Biomedicines*. 2022;10(6). doi:10.3390/BIOMEDICINES10061372

47. Alwazzan M, Newman E, Hamshere MG, Brook JD. Myotonic Dystrophy Is Associated with a Reduced Level of RNA from the DMWD Allele Adjacent to the Expanded Repeat. *Hum Mol Genet*. 1999;8(8):1491-1497. doi:10.1093/hmg/8.8.1491

48. Inukai A, Doyu M, Kato T, et al. Reduced expression of DMAHP/SIX5 gene in myotonic dystrophy muscle. *Muscle Nerve*. 2000;23(9):1421-1426. doi:10.1002/1097-4598(200009)23:9<1421::aid-mus14>3.0.co;2-y

49. Mateos-Aierdi AJ, Goicoechea M, Aiastui A, et al. Muscle wasting in myotonic dystrophies: a model of premature aging. *Front Aging Neurosci*. 2015;7. doi:10.3389/fnagi.2015.00125

50. Taneja KL, McCurrach M, Schalling M, Housman D, Singer RH. Foci of trinucleotide repeat transcripts in nuclei of myotonic dystrophy cells and tissues. *Journal of Cell Biology*. 1995;128(6):995-1002. doi:10.1083/jcb.128.6.995

51. Mankodi A, Logigian E, Callahan L, et al. Myotonic dystrophy in transgenic mice expressing an expanded CUG repeat. *Science*. 2000;289(5485):1769-1773. doi:10.1126/science.289.5485.1769

52. Ballester-Lopez A, Núñez-Manchón J, Koehorst E, et al. Three-dimensional imaging in myotonic dystrophy type 1: Linking molecular alterations with disease phenotype. *Neurol Genet*. 2020;6(4):e484. doi:10.1212/NXG.0000000000000484

53. Botta A, Rinaldi F, Catalli C, et al. The CTG repeat expansion size correlates with the splicing defects observed in muscles from myotonic dystrophy type 1 patients. *J Med Genet*. 2008;45(10):639-646. doi:10.1136/jmg.2008.058909

54. Pascual M, Vicente M, Monferrer L, Artero R. The Muscleblind family of proteins: an emerging class of regulators of developmentally programmed alternative splicing. *Differentiation*. 2006;74(2-3):65-80. doi:10.1111/j.1432-0436.2006.00060.x

55. Fardaei M, Rogers MT, Thorpe HM, et al. Three proteins, MBNL, MBLL and MBXL, co-localize in vivo with nuclear foci of expanded-repeat transcripts in DM1 and DM2 cells. *Hum Mol Genet*. 2002;11(7):805-814. doi:10.1093/hmg/11.7.805

56. Kuyumcu-Martinez NM, Wang GS, Cooper TA. Increased Steady-State Levels of CUGBP1 in Myotonic Dystrophy 1 Are Due to PKC-Mediated Hyperphosphorylation. *Mol Cell*. 2007;28(1):68-78. doi:10.1016/j.molcel.2007.07.027

57. Chau A, Kalsotra A. Developmental insights into the pathology of and therapeutic strategies for DM1: Back to the basics. *Developmental Dynamics*. 2015;244(3):377-390. doi:10.1002/dvdy.24240

58. López-Martínez A, Soblechero-Martín P, de-la-Puente-Ovejero L, Nogales-Gadea G, Arechavala-Gomeza V. An Overview of Alternative Splicing Defects Implicated in Myotonic Dystrophy Type I. *Genes (Basel)*. 2020;11(9). doi:10.3390/genes11091109

59. Lueck JD, Mankodi A, Swanson MS, Thornton CA, Dirksen RT. Muscle Chloride Channel Dysfunction in Two Mouse Models of Myotonic Dystrophy. *J Gen Physiol*. 2007;129(1):79-94. doi:10.1085/jgp.200609635

60. Savkur RS, Philips A V., Cooper TA. Aberrant regulation of insulin receptor alternative splicing is associated with insulin resistance in myotonic dystrophy. *Nat Genet*. 2001;29(1):40-47. doi:10.1038/ng704

61. Kimura T, Nakamori M, Lueck JD, et al. Altered mRNA splicing of the skeletal muscle ryanodine receptor and sarcoplasmic/endoplasmic reticulum Ca2+-ATPase in myotonic dystrophy type 1. *Hum Mol Genet*. 2005;14(15):2189-2200. doi:10.1093/hmg/ddi223

62. Fugier C, Klein AF, Hammer C, et al. Misregulated alternative splicing of BIN1 is associated with T tubule alterations and muscle weakness in myotonic dystrophy. *Nat Med*. 2011;17(6):720-725. doi:10.1038/nm.2374

63. Rau F, Lainé J, Ramanoudjame L, et al. Abnormal splicing switch of DMD's penultimate exon compromises muscle fibre maintenance in myotonic dystrophy. *Nat Commun*. 2015;6(1):7205. doi:10.1038/ncomms8205

64. Konieczny P, Stepniak-Konieczna E, Sobczak K. MBNL proteins and their target RNAs, interaction and splicing regulation. *Nucleic Acids Res*. 2014;42(17):10873-10887. doi:10.1093/nar/gku767

65. Freyermuth F, Rau F, Kokunai Y, et al. Splicing misregulation of SCN5A contributes to cardiac-conduction delay and heart arrhythmia in myotonic dystrophy. *Nat Commun*. 2016;7(1):11067. doi:10.1038/ncomms11067

66. Nakamori M, Sobczak K, Puwanant A, et al. Splicing biomarkers of disease severity in myotonic dystrophy. *Ann Neurol*. 2013;74(6):862-872. doi:10.1002/ana.23992

67. Goodwin M, Mohan A, Batra R, et al. MBNL Sequestration by Toxic RNAs and RNA Misprocessing in the Myotonic Dystrophy Brain. *Cell Rep*. 2015;12(7):1159-1168. doi:10.1016/j.celrep.2015.07.029

68. Jiang H, Mankodi A, Swanson MS, Moxley RT, Thornton CA. Myotonic dystrophy type 1 is associated with nuclear foci of mutant RNA, sequestration of muscleblind proteins and deregulated alternative splicing in neurons. *Hum Mol Genet*. 2004;13(24):3079-3088. doi:10.1093/hmg/ddh327

69. Maeda M, Taft CS, Bush EW, et al. Identification, tissue-specific expression, and subcellular localization of the 80- and 71-kDa forms of myotonic dystrophy kinase protein. *J Biol Chem*. 1995;270(35):20246-20249. doi:10.1074/jbc.270.35.20246

70. Lam LT, Pham YC, Nguyen TM, Morris GE. Characterization of a monoclonal antibody panel shows that the myotonic dystrophy protein kinase, DMPK, is expressed almost exclusively in muscle and heart. *Hum Mol Genet*. 2000;9(14):2167-2173. doi:10.1093/hmg/9.14.2167

71. Wansink DG, van Herpen REMA, Coerwinkel-Driessen MM, Groenen PJTA, Hemmings BA, Wieringa B. Alternative splicing controls myotonic dystrophy protein kinase structure, enzymatic activity, and subcellular localization. *Mol Cell Biol*. 2003;23(16):5489-5501. doi:10.1128/MCB.23.16.5489-5501.2003

72. Kaliman P, Llagostera E. Myotonic dystrophy protein kinase (DMPK) and its role in the pathogenesis of myotonic dystrophy 1. *Cell Signal*. 2008;20(11):1935-1941. doi:10.1016/j.cellsig.2008.05.005

73. Y H Fu 1, D L Friedman, S Richards, J A Pearlman, R A Gibbs, A Pizzuti, T Ashizawa, M B Perryman, G Scarlato RGFJ. Decreased expression of myotonin-protein kinase messenger RNA and protein in adult form of myotonic dystrophy. *Science (1979)*. 1993;260(5105). doi:10.1126/science.8469976.

74. Berul CI, Maguire CT, Aronovitz MJ, et al. DMPK dosage alterations result in atrioventricular conduction abnormalities in a mouse myotonic dystrophy model. *J Clin Invest*. 1999;103(4):R1-7. doi:10.1172/JCI5346

75. Jansen G, Groenen PJ, Bächner D, et al. Abnormal myotonic dystrophy protein kinase levels produce only mild myopathy in mice. *Nat Genet*. 1996;13(3):316-324. doi:10.1038/ng0796-316

76. Eriksson M, Hedberg B, Carey N, Ansved T. Decreased DMPK transcript levels in myotonic dystrophy 1 type IIA muscle fibers. *Biochem Biophys Res Commun*. 2001;286(5):1177-1182. doi:10.1006/bbrc.2001.5516

77. Carango P, Noble JE, Marks HG, Funanage VL. Absence of myotonic dystrophy protein kinase (DMPK) mRNA as a result of a triplet repeat expansion in myotonic dystrophy. *Genomics*. 1993;18(2):340-348. doi:10.1006/geno.1993.1474

78. Alwazzan M, Newman E, Hamshere MG, Brook JD. Myotonic dystrophy is associated with a reduced level of RNA from the DMWD allele adjacent to the expanded repeat. *Hum Mol Genet*. 1999;8(8):1491-1497. doi:10.1093/hmg/8.8.1491

79. Frisch R, Singleton KR, Moses PA, et al. Effect of triplet repeat expansion on chromatin structure and expression of DMPK and neighboring genes, SIX5 and DMWD, in myotonic dystrophy. *Mol Genet Metab*. 2001;74(1-2):281-291. doi:10.1006/mgme.2001.3229

80. Korade-Mirnics Z, Tarleton J, Servidei S, et al. Myotonic dystrophy: tissue-specific effect of somatic CTG expansions on allele-specific DMAHP/SIX5 expression. *Hum Mol Genet*. 1999;8(6):1017-1023. doi:10.1093/hmg/8.6.1017

81. Klesert TR, Cho DH, Clark JI, et al. Mice deficient in Six5 develop cataracts: implications for myotonic dystrophy. *Nat Genet*. 2000;25(1):105-109. doi:10.1038/75490

82. Barbé L, Lanni S, López-Castel A, et al. CpG Methylation, a Parent-of-Origin Effect for Maternal-Biased Transmission of Congenital Myotonic Dystrophy. *Am J Hum Genet*. 2017;100(3):488-505. doi:10.1016/j.ajhg.2017.01.033

83. Sarkar PS, Paul S, Han J, Reddy S. Six5 is required for spermatogenic cell survival and spermiogenesis. *Hum Mol Genet*. 2004;13(14):1421-1431. doi:10.1093/hmg/ddh161

84. Yin Q, Wang H, Li N, et al. Dosage effect of multiple genes accounts for multisystem disorder of myotonic dystrophy type 1. *Cell Res*. 2020;30(2):133-145. doi:10.1038/S41422-019-0264-2

85. Dexheimer PJ, Cochella L. MicroRNAs: From Mechanism to Organism. *Front Cell Dev Biol*. 2020;8:409. doi:10.3389/fcell.2020.00409

86. Latronico MVG, Condorelli G. MicroRNAs and cardiac pathology. *Nat Rev Cardiol*. 2009;6(6):419-429. doi:10.1038/nrcardio.2009.56

87. Lee ST, Chu K, Im WS, et al. Altered microRNA regulation in Huntington's disease models. *Exp Neurol*. 2011;227(1):172-179. doi:10.1016/j.expneurol.2010.10.012

88. Deiuliis JA. MicroRNAs as regulators of metabolic disease: pathophysiologic significance and emerging role as biomarkers and therapeutics. *Int J Obes (Lond)*. 2016;40(1):88-101. doi:10.1038/ijo.2015.170

89. Peng Y, Croce CM. The role of MicroRNAs in human cancer. *Signal Transduct Target Ther*. 2016;1:15004. doi:10.1038/sigtrans.2015.4

90. Eisenberg I, Eran A, Nishino I, et al. Distinctive patterns of microRNA expression in primary muscular disorders. *Proc Natl Acad Sci U S A*. 2007;104(43):17016-17021. doi:10.1073/pnas.0708115104

91. Condrat CE, Thompson DC, Barbu MG, et al. miRNAs as Biomarkers in Disease: Latest Findings Regarding Their Role in Diagnosis and Prognosis. *Cells*. 2020;9(2):276. doi:10.3390/cells9020276

92. Koehorst E, Ballester-Lopez A, Arechavala-Gomeza V, Martínez-Piñeiro A, Nogales-Gadea G. The Biomarker Potential of miRNAs in Myotonic Dystrophy Type I. *J Clin Med*. 2020;9(12):3939. doi:10.3390/jcm9123939

93. Rau F, Freyermuth F, Fugier C, et al. Misregulation of miR-1 processing is associated with heart defects in myotonic dystrophy. *Nat Struct Mol Biol*. 2011;18(7):840-845. doi:10.1038/nsmb.2067

94. Koehorst E, Ballester-Lopez A, Arechavala-Gomeza V, Martínez-Piñeiro A, Nogales-Gadea G. The Biomarker Potential of miRNAs in Myotonic Dystrophy Type I. *J Clin Med*. 2020;9(12):3939. doi:10.3390/jcm9123939

95. Mankodi A, Logigian E, Callahan L, et al. Myotonic Dystrophy in Transgenic Mice Expressing an Expanded CUG Repeat. *Science (1979)*. 2000;289(5485):1769-1772. doi:10.1126/science.289.5485.1769

96. Sicot G, Gomes-Pereira M. RNA toxicity in human disease and animal models: From the uncovering of a new mechanism to the development of promising therapies. *Biochimica et Biophysica Acta (BBA) - Molecular Basis of Disease*. 2013;1832(9):1390-1409. doi:10.1016/j.bbadis.2013.03.002

97. Orengo JP, Chambon P, Metzger D, Mosier DR, Snipes GJ, Cooper TA. Expanded CTG repeats within the DMPK 3' UTR causes severe skeletal muscle wasting in an inducible mouse model for myotonic dystrophy. *Proc Natl Acad Sci U S A*. 2008;105(7):2646-2651. doi:10.1073/pnas.0708519105

98. Kanadia RN, Johnstone KA, Mankodi A, et al. A muscleblind knockout model for myotonic dystrophy. *Science*. 2003;302(5652):1978-1980. doi:10.1126/science.1088583

99. Yin Q, Wang H, Li N, et al. Dosage effect of multiple genes accounts for multisystem disorder of myotonic dystrophy type 1. *Cell Res*. 2020;30(2):133-145. doi:10.1038/s41422-019-0264-2

100. Koshelev M, Sarma S, Price RE, Wehrens XHT, Cooper TA. Heart-specific overexpression of CUGBP1 reproduces functional and molecular

abnormalities of myotonic dystrophy type 1. *Hum Mol Genet*. 2010;19(6):1066-1075. doi:10.1093/hmg/ddp570

101. Lawlor KT, O'Keefe L V, Samaraweera SE, van Eyk CL, Richards RI. Ubiquitous expression of CUG or CAG trinucleotide repeat RNA causes common morphological defects in a Drosophila model of RNA-mediated pathology. *PLoS One*. 2012;7(6):e38516. doi:10.1371/journal.pone.0038516

102. Wang LC, Chen KY, Pan H, et al. Muscleblind participates in RNA toxicity of expanded CAG and CUG repeats in Caenorhabditis elegans. *Cell Mol Life Sci*. 2011;68(7):1255-1267. doi:10.1007/s00018-010-0522-4

103. Machuca-Tzili L, Thorpe H, Robinson TE, Sewry C, Brook JD. Flies deficient in Muscleblind protein model features of myotonic dystrophy with altered splice forms of Z-band associated transcripts. *Hum Genet*. 2006;120(4):487-499. doi:10.1007/s00439-006-0228-8

104. Spilker KA, Wang GJ, Tugizova MS, Shen K. Caenorhabditis elegans Muscleblind homolog mbl-1 functions in neurons to regulate synapse formation. *Neural Dev*. 2012;7:7. doi:10.1186/1749-8104-7-7

105. Machuca-Tzili LE, Buxton S, Thorpe A, et al. Zebrafish deficient for Muscleblind-like 2 exhibit features of myotonic dystrophy. *Dis Model Mech*. 2011;4(3):381-392. doi:10.1242/dmm.004150

106. Konieczny P, Selma-Soriano E, Rapisarda AS, Fernandez-Costa JM, Perez-Alonso M, Artero R. Myotonic dystrophy: candidate small molecule therapeutics. *Drug Discov Today*. 2017;22(11):1740-1748. doi:10.1016/j.drudis.2017.07.011

107. Amack JD, Paguio AP, Mahadevan MS. Cis and trans effects of the myotonic dystrophy (DM) mutation in a cell culture model. *Hum Mol Genet*. 1999;8(11):1975-1984. doi:10.1093/hmg/8.11.1975

108. Matloka M, Klein AF, Rau F, Furling D. Cells of Matter-In Vitro Models for Myotonic Dystrophy. *Front Neurol*. 2018;9:361. doi:10.3389/fneur.2018.00361

109. Mamchaoui K, Trollet C, Bigot A, et al. Immortalized pathological human myoblasts: towards a universal tool for the study of neuromuscular disorders. *Skelet Muscle*. 2011;1:34. doi:10.1186/2044-5040-1-34

110. Arandel L, Polay Espinoza M, Matloka M, et al. Immortalized human myotonic dystrophy muscle cell lines to assess therapeutic compounds. *Dis Model Mech*. 2017;10(4):487-497. doi:10.1242/dmm.027367

111. Pantic B, Borgia D, Giunco S, et al. Reliable and versatile immortal muscle cell models from healthy and myotonic dystrophy type 1 primary human myoblasts. *Exp Cell Res*. 2016;342(1):39-51. doi:10.1016/j.yexcr.2016.02.013

112. Bigot A, Klein AF, Gasnier E, et al. Large CTG repeats trigger p16-dependent premature senescence in myotonic dystrophy type 1 muscle precursor cells. *Am J Pathol*. 2009;174(4):1435-1442. doi:10.2353/ajpath.2009.080560

113. Takahashi K, Tanabe K, Ohnuki M, et al. Induction of pluripotent stem cells from adult human fibroblasts by defined factors. *Cell*. 2007;131(5):861-872. doi:10.1016/j.cell.2007.11.019

114. Gutiérrez Gutiérrez G, Díaz-Manera J, Almendrote M, et al. Clinical guide for the diagnosis and follow-up of myotonic dystrophy type 1, MD1 or Steinert's disease. *Neurologia*. 2020;35(3):185-206. doi:10.1016/j.nrl.2019.01.001

115. Heatwole C, Luebbe E, Rosero S, et al. Mexiletine in Myotonic Dystrophy Type 1: A Randomized, Double-Blind, Placebo-Controlled Trial. *Neurology*. 2021;96(2):e228-e240. doi:10.1212/WNL.0000000000011002

116. Logigian EL, Martens WB, Moxley RT, et al. Mexiletine is an effective antimyotonia treatment in myotonic dystrophy type 1. *Neurology*. 2010;74(18):1441-1448. doi:10.1212/WNL.0b013e3181dc1a3a

117. García-Puga M, Saenz-Antoñanzas A, Matheu A, López de Munain A. Targeting Myotonic Dystrophy Type 1 with Metformin. *Int J Mol Sci*. 2022;23(5). doi:10.3390/ijms23052901

118. Bassez G, Audureau E, Hogrel JY, et al. Improved mobility with metformin in patients with myotonic dystrophy type 1: a randomized controlled trial. *Brain*. 2018;141(10):2855-2865. doi:10.1093/brain/awy231

119. Horrigan J, Gomes TB, Snape M, et al. A Phase 2 Study of AMO-02 (Tideglusib) in Congenital and Childhood-Onset Myotonic Dystrophy Type 1 (DM1). *Pediatr Neurol*. 2020;112:84-93. doi:10.1016/j.pediatrneurol.2020.08.001

120. Sarfraz N, Okuampa D, Hansen H, et al. pitolisant, a novel histamine-3 receptor competitive antagonist, and inverse agonist, in the treatment of

excessive daytime sleepiness in adult patients with narcolepsy. *Health Psychol Res*. 2022;10(3):34222. doi:10.52965/001c.34222

121. Nakamori M, Taylor K, Mochizuki H, Sobczak K, Takahashi MP. Oral administration of erythromycin decreases RNA toxicity in myotonic dystrophy. *Ann Clin Transl Neurol*. 2016;3(1):42-54. doi:10.1002/acn3.271

122. Pascual-Gilabert M, Artero R, López-Castel A. The myotonic dystrophy type 1 drug development pipeline: 2022 edition. *Drug Discov Today*. 2023;28(3):103489. doi:10.1016/j.drudis.2023.103489

123. Pascual-Gilabert M, López-Castel A, Artero R. Myotonic dystrophy type 1 drug development: A pipeline toward the market. *Drug Discov Today*. 2021;26(7):1765-1772. doi:10.1016/j.drudis.2021.03.024

124. Y. Zhu · T. Kwan · Q. Meng · L. Tai · H. Cho · M. Lee · H. Younis · A. Levin · M. Flanagan. VP48 AOC 1001 demonstrates DMPK reduction and spliceopathy improvement in a phase 1/2 study in myotonic dystrophy type 1 (DM1) (MARINA). *Neuromuscular Disorders*. 2023;33(1):70-70.

125. Pascual-Gilabert M, Artero R, López-Castel A. The myotonic dystrophy type 1 drug development pipeline: 2022 edition. *Drug Discov Today*. 2023;28(3):103489. doi:10.1016/j.drudis.2023.103489

126. Cerro-Herreros E, González-Martínez I, Moreno N, et al. Preclinical characterization of antagomiR-218 as a potential treatment for myotonic dystrophy. *Mol Ther Nucleic Acids*. 2021;26:174-191. doi:10.1016/j.omtn.2021.07.017

127. Overby SJ, Cerro-Herreros E, Espinosa-Espinosa J, et al. BlockmiR AONs as Site-Specific Therapeutic MBNL Modulation in Myotonic Dystrophy 2D and 3D Muscle Cells and HSALR Mice. *Pharmaceutics*. 2023;15(4). doi:10.3390/pharmaceutics15041118

128. Cerro-Herreros E, González-Martínez I, Moreno-Cervera N, et al. Therapeutic Potential of AntagomiR-23b for Treating Myotonic Dystrophy. *Mol Ther Nucleic Acids*. 2020;21:837-849. doi:10.1016/j.omtn.2020.07.021

129. Cerro-Herreros E, Sabater-Arcis M, Fernandez-Costa JM, et al. miR-23b and miR-218 silencing increase Muscleblind-like expression and alleviate myotonic dystrophy phenotypes in mammalian models. *Nat Commun*. 2018;9(1):2482. doi:10.1038/s41467-018-04892-4

130. Lo Scrudato M, Poulard K, Sourd C, et al. Genome Editing of Expanded CTG Repeats within the Human DMPK Gene Reduces Nuclear RNA Foci in the Muscle of DM1 Mice. *Mol Ther*. 2019;27(8):1372-1388. doi:10.1016/j.ymthe.2019.05.021

131. Dastidar S, Ardui S, Singh K, et al. Efficient CRISPR/Cas9-mediated editing of trinucleotide repeat expansion in myotonic dystrophy patient-derived iPS and myogenic cells. *Nucleic Acids Res*. 2018;46(16):8275-8298. doi:10.1093/nar/gky548

132. Wang Y, Hao L, Wang H, et al. Therapeutic Genome Editing for Myotonic Dystrophy Type 1 Using CRISPR/Cas9. *Mol Ther*. 2018;26(11):2617-2630. doi:10.1016/j.ymthe.2018.09.003

133. Batra R, Nelles DA, Roth DM, et al. The sustained expression of Cas9 targeting toxic RNAs reverses disease phenotypes in mouse models of myotonic dystrophy type 1. *Nat Biomed Eng*. 2021;5(2):157-168. doi:10.1038/s41551-020-00607-7

134. Izzo M, Battistini J, Provenzano C, Martelli F, Cardinali B, Falcone G. Molecular Therapies for Myotonic Dystrophy Type 1: From Small Drugs to Gene Editing. *Int J Mol Sci*. 2022;23(9). doi:10.3390/ijms23094622

135. Seim I, Ma S, Gladyshev VN. Gene expression signatures of human cell and tissue longevity. *NPJ Aging Mech Dis*. 2016;2:16014. doi:10.1038/npjamd.2016.14

136. X. Xing RMTGSBDJNMWJDB. Regulation of Toxic RNA Foci and Mutant DMPK Transcripts: Role of MBNL Proteins and RNA Decay Pathway. *bioRxiv [Preprint]*. Published online 2023.

137. Dansithong W, Paul S, Comai L, Reddy S. MBNL1 is the primary determinant of focus formation and aberrant insulin receptor splicing in DM1. *J Biol Chem*. 2005;280(7):5773-5780. doi:10.1074/jbc.M410781200

138. Benizri S, Gissot A, Martin A, Vialet B, Grinstaff MW, Barthélémy P. Bioconjugated Oligonucleotides: Recent Developments and Therapeutic Applications. *Bioconjug Chem*. 2019;30(2):366-383. doi:10.1021/acs.bioconjchem.8b00761

139. Morales F, Couto JM, Higham CF, et al. Somatic instability of the expanded CTG triplet repeat in myotonic dystrophy type 1 is a heritable quantitative

trait and modifier of disease severity. *Hum Mol Genet*. 2012;21(16):3558-3567. doi:10.1093/hmg/dds185

140. Jones PA, Wolkowicz MJ, Rideout WM, et al. De novo methylation of the MyoD1 CpG island during the establishment of immortal cell lines. *Proc Natl Acad Sci U S A*. 1990;87(16). doi:10.1073/pnas.87.16.6117.

141. Antequera F, J Boyes AB. High levels of de novo methylation and altered chromatin structure at CpG islands in cell lines. *Cell*. 1990;62(3). doi:10.1016/0092-8674(90)90015-7

142. Jones PA. Functions of DNA methylation: islands, start sites, gene bodies and beyond. *Nat Rev Genet*. 2012;13(7):484-492. doi:10.1038/NRG3230

143. Carrió E, Díez-Villanueva A, Lois S, et al. Deconstruction of DNA methylation patterns during myogenesis reveals specific epigenetic events in the establishment of the skeletal muscle lineage. *Stem Cells*. 2015;33(6):2025-2036. doi:10.1002/STEM.1998

144. Reik W. Stability and flexibility of epigenetic gene regulation in mammalian development. *Nature*. 2007;447(7143):425-432. doi:10.1038/NATURE05918

145. Fu YH, Friedman DL, Richards S, et al. Decreased expression of myotonin-protein kinase messenger RNA and protein in adult form of myotonic dystrophy. *Science*. 1993;260(5105):235-238. doi:10.1126/SCIENCE.8469976

146. T R Klesert, A D Otten, T D Bird SJT. Trinucleotide repeat expansion at the myotonic dystrophy locus reduces expression of DMAHP. *Nat Genet*. 1997;16(4). doi:10.1038/ng0897-402

147. M Alwazzan, E Newman, M G Hamshere JDB. Myotonic dystrophy is associated with a reduced level of RNA from the DMWD allele adjacent to the expanded repeat. *Hum Mol Genet*. 1999;8(8). doi:10.1093/hmg/8.8.1491.

148. Yin Q, Wang H, Li N, et al. Dosage effect of multiple genes accounts for multisystem disorder of myotonic dystrophy type 1. *Cell Res*. 2020;30(2):133-145. doi:10.1038/S41422-019-0264-2

149. Ballester-Lopez A, Núñez-Manchón J, Koehorst E, et al. Three-dimensional imaging in myotonic dystrophy type 1: Linking molecular alterations with disease phenotype. *Neurol Genet*. 2020;6(4). doi:10.1212/NXG.0000000000000484

150. Arandel L, Espinoza MP, Matloka M, et al. Immortalized human myotonic dystrophy muscle cell lines to assess therapeutic compounds. *DMM Disease Models and Mechanisms*. 2017;10(4):487-497. doi:10.1242/dmm.027367

151. Manning KS, Rao AN, Castro M, Cooper TA. BNANC Gapmers Revert Splicing and Reduce RNA Foci with Low Toxicity in Myotonic Dystrophy Cells. *ACS Chem Biol*. 2017;12(10):2503-2509. doi:10.1021/ACSCHEMBIO.7B00416/SUPPL_FILE/CB7B00416_SI_001.PDF

*Introduction figures were designed with Biorender.

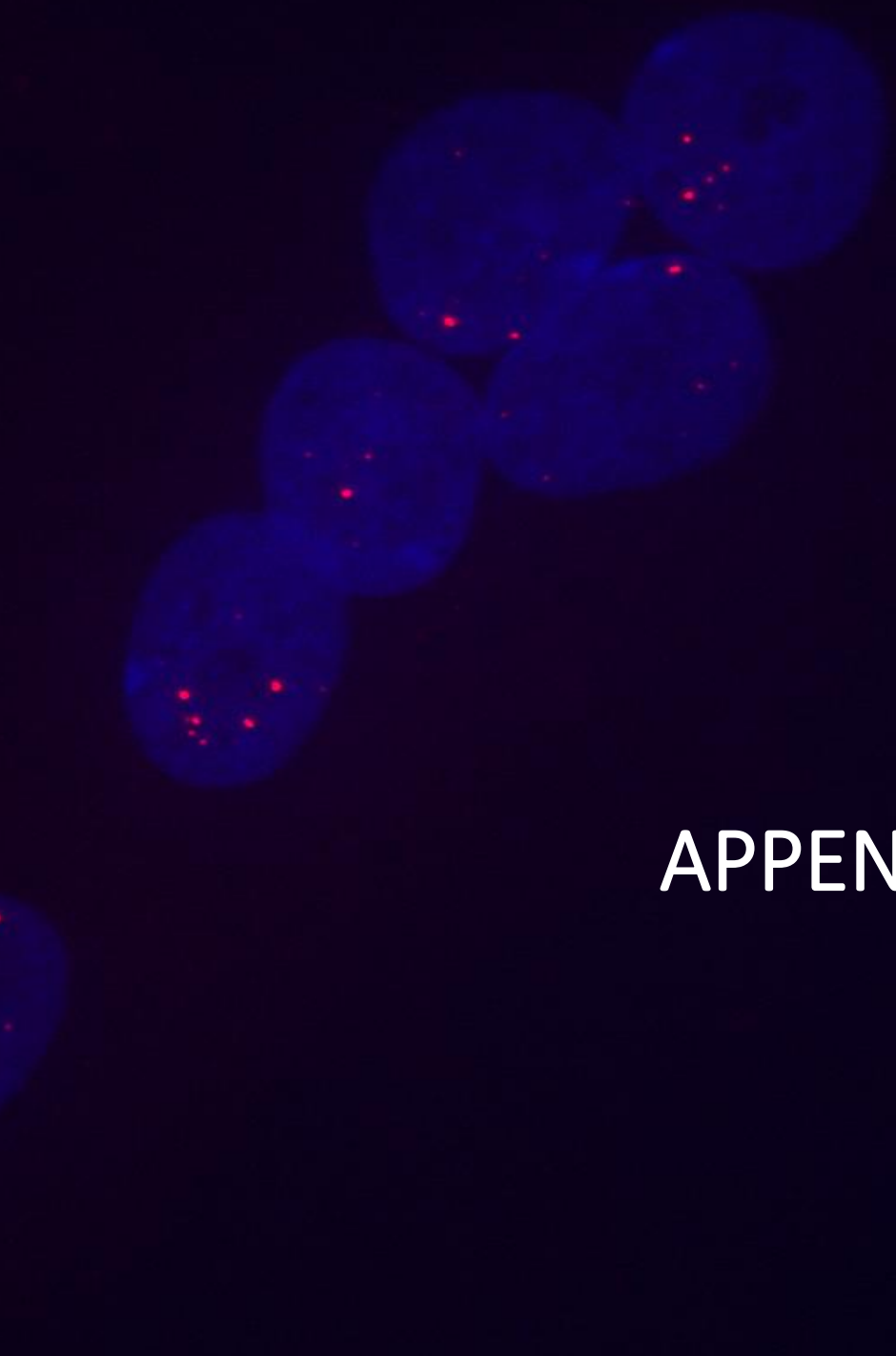

APPENDIX

List of publications in which I participated during the PhD

Koehorst E, Núñez-Manchón J, Ballester-López A, Almendrote M, Lucente G, Arbex A, Chojnacki J, Vázquez-Manrique RP, Gómez-Escribano AP, Pintos Morell G, Coll-Cantí J, Ramos-Fransi A, Martínez-Piñeiro A, Suelves M, Nogales-Gadea G. Characterization of RAN Translation and Antisense Transcription in Primary Cell Cultures of Patients with Myotonic Dystrophy Type 1. J Clin Med. 2021 Nov 25;10(23):5520. doi: 10.3390/jcm10235520. PMID: 34884222; PMCID: PMC8658563.

Koehorst E, Odria R, Capó J, Núñez-Manchón J, Arbex A, Almendrote M, Linares-Pardo I, Natera-de Benito D, Saez V, Nascimento A, Ortez C, Rubio MÁ, Díaz-Manera J, Alonso-Pérez J, Lucente G, Rodriguez-Palmero A, Ramos Fransi A, Martínez-Piñeiro A, Nogales-Gadea G, Suelves M. An Integrative Analysis of DNA Methylation Pattern in Myotonic Dystrophy Type 1 Samples Reveals a Distinct DNA Methylation Profile between Tissues and a Novel Muscle-Associated Epigenetic Dysregulation. Biomedicines. 2022 Jun 10;10(6):1372. doi: 10.3390/biomedicines10061372. PMID: 35740394; PMCID: PMC9220235.

Judit Núñez-Manchón, Júlia Capó , Alicia Martínez-Piñeiro, Eduard Juanola, Jovan Pesovic, Laura Mosqueira-Martín, Klaudia González-Imaz, Pau Maestre-Mora, Renato Odria, Dusanka Savic-Pavicevic, Ainara Vallejo-Illarramendi, Kamel Mamchaoui, Anne Bigot, Vincent Mouly, Mònica Suelves, Gisela Nogales-Gadea. Immortalized human myotonic dystrophy type 1 muscle cell lines to address patient heterogeneity. iScience. 2024 May 7;27(6):109930. doi: 10.1016/j.isci.2024.109930. PMID: 38832025 PMCID: PMC11144749.

Estefanía Cerro-Herreros, Judit Núñez-Manchón, Neia Naldaiz-Gastesi, Marc Carrascosa-Sàez, Andrea García-Rey, Diego Piqueras Losilla, Irene González-Martínez, Jorge Espinosa-Espinosa, Kevin Moreno, Javier Poyatos-García, Juan J Vilchez, Adolfo López de Munain, Mònica Suelves, Gisela Nogales-Gadea, Beatriz Llamusí and Rubén Artero. AntimiR treatment corrects myotonic dystrophy primary cell defects across several CTG repeat expansions with a dual mechanism of action. Science Advances. Accepted for publication.

In the following pages there is a printed copy of each of the publications.

Journal of *Clinical Medicine*

MDPI

Article

Characterization of RAN Translation and Antisense Transcription in Primary Cell Cultures of Patients with Myotonic Dystrophy Type 1

Emma Koehorst [1], Judit Núñez-Manchón [1], Alfonsina Ballester-López [1,2], Miriam Almendrote [1,3], Giuseppe Lucente [1,3], Andrea Arbex [1,3], Jakub Chojnacki [4], Rafael P. Vázquez-Manrique [2,5,6], Ana Pilar Gómez-Escribano [2,5,6], Guillem Pintos-Morell [1,7], Jaume Coll-Cantí [1,3], Alba Ramos-Fransi [1,3], Alicia Martínez-Piñeiro [1,3,†], Mònica Suelves [1,†] and Gisela Nogales-Gadea [1,2,*,†]

1 Neuromuscular and Neuropediatric Research Group, Institut d'Investigació en Ciències de la Salut Germans Trias i Pujol (IGTP), Campus Can Ruti, Universitat Autònoma de Barcelona, 08916 Badalona, Spain; ekoehorst@igtp.cat (E.K.); jnunez@igtp.cat (J.N.-M.); aballester@igtp.cat (A.B.-L.); malmendrote.germanstrias@gencat.cat (M.A.); glucente@igtp.cat (G.L.); aarbex@igtp.cat (A.A.); gpintos@igtp.cat (G.P.-M.); jcoll@igtp.cat (J.C.-C.); aramosf@igtp.cat (A.R.-F.); amartinezp.germanstrias@gencat.cat (A.M.-P.); msuelves@igtp.cat (M.S.)
2 Centre for Biomedical Network Research on Rare Diseases (CIBERER), Instituto de Salud Carlos III, 28029 Madrid, Spain; rafael_vazquez@isslafe.es (R.P.V.-M.); ana_pilar_gomez@iislafe.es (A.P.G.-E.)
3 Neuromuscular Pathology Unit, Neurology Service, Neuroscience Department, Hospital Universitari Germans Trias i Pujol, 08916 Badalona, Spain
4 IrsiCaixa AIDS Research Institute, 08916 Badalona, Spain; jchojnacki@irsicaixa.es
5 Laboratory of Molecular, Cellular and Genomic Biomedicine, Instituto de Investigación Sanitaria La Fe, 46026 Valencia, Spain
6 Joint Unit for Rare Diseases IIS La Fe-CIPF, 46012 Valencia, Spain
7 Reference Unit for Hereditary Metabolic Disorders (MetabERN), Vall d'Hebron University Hospital, 08035 Barcelona, Spain
* Correspondence: gnogales@igtp.cat; Tel.: +34-930330530
† Equal contribution.

check for updates

Citation: Koehorst, E.; Núñez-Manchón, J.; Ballester-López, A.; Almendrote, M.; Lucente, G.; Arbex, A.; Chojnacki, J.; Vázquez-Manrique, R.P.; Gómez-Escribano, A.P.; Pintos-Morell, G.; et al. Characterization of RAN Translation and Antisense Transcription in Primary Cell Cultures of Patients with Myotonic Dystrophy Type 1. *J. Clin. Med.* **2021**, *10*, 5520. https://doi.org/10.3390/jcm10235520

Academic Editor: Sabrina Ravaglia

Received: 30 October 2021
Accepted: 19 November 2021
Published: 25 November 2021

Publisher's Note: MDPI stays neutral with regard to jurisdictional claims in published maps and institutional affiliations.

Abstract: Myotonic Dystrophy type 1 (DM1) is a muscular dystrophy with a multi-systemic nature. It was one of the first diseases in which repeat associated non-ATG (RAN) translation was described in 2011, but has not been further explored since. In order to enhance our knowledge of RAN translation in DM1, we decided to study the presence of DM1 antisense (DM1-AS) transcripts (the origin of the polyglutamine (polyGln) RAN protein) using RT-PCR and FISH, and that of RAN translation via immunoblotting and immunofluorescence in distinct DM1 primary cell cultures, e.g., myoblasts, skin fibroblasts and lymphoblastoids, from ten patients. DM1-AS transcripts were found in all DM1 cells, with a lower expression in patients compared to controls. Antisense RNA foci were found in the nuclei and cytoplasm of a subset of DM1 cells. The polyGln RAN protein was undetectable in all three cell types with both approaches. Immunoblots revealed a 42 kD polyGln containing protein, which was most likely the TATA-box-binding protein. Immunofluorescence revealed a cytoplasmic aggregate, which co-localized with the Golgi apparatus. Taken together, DM1-AS transcript levels were lower in patients compared to controls and a small portion of the transcripts included the expanded repeat. However, RAN translation was not present in patient-derived DM1 cells, or was in undetectable quantities for the available methods.

Keywords: RAN translation; antisense transcription; myotonic dystrophies; primary cell cultures; phenotypic modulators

1. Introduction

Myotonic Dystrophy type 1 (DM1) is an autosomal dominant inherited muscular dystrophy with a multi-systemic nature. Patients display a wide variety of symptoms,

including muscle weakness, myotonia, respiratory failure, cardiac conduction defects, cataracts, and endocrine disturbances. In addition, the age of onset varies greatly, from birth up to >70 years. The cause of the variability in clinical manifestation is poorly understood. DM1 is viewed as an RNA gain of function disorder, wherein a CTG expansion in the 3′ untranslated region of the myotonic dystrophy protein kinase (*DMPK*) gene causes the accumulation of expanded transcripts as intranuclear RNA foci, which sequester a number of splicing factors, resulting in loss of function and downstream deregulation of the alternative splicing of several genes [1]. In recent years, the view of DM1 as solely an RNA gain-of-function disorder has changed. Several new discoveries, such as antisense transcription and repeat associated non-ATG (RAN) translation, have added to the complexity of this disease. DM1 antisense (DM1-AS) transcription was first described by Cho and collaborators in 2005 [2]. They reported an antisense transcript, emanating from the adjacent SIX5 regulatory region, which was converted into 21 nt siRNAs. These siRNAs were proposed to have a regulatory role in heterochromatin formation. Huguet and collaborators, however, showed that DM1-AS transcription extends across the CAG repeat, as they could detect DM1-AS RNA after the repeat in the 3′ region of DM1 tissue and they also showed the presence of antisense RNA foci, which did not co-localize with sense RNA foci, in adult mouse models [3]. Similar results were found by Michel and collaborators in human fetal samples [4]. The inclusion of the expanded repeat was confirmed by Gudde and collaborators in 2017, although they found DM1-AS transcripts to be low in abundance and with varying lengths, both including and excluding the CAG repeat [5]. In addition, the DM1-AS strand was found by Zu and collaborators to give rise to RAN-translated polyglutamine stretches [6]. RAN translation is a typical phenomenon seen in repeat expansion disorders, in which peptides are produced from all frames without ATG start codon recognition. Zu and collaborators discovered a novel polyglutamine (polyGln) RAN protein expressed from the antisense CAG expansion transcript of the *DMPK* gene [6]. Nuclear polyGln RAN protein aggregates were found at a low frequency in a DM1 patient's myoblasts and skeletal muscle ($n = 1$) and at a higher frequency in leukocytes from peripheral blood ($n = 1$) [6]. The nuclear aggregates co-localized with caspase-8, an early indicator of polyGln-induced apoptosis. This suggests that RAN proteins may be an additional mechanism of cytotoxicity in DM1 cells.

Since its first discovery in 2011 by Zu and collaborators, RAN translation has been extensively studied in multiple expansion disorders and great advances have been made [7]. However, the contribution of RAN translation to DM1 pathology has not been further studied since its first report in 2011. Much remains unknown regarding the presence of RAN translation and its mechanism in DM1. Is it equally present across patients, and is its distribution across tissues similar? To what extent does it contribute to the pathology of the disease? In order to further enhance our knowledge of RAN translation in DM1, we decided to study the presence of RAN translation in DM1 primary cell cultures—myoblasts, skin fibroblasts and lymphoblastoids—derived from ten DM1 patients, with a heterogeneous display of subtypes. The RAN-translated polyGln has been described to originate from the antisense strand of the *DMPK* gene. We therefore validated the presence of DM1-AS transcription in our three patient-derived cellular models and lower expression levels were found in patients compared to controls. Additionally, we found that the DM1-AS transcripts were found in both the nucleus and the cytoplasm, of which at least a portion contained the expanded repeat, as shown by the presence of antisense RNA foci in patients. However, the polyGln RAN protein was not present in patient-derived DM1 cells, or was present in such low quantities that it was below the detection limit of the currently available techniques.

2. Materials and Methods

2.1. Samples

This study was approved by the Ethics Committee of the University Hospital Germans Trias i Pujol and was performed in accordance with the Declaration of Helsinki for

Human Research. Written informed consent was obtained from all participants. The study included ten patients with DM1 and thirteen controls with no previous family history of neuromuscular disorders (recruited from the traumatology department, in whom surgery was needed). DM1 diagnosis was confirmed or discarded via triplet-primed PCR in all the study participants. Clinical information of DM1 patients was obtained from medical records and updated at the last visit. We obtained three different samples from eight patients and eleven controls: blood, muscle biopsy, and skin biopsy. The other two patients and two controls only provided a blood sample. All samples were simultaneously obtained from patients with confirmed juvenile, adult or late-onset DM1. The muscle biopsy was obtained from biceps brachii ($n = 7$) or vastus lateralis ($n = 1$) of DM1 patients and from intrinsic forearm or hand muscles of eleven non-DM1 patients. Skin biopsy was obtained with a 0.5 cm skin punch.

2.2. Small Pool PCR for Sizing the CTG Repeat

Total genomic DNA was extracted from peripheral blood samples, as previously described [8]. To estimate the length of the expanded mode allele, small-pool PCR (SP-PCR) was carried out with small amounts of input DNA (300 pg), using flanking primers DM-C and DM-DR, as previously described [9,10]. PCR was performed using a Custom PCR Master Mix (Thermo Fisher Scientific, Waltham, MA, USA) supplemented with 69 mM 2-mercaptoethanol, and Taq polymerase (Sigma-Aldrich, Gillingham, UK) at 1 unit per 10 µL. All reactions were supplemented with 5% DMSO and the annealing temperature was 63.5 °C. DNA fragments were resolved by electrophoresis on a 1% agarose gel, and Southern blot hybridized as described in references [9,10]. Autoradiographic images were scanned and the CTG size of the mode was estimated through comparison against the molecular weight ladder using GelAnalyzer 19.1 software (www.gelanalyzer.com, by Istvan Lazar Jr. and Istvan Lazar Sr.).

2.3. Cell Culture

Myoblasts were isolated from the biopsied tissue by CD56 magnetic separation. Myoblasts were grown until 60–70% confluency on 0.1% gelatin-coated coverslips in six-well tissue-culture plates in a proliferation medium containing DMEM supplemented with 10% FBS, 22% M-199, 1× PSF, insulin 1.74 µM, L-glutamine 2 mM, FGF 1.39 nM and EGF 0.135 mM. Skin fibroblasts were isolated from biopsied tissue using the explant method. Skin fibroblasts were grown until 70% confluency on 0.5% poly-D-lysin coated coverslips in a six-well tissue culture plate in a proliferation medium containing DMEM, supplemented with 10% FBS and 1× PSF. Peripheral blood mononuclear cells were isolated from blood collected in heparin tubes according to the Ficoll gradient and immortalized using Epstein–Barr virus. Lymphoblastoids were grown until 70% confluency on 0.1% poly-D-lysin coated coverslips in a six-well tissue culture plate in a proliferation medium containing RPMI, supplemented with 10% FBS, 1× PSF and 2 mM L-glutamine. HEK293 cells were cultured until 80% confluency on 0.5% poly-D-lysin coated coverslips in a six-well tissue culture plate in MEM, supplemented with 5% horse serum, 5% FBS, 1% Glutamine and 1% PSF. In addition to the coverslips, cell pellets from each of the cell types were extracted and stored for later use in RNA and protein studies.

2.4. cDNA Construct Huntingtin and HEK293 Transfection

The Q17 vector was generously provided to us by R.P.V.-M.. In short, the construct is part of the cDNA of human huntingtin (585 amino acids), containing 17 CAGs, and was cloned into a pcDNA3.1-Gateway. The human huntingtin with the 17 CAGs was in frame with mCherry, a fluorescent. DNA transfections were performed when HEK293 cells reached 80% confluency using Lipofectamine 2000 reagent (Thermo Fisher Scientific, Waltham, MA, USA), according to the manufacturer's instructions. DNA:lipofectamine ratio was 1:2 and incubation lasted 48 h.

2.5. RNA Isolation and Subcellular Fractionation

Total RNA from cultured myoblast, skin fibroblast and lymphoblastoid cell lines was isolated using TRIzol reagent (Thermo Fisher Scientific, Waltham, MA, USA) or the RNeasy plus mini kit (Qiagen, Hilden, Germany), according to the manufacturer's instructions. Total RNA from a healthy human heart was used as a positive control in all RT-PCR analyses (AM7966, Thermo Fisher Scientific, Waltham, MA, USA).

For RNA isolation from the subcellular fractions, skin fibroblasts were grown to 80% confluency, collected through trypsinization and pelleted through centrifugation at 2000 rpm for 5 min at 4 °C. Cell pellets were washed twice with ice-cold PBS. Cells were resuspended in ice-cold cell disruption buffer (10 mM KCl, 1.5 mM $MgCl_2$, 20 mM Tris-Cl (pH 7.5), 1 mM DTT) and incubated on ice for 10 min [11]. Samples were homogenized using a tissue disruptor for 30 s and then Triton X-100 was added to a final concentration of 0.1%. The lysate was centrifuged at 2000 rpm for 5 min at 4 °C, after which the supernatant (cytoplasmic fraction) was removed. Both cytoplasmic and nuclear fraction underwent RNA isolation by the RNeasy plus mini kit (Qiagen, Hilden, Germany), according to the manufacturer's instructions.

2.6. RT-PCR Analysis for DM1-AS Transcript Detection

For detection of the DM1-AS transcripts, a similar strategy to Zu et al. was followed [6], with some minor changes. In brief, an equivalent of 1 µg total RNA was subjected to cDNA synthesis using SuperScript IV reverse transcriptase (Thermo Fisher Scientific, Waltham, MA, USA) at 55 °C, using random hexamers (50 µM, N8080127, Thermo Fisher Scientific, Waltham, MA, USA). The subsequent PCR was carried out using DM1-AS specific primers LK1, together with anti-N3 or anti-1B, and LK2, together with anti-N3 (Figure 1A; primer details and PCR conditions can be found in Table S1). Both LK1 and LK2 contained a linker sequence, for which a specific primer was created and used in some of the PCR reactions. For endogenous controls GAPDH, β2-microglobulin (β2-MG) and PSMC4 a similar approach was followed (primer details and PCR condition found in Table S1).

To analyze nuclear and cytoplasmic RNA fractions, 150 ng RNA was used for the RT reaction for both fractions. RNA was reverse transcribed using SuperScript IV reverse transcriptase (Thermo Fisher Scientific, Waltham, MA, USA) at 55 °C, using random hexamers (50 µM, N8080127, Thermo Fisher Scientific, Waltham, MA, USA). For RT-PCR analyses, the same approach was used as described above with primer combinations LK1/anti-N3 and LK2/anti-N3. As a nuclear marker, pre-mRNA DMPK was used and GAPDH as an endogenous control (primers and PCR conditions in Table S1).

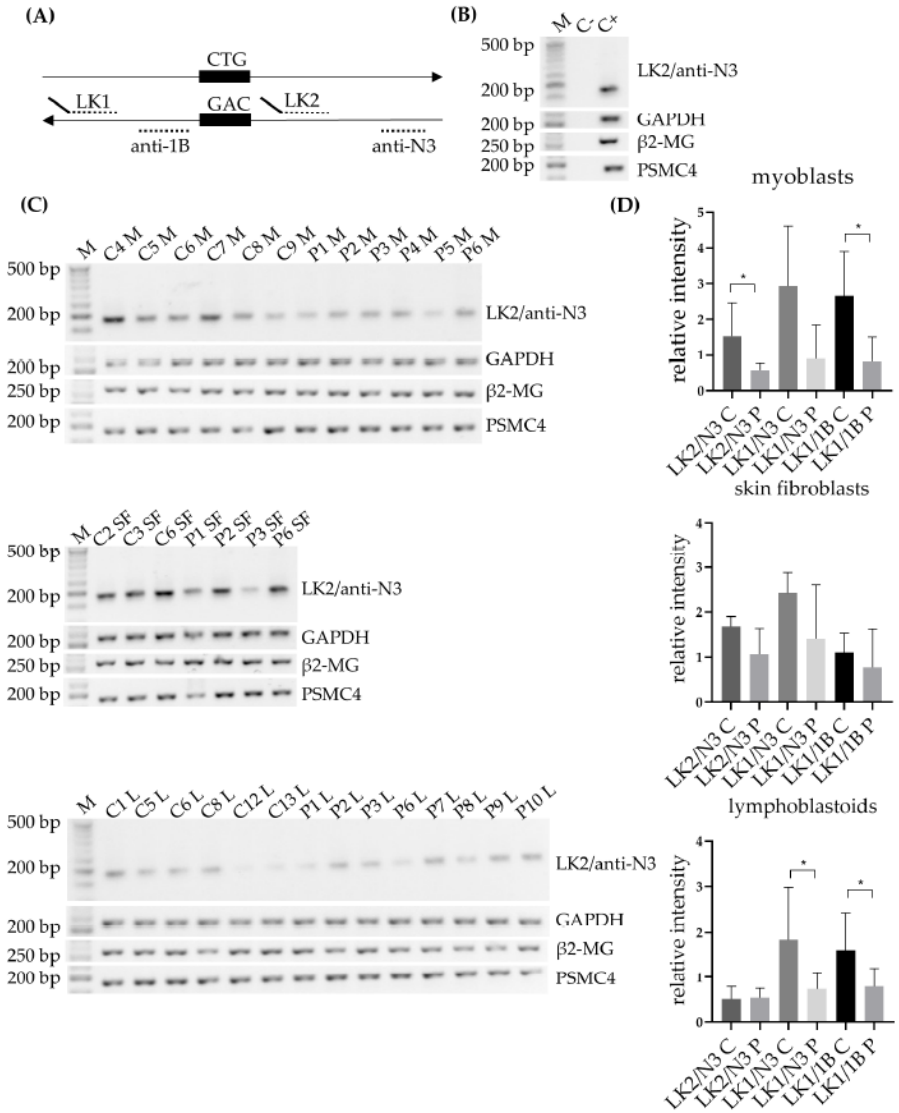

Figure 1. DM1 antisense (DM1-AS) transcripts in DM1 cells. (**A**) Schematic diagram indicating the location of the primers used for the DM1-AS amplification. Both DM1-AS specific primers (LK1 and LK2) have a linker sequence attached, indicated by the tail. Either a linker primer or the strand-specific primers were used for the RT-PCR reactions. A total of three primer combinations were used, LK1 with primers anti-1B/anti-N3 and LK2 with primer anti-N3. (**B**) Positive and negative controls from the RT-PCR reactions; C- = no DNA in the RT-reaction; C+ = control heart RNA as input, the tissue used in the original paper. (**C**) Strand-specific RT-PCRs of the DM1-AS with the DM1-AS specific primers LK2 and anti-N3 in all three primary cell cultures. GAPDH, β2-MG and PSMC4 were used as an endogenous controls. (**D**) Expression of DM1-AS determined by measuring intensity with ImageJ, normalized against the mean of the endogenous controls for all three primer combinations in all three primary cell cultures. Gels of the other two primer combinations can be found in Figure S1. Error bars indicate standard deviations. * = *p*-value below 0.05. Abbreviations: M = marker; C = control; P = DM1 patient; M = myoblasts; SF = skin fibroblasts; L = lymphoblastoids.

2.7. Immunoblotting

The cell pellets collected from the cell cultures were lysed in a RIPA buffer, supplemented with a cOmplete™ Protease Inhibitor Cocktail (Roche, Basel, Switzerland) and homogenized with a tissue disruptor. After centrifugation, the supernatant was collected and the protein concentration determined with a DC™ Protein Assay Kit II (Bio-Rad Laboratories, Hercules, CA, USA). 20–70 µg of protein was separated on a 3–8% gradient Tris-Acetate gel or an 8% acrylamide gel. Gel proteins were transferred by the iBlot2 system (Thermo Fisher Scientific, Waltham, MA, USA) for Tris-Acetate gels to a nitrocellulose membrane and by wet transfer to a PVDF membrane for the acrylamide gels (Merck, Darmstadt, Germany). Membranes were blocked for one hour in Intercept (TBS) blocking buffer (LI-COR, Lincoln, NE, USA). Immunoblotting was performed with α-DM1 antibody (1:1000, kindly provided by Laura Ranum), 1C2 (clone 5TF1-1C2, 1:250-1:1000, Merck, Darmstadt, Germany), #1874 (clone 3B5H10, Merck, Darmstadt, Germany, 1:1000), TATA-box-binding protein (TBP) (1:250-1:1000, Abcam, Cambridge, UK) or α-tubulin (1:5000, Merck, Darmstadt, Germany) overnight at 4 °C. Appropriate secondary antibodies, anti-rabbit 1:8000 conjugated with IRDye 680RD and anti-mouse 1:8000 conjugated with IRDye 800CW or IRDye 680RD (Thermo Fisher Scientific, Waltham, MA, USA), were used. Band pattern was revealed with an Odyssey Imager (LI-QOR, Lincoln, NE, USA). For favoring the detection of bigger proteins, one of the membranes was stripped with a mild stripping buffer (20 mM glycine, 3 mM SDS, 0.1% Tween 20 in deionized water, with a pH of 2.2), after which the membrane was cut below the 50kD marker and re-blocked and probed with #1874.

2.8. Fluorescence In Situ Hybridization (FISH) and Immunofluorescence

Myoblasts, skin fibroblasts and lymphoblastoids grown on coverslips were fixed in 4% paraformaldehyde for 30 min and permeabilized with 0.3% Triton X-100 at 4 °C for 5 min (0.1% Triton X-100 for lymphoblastoids).

For the FISH, coverslips were incubated with 30% formamide in 2× SSC buffer for 30 min at room temperature, followed by an overnight incubation at 37 °C in darkness with a hybridization buffer, containing 0.01 µM Cy3-labelled $(CAG)_{10}$ or $(CTG)_{10}$ probe, 30% formamide, 1% dextran sulfate, 0.02% BSA and 2 mM vanadyl in 2× SSC buffer. The following day, the coverslips were washed with 30% formamide in 2× SSC buffer at 45 °C, 1× SSC buffer at 37 °C and 1× PBS at room temperature, and mounted with ProLong Gold Anti-Fade Mountant with DAPI (Thermo Fisher Scientific, Waltham, MA, USA).

For immunofluorescence, three approaches were followed: a simple immunofluorescence for the detection of RAN-translated polyglutamine protein in all three primary cell cultures, a single-step double immunofluorescence to compare one of the commercial antibodies with the custom antibody used and a two-step double immunofluorescence to assess the co-localization of the found protein with the Golgi apparatus.

For the simple immunofluorescence, coverslips with myoblasts, skin fibroblasts or lymphoblastoids were blocked for 1 h in 5% filtered NGS and incubated overnight at 4 °C with either α-DM1 (1:200, kindly provided by Laura Ranum), 1C2 (Merck, Darmstadt, Germany, ref MAB1574, 1:1000) or #1874 (Merck, Darmstadt, Germany, ref P1874, 1:1000). Next, cells were washed and incubated with goat anti-rabbit conjugated with alexa fluor 488 (Thermo Fisher Scientific, Waltham, MA, USA) for α-DM1 and goat anti-mouse conjugated with alexa fluor 488 (Thermo Fisher Scientific, Waltham, MA, USA) for 1C2 and #1874 for 1 h at room temperature, in darkness. After another round of washes in 1× PBS supplemented with 0.025% Tween-20, coverslips were mounted with ProLong Gold or Diamond Anti-Fade Mountant with DAPI (Thermo Fisher Scientific, Waltham, MA, USA).

For the single-step double immunofluorescence, coverslips were blocked for 1 h in 5% filtered NGS and incubated overnight at 4 °C with two antibodies in the same mix, α-DM1 (1:500 for myoblasts and skin fibroblasts and 1:5000 for lymphoblastoids, kindly provided by Laura Ranum) and 1C2 (1:500, Merck, Darmstadt, Germany). Next, cells were washed and incubated with goat anti-rabbit conjugated with alexa fluor 488 (Thermo Fisher Scientific, Waltham, MA, USA) and goat anti-mouse conjugated with alexa fluor 594

(Thermo Fisher Scientific, Waltham, MA, USA). After another round of washes in 1× PBS, coverslips were mounted with ProLong Gold Anti-Fade Mountant with DAPI (Thermo Fisher Scientific, Waltham, MA, USA).

For the two-step immunofluorescence, coverslips, containing either skin fibroblasts or myoblasts, were blocked for 30 min with the horse blocking solution, containing 5% normal horse serum, 10% normal human serum and 0.02% bovine serum albumin in 1× TBS. Subsequently, the coverslips were incubated overnight at 4 °C with 1C2 (1:200, Merck, Darmstadt, Germany). The following day, the cells were washed three times for 5 min with 1× TBS and incubated at room temperature for 1 h with biotin-labeled horse anti-mouse (1:2000, Thermo Fisher Scientific, Waltham, MA, USA). After another round of washes, the cells were incubated at room temperature for 1 h with streptavidin conjugated with alexa fluor 594 (1:2000, Thermo Fisher Scientific, Waltham, MA, USA). Next, the cells were washed and blocked with the goat blocking solution, containing 5% normal goat serum, 10% normal human serum, 10% Goat anti-horse IgG (Thermo Fisher Scientific, Waltham, MA, USA) and 0.02% bovine serum albumin in 1× TBS. Subsequently, the coverslips were incubated overnight at 4 °C with TGN-38 (1:200, Merck, Darmstadt, Germany). The following day, the cells were washed three times for 5 min with 1× TBS and incubated at room temperature for 1 h with goat anti-mouse conjugated with alexa fluor 488 (1:500, Thermo Fisher Scientific, Waltham, MA, USA). After another round of washes, the cells were mounted with ProLong Gold Anti-Fade Mountant with DAPI (Thermo Fisher Scientific, Waltham, MA, USA).

2.9. Image and Statistical Analysis

To assess DM1-AS expression and protein quantity, intensity measurements were taken using ImageJ software, and normalized against the endogenous controls. Differences in transcript expression were calculated using the Mann–Whitney's non-parametric U test with Graphpad Prism 9.1.2 software; significance level was set at 0.05.

3. Results

3.1. The DM1 Clinical Phenotype of the Studied Cohort

Our study population consisted of ten DM1 patients, of which the clinical characteristics have been, in part, described previously (Table 1, [12,13]). Eight out of ten DM1 patients provided skin and muscle biopsies, whereas from the other two only lymphoblastoid cell lines were available. The studied DM1 cohort consisted of eight females and two males with an age of onset ranging from 15 to 50 years. Seven individuals were unrelated and three were sisters (P3, P4 and P8). All patients presented with clinical myotonia, but mild muscle impairment was only observed in two patients, reflected by a Biceps MRC of four. Performance in the six-min walking distance test averaged 377 m (range 251–519 m). The muscular impairment rating scale (MIRS) revealed minimal signs of muscular impairment in three of the patients, while five patients showed distal weakness and two patients had mild-moderate proximal weakness. Cardiac problems occurred in all patients, except P3 and P10. Six DM1 patients showed minor ECG alterations, one (P2) a structural cardiopathy (valvulopathy) and P5 had a pacemaker. Five patients needed nocturnal mechanical ventilation, whereas three patients only showed mild changes in the respiratory function test and two patients (P7 and P10) showed no altered respiration. The majority of patients were independent in daily life activities (score of 0–2 on the modified Rankin (mRS) scale), and two patients (P5 and P9) had a moderate to moderately severe disability (scores of 3 and 4, respectively). The average repeat size in blood was 387 CTGs (range 130–619 CTGs) and one patient presented with CCG variant repeats (P7, previously reported [14]).

Table 1. Clinical characteristics of Myotonic Dystrophy type 1 (DM1) patients.

Patient	Sex	Age of Onset (y)	Age at Sampling (y)	Biceps MRC	Myotonia (s)	6-MWD (m)	MIRS	mRS	Cataracts	Cardiopathy	Spirometry	Repeat Size (CTGs)
P1	F	15 *	36	4	0.52	348	4	2	no	LAFB	Altered PFT	445
P2	M	48	54	5	0.67	251	3	2	yes	Valvulopathy	NMV	381
P3	F	36	41	5	0.73	368	2	1	yes	none	NMV	338
P4	F	42	46	5	0.98	338	3	1	yes	1st-degree AV block	NMV	246
P5	F	27	40	4	NP	NP	4	4	yes	Pacemaker	Altered PFT	374
P6	M	36	41	5	0.96	519	3	2	no	LAFB	Altered PFT	130
P7	F	50	62	5	NP	436	2	1	yes	1st-degree AV block	none	561
P8	F	35	38	5	NP	NP	3	2	no	1st-degree AV block	NMV	619
P9	F	30	51	5	NP	NP	4	3	yes	1st-degree AV block	NMV	NP
P10	F	18	34	5	NP	NP	3	2	yes	none	none	NP

F = female; M = male; MRC = Medical Research Council; NP = not performed; 6MWD = 6-min walking test; AV = atrioventricular; LAFB = left anterior fascicular block; mRS = modified Rankin Scale; MIRS = Muscular Impairment Rating Scale; NMV = nocturnal mechanical ventilation; PFT = pulmonary function test; * Although the exact age of disease onset was impossible to determine, based on the symptoms displayed at first visit (age 36), which commonly appear with an early onset (including oval pallor and temporal atrophy), disease onset was considered to have been during adolescence.

3.2. Lower Expression of DM1-AS Transcripts Found in DM1 Patients Compared to Controls

The RAN-translated polyGln has been described to originate from the antisense strand of the *DMPK* gene. We therefore decided to first validate the presence of DM1-AS transcripts in our three patient-derived primary cell cultures (myoblasts, skin fibroblasts and lymphoblastoids) by using three DM1-AS specific primer combinations, previously described ([6], Figure 1A). The original set-up published by Cho and collaborators and used in the original paper on DM1 RAN translation consisted of using DM1-AS specific primers with a linker sequence attached for strand-specific priming, and a primer complementary to that linker sequence for the subsequent PCRs [2]. However, in our cohort, this setup resulted in an inability to find the DM1-AS transcripts, including our positive control consisting of RNA of a heart control (data not shown), the tissue of origin used in the original paper [6]. When using the DM1-AS specific primers for the subsequent PCRs instead of the linker primer, we detected extreme variability in both DM1-AS transcripts and endogenous controls. We therefore opted for the use of random hexamers for cDNA synthesis and the use of the DM1-AS specific primers for the subsequent PCR. This allowed us to show DM1-AS transcription in all patients and controls with all three primer combinations and with a homogenous housekeeping gene distribution (Figures 1B,C and S1). PCR products were validated by Sanger sequencing. Overall, a lower expression was found in DM1 patients compared to controls with all three primer combinations, which reached significance for LK2/anti-N3 and LK1/anti-1B in myoblasts and LK1/anti-N3 and LK1/anti-1B in lymphoblastoids (Figure 1D). Expression was normalized against each housekeeping gene individually and against the mean of the three endogenous controls. Similar results were obtained with each approach, and the latter was used for the normalization shown in Figure 1. Of note, the LK1/anti-N3 combination, which included the CTG expansion, showed two distinct bands in some of the controls, indicating heterogeneity in their wild-type alleles (Figure S1). This primer combination seemed to favor the wild-type allele, as for the DM1 patients only one patient showed an extra band, which could be the expanded allele, based on the 130 CTG repeat this patient carried (Figure S1A,B).

3.3. DM1-AS Transcripts Are Present in the Cytoplasm of DM1 Cells

The results shown above indicate the presence of the DM1-AS transcript in both patients and controls, but for RAN translation to occur, these transcripts need to be able to reach the cytoplasm. To study this, we decided on a dual approach. The first approach was subcellular fractionation of the DM1 cells prior to RNA isolation. We verified the absence of nuclear pre-mRNA *DMPK* in the cytoplasmic fraction to ensure that no nuclear contamination could alter our results. RT-PCRs revealed that, in both patients and controls, the DM1-AS transcripts of two different regions were present in the cytoplasm (Figure 2A). The signal was higher in the nucleus compared to the cytoplasm, and this was slightly more apparent in patients (Figure 2B). In addition, we performed FISH using a Cy3-labeled $(CTG)_{10}$ probe to detect antisense RNA foci and a Cy3-labeled $(CAG)_{10}$ to detect sense RNA foci in DM1 cells. We showed the presence of antisense and sense RNA foci in all DM1 cells (Figures 2C and S2A). Notably, for myoblasts and skin fibroblasts, these antisense RNA foci were also present in the cytoplasm (12.5% of myoblasts and 8.75% of skin fibroblasts). However, this percentage was highly dependent on the patient, as some patients showed only 5% of cells with cytoplasmic antisense RNA foci, whereas others showed 30% (Tables S3 and S5). This variability could not be correlated to, for example, the CTG repeat size. As expected, no sense or antisense RNA foci were found in controls (Figure S2B). Overall, the presence of antisense RNA foci was shown in DM1 cells, although they were less abundant compared to sense RNA foci (Tables S3–S7). Importantly, antisense RNA foci were detected in cytoplasm, indicating that RAN translation is theoretically possible.

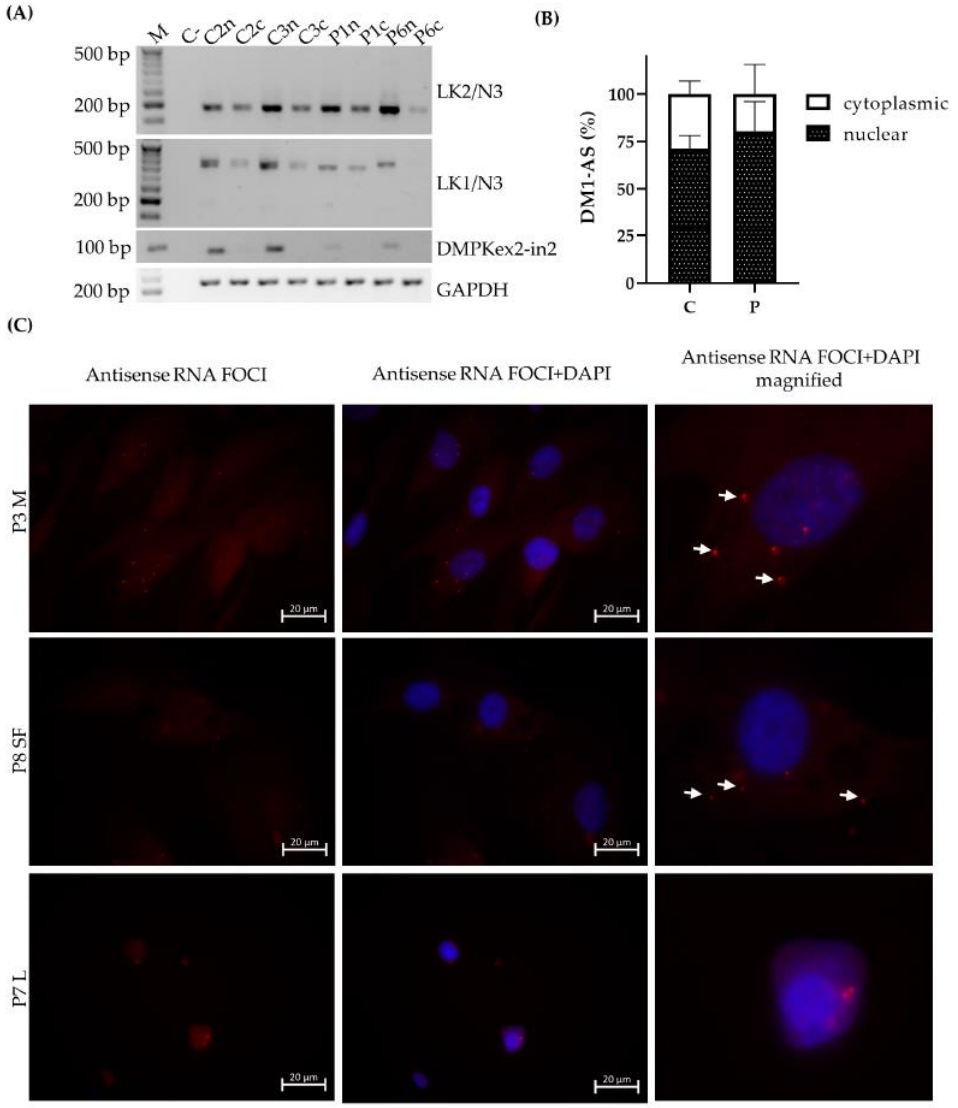

Figure 2. DM1-AS presence in the cytoplasm. (A) DM1-AS specific RT-PCR for subcellular fractionated skin fibroblasts with two primer combinations, LK2/anti-N3 and LK1/anti-N3. (B) Quantification of DM1-AS signals; bars represent mean +SD. (C) Presence of antisense RNA foci in all three cell types of DM1 patients. Cy3-labeled $(CTG)_{10}$ probe (RED) showing antisense RNA foci; nuclei indicated by DAPI (blue) and white arrows indicate cytoplasmic antisense RNA foci. Abbreviations: C = control; P = DM1 patient; *n* = nuclear; c = cytoplasmic; DMPKex2-in 2 = pre-mRNA DMPK as a nuclear marker; GAPDH = endogenous control; M = myoblasts; SF = skin fibroblasts; L = lymphoblastoids.

3.4. RAN Protein Was Undetectable in All Three Primary Cell Cultures

After validation that the origin of the RAN-translated polyGln was detectable in our primary cell cultures, we moved on to detection of the protein itself. For this, we used three different antibodies, of which two detect polyGln and are commercially available (1C2 and #1874), and one custom antibody, α-DM1, directed against the C-terminus of a predicted glutamine frame of DM1 in the CAG direction (generously provided by Laura Ranum). To make sure our commercial antibodies were able to recognize longer stretches of polyGln, we added two positive controls to our experiments: firstly a huntingtin vector containing 17 glutamines (Q17), in frame with mCherry, transfected into HEK293 cells, with an expected size of approximately 85 kD and secondly a Huntington's patient lymphoblastoid cell line (Huntingtin expected size: 340–350 kD). The commercially available anti-polyGln antibody #1874 was able to detect the polyGln-containing proteins in the two positive controls, and 1C2 was able to detect the Q17 vector as well (Figure S3A,B), indicating that our approach was able to show polyGln-containing proteins as large as 350 kD. In addition, HEK293 untransfected cells were added as a negative control and only showed a 42 kD protein (Figures 3A and S3B). Protein blots with 1C2 and #1874 in most cases showed a 42 kD protein in both controls and patients in all primary cell cultures, which was also present in both our negative and positive controls (Figures 3A and S3B). This protein was later identified as the TATA-box binding protein (TBP) (Figure 3B). Cutting the membrane above the 42 kD band to favor binding to other proteins did not alter our results (Figure S3C). α-DM1 revealed several different sizes of proteins in all three cell types, ranging from 26 kD to 150 kD, but these were visible in both patients and controls and with no significant differences in intensity (Figure S3D). In addition, the striking observation here was the different size of the polyGln-containing protein that both antibodies bound. Although small, the double staining method clearly showed a different band and the antibodies therefore did not bind the same protein (Figure S3E). The only cellular model to show a band that might correspond to the RAN protein were the lymphoblastoid cell lines, as four out of six patients showed polyGln containing proteins in the upper regions, which were not visible in the controls (Figure 3C). However, these proteins were not recognized by the α-DM1 antibody, which showed several bands in the 37 to 75 kD region in both patients and controls (Figure 3D), and these higher located polyGln-containing proteins could therefore not be validated as a polyGln RAN protein.

Although the protein blots did not reveal the polyGln RAN-translated protein, we opted to use a second approach to validate our findings, using immunocytochemistry. By use of the Q17-transfected HEK293 cells we validated the use of our commercial anti-polyGln antibodies in immunocytochemistry (Figure S3F). No differences were observed between patients and controls in all three primary cell cultures (Figure 4). A wide range of concentrations from 1:200 to 1:20,000 was used, but did not alter the original findings (data not shown). Both anti-polyGln antibodies, 1C2 and #1874, showed infrequent staining of the nucleus and an intense aggregate around the nucleus in myoblasts and skin fibroblasts in all cells of both patients and controls (Figures 4A,B, S4 and S5). In lymphoblastoids, due to the limited amount of cytoplasm, it did not show as an aggregate, but rather as an overall intense staining (Figures 4C, S4 and S5). This staining was present in approximately half of the cells, but still visible in both DM1 patients and controls. With the α-DM1, we saw an overall staining of the cytoplasm, with a more intense staining around the nucleus in both DM1 patients and controls and again infrequent staining of the nucleus (Figure S6). In myoblasts, in addition to the intense staining around the nucleus, small bright dots were observed in approximately half of the cells. Again, these were seen in both DM1 patients and controls (Figure S6). This more intense staining was roughly at the same place as the aggregates found with 1C2 and #1874, as illustrated by the double staining (Figure S7).

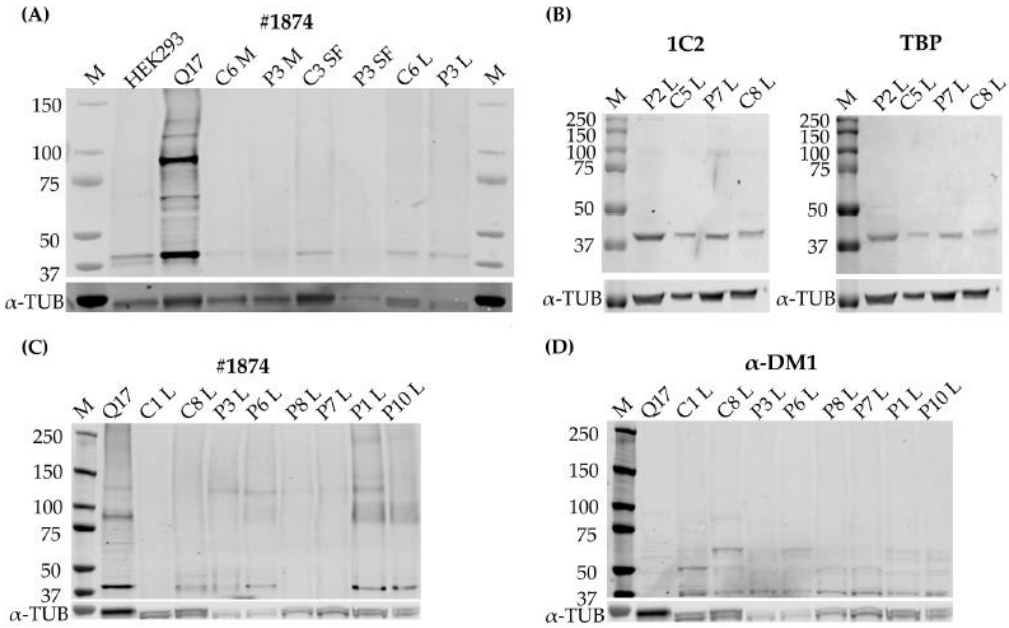

Figure 3. Quantitative analysis of repeat associated non-ATG (RAN) translated polyglutamine (polyGln) protein. (A) A representative immunoblot with #1874 1:1000, including all three primary cell cultures, our positive control, a huntingtin vector containing 17 polyglutamine stretches (Q17), and a negative control, consisting of untransfected HEK293 cells (C: $n = 4$, P: $n = 4$). (B) Immunoblot showing co-localization of the 42 kD protein found with #1874 and 1C2 with TATA-box-binding protein (TBP) in lymphoblastoids. The antibody shown here is 1C2. (C) Immunoblot of lymphoblastoid cell lines, two controls and six patients with #1874 showing several higher bands in certain DM1 patients. (D) Immunoblot with the custom antibody α-DM1, showing several non-specific bands, but none that overlap with the bands found with #1874. Abbreviations: M = marker; C = control; P = DM1 patient; HEK293 = untransfected HEK293 cells; Q17 = Q17 huntingtin vector; M = myoblasts; SF = skin fibroblasts; L = lymphoblastoids. #1874 = commercial antibody recognizing polyGln; α-DM1 = custom antibody against the predicted C-terminus of the polyGln RAN protein; α-TUB = α-tubulin as endogenous control.

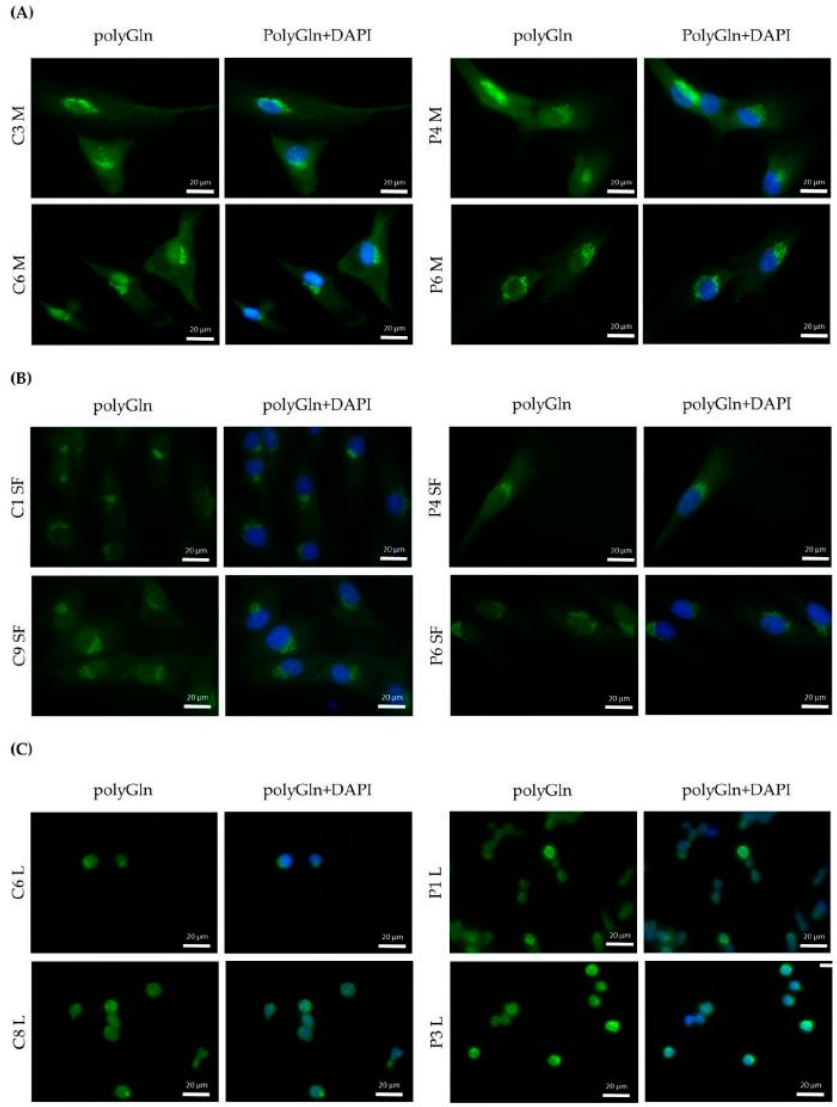

Figure 4. Qualitative analysis of polyGln RAN proteins in all DM1 cells. (A) Immunofluorescence polyGln staining with #1874 (alexa fluor-488, green) of human control and DM1 myoblasts. Nuclei indicated by DAPI (blue) (C: $n = 5$, P: $n = 6$) (B) Immunofluorescence polyGln staining with #1874 (alexa fluor-488, green) of human control and DM1 skin fibroblasts. Nuclei indicated by DAPI (blue) (C: $n = 5$, P: $n = 8$). (C) Immunofluorescence polyGln staining with #1874 (alexa fluor-488, green) of human control and DM1 lymphoblastoids (C: $n = 4$, P: $n = 5$). Nuclei indicated by DAPI (blue). Abbreviations: C = control; P = DM1 patient; polyGln = polyglutamine; M = myoblasts; SF = skin fibroblasts; L = lymphoblastoids.

3.5. The Polyglutamine Containing Protein Found Resides in the Golgi Apparatus

Due to the unexpected result of finding a positive staining in both DM1 patients and controls, we decided to further study the origin of this positive staining. The distinct structure found with the 1C2 and #1874 antibody resembled the structure of an organelle and we therefore decided to investigate this hypothesis. A double immunostaining with TGN-38, a marker for the Golgi apparatus, showed an exact match to the structure we found with the 1C2 antibody in DM1 cells (Figure 5).

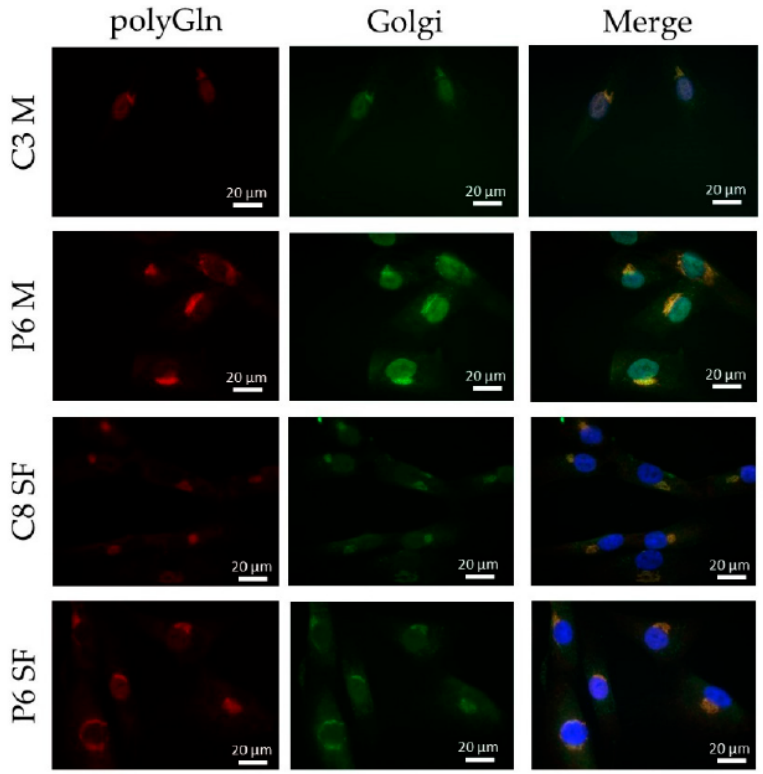

Figure 5. Determination of the origin of the polyGln containing proteins found via the immunofluorescence. Immunofluorescence showing co-localization of the polyGln aggregate found in myoblasts and skin fibroblasts with the commercial antibodies (1C2, alexa fluor-594, red) with the Golgi apparatus (TGN-38, alexa fluor-488 in green). Nuclei stained with DAPI (blue). Abbreviations: C = control; P = DM1 patient; M = myoblasts; SF = skin fibroblasts; polyGln = polyglutamine; Golgi = Golgi apparatus.

4. Discussion

We studied the presence of antisense transcription and polyGln RAN protein in three primary cell cultures of patients with DM1, namely myoblast, skin fibroblast and lymphoblastoid cell lines, in order to further elucidate its contribution to DM1 pathology.

The presence of antisense transcription, the origin of RAN-translated polyGln, was validated in our three primary cell cultures with three different primer combinations, and lower levels of expression were observed in DM1 patients compared to controls, which reached significance for LK2/anti-N3 and LK1/anti-1B in myoblasts and LK1/anti-N3 and LK1/anti-1B in lymphoblastoids. Of note, the LK1/anti-N3 primer combination, which

encompasses the repeat region, revealed that it primarily detected the smaller transcripts, most likely corresponding to the wild-type allele. Only P6 showed an additional band in myoblasts and skin fibroblasts, which, based on the CTG repeat size, could correspond to the expanded repeat. P6 had the smallest expanded repeat (130 repeats) in our cohort and it could be that the other patients, carrying much larger expanded repeats, could not be detected by this method. This could be a potential explanation for the lower levels of expression seen in patients compared to controls. However, the lower levels were also observed with the other two primer combinations that did not encompass the expanded repeat, making it highly unlikely that the lower levels seen were solely due to the binding of the wild-type allele. DM1-AS expression has only been studied by a handful of other groups. Zu and collaborators showed its presence in a heart sample of a DM1 patient and a healthy control; however, the expression patterns were hard to interpret, since an endogenous control was lacking [6]. A study by Gudde and collaborators showed a slightly higher expression in muscle biopsies of DM1 patients when studying RNA-seq data from the myotonic dystrophy deep sequencing data repository [5]. They did, however, mention that globally no obvious differences in read density were observed between DM1 patients and controls. However, when stratified based on inferred MBNL concentration, the most severely affected patients showed a three-fold increase in DM1-AS expression compared to controls, which was in vast contrast to the lower expression levels found in our cohort [5]. Another study, performed by Brouwer and collaborators, showed that in mouse models with increasing CTG repeat length, the DM1-AS transcription levels remained unchanged [15]. Unfortunately, disease severity in Gudde and collaborators' report was based on the inferred MBNL concentration of DM1 patients, and this was not available for our patients, which meant we could not do a similar stratification. We did, however, have extensive knowledge on the clinical phenotype of our DM1 cohort and had patients from three different clinical subtypes included in our studies, namely juvenile, adult and late-onset. Upon revision, a correlation between expression levels and clinical phenotype could not be found, based on for example, age of onset, muscle involvement (muscle weakness, myotonia) or CTG repeat size, the latter in agreement with the report of Brouwer and collaborators [15]. The sample size of our cohort was rather small for such comparisons or stratification, hindering the analysis. To determine whether DM1-AS transcript expression is linked to disease severity, a bigger cohort is needed.

The presence of DM1-AS transcripts in DM1 cells does not necessarily mean that these transcripts can reach the cytoplasm and be RAN-translated. To further elucidate the localization of these transcripts, cellular fractionation was performed and revealed the presence of DM1-AS transcripts in the cytoplasm of both patients and controls, with a higher percentage in the nuclear fraction. The presence of cytoplasmic DM1-AS transcripts was previously reported by Gudde and collaborators, as they showed the presence of DM1-AS transcripts in the cytoplasmic fraction of myoblasts [5]. However, in both the fractionated and unfractionated DM1-AS pool, it was unclear whether the transcripts possessed the expanded repeat. The LK1/anti-N3 combination already hinted that not all of the DM1-AS transcripts had the expanded repeat. This was also shown by Gudde and collaborators, who found a heterogeneous pool of DM1-AS transcript sizes, with and without the expanded repeat [5]. To determine whether the DM1-AS transcripts in DM1 cells included the expanded repeat, we performed a FISH to detect antisense RNA foci and found that antisense RNA foci were present in both the nucleus and cytoplasm of DM1 cells, indicating that these DM1-AS transcripts contained the expanded repeat and RAN translation was therefore, hypothetically, possible. However, the number of antisense RNA foci compared to sense RNA foci was much lower and they were not present in all cells. In addition, the cytoplasmic antisense RNA foci were even rarer, with only approximately 10% of myoblasts and skin fibroblasts containing cytoplasmic RNA foci, indicating that the presence of DM1-AS transcripts with the expanded repeat in the cytoplasm was quite low. Previous reports on antisense RNA foci in DM1 have also shown that the amount of antisense RNA foci in the nucleus was less compared to sense RNA

foci [3,4]. The polyGln RAN protein was undetectable in all three of our primary cell cultures via two different approaches. Western blots revealed a 42 kD polyGln-containing protein with the two commercial anti-polyGln antibodies, which was most likely TBP. In fact, the original immunogen for the 1C2 antibody was the general transcription factor TBP, which contains a 38-Gln stretch and therefore matches our results. It was shown, however, that although TBP will always show up on Western blots in both patients and controls, the antibody favored the binding of longer stretches of polyGln, such as were present in Huntington's disease and cerebellar ataxia type 1 and 3 [16]. Accordingly, a certain subset of lymphoblastoids did show a band that might correspond to the polyGln RAN protein, but the custom α-DM1 antibody showed a range of non-specific bands in both patients and controls and we were therefore unable to determine the origin of this protein with certainty. In addition, it is difficult to know the exact size of the polyGln RAN protein produced by the DM1-AS, as the disease is prone to somatic mosaicism. This means that cells of the same tissue can carry different CTG expansion sizes and it is therefore also possible to have a range of potential sizes for the protein originating from these transcripts [17,18]. However, Zu and collaborators showed a band just below 60 kD in a patient carrying 85 CTG·CAGs [6]. Our patients carried expansions much larger than that, and when estimating the molecular weight based on the CTG expansion size, it was possible to have polyGln RAN proteins in the range we found within the lymphoblastoid cell lines. This will remain, however, hypothetical, as it seems we do not have a proper functional custom DM1 polyGln RAN antibody and no positive control available to test its functionality.

Immunofluorescence revealed a cytoplasmic aggregate surrounding the nucleus in myoblasts and skin fibroblasts with both commercial anti-polyGln antibodies, which was found to be co-localized with the Golgi apparatus. Since the aggregate was visible in both patients and controls and no apparent differences were seen, this might indicate the detection of another endogenous polyGln-containing protein. For example, ataxin-2, the product of the spinocerebellar ataxia type 2 gene, contains 22 glutamines and resides in the Golgi apparatus [19]. In addition, our immunofluorescence did show staining of the nucleus at high antibody concentrations, which might be due to binding of the transcription factor TBP, also detected by the immunoblots (42 kD band). Taken together, this would mean that both commercial anti-polyGln antibodies bind to several endogenous polyGln-containing proteins, especially at higher antibody concentrations. However, no apparent differences were found between patients and controls across a wide range of concentrations, and the use of α-DM1 antibody did not reveal these similar aggregates. This is in vast contrast to the results previously reported by Zu and collaborators, as they found nuclear polyGln RAN protein aggregates at low frequencies in a DM1 patient's myoblasts and skeletal muscle (n = 1) and at higher frequencies in leukocytes from peripheral blood (n = 1) [6]. The 1C2 antibody was used in their experiments to validate the specificity of their custom α-DM1 antibody. Although one of the cell types we used was the same as theirs, i.e., myoblasts, neither antibody was able to find the polyGln RAN protein in our myoblast cell lines, nor in the other two primary cell cultures. In fact, although both types of antibodies showed a protein of approximately 42 kD, our simultaneous staining showed that it was not the same protein, indicating that the antibodies were not able to recognize the same proteins. This was surprising, as the commercial antibody was used to validate the custom antibody in the paper of Zu and collaborators [6]. Our DM1-AS results suggested that the presence of DM1-AS transcripts containing the expanded repeat in the cytoplasm of DM1 cells is quite a rare occurrence. This highly affects the chance of producing polyGln RAN proteins. In addition, polyGln-containing proteins are very common in healthy subjects. Taking these two notions together, it might be plausible that with current techniques, sensitivity is too low to detect such low quantities of the polyGln RAN protein, which in addition is hindered by the presence of other polyGln containing proteins.

APPENDIX

Although we were unable to detect polyGln RAN proteins in our DM1 cells, much progress has been made in other repeat expansion disorders displaying RAN translation, which could help in the field of DM1. Nine expansion disorders have been added since the first discovery of RAN translation in SCA8 and DM1: C9orf72 amyotrophic lateral sclerosis/frontotemporal dementia [20–22], fragile X tremor/ataxia syndrome [23], Huntington's disease (HD) [24,25], spinocerebellar ataxia 3 and 31 [26,27], Fuchs' endothelial corneal dystrophy [28] and myotonic dystrophy type 2 (DM2) [29]. Of these, SCA8, SCA3 and HD are the three repeat expansion disorders in which the RAN proteins originate from a CAG expansion, and can therefore result in polyGln RAN proteins. Interestingly, in vivo, none of these diseases show polyGln RAN proteins, but instead produce poly-alanine, and for HD additionally poly-serine RAN proteins. It might be interesting to include custom antibodies for the two additional homo-polymeric protein possibilities with regard to DM1. Although the name suggests a close relationship between DM1 and DM2, the underlying expansion in DM2 is a CCTG expansion and therefore results in complex poly-LPAC (sense) or poly-QAGR (antisense) RAN proteins, and is thus not hindered by the presence of endogenous polyGln proteins. The study was performed in autopsy brains, a tissue not yet studied for DM1, which might also be worth exploring.

In conclusion, DM1-AS transcript levels were lower in patients compared to controls and were present in both the nucleus and the cytoplasm of DM1 cells. Only a small portion of the DM1-AS transcripts contained the expanded repeat, substantially lowering the possibility of RAN translation in DM1. The polyGln RAN protein was not present in patient-derived DM1 cells, or was present in such low quantities that it is below the detection limit of the currently available techniques.

Supplementary Materials: The following are available online at https://www.mdpi.com/article/10.3390/jcm10235520/s1. Table S1: Primer sequences. Figure S1: DM1-AS transcripts in DM1 cells of the additional two primer combinations studied. Figure S2: RNA foci overview. Table S2: Sense RNA foci details in DM1 myoblasts. Table S3: Antisense RNA foci details in DM1 myoblasts. Table S4: Sense RNA foci details in DM1 skin fibroblasts. Table S5: Antisense RNA foci details in DM1 skin fibroblasts. Table S6: Sense RNA foci details in DM1 lymphoblastoids. Table S7: Antisense RNA foci details in DM1 lymphoblastoids. Figure S3: Quantitative analysis of the polyGln RAN protein and antibody validation. Figure S4: Qualitative analysis of polyGln RAN proteins with the #1874 antibody of additional samples. Figure S5: Qualitative analysis of polyGln RAN proteins with the 1C2 antibody. Figure S6: Qualitative analysis of polyGln RAN proteins with the α-DM1 antibody. Figure S7: Double immunofluorescence with the α-DM1 antibody and 1C2 antibody.

Author Contributions: Conceptualization, G.N.-G. and E.K.; methodology, E.K., M.S., G.N.-G. and J.C.; validation, M.S. and G.N.-G.; formal analysis, E.K.; investigation, E.K., J.N.-M., A.B.-L., J.C., A.P.G.-E., M.A., G.L., A.A., G.P.-M., J.C.-C., A.R.-F. and A.M.-P.; resources, G.N.-G. and R.P.V.-M.; data curation, G.N.-G.; writing—original draft preparation, E.K.; writing—review and editing, G.N.-G., M.S., A.M.-P., J.N.-M., A.B.-L., M.A., G.L., A.A., J.C., R.P.V.-M., A.P.G.-E., G.P.-M., J.C.-C. and A.R.-F.; visualization, E.K. and J.C.; supervision, M.S. and G.N.-G.; project administration, E.K., M.S. and G.N.-G.; funding acquisition, G.N.-G., M.S. and A.M.-P. All authors have read and agreed to the published version of the manuscript.

Funding: The research of G. Nogales-Gadea and A. Ramos-Fransi is funded by Instituto de Salud Carlos III (grant numbers PI15/01756 and PI18/00713) and co-financed by Fondos FEDER. G. Nogales-Gadea is supported by a Miguel Servet research contract (ISCIII CD14/00032, ISCIII CPII19/00021, and FEDER) and by a Trampoline Grant #21108 from AFM Telethon. E. Koehorst is funded by the La Caixa Foundation (ID 100010434), fellowship code LCF/BQ/IN18/11660019, cofunded by the European Union's Horizon 2020 research and innovation program under the Marie Skłodowska-Curie grant agreement no. 713673. The research of M. Suelves is funded by Ministerio de Ciencia e Innovación (grant number PID2020-118730RB-I00) and co-financed by Fondos FEDER. J. Núñez-Manchón is funded by Instituto de Salud Carlos III I-PFIS fellowship (grant number IFI20/00022). G. Lucente is supported by a Rio Hortega contract (ISCIII CM16/00016 and FEDER). J. Chojnacki is supported by European Union's Horizon 2020 research and innovation program under the Marie Skłodowska-Curie grant agreement no. 793830. The work of A.P. Gómez-Escribano and R.P. Vázquez-

APPENDIX

Manrique is funded by the ISCIII (CPII16/00004, PI17/00011 and PI20/00114) and the Fundación Ramón Areces (CIVP19S8119). This work was supported by the CERCA program/ Government of Catalonia. The funding bodies had no role in the design of the study and the collection, analysis, and interpretation of data.

Institutional Review Board Statement: The study was conducted according to the guidelines of the Declaration of Helsinki, and approved by the Institutional Review Board (or Ethics Committee) of Hospital Universitario Germans Trias i Pujol, protocol code PI15/01756, date of approval 27 November 2015.

Informed Consent Statement: Informed consent was obtained from all subjects involved in the study.

Data Availability Statement: The data presented in this study are available on request from the corresponding author.

Acknowledgments: The authors wish to thank Laura Ranum for generously providing the custom α-DM1 antibody and Darren Monckton and Sarah Cumming for their help with the SP-PCRs. The authors also wish to thank Manuel Rodriguez-Allue and Daniel del Toro-Ruiz for their helpful comments and sug-gestions and the DM1 patients and the Huntington's patient for providing the samples needed to perform this study. We thank the IGTP core facilities for their contribution to this publication.

Conflicts of Interest: G. Pintos-Morell reports personal honoraria from Shire-Takeda, Amicus, and Sanofi-Genzyme, outside the submitted work.

References

1. Meola, G.; Cardani, R. Myotonic dystrophies: An update on clinical aspects, genetic, pathology, and molecular pathomechanisms. *Biochim. Biophys. Acta Mol. Basis Dis.* **2015**, *1852*, 594–606. [CrossRef]
2. Cho, D.H.; Thienes, C.P.; Mahoney, S.E.; Analau, E.; Filippova, G.N.; Tapscott, S.J. Antisense transcription and heterochromatin at the DM1 CTG repeats are constrained by CTCF. *Mol. Cell* **2005**, *20*, 483–489. [CrossRef]
3. Huguet, A.; Medja, F.; Nicole, A.; Vignaud, A.; Guiraud-Dogan, C.; Ferry, A.; Decostre, V.; Hogrel, J.Y.; Metzger, F.; Hoeflich, A.; et al. Molecular, Physiological, and Motor Performance Defects in DMSXL Mice Carrying >1000 CTG Repeats from the Human DM1 Locus. *PLoS Genet.* **2012**, *8*, e1003043. [CrossRef]
4. Michel, L.; Huguet-Lachon, A.; Gourdon, G. Sense and antisense DMPK RNA foci accumulate in DM1 tissues during development. *PLoS ONE* **2015**, *10*, e1003043. [CrossRef]
5. Gudde, A.E.E.G.; van Heeringen, S.J.; de Oude, A.I.; van Kessel, I.D.G.; Estabrook, J.; Wang, E.T.; Wieringa, B.; Wansink, D.G. Antisense transcription of the myotonic dystrophy locus yields low-abundant RNAs with and without (CAG)n repeat. *RNA Biol.* **2017**, *14*, 1374–1388. [CrossRef]
6. Zu, T.; Gibbens, B.; Doty, N.S.; Gomes-Pereira, M.; Huguet, A.; Stone, M.D.; Margolis, J.; Peterson, M.; Markowski, T.W.; Ingram, M.A.C.; et al. Non-ATG-initiated translation directed by microsatellite expansions. *Proc. Natl. Acad. Sci. USA* **2011**, *108*, 260–265. [CrossRef]
7. Nguyen, L.; Cleary, J.D.; Ranum, L.P.W. Repeat-Associated Non-ATG Translation: Molecular Mechanisms and Contribution to Neurological Disease. *Annu. Rev. Neurosci.* **2019**, *42*, 227–247. [CrossRef]
8. Miller, S.A.; Dykes, D.D.; Polesky, H.F. A simple salting out procedure for extracting DNA from human nucleated cells. *Nucleic Acids Res.* **1988**, *16*, 1215. [CrossRef] [PubMed]
9. Gomes-Pereira, M.; Bidichandani, S.I.; Monckton, D.G. Analysis of Unstable Triplet Repeats Using Small-Pool Polymerase Chain Reaction. In *Trinucleotide Repeat Protocols*; Humana Press: Totowa, NJ, USA, 2004; Volume 277, pp. 61–76.
10. Monckton, D.G.; Wong, L.J.; Ashizawa, T.; Caskey, C.T. Somatic mosaicism, germline expansions, germline reversions and intergenerational reductions in myotonic dystrophy males: Small pool PCR analyses. *Hum. Mol. Genet.* **1995**, *4*, 1–8. [CrossRef]
11. Rio, D.C.; Ares, M.; Hannon, G.J.; Nilsen, T.W. Preparation of cytoplasmic and nuclear RNA from tissue culture cells. *Cold Spring Harb. Protoc.* **2010**, *2010*, pdb.prot5441. [CrossRef] [PubMed]
12. Ballester-Lopez, A.; Koehorst, E.; Linares-Pardo, I.; Núñez-Manchón, J.; Almendrote, M.; Lucente, G.; Arbex, A.; Alonso, C.P.; Lucia, A.; Monckton, D.G.; et al. Preliminary findings on ctg expansion determination in different tissues from patients with myotonic dystrophy type 1. *Genes* **2020**, *11*, 1321. [CrossRef]
13. Ballester-Lopez, A.; Núñez-Manchón, J.; Koehorst, E.; Linares-Pardo, I.; Almendrote, M.; Lucente, G.; Guanyabens, N.; Lopez-Osias, M.; Suárez-Mesa, A.; Hanick, S.A.; et al. Three-dimensional imaging in myotonic dystrophy type 1. *Neurol. Genet.* **2020**, *6*, e484. [CrossRef]
14. Ballester-Lopez, A.; Koehorst, E.; Almendrote, M.; Martínez-Piñeiro, A.; Lucente, G.; Linares-Pardo, I.; Núñez-Manchón, J.; Guanyabens, N.; Cano, A.; Lucia, A.; et al. A DM1 family with interruptions associated with atypical symptoms and late onset but not with a milder phenotype. *Hum. Mutat.* **2020**, *41*, 420–431. [CrossRef]

APPENDIX

15. Brouwer, J.R.; Huguet, A.; Nicole, A.; Munnich, A.; Gourdon, G. Transcriptionally repressive chromatin remodelling and CpG methylation in the presence of expanded CTG-repeats at the DM1 locus. *J. Nucleic Acids* **2013**, *2013*, 567435. [CrossRef] [PubMed]
16. Trottier, Y.; Lutz, Y.; Stevanin, G.; Imbert, G.; Devys, D.; Cancel, G.; Saudou, F.; Weber, C.; David, G.; Tora, L.; et al. Polyglutamine expansion as a pathological epitope in Huntington's disease and four dominant cerebellar ataxias. *Nature* **1995**, *378*, 403–406. [CrossRef]
17. Morales, F.; Couto, J.M.; Higham, C.F.; Hogg, G.; Cuenca, P.; Braida, C.; Wilson, R.H.; Adam, B.; del Valle, G.; Brian, R.; et al. Somatic instability of the expanded CTG triplet repeat in myotonic dystrophy type 1 is a heritable quantitative trait and modifier of disease severity. *Hum. Mol. Genet.* **2012**, *21*, 3558–3567. [CrossRef] [PubMed]
18. Morales, F.; Vásquez, M.; Corrales, E.; Vindas-Smith, R.; Santamaría-Ulloa, C.; Zhang, B.; Sirito, M.; Estecio, M.; Krahe, R.; Monckton, D. Longitudinal increases in somatic mosaicism of the expanded CTG repeat in myotonic dystrophy type 1 are associated with variation in age-at-onset. *Hum. Mol. Genet.* **2020**, *29*, 2496–2507. [CrossRef]
19. Huynh, D.P.; Yang, H.T.; Vakharia, H.; Nguyen, D.; Pulst, S.M. Expansion of the polyQ repeat in ataxin-2 alters its Golgi localization, disrupts the Golgi complex and causes cell death. *Hum. Mol. Genet.* **2003**, *12*, 1485–1496. [CrossRef]
20. Ash, P.E.A.; Bieniek, K.F.; Gendron, T.F.; Caulfield, T.; Lin, W.-L.; Dejesus-Hernandez, M.; van Blitterswijk, M.M.; Jansen-West, K.; Paul, J.W.; Rademakers, R.; et al. Unconventional translation of C9ORF72 GGGGCC expansion generates insoluble polypeptides specific to c9FTD/ALS. *Neuron* **2013**, *77*, 639–646. [CrossRef] [PubMed]
21. Zu, T.; Liu, Y.; Bañez-Coronel, M.; Reid, T.; Pletnikova, O.; Lewis, J.; Miller, T.M.; Harms, M.B.; Falchook, A.E.; Subramony, S.H.; et al. RAN proteins and RNA foci from antisense transcripts in C9ORF72 ALS and frontotemporal dementia. *Proc. Natl. Acad. Sci. USA* **2013**, *110*, E4968–E4977. [CrossRef]
22. Mori, K.; Weng, S.M.; Arzberger, T.; May, S.; Rentzsch, K.; Kremmer, E.; Schmid, B.; Kretzschmar, H.A.; Cruts, M.; Van Broeckhoven, C.; et al. The C9orf72 GGGGCC repeat is translated into aggregating dipeptide-repeat proteins in FTLD/ALS. *Science* **2013**, *339*, 1335–1338. [CrossRef] [PubMed]
23. Todd, P.K.; Oh, S.Y.; Krans, A.; He, F.; Sellier, C.; Frazer, M.; Renoux, A.J.; Chen, K.; Scaglione, K.M.; Basrur, V.; et al. CGG repeat-associated translation mediates neurodegeneration in fragile X tremor ataxia syndrome. *Neuron* **2013**, *78*, 440–455. [CrossRef]
24. Banez-Coronel, M.; Ayhan, F.; Tarabochia, A.D.; Zu, T.; Perez, B.A.; Tusi, S.K.; Pletnikova, O.; Borchelt, D.R.; Ross, C.A.; Margolis, R.L.; et al. RAN Translation in Huntington Disease. *Neuron* **2015**, *88*, 667–677. [CrossRef]
25. Davies, J.E.; Rubinsztein, D. Polyalanine and polyserine frameshift products in Huntington's disease. *J. Med. Genet.* **2006**, *43*, 893–896. [CrossRef]
26. Ishiguro, T.; Sato, N.; Ueyama, M.; Fujikake, N.; Sellier, C.; Kanegami, A.; Tokuda, E.; Zamiri, B.; Gall-Duncan, T.; Mirceta, M.; et al. Regulatory Role of RNA Chaperone TDP-43 for RNA Misfolding and Repeat-Associated Translation in SCA31. *Neuron* **2017**, *94*, 108–124.e7. [CrossRef]
27. Toulouse, A.; Au-Yeung, F.; Gaspar, C.; Roussel, J.; Dion, P.; Rouleau, G.A. Ribosomal frameshifting on MJD-1 transcripts with long CAG tracts. *Hum. Mol. Genet.* **2005**, *14*, 2649–2660. [CrossRef] [PubMed]
28. Soragni, E.; Petrosyan, L.; Rinkoski, T.A.; Wieben, E.; Baratz, K.; Fautsch, M.; Gottesfeld, J. Repeat-Associated Non-ATG (RAN) Translation in Fuchs' Endothelial Corneal Dystrophy. *Investig. Ophthalmol. Vis. Sci.* **2018**, *59*, 1888–1896. [CrossRef]
29. Zu, T.; Cleary, J.D.; Liu, Y.; Bañez-Coronel, M.; Bubenik, J.L.; Ayhan, F.; Ashizawa, T.; Xia, G.; Clark, H.B.; Yachnis, A.T.; et al. RAN Translation Regulated by Muscleblind Proteins in Myotonic Dystrophy Type 2. *Neuron* **2017**, *95*, 1292–1305.e5. [CrossRef] [PubMed]

biomedicines

MDPI

Article

An Integrative Analysis of DNA Methylation Pattern in Myotonic Dystrophy Type 1 Samples Reveals a Distinct DNA Methylation Profile between Tissues and a Novel Muscle-Associated Epigenetic Dysregulation

Emma Koehorst [1], Renato Odria [1], Júlia Capó [1], Judit Núñez-Manchón [1], Andrea Arbex [1,2], Miriam Almendrote [1,2], Ian Linares-Pardo [1], Daniel Natera-de Benito [3], Verónica Saez [3], Andrés Nascimento [3], Carlos Ortez [3], Miguel Ángel Rubio [4], Jordi Díaz-Manera [5,6], Jorge Alonso-Pérez [5], Giuseppe Lucente [1,2], Agustín Rodriguez-Palmero [1,7], Alba Ramos-Fransi [1,2], Alicia Martínez-Piñeiro [1,2], Gisela Nogales-Gadea [1,†] and Mònica Suelves [1,*,†]

[1] Neuromuscular and Neuropediatric Research Group, Institut d'Investigació en Ciències de la Salut Germans Trias i Pujol (IGTP), Campus Can Ruti, Universitat Autònoma de Barcelona, 08916 Badalona, Spain; ekoehorst@igtp.cat (E.K.); rrodria@igtp.cat (R.O.); jcapo@igtp.cat (J.C.); jnunez@igtp.cat (J.N.-M.); aarbexb.germanstrias@gencat.cat (A.A.); malmendrote.germanstrias@gencat.cat (M.A.); ilinares@igtp.cat (I.L.-P.); glucente@igtp.cat (G.L.); arodriguezpalmero.germanstrias@gencat.cat (A.R.-P.); aramosf@igtp.cat (A.R.-F.); amartinezp.germanstrias@gencat.cat (A.M.-P.); gnogales@igtp.cat (G.N.-G.)

[2] Neuromuscular Pathology Unit, Neurology Service, Neuroscience Department, Hospital Universitari Germans Trias i Pujol, 08916 Badalona, Spain

[3] Neuromuscular Unit, Neuropediatric Department, Institut de Recerca Pediàtrica Hospital Sant Joan de Déu, L'Hospitalet de Llobregat, 08950 Barcelona, Spain; daniel.natera@sjd.es (D.N.-d.B.); veroisabelsaez@gmail.com (V.S.); anascimento@sjdhospitalbarcelona.org (A.N.); ciortez@sjdhospitalbarcelona.org (C.O.)

[4] Neuromuscular Unit, Department of Neurology, Hospital del Mar, 08003 Barcelona, Spain; marubio@psmar.cat

[5] Neuromuscular Diseases Unit, Department of Neurology, Hospital de la Santa Creu i Sant Pau, 08025 Barcelona, Spain; jordi.diaz-manera@newcastle.ac.uk (J.D.-M.); jalonsop@santpau.cat (J.A.-P.)

[6] John Walton Muscular Dystrophy Research Centre, Newcastle University and Newcastle Hospitals NHS Foundation Trust, Newcastle upon Tyne NE1 3BZ, UK

[7] Pediatric Neurology Unit, Department of Pediatrics, Hospital Universitari Germans Trias i Pujol, Universitat Autònoma de Barcelona, 08916 Badalona, Spain

* Correspondence: msuelves@igtp.cat

† These authors contributed equally to this work.

check for updates

Citation: Koehorst, E.; Odria, R.; Capó, J.; Núñez-Manchón, J.; Arbex, A.; Almendrote, M.; Linares-Pardo, I.; Natera-de Benito, D.; Saez, V.; Nascimento, A.; et al. An Integrative Analysis of DNA Methylation Pattern in Myotonic Dystrophy Type 1 Samples Reveals a Distinct DNA Methylation Profile between Tissues and a Novel Muscle-Associated Epigenetic Dysregulation. *Biomedicines* **2022**, *10*, 1372. https://doi.org/10.3390/biomedicines10061372

Academic Editor: Nina Entelis

Received: 22 April 2022
Accepted: 7 June 2022
Published: 10 June 2022

Publisher's Note: MDPI stays neutral with regard to jurisdictional claims in published maps and institutional affiliations.

Abstract: Myotonic dystrophy type 1 (DM1) is a progressive, non-treatable, multi-systemic disorder. To investigate the contribution of epigenetics to the complexity of DM1, we compared DNA methylation profiles of four annotated CpG islands (CpGis) in the *DMPK* locus and neighbouring genes, in distinct DM1 tissues and derived cells, representing six DM1 subtypes, by bisulphite sequencing. In blood, we found no differences in CpGi 74, 43 and 36 in DNA methylation profile. In contrast, a CTCF1 DNA methylation gradient was found with 100% methylation in congenital cases, 50% in childhood cases and 13% in juvenile cases. CTCF1 methylation correlated to disease severity and CTG expansion size. Notably, 50% of CTCF1 methylated cases showed methylation in the CTCF2 regions. Additionally, methylation was associated with maternal transmission. Interestingly, the evaluation of seven families showed that unmethylated mothers passed on an expansion of the CTG repeat, whereas the methylated mothers transmitted a contraction. The analysis of patient-derived cells showed that DNA methylation profiles were highly preserved, validating their use as faithful DM1 cellular models. Importantly, the comparison of DNA methylation levels of distinct DM1 tissues revealed a novel muscle-specific epigenetic signature with methylation of the CTCF1 region accompanied by demethylation of CpGi 43, a region containing an alternative *DMPK* promoter, which may decrease the canonical promoter activity. Altogether, our results showed a distinct DNA methylation profile across DM1 tissues and uncovered a novel and dual epigenetic signature in DM1 muscle samples, providing novel insights into the epigenetic changes associated with DM1.

APPENDIX

Keywords: myotonic dystrophy; CpG islands; DNA methylation; epigenetics; phenotype severity; DM1 biopsies; cellular models

1. Introduction

Myotonic dystrophy type 1 (DM1) is an autosomal dominant inherited, multi-systemic disorder, with predominant muscle involvement and an estimated incidence of 1:8000 [1]. DM1 has been recognized as one of the muscle dystrophies with the more variable phenotype, as it affects several tissues and systems, and because it has varied manifestations. It can be classified into five different clinical subtypes, which are based on the age of onset, ranging from foetal to late-adult onset [2]. These clinical subtypes show an increasing disease severity with decreasing age of onset, and although they share a core set of symptoms, each subtype has unique additional features (Table 1) [2–12]. In addition to the five clinical categories, there is another special set of 'DM1' patients, the asymptomatic or paucisymptomatic DM1 category, characterized by the absence or just minor symptoms across an individual's life span. The causes of the clinical variability observed in DM1 are poorly understood.

Table 1. Clinical manifestations of the different DM1 subcategories.

Clinical Subtype	Age of Onset	Main Symptoms
Congenital	<1 year	Poor fetal movement Hypotonia Feeding difficulties Clubfoot deformities Respiratory failure Learning disability Cardiorespiratory complications
Childhood	1–10 years	Cognitive and learning disabilities Facial weakness Myotonia Conduction defects
Juvenile	11–20 years	Skeletal muscle weakness Myotonia Cognitive and learning disabilities Conduction defects
Adult	21–40 years	Progressive muscle weakness Myotonia Early-onset cataracts Conduction defects Endocrine dysfunction
Late-onset	>40 years	Low-grade muscle weakness Early-onset cataracts alopecia

Epigenetics is defined as heritable changes that do not affect the DNA sequence itself but influence gene expression and it includes DNA methylation, histone modifications, and non-coding RNAs [13]. DNA methylation is the most widely studied epigenetic mark, which is essential for mammalian development, crucial for the establishment and maintenance of cell identity, and it affects gene expression by regulating promoters and distal regulatory elements, such as enhancers and insulators [14–16]. It occurs most often on a cytosine leading a guanine, which are referred to as CpG dinucleotides. They are globally underrepresented in the genome, except in CpG islands. CpG islands are CpG-dense regions largely resistant to DNA methylation [17,18]. They are generally found at

promoters of housekeeping and developmental genes, and are represented in 70% of the promoters, but can be also found in exons, introns and regulatory regions [19].

The dystrophia myotonica protein kinase (*DMPK)* gene (the gene carrying the disease causing CTG expansion in its 3′ untranslated region) and neighbouring genes (henceforth referred to as the *DMPK* locus) contain several CpG islands (CpGis). CpGi 374 has gained the most attention because this 3.5 kb island contains the expanded repeat. In addition, the CTG repeat is flanked by two CCTC-binding factor (CTCF) binding sites, named CTCF1 and CTCF2. Early studies suggested that the two CTCF binding sites together with the expanded repeat established an insulator element between the *DMPK* promoter and the six homeobox 5 (*SIX5*) enhancer, affecting chromatin dynamics [20]. Several studies have found aberrant DNA methylation profiles in CTCF1 and CTCF2 regions in DM1, but they do not reach consensus [20–30]. The effect of aberrant DNA methylation profiles in the CTCF1 region on clinical phenotype is still largely unknown. In a previous study, Yanovsky-Dagan and collaborators identified a new differentially methylated region in DM1-affected human embryonic stem cell lines, at the beginning of CpGi 374, 900 bp upstream of the CTG expansion, which corresponded to a SIX5 regulatory element within the *DMPK* coding sequence [30]. This finding showed the importance of DNA methylation changes inside the *DMPK* gene body (not only in the regions closest to the CTG expansion, containing the CTCF binding sites), and raises an interest for the study of the epigenetic state of the other CpG islands located at the *DMPK* gene in DM1.

The *DMPK* locus harbours three more CpG islands, one in the neighbouring myotonic dystrophy WD repeat containing *(DMWD)* gene, CpGi 74, and two in the *DMPK* gene, namely CpGi 43 and 36; however, nothing is known about the epigenetic state of these CpG islands in DM1. To date, only one publication has looked at the entire *DMPK* locus and this was solely done in control tissues and cell cultures [31]. Interestingly, they described muscle-associated DNA hyper- and hypomethylation in the *DMPK* gene neighbourhood, in regions containing CpGi 43 and CpGi 74, respectively. Furthermore, CpGi 43 overlaps with a proposed alternative *DMPK* promoter, which could be tissue-specific and epigenetically regulated. Therefore, the main goal of this study was to elucidate the DNA methylation profiles across the four CpG islands residing in the *DMPK* locus in distinct DM1 tissues and tissue-derived cells across the different clinical phenotypes. Our results showed a CTCF1 DNA methylation gradient in blood of the developmental cases and CTCF1 methylation correlated to disease severity and CTG expansion size. Methylated cases showed a higher chance of maternal transmission and CTCF1 methylation in the parent was associated with a contraction of the CTG expansion upon generational transmission. Notably, DM1 patient-derived cells preserved the DNA methylation profiles observed in tissues. Finally, our results showed a DM1 muscle-specific epigenetic landscape, with a loss of methylation at CpGi 43, a region containing an alternative *DMPK* promoter, accompanied by a gain of methylation in the CTCF1 region in muscle and muscle-derived cells. Altogether, our results offer novel insights into the epigenetic changes in DM1.

2. Materials and Methods

2.1. Patient Registry

This study was approved by the Ethics Committee of the University Hospital Germans Trias i Pujol and was performed in accordance with the Declaration of Helsinki for Human Research. Written informed consent was obtained for all participants. The study included 65 DM1 patients and 8 controls with no previous family history of neuromuscular disorders (recruited from the traumatology department in whom surgery was needed). DM1 diagnosis was confirmed or discarded with triplet primed-PCR in all the study participants. Clinical information of DM1 patients was obtained from the medical records and updated in the last visit by neurologists. Patients were subdivided into five different categories based on age of onset: congenital = first year of life, childhood = 1–10 years, juvenile = 11–20 years, adult = 21–40 years, late-onset > 40 years. Additionally, a group of asymptomatic patients was added. For three patients the exact year of age of onset could

not be determined, but based on the clinical information all three were classified as adults. Clinical information included family history, and details on the last ophthalmological, cardiological and respiratory examination by the corresponding specialists, including the electrocardiograms, echocardiograms and spirometry tests performed in the last year. A full neurological work-up was performed by neurologists, including the presence of myotonia, ptosis, axial and facial weakness, muscle strength with the manual Medical Research Council (MRC) scale, and muscle impairment by the Muscular Impairment Rating scale (MIRS). In addition, the presence of cataracts, alopecia, intestinal problems, and sleep disturbances were catalogued and the functional status and degree of disability were evaluated using the DM1-Activ questionnaire and modified Rankin Scale (mRS), respectively.

2.2. Tissue and Cell Culture

A total of three different samples from patients and controls were obtained: blood, muscle biopsy, and skin biopsy. Blood was obtained from all patients and lymphoblastoids were isolated when possible. From a subset of patients and controls, an additional muscle (biceps brachialis or vastus lateralis) and skin biopsy were taken, of which muscle and skin-derived cell cultures were obtained. Of note, to increase the number of biopsies, a subset of biopsies for which no blood was available were included. They included three extra patients and two controls. All samples were obtained at the same time and processed as described previously by Ballester-López and collaborators [32]. Cell isolation and subsequent culturing was performed as previously described by Koehorst and collaborators [33].

2.3. DNA Isolation

Genomic DNA was isolated from peripheral blood by the use of the QIAamp DNA mini kit (Qiagen, Hilden, Germany), the PureLink genomic DNA mini kit (Thermo Fisher Scientific, Waltham, MA, USA) or a simple salting procedure, as previously described by Miller and collaborators [34]. Genomic DNA from muscle and skin tissue was extracted as previously described by Ballester-López and collaborators [32].

2.4. CTG Expansion Size Analysis

To estimate the length of the expanded progenitor allele, a specific long PCR with digested DNA, followed by a Southern Blot was carried out. First, 250 ng DNA was digested with EcoR I (New England Biolabs, Ipswich, MA, USA), according to the manufacturer's protocol. Then, 750 pg of digested DNA was used in the subsequent PCR, with the Expand Long Template PCR System (Roche, Basel, Switzerland) and primers DM-C and DM-DR (Table S1), according to the manufacturer's guidelines, supplemented with 2% DMSO. The following thermocycler conditions were used: initial 3 min at 96 °C, followed by 28 cycles of 15 s 96 °C, 45 s 63.5 °C, 5 min 68 °C, and a final extension step of 1 min 63.5 °C and 7 min 68 °C. DNA fragments were resolved by electrophoresis on a 1% agarose gel. The gel was run for an initial 10 min at 200 V, followed by ±19 h at 27 V and blotted onto a positively charged nylon membrane (Roche, Basel, Switzerland). The membrane was hybridized with a digoxigenin labelled seven CAG LNA probe overnight and detected by chemiluminescence using the anti-Dig-CDP-Star system (Roche, Basel, Switzerland). Two CTG expansion sizes were estimated through comparison against the molecular weight ladder using GelAnalyzer 19.1 software (www.gelanalyzer.com, by Istvan Lazar Jr. and Istvan Lazar Sr., accessed on 16 February 2022). The CTG size of the progenitor (ePAL), which is the lowest range of band thought to originate from the transmitting parent, and the modal allele, which shows the densest collection of CTG sizes and thought to be the most representative size for the patient at that specific time.

2.5. Bisulphite Treatment and Sanger Sequencing of Four CpG Islands

The methylation status of four annotated CpG islands (CpGi) in the *DMPK* locus, divided into five individual areas, was studied by using bisulphite treatment and subsequent Sanger sequencing. For CpGi 74, CpGi 43 and CpGi 36, 19, 15 and 17 CpGs were studied

respectively (Figure S1A–C for detailed location). In the CPGi 374, two separate regions were studied, namely CTCF1 and CTCF2, which surround the CTG expansion and each hold a CTCF binding site. For CTCF1, 25 CpGs were studied and for CTCF2, 11 CpGs were studied (Figure S1D,E for detailed information).

A total of 200–400 ng of DNA was bisulphite treated using the EZ DNA Methylation Gold kit (Zymo Research, Irvine, CA, USA), according to the manufacturer's guidelines. Bisulphite-treated DNA was amplified using nested and hemi-nested PCR for the CTCF1 and CTCF2 region, located in the CpGi 374 surrounding the CTG expansion, previously described by Barbé and collaborators [21], with some minor modifications. Here we used the TaKaRa Taq DNA polymerase (TaKaRa Bio Inc., Kioto, Japan) on a Mastercycler nexus X2 thermocycler, primer combinations and thermocycler settings are listed in Table S1. Additionally, three regions further upstream of the CTG repeat were analysed, namely the CpGi 36, CpGi 43 and CpGi 74 regions, in a similar fashion, using different primer combinations and thermocycler settings (Table S1).

Amplicons were purified using Illustra™ ExoProStar 1-Step (Merck, Darmstadt, Germany), according to the manufacturer's protocol. This was followed by sequencing using the BigDye Terminator v3.1 cycle sequencing kit (Thermo Fisher Scientific, Waltham, MA, USA), following the manufacturer's guidelines. Afterwards, amplicons were run on an ABI Prism 3130 Genetic Analyzer (Applied Biosystems, Waltham, MA, USA) and analysed using Chromas software version 2.6.6 or FinchTV software version 1.5.0, as detailed in Carrió et al. 2016 [35]. Sodium bisulphite sequencing data were represented with the Methylation Plotter web tool [36]. A CpG island was considered methylated when the majority of CpGs studied for that particular island (>50%) showed ≥10% methylation.

2.6. Statistical Analysis

Dichotomous variable CTCF1 methylation status, the occurrence of abnormal methylation upstream of the repeat, was modelled as a dependent variable using a logistic regression model, against the independent variable ePAL and modal allele. The program used was SPSS 28.0.0.0 and the significance level was set at 0.05.

3. Results

3.1. A Study Cohort Encompassing All Clinical Subtypes of DM1

For this study, DM1 patients from six different subcategories were included. The first five categories are the different established clinical phenotypes: congenital, childhood, juvenile, adult and late-onset. The sixth category is a special subset of patients, which are known to carry the CTG expansion, but are as of yet asymptomatic. Congenital ($n = 6$), childhood ($n = 6$) and juvenile ($n = 23$) will also be referred to as the developmental cases, whereas adult ($n = 22$), late onset ($n = 6$) and asymptomatic ($n = 2$) will be referred to as the non-developmental cases. Age of onset ranged from first year of life until 67 years, with a mean of seven years for childhood, 15 years for juvenile, 31 years for adult and 52 years for late-onset. The presence of seven families was identified in this cohort. In 59 out of 65 patients, the CTG expansion could be sized, ranging from 115 to 1011 CTG repeats. Detailed information on the clinical phenotypes can be found in Table 2.

Table 2. Clinical characteristics cohort.

Clinical Subtype	*n* Patients	Age of Onset (Years)	Age at Sampling (Years)	Inheritance Maternal	Gender (Male)	ePAL (CTGs)	Myotonia	Biceps MRC Scale	MIRS	Cardiac Involvement	NVM	Cataracts	mRS
Congenital	6	At birth	12.83 ± 5.43	(6/6)	(4/6)	610 (222–1011)	(2/6)	4.25 (3–5)	3.80 (3–5)	(1/6)	(2/6)	(0/6)	3.60 (2–5)
Childhood	6	6.83 ± 2.99	41.83 ± 12.04	(2/6)	(5/6)	549 (296–796)	(6/6)	4.17 (3–5)	3.33 (2–4)	(4/6)	(4/6)	(3/6)	3.33 (2–4)
Juvenile	23	15.05 ± 2.50	27.09 ± 12.54	(7/23)	(11/22)	317 (189–642)	(23/23)	4.87 (4–5)	2.30 (1–4)	(6/23)	(6/23)	(3/23)	1.48 (1–3)
Adult	22	31.50 ± 4.50	49.00 ± 9.33	(4/13)	(6/22)	290 (115–628)	(21/21)	4.86 (4–5)	2.57 (1–4)	(7/21)	(7/21)	(8/21)	1.62 (0–4)
Late Onset	6	52.17 ±7.99	61.33 ± 10.23	(0/4)	(5/6)	332 (131–911)	(3/5)	5.00 (5–5)	2.40 (1–4)	(5/5)	(1/5)	(5/5)	2.00 (0–4)
Asymptomatic	2	N/A	30.00 ± 22.63	(0/2)	(2/2)	238 [a]	(0/2)	5.00 (5–5)	1 (1–1)	(0/2)	(0/2)	(0/2)	0 (0–0)

[a] CTG size of only one of the two patients available. Age of onset and sampling is given as mean ± SD; MRC scale, MIRS scale, mRS scale and ePAL are given as mean (range); Abbreviations: MRC = Medical Research Council; MIRS = Muscular Impairment Rating Scale; NVM = nocturnal mechanical ventilation; mRS = modified Rankin Scale; ePAL = estimated progenitor CTG size. N/A = not applicable.

Table 3. Clinical characteristics of childhood cases.

Patient	Methyl CTCF1/2	Age of Onset (Years)	Age at Sampling (Years)	Gender	ePAL (CTGs)	Myotonia	Facial Weakness	Axial Weakness	Limb Weakness	MIRS	Cardiac Involvement	NVM	CNS Involvement	Hyperso-mnolence	Cataracts	mRS	DM1-ACTIV
P7	yes/no	6	56	male	756	yes	moderate	moderate	severe distal	4	pacemaker	yes	Moderate learning disability	yes	yes	4	9
P8	no/no	7	43	male	296	yes	mild	mild	mild distal	3	no	yes	no	no	no	2	25
P9	no/no	2	20	male	476	yes	moderate	mild	mild distal	2	1°AV block	no	moderate learning disability	no	no	4	22
P10	yes/no	6	40	female	324	yes	severe	moderate	mild distal	3	no	no	severe cognitive delay	yes	yes	3	14
P11	no/no	10	44	male	644	yes	mild	moderate	mild proximal + distal	4	1°AV block	yes	no	no	yes	3	38
P12	yes/no	10	48	male	796	yes	moderate	moderate	severe proximal + distal	4	pacemaker	yes	severe cognitive delay	yes	no	4	14

Abbreviations: Methyl CTCF1/2 = methylated at the CTCF1 and CTCF2 site; ePAL = estimated progenitor allele size; AV = atrioventricular; MIRS = Muscular Impairment Rating Scale mRS = modified Rankin Scale; NMV = nocturnal mechanical ventilation; CNS = central nervous system.

3.2. DNA Methylation Profiles across the DMPK Locus in Blood

This study aimed to elucidate the DNA methylation profiles across the four CpG islands residing in the *DMPK* locus in distinct DM1 patient samples and derived primary cell cultures. The four CpGis were divided into five distinct regions: CpGi 74, CpGi 43, CpGi 36, CTCF1 and CTCF2. The latter two reside in the same CpG island and refer to the two regions that contain a CTCF binding site and also encompass the CTG expansion (Figure 1A). In blood samples, for the first three CpGis, no differences in DNA methylation levels across the six phenotypes and the controls were observed. CpGi 74 and CpGi 36 showed high levels of methylation (90–100%) across the 19 and 17 CpGs studied, respectively (Figure 1B and Tables S2 and S4), meanwhile CpGi 43 showed no methylation across the 15 CpG sites studied (Figure 1B and Table S3). For the CTCF1 region upstream of the CTG repeat, 25 CpG sites were studied and increased levels of methylation were observed almost exclusively in the developmental cases, with 100% of the congenital cases, 50% of the childhood cases and 13% of the juvenile cases (Figure 1C and Table S5). No methylation was found in the non-developmental cases and the controls, except for one adult case out of 30 (P50). The two CpGs (CpG 18 and 19) that reside inside the proposed CTCF1 binding site were both highly methylated in the methylated cases. Regarding the CTCF2 region found downstream of the CTG repeat, eleven CTG sites were studied and fifty percent of the CTCF1 methylated cases also showed methylation in the CTCF2 region (Figure 1C and Table S6). No CTCF2 methylation was found in cases that were not methylated in CTCF1. CpG 5 resides in the CTCF2 binding site and it was partially methylated in the found methylated cases. Interestingly, for one of the congenital cases (P1), we obtained another blood sample from a five-year follow-up. The methylation pattern that this patient showed in the CTCF1 region was preserved after five years, whereas CTCF2 remained unmethylated (Tables S5 and S6, annotated as P1 and P1–2).

3.3. Aberrant DNA Methylation Profiles of CTCF1 Associated with Higher Disease Severity in Childhood Cases

Since the methylation profiles showed exclusive methylation in the CTCF1 region of the developmental cases, we reviewed their clinical phenotypes in-depth to see whether this aberrant methylation profile is associated with a differential disease severity. The congenital cases all showed high methylation and no clinical phenotype distinction based on DNA methylation status could be made (detailed clinical information in Table S7). Our focus was therefore on the childhood and juvenile cases. In the group of childhood-onset DM1, three out of six patients showed methylation (detailed clinical information in Table 3). One case with methylation was female; all the other childhood cases were male. Age of onset was on average 6.83 years old, but the age at sampling was a few decades later with a mean of 41.83 years.

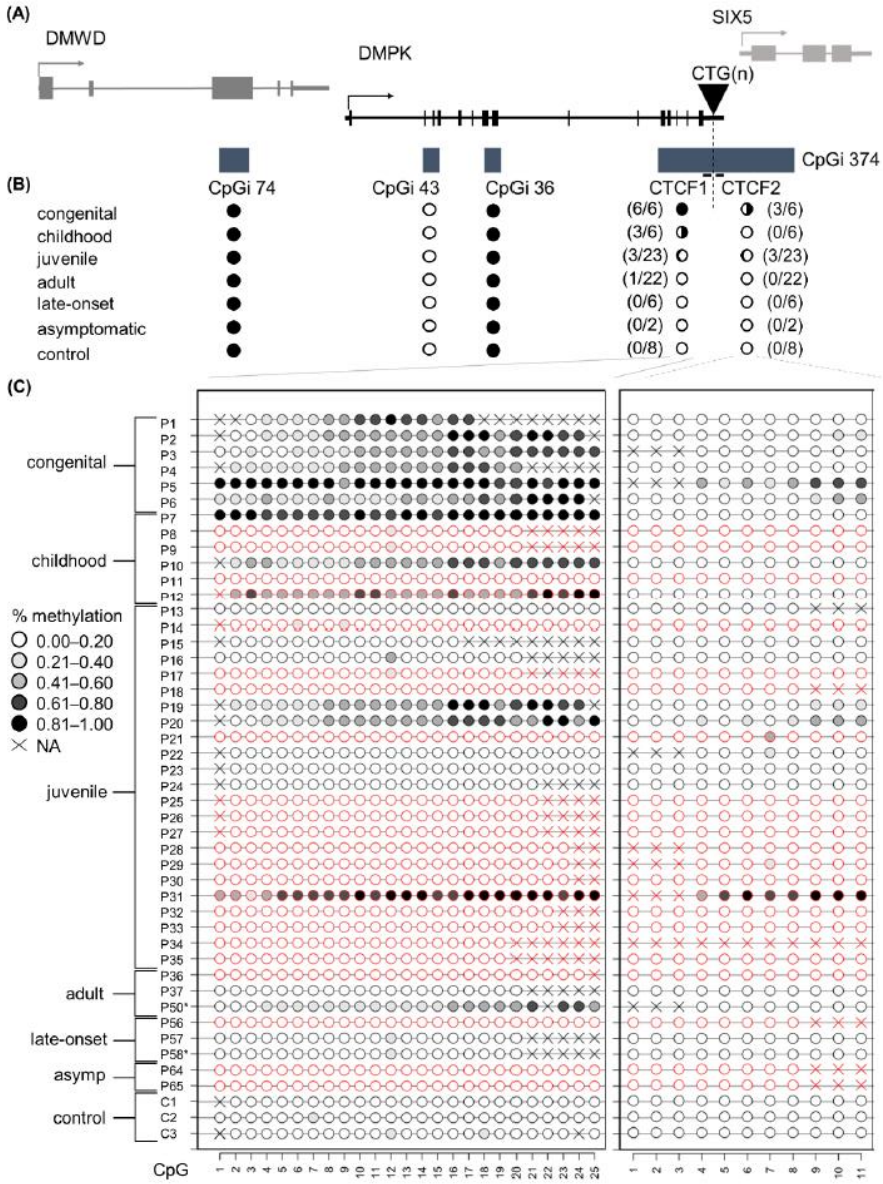

Figure 1. DNA methylation profile at the *DMPK* locus in DM1 blood samples representing all clinical subtypes. (A) Schematic representation of the four CpGis residing in the *DMPK* locus and neighboring genes. CpGi 374 is divided into the CTCF1 and CTCF2 region, harboring the CTCF binding sites and encompassing the CTG expansion. (B) Summary of the methylation profiles of the five CpG regions across the *DMPK* locus in the studied clinical subtypes, in which black indicates the degree of methylation. Congenital $n = 6$, Childhood $n = 6$, Juvenile $n = 23$, Adult $n = 22$, Late onset $n = 6$, asymptomatic $n = 2$, Controls $n = 8$. (C) Detailed DNA methylation profiles of the clinical subtypes

in the CTCF1 and CTCF 2 regions. Each circle represents a CpG dinucleotide. The colour gradient represents the level of methylation indicated in the legend assessed by sodium bisulphite sequencing. Red indicates paternal inheritance. Black indicates maternal inheritance. * means unknown inheritance. For the non-developmental cases, only a representative subset of three samples is displayed. Detailed methylation profiles of all patients in all categories can be found in the supplemental tables. Abbreviations: DMWD = dystrophia myotonica WD repeat-containing gene, *DMPK* = myotonic dystrophy protein kinase gene, SIX5 = six homeobox 5 gene, CTG(n) = the CTG expansion, CpGi = CpG island, Asymp = asymptomatic, C = control, P = DM1 patient.

At the time of revision, all patients showed muscle weakness and myotonia, but the muscular symptoms seemed to be more significant in the methylated group. Two out of three of the methylated patients experienced cramps and myalgia, while just one non-methylated patient suffered this symptom. All six patients had the characteristic facial dysmorphia and ptosis. The ptosis seemed to be more pronounced in the methylated patients: two of the patients had a severe ptosis covering the pupil and the last one had a moderate ptosis covering part of the pupil. In the non-methylated group, just one patient had a moderate ptosis, while the other two had a mild ptosis. Facial weakness was also present in all childhood-onset-DM1 patients, being severe in 1/3 and moderate in 2/3 of the methylated patients; whereas the non-methylated group showed only mild (two patients) and moderate facial weakness (one patient). Dysarthria was present in all patients, but to a higher degree in methylated patients, where it ranged from moderate to severe, compared to mild to moderate in non-methylated patients. Axial and limb weakness was also more pronounced in the methylated versus the non-methylated group. In the methylated cases, 2/3 had a severe limb weakness (MRC scale of 1–2): one of the patients had a proximal and distal weakness, requiring a wheelchair and the other patient showed a proximal and distal weakness pattern needing just a cane for walking. The last one of the methylated childhood cases had a mild distal weakness (MRC scale 3–4). In the non-methylated group, all of the patients showed a mild weakness (MRC of 3–4), two of the patients with a distal pattern and one patient with proximal/distal weakness.

Cardiac manifestations were more severe in the methylated group, as 2/3 patients had a pacemaker, whereas in the case of the non-methylated group only mild changes in electrocardiogram were seen, such as a mild first grade AV block in 2/3 cases. Two of the methylated patients and one of the non-methylated patients used ventilatory support. Cognitive manifestations were noticed in all methylated childhood DM1 patients: two of the patients had severe cognitive delay, while moderate learning difficulty was observed in the third patient. In the non-methylated group, just one patient had learning difficulties, while the others showed no mental disabilities. All methylated patients experienced hypersomnolence and none of the non-methylated patients suffered this symptom. Intestinal rhythm dysfunction was found exclusively in the methylated patients, while alopecia was found in the non-methylated patients only.

At the time of revision, all patients had some degree of dependence in the mRS. In the methylated group, 2/3 needed help in the basic activities of daily life but did not require continuous supervision (mRS 4), while the other one required help for instrumental activities (mRS 3). The average score in the DM1-ACTIV scale was 12.33. In the non-methylated group, we found one patient with mRS 4, another one with mRS 3 and the last one had a milder dependence (mRS 2) and the average score in the DM1-ACTIV scale was 28.33, which means they were better at performing daily and social activities. Considering all this data as a whole, there seemed to be a more severe muscular, cardiac, and cognitive manifestation of the disease in the methylated childhood cases.

Upon revision of the juvenile cases, no such differences in muscular, cardiac and cognitive manifestation could be found between the methylated ($n = 3$) and non-methylated group ($n = 20$). Although, this might be due to the low number of cases, and analysis of a larger cohort of this DM1 subcategory would be needed to address the impact of CTCF1 methylation on this clinical subtype (detailed information in Table S8).

3.4. A Higher Chance of Methylation in CTCF1 with Increasing CTG Expansion Size

As mentioned before, methylation of the CTCF1 region is almost exclusively found in the developmental subtypes. These subtypes are associated with a higher disease severity and overall greater CTG expansion sizes. To see whether methylation status in DM1 patients is associated with the CTG expansion size, we performed a logistic regression on the entire cohort using the ePAL and modal allele. This revealed a positive association between ePAL and methylation status of the CTCF1 region in DM1 patients (Table S9, model 1, $p = 0.004$) and between the modal allele and the methylation status (Table S9, model 2, $p = 0.001$), which suggests that the larger the ePAL/modal, the more likely methylation at the CTCF1 regions is going to occur.

3.5. Increased, but Not Exclusive, Maternal Transmission in CTCF1 Methylated Cases

It has been reported that the methylation observed in DM1 cases is associated with maternal transmission. We therefore decided to evaluate, where possible, the transmission in this DM1 cohort (Figure 1C). We found that all congenital cases, which were all hypermethylated, were maternally transmitted. In both childhood and juvenile cases, two out of the three methylated cases in each category were maternally transmitted. For the childhood subcategory as a whole, a total of two maternal transmissions were registered, meaning that all maternally transmitted cases reside in the methylated group. However, for the juvenile subcategory, a total of seven patients were maternally transmitted, of which only two reside in the methylated group. Taken together, we could corroborate a higher chance of maternal transmission when methylated, but notably there were patients that were methylated and paternally transmitted.

3.6. Methylation Status Is Not Inheritable and Associated with the Transmission of CTG Repeat Contractions

This study cohort included seven families, giving us the opportunity to study the inheritance of the differential DNA methylation profiles shown in CTCF1 and CTCF2 (pedigrees in Figure 2). Of five out of six congenital cases, the mother was included in the study cohort as well. Only one of the mothers showed methylation at both the CTCF1 and CTCF2 region, whereas the other four were unmethylated. This methylated mother belonged to the juvenile subtype. For the childhood subset, only one family could be studied, where both the childhood case and the adult-onset father were unmethylated. For the juvenile subset, one family consisting of two siblings with both juvenile onsets could be studied. These two siblings were both methylated at the CTCF1 and CTCF2 regions and interestingly the mother was the only adult methylated case in our cohort, showing only CTCF1 methylation. Of note, when reviewing the CTG expansion sizes, the unmethylated mothers passed on an expansion of the CTG repeat, whereas the methylated mothers transmitted a contraction of the CTG repeat.

3.7. DNA Methylation Profiles Are Preserved in Blood-Derived Cells

To see whether lymphoblastoids preserve the epigenetic landscape and can be used as a faithful DM1 cellular model, we decided to study whether the DNA methylation profiles are similar between blood and the blood-derived lymphoblastoids (Figure 3). CpGi 74, CpGi 43 and CpGi 36 showed no differences between blood and lymphoblastoids across all clinical subtypes (Figure 3A and Tables S10–S12). Both CpGi 74 and CpGi 36 remained completely highly methylated regions, whereas CpGi 43 was totally unmethylated. For CTCF1, the pattern observed in blood, a gradient of methylation in the developmental cases was preserved in all the studied lymphoblastoids (Figure 3B), except for P7, which showed methylation in blood, but not in lymphoblastoid cells in CTCF1 (Table S13). Regarding CTCF2, the patients that displayed methylation of the CTCF2 region in blood, preserved their methylation status in the studied lymphoblastoids (Figure 3B and Table S14). However, two patients that were not methylated in blood for CTCF2 (P4 and P10) showed low-grade methylation in lymphoblastoids (~10% methylation) (Table S14).

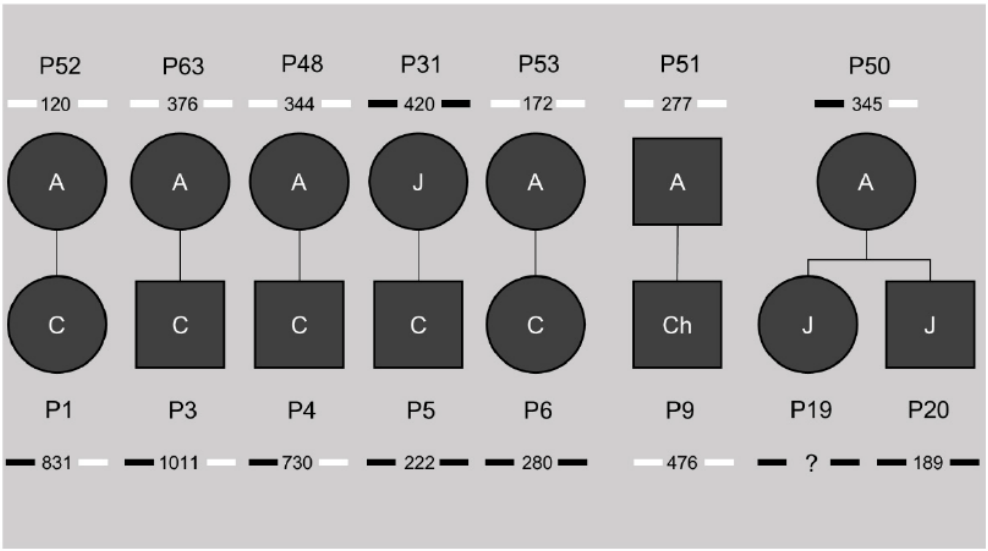

Figure 2. Pedigrees of the known families in our study cohort. The number beneath the patient identification code indicates the ePAL (estimated progenitor allele size), with the bars next to it indicating methylation status of CTCF1 (left) and CTCF2 (right). Black indicates methylation, white no methylation. A = adult, J = juvenile, Ch = childhood, C = congenital. ? = unknown CTG expansion size.

3.8. DM1 Is Associated with Hypomethylation of CpGi 43 in Muscle Tissue and Muscle-Derived Cells

Next, we wanted to study the DNA methylation profiles of the five regions in tissues other than blood to address whether tissue-specific epigenetics at the *DMPK* locus exists in DM1. For this, we acquired a muscle and skin biopsy from a subset of patients (juvenile, adult and late-onset origin). From these biopsies, cells were isolated to assess whether cellular models accurately reflect the origin tissue in terms of DNA methylation status. In CpGi 74 and CpGi 36, high DNA methylation levels were found in skin and muscle of both DM1 patients and controls, similar to what was found in blood (Figure 4A,B). Additionally, the tissue-derived cells of both muscle and skin preserved the observed methylation (Tables S15–S18). Regarding CpGi 43, skin samples and skin-derived cells showed no methylation in the DM1 patients and controls, similar to the observations in blood, with the exception of one patient and one control in skin fibroblasts (Figure 4C, Table S19). Interestingly, a distinct DNA methylation pattern was observed in muscle tissue, with overall high methylation in control samples, which was much lower in DM1 muscles, showing reductions as high as 70% in some CpGs (Figure 4C,D and Table S20). This muscle-specific DNA methylation profile was preserved in both control- and patient-derived myoblasts and myotubes (Figure 4D and Table S20). Interestingly, DM1 myoblasts or myogenic precursor cells showed the biggest DNA demethylation compared to controls.

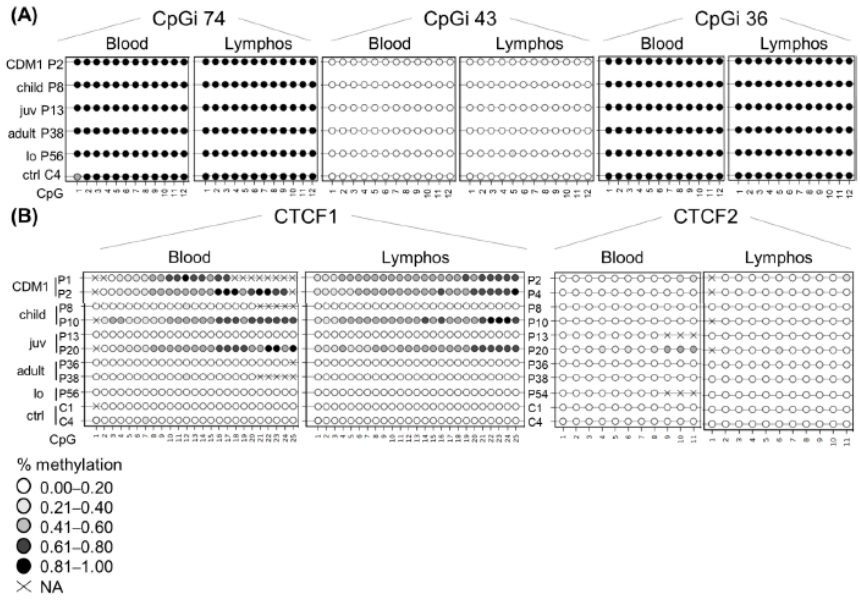

Figure 3. DNA methylation profile is preserved at the *DMPK* locus in patient-derived lymphoblastoids. Comparison of the DNA methylation profile between blood and lymphoblastoid cell lines of the same individual across the five annotated CpG regions: (A) CpGi 74, 43 and 36. (B) CTCF1 and CTCF2. Each circle represents a CpG dinucleotide. The colour gradient represents the level of methylation indicated in the legend assessed by sodium bisulphite sequencing. Abbreviations: C = control, P = DM1 patient; CDM1 = congenital, child = childhood, juv = juvenile, lo = late-onset, ctrl = controls, lymphos = lymphoblastoids.

3.9. DM1 Is Associated with Hypermethylation in CTCF1 in Muscle Tissue and Muscle Derived Cells

The CTCF1 region showed similar DNA methylation profiles in skin and skin-derived cells compared to blood (Figure 5A and Table S21). However, one DM1 skin fibroblast sample showed low-grade methylation (average of around 10%), but none in controls (Table S21). Due to difficulties with the sequencing analysis, only in one patient could both the skin and the skin-derived fibroblasts be analysed. For the other samples, we analysed DM1 skin fibroblasts that were not derived from the analysed skin biopsies; therefore, we cannot rule out the possibility that this sample already showed a partial methylation, especially since it is a juvenile sample. Interestingly, six out of seven DM1 muscle biopsies showed hypermethylation compared to controls, with half of the samples showing a gain of methylation in at least 50% of analysed CpGs (Figure 5B and Table S22). Notably, the highest methylation average was found in the youngest biopsy, belonging to a juvenile case. Of these biopsies, we have the CTG expansion size available in muscle and blood (Table S23). However, CTG expansion size could not be linked to the degree of methylation. Surprisingly, the two CpGs residing in the CTCF1 binding site (CpG 18 and 19) were not methylated in these biopsies, with the exception of CpG 18 in the biopsy of P68. Total unmethylation in all CpGs was observed in the control biopsies. This methylation profile was maintained in the muscle-derived cells (Figure 5C and Table S22). Of note, the differences in myogenic precursor cells between patients and controls were the highest (Figure 5C). The last analysed region, CTCF2, showed no methylation in the tissues and tissue-derived cells

studied from the patients of which we have the biopsies (Tables S24 and S25), suggesting that muscle-specific hypermethylation only happens in the CTCF1 region.

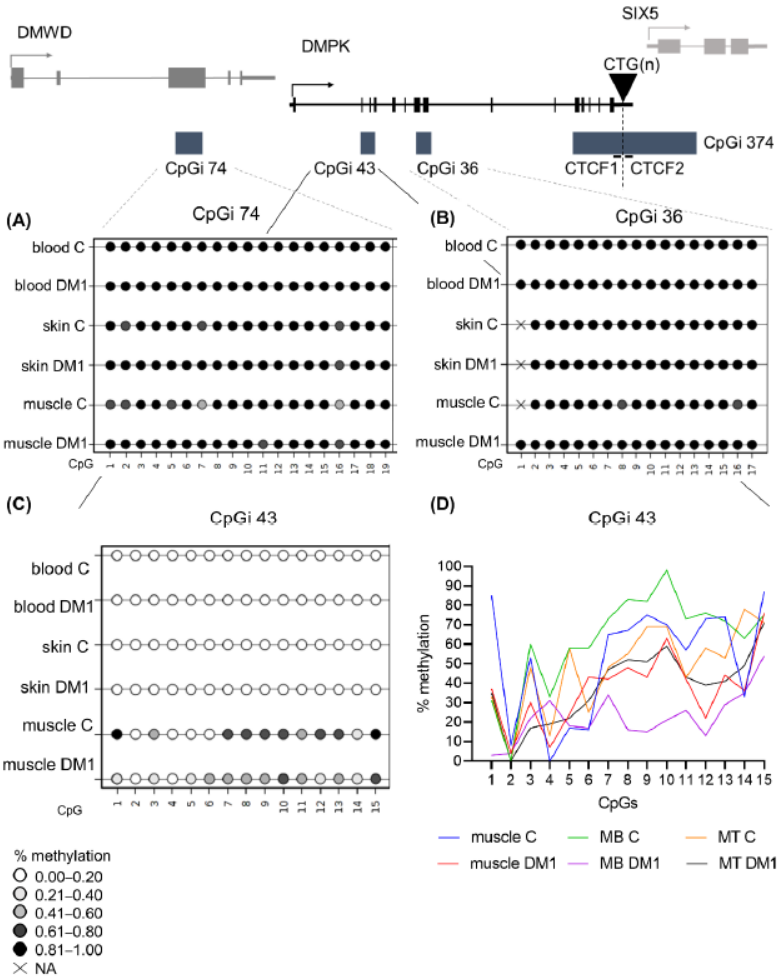

Figure 4. DNA methylation profile at CpGi 43 showed specific hypomethylation in DM1 muscle tissue and muscle-derived cells. (A–C) Averages of DNA methylation profiles across the three studied tissues, blood, skin and muscle, in patients versus controls for CpGi 74 (A), for CpGi 36 (B) and CpGi 43 (C). Included patients are from the juvenile, adult and late onset clinical category (n = 5 for blood, n = 3 for skin, n = 7 for muscle and n = 4 for controls). Each circle represents a CpG dinucleotide. The colour gradient represents the level of methylation indicated in the legend assessed by sodium bisulphite sequencing. (D) Representation of the DNA methylation profiles of muscle and muscle-derived cells (myoblasts and myotubes) in CpGi 43 assessed by bisulphite sequencing.

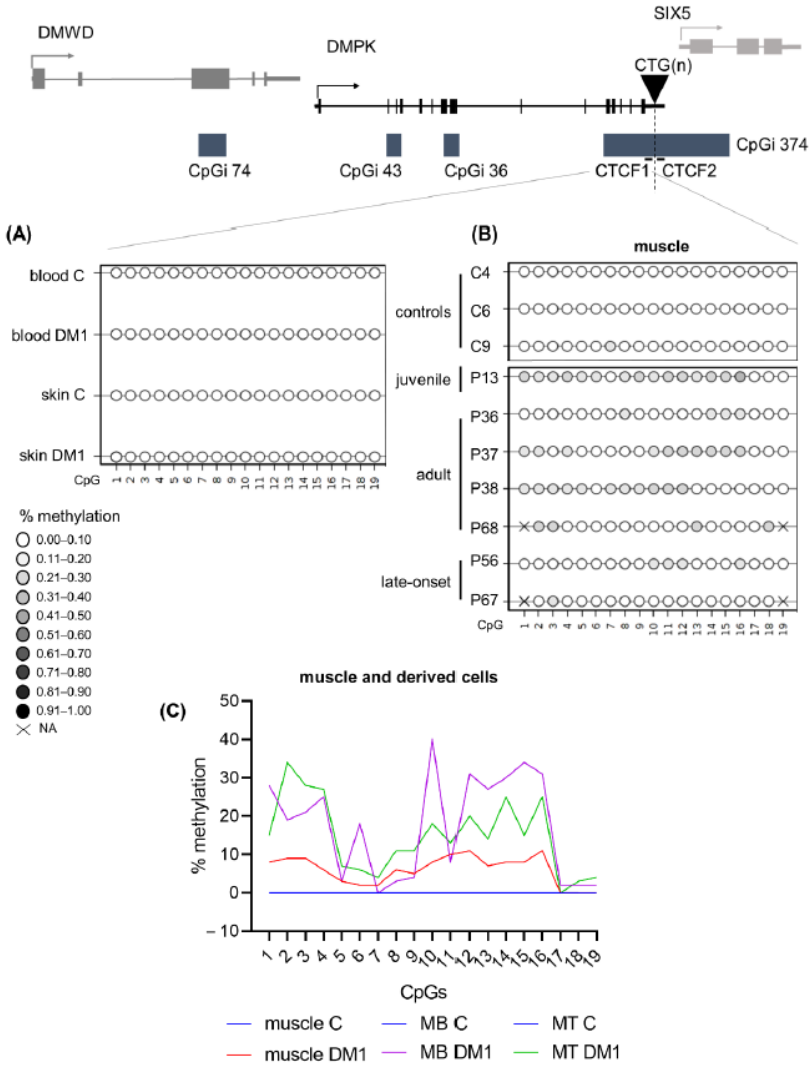

Figure 5. DNA methylation profiles at the CTCF1 regions were tissue-specific and increased in DM1 muscle samples. (A) Averages of DNA methylation profiles across blood and skin in patients versus controls for CTCF1. Included patients are from the juvenile, adult and late onset clinical category (n = 5 for blood, n = 3 for skin and n = 4 for controls). (B) Overview of the muscle biopsy DNA methylation profiles of DM1 patients and controls. Each circle represents a CpG dinucleotide. The color gradient represents the level of methylation indicated in the legend assessed by sodium bisulfite sequencing. (C) Representation of the DNA methylation profiles of muscle and muscle-derived cells (myoblasts and myotubes) in CTCF1. For CTCF1 all control muscle cells are at zero and have been given the same color to aid visualization.

4. Discussion

The overall goal of this study was to investigate the contribution of epigenetics to DM1 pathology, by analysing for the first time the DNA methylation profiles across the

four CpG islands residing in the *DMPK* locus in several tissues and tissue-derived cells in all clinical subtypes of DM1. Our results showed a distinct DNA methylation profile across DM1 tissues and uncovered a novel and dual epigenetic signature in DM1 muscle samples, involving a gain of DNA methylation in the flanking region of the CTG expansion accompanied by specific DNA demethylation in the *DMPK* gene body (Figure 6).

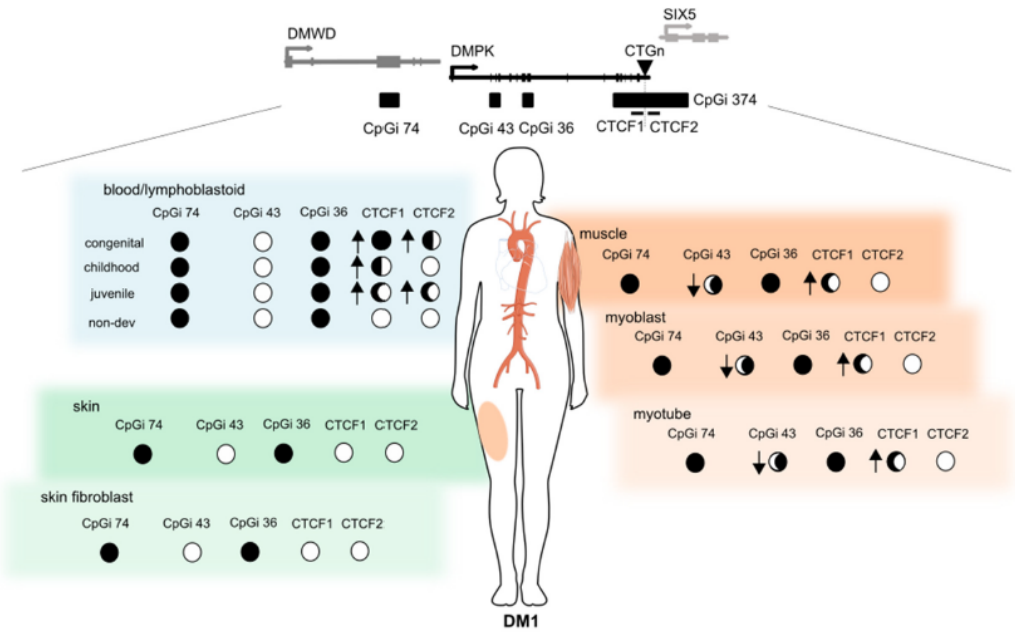

Figure 6. Summary of the epigenetic landscape of the *DMPK* locus in DM1. An overview is given of the methylation status across the *DMPK* locus in muscle, skin and blood and their derived cells in DM1 patients. The circle underneath each CpG island represents its methylation status, ranging from fully methylated (black) to completely unmethylated (white) in DM1 patients. The arrows indicate the changes compared to controls, where an upward arrow means increased methylation in DM1 compared to controls. This figure was partially made using Servier Medical Art (smart.servier.com, accessed on 31 March 2022).

Previously, it was reported that in leukocytes derived from control individuals, CpGi 36 and 74 (located in the *DMPK* and *DMWD* gene bodies, respectively) were highly methylated, while CpGi 43 (located in *DMPK* gene body and overlapping with a proposed alternative promoter) was unmethylated [31]. Our results showed that in DM1 blood samples, the DNA methylation profile of CpGi 36, 43, and 74 does not change in the distinct DM1 subtypes. Conversely, the CTCF1 and CTCF2 regions did show a change in DNA methylation levels in DM1 compared to controls. Developmental cases showed an upward gradient of methylation with increasing severity of the disease and decreasing age of onset. No methylation was observed in the non-developmental cases, except for a single adult case. Additionally, fifty percent of the CTCF1 methylated cases also showed methylation in the CTCF2 region, but interestingly, CTCF2 methylation without CTCF1 methylation was not observed in any case. This may indicate that the beginning of the aberrant DNA methylation is not random and it spreads beyond the CTG repeat only in certain cases/conditions. The mechanism behind the high methylation levels observed in the CTCF1 region and why the mechanism seems to be biased towards developmental cases are still relevant questions that need addressing in the DM1 field.

The current studies on DNA methylation profiles in the two CTCF binding regions are controversial. Nevertheless, several studies have shown a similar trend in the levels of CTCF1 methylation as we observed in our developmental cases [21,23,27,28]. Regarding the CTCF2 region, our results corroborate previous findings that CTCF2 is less methylated than the CTCF1 region [21,27,28]. Several studies have focused solely on adult cases, and have found methylation among these non-developmental cases, contradictory to our findings [24,25,37], although the methylation levels were very small in these studies. The differences found between the published works could be due to the different techniques used to assess DNA methylation levels, the different criteria used to decide what is considered methylated, and the difficulties to establish the age of onset in DM1. To better identify the DNA methylation differences in DM1 samples, a general consensus in DM1 DNA methylation studies would be needed. In our cohort we could see whether the methylation status changes over time, since we had the five-year follow-up of one of the congenital cases, where we found that the methylation status was stable, which is in concordance with previous studies [24–26].

Few studies have addressed the link between clinical phenotype and DNA methylation profiles. Due to the extensive clinical data obtained from this cohort, we had the opportunity to assess whether DNA methylation status was associated with clinical phenotype. Methylated childhood cases showed more severe muscular, cardiac, and cognitive manifestations of the disease. This type of phenotypic association in this particular disease subtype has not been made previously and the few available studies on clinical phenotype correlations are from adults. Légaré and collaborators have shown that methylation status is linked to muscular and respiratory profiles in adults [37] and Breton found a correlation between hypermethylation and a decline in cognitive function [24]. However, it has been stipulated that methylation seems to be associated with the more severe forms of the disease, as methylation is found overwhelmingly in CDM1 cases [21,27–29]. Our study supports this notion and adds the novel finding that it is also linked to the more severe cases of childhood DM1. Caution must be taken, however, as our sample size was quite low and further studies are needed to confirm this association.

Disease severity and age of onset have been previously linked to the CTG expansion size, where the more severe disease forms and earlier age of onset correlate with the greater CTG expansion sizes [38,39]. We found a positive association between two CTG size predictors and methylation status of CTCF1. This suggests that the larger the CTG expansion size, the higher the likelihood of CTCF1 methylation. This association has been found previously by several studies, both for ePAL [27] and modal allele [25,28,37]. However, not all studies were able to find such an association between CTG expansion size and the methylation status [21,23].

Our study cohort included several families, giving us the opportunity to study inheritance of the DNA methylation profiles. We found the DNA methylation status of our patients to be not inheritable, as several unmethylated mothers gave birth to methylated cases. This is in accordance with previous studies [21,27]. Interestingly, we observed that the offspring of methylated mothers carried contractions of the CTG expansion, while the offspring of unmethylated mothers carried expansions of the repeat. This suggests that although the bigger CTG expansion sizes are associated with methylation, when a methylated parent passes on the methylation status, it coincides with the transference of a smaller CTG expansion. Some authors have evaluated the effect of DNA methylation on the stability of the CTG expansion repeat [40]. When using bacterial and primate cellular models of 83 to 100 CTG repeat expansions, DNA methylation was found to be associated with a stabilization of the repeat size. However, caution must be taken with these observations, as the sample size in their study and our study was low and further studies are needed to further elucidate this observation.

We found an increased maternal transmission rate in CTCF1 methylated cases. However, this was not absolute. Barbé and collaborators have suggested the presence of a parent-of-origin effect, where DNA methylation may account for the maternal bias for CDM1 transmission, the larger maternal CTG expansions, age of onset, and clinical phe-

notype [21]. The hypothesis is based on the potentially reduced survival of spermatozoa due to the hypermethylation of the CTCF1 region, disrupting the insulator element and decreasing levels of *SIX5*, which is essential for spermatozoa survival. Although we do see a similar trend, as all our CDM1 cases are both maternally transmitted and methylated, parental inheritance might not be a good predictor for methylation status or vice versa for the other clinical phenotypes. This is strengthened by the observation made by Morales and collaborators, where a large family showed several paternally transmitted methylated cases [27]. Furthermore, a very recent study in DM1 spermatozoa found that methylation did not affect sperm viability and these spermatozoa were compatible with "in vitro" fertilization [41], which goes against the hypothesis that reduced survival is associated with methylated spermatozoa, preventing the transmission of CDM1 [3], and therefore, other explanations for this maternal bias should be explored.

Buckley and collaborators extensively studied the epigenetics in the *DMPK* locus in several control tissues and cell types. Interestingly, they reported the existence of a *DMPK* alternative promoter (also referred to as the downstream promoter, which overlaps with CpGi 43), as well as cell type-dependent differences in promoter usage, according to epigenetic features [31]. The data presented by Buckley and collaborators showed a predominant use of the canonical upstream promotor in skeletal muscle and myogenic cells from control individuals, by RNA-CAGE (cap analysis gene expression) data, supported by complete hypomethylation of this promoter and hypermethylation of the alternative downstream promoter [31]. Conversely, in blood, a predominant usage of the alternative *DMPK* promoter (in CpGi 43) was suggested, by showing its hypomethylation together with hypermethylation of the canonical promoter, strong binding of CTCF and high levels of H3K4me3 in control leukocytes [31]. Interestingly, our study of DM1 muscle samples revealed a novel epigenetic change by specific demethylation of this alternative promoter located at CpGi 43, in skeletal muscle tissue and muscle-derived cells. This could potentially alter chromatin conformation and result in a shift in the promoter usage from the strongest/canonical one to the weak/alternative promoter, decreasing *DMPK* expression levels in DM1 myogenic samples.

Additionally, this DM1 tissue-dependent demethylation was accompanied by a gain of methylation in the CTCF1, but not the CTCF2 region. Previous studies showed that CTCF, a transcription factor that can function as an insulator, binds strongly to CTCF1, but not CTCF2, in a methylation-dependent manner [20]. Importantly, the hypermethylation of the CTCF regions could inhibit CTCF-binding and disrupt the insulator element formed by the CTG expansion and the two CTCF-binding sites, affecting *DMPK* and *SIX5* expression. The loss of the insulator activity by DNA methylation would allow the interaction of the *SIX5* enhancer with the *DMPK* promoter, increasing *DMPK* expression, while reducing *SIX5* expression [20]. Notably, our results showed that in blood samples and derived-leukocytes, the CpGs located inside the CTCF1 and CTCF2 binding sites were hypermethylated in all methylated cases (almost exclusively developmental cases), while in muscle samples, these remained unmethylated (almost exclusively non-developmental cases). This may imply that although there is a disease-specific gain of methylation for the CTCF1 region in muscle, the CTCF binding site is not disrupted, allowing CTCF binding. However, this hypermethylation might affect other chromatin interactions, in turn affecting gene expression. The analysis of publicly available ChIP-seq data of histone post translational modifications (H3K4me3, H3K4me1 and H3K27ac), done by Buckley and collaborators at *DMPK* and neighbouring genes, showed that CTCF regions and intragenic regions of *DMWD* and radial spoke head 6 homolog A genes (*RSPH6A*), located next to the *DMPK* gene, displays enhancer chromatin features in control muscle cells [31]. This is interesting since *DMPK* lies in the middle of a chromosomal domain with three genes preferentially expressed in testis, indicating that its expression, mainly in skeletal muscle and heart, has to be tightly regulated. Additionally, Brouwer and collaborators showed an increase in the H3K9me3 chromatin repressive mark, together with gain of DNA methylation, in the CTCF1 region (and to a lesser extent in CTCF2) in DM1 mice hearts, which correlates

with decreased *DMPK* expression [22]. To address whether DNA methylation changes in the CTCF1 region in DM1 skeletal muscles may alter chromatin interactions between the *DMPK* promoter and these potential myogenic enhancers, further experiments are needed.

Finally, this study addressed for the first time the DNA methylation status of patient-derived DM1 cells. The availability of several DM1 tissues and their corresponding tissue-derived cells gave us the opportunity to determine that most cellular models maintained the DNA methylation state observed in the original tissue. However, in some cases, we observed a slight gain of methylation in cultured cells (e.g., some DM1 lymphoblastoids, skin fibroblasts and myoblast/myotubes) versus the corresponding tissues. This can be explained by the observation that cellular models, especially immortalized cell lines or primary cell cultures that have been in culture for a substantial amount of time, can increase DNA methylation levels [13,42,43] and/or because of the purity of cell cultures compared to tissues containing distinct cell types. Overall, our results showed that the DM1 patient-derived cells preserve the genetic and epigenetic features, which makes them excellent models to study DM1 pathology.

5. Conclusions

In conclusion, our results showed a distinct DNA methylation profile across DM1 tissues and uncovered a novel, dual epigenetic signature involving a gain of DNA methylation in the flanking region of the CTG expansion, accompanied by specific DNA demethylation in the *DMPK* gene body of DM1 muscle samples, which provided novel insights into the epigenetic changes occurring in DM1.

Supplementary Materials: The following supporting information can be downloaded at: https://www.mdpi.com/article/10.3390/biomedicines10061372/s1, Figure S1. The location of the primers and CpGs investigated in this study for the five annotated regions. Table S1. Primer combinations and thermocycler settings. Table S2. DNA methylation analysis of CpGi 74 in blood samples across the clinical DM1 subtypes. Table S3. DNA methylation analysis of CpGi 43 in blood across the DM1 clinical subtypes. Table S4. DNA methylation analysis of CpGi 36 in blood across the DM1 clinical subtypes. Table S5. DNA methylation analysis of CTCF1 in blood across the DM1 clinical subtypes. Table S6. DNA methylation analysis of CTCF2 in blood across the DM1 clinical subtypes. Table S7. Clinical characteristics of congenital cases. Table S8. Clinical characteristics of juvenile cases. Table S9. Logistic regression model ePAL/mode vs. Methylation status. Table S10. DNA methylation analysis of CpGi 74 in lymphoblastoids. Table S11. DNA methylation analysis of CpGi 43 in lymphoblastoids. Table S12. DNA methylation analysis of CpGi 36 in lymphoblastoids. Table S13. DNA methylation analysis of CTCF1 in lymphoblastoids. Table S14. DNA methylation analysis of CTCF2 in lymphoblastoids. Table S15. DNA methylation analysis of CpGi 74 in skin and skin-derived cells. Table S16. DNA methylation analysis of CpGi 74 in muscle and muscle-derived cells. Table S17. DNA methylation analysis of CpGi 36 in skin and skin-derived cells. Table S18. DNA methylation analysis of CpGi 36 in muscle and muscle-derived cells. Table S19. DNA methylation analysis of CpGi 43 in skin and skin-derived cells. Table S20. DNA methylation analysis of CpGi 43 in muscle and muscle-derived cells. Table S21. DNA methylation analysis of CTCF1 in skin and skin-derived cells. Table S22. DNA methylation analysis of CTCF1 in muscle and muscle-derived cells. Table S23. CTG expansion sizes in blood and muscle of the patients providing a muscle biopsy. Table S24. DNA methylation analysis of CTCF2 in skin and skin-derived cells. Table S25. DNA methylation analysis of CTCF2 in muscle and muscle-derived cells.

Author Contributions: Conceptualization, M.S., G.N.-G. and E.K.; methodology, E.K. and M.S.; validation, M.S. and G.N.-G.; formal analysis, E.K.; investigation, E.K., R.O., J.C., J.N.-M., I.L.-P., A.A., M.A., D.N.-d.B., V.S., A.N., C.O., M.Á.R., J.D.-M., J.A.-P., G.L., A.R.-P., A.R.-F. and A.M.-P.; visualization, E.K., M.S. and G.N.-G.; resources, M.S. and G.N.-G.; data curation, E.K., M.S. and G.N.-G. writing—original draft preparation, E.K., M.S. and G.N.-G.; writing—review and editing, E.K., M.S., G.N.-G., R.O., J.C., J.N.-M., A.A., M.A., D.N.-d.B., V.S., A.N., C.O., M.Á.R., J.D.-M., J.A.-P., G.L., A.R.-P., A.R.-F. and A.M.-P.; visualization, E.K., M.S. and G.N.-G.; supervision, M.S. and G.N.-G.; project administration, E.K., M.S., G.N.-G.; funding acquisition, M.S. and G.N.-G. All authors have read and agreed to the published version of the manuscript.

Funding: This research was funded by Instituto de Salud Carlos III (grant number PI18/00713 to G. Nogales-Gadea and A. Ramos-Fransi), Trampoline Grant (#21108) from AFM-Telethon to G. Nogales-Gadea, Ministerio de Ciencia e Innovación (grant number PID2020-118730RB-I00) and Grant Project (#23557) from AFM-Telethon to M. Suelves, and co-financed by Fondos FEDER. E. Koehorst is funded by the La Caixa Foundation (ID 100010434), fellowship code LCF/BQ/IN18/11660019, cofunded by the European Union's Horizon 2020 research and innovation program under the Marie Skłodowska-Curie grant agreement no. 713673. J. Núñez-Manchón is funded by Instituto de Salud Carlos III I-PFIS fellowship (grant number IFI20/00022). G. Nogales-Gadea is supported by a Miguel Servet research contract (ISCIII CPII19/00021, and FEDER). This work was supported by the CERCA program/Government of Catalonia. The funding bodies had no role in the design of the study and the collection, analysis, and interpretation of data.

Institutional Review Board Statement: The study was conducted according to the guidelines of the Declaration of Helsinki, and approved by the Institutional Review Board (or Ethics Committee) of Hospital Universitario Germans Trias i Pujol, protocol code PI15/01756, date of approval 27 November 2015.

Informed Consent Statement: Informed consent was obtained from all subjects involved in the study.

Acknowledgments: The authors wish to thank the DM1 patients for providing the samples needed to perform this study. We also thank the IGTP core facilities for their contribution to this publication.

Conflicts of Interest: The authors declare no conflict of interest.

References

1. Harper, P.S. *Major Problems in Neurology: Myotonic Dystrophy*, 3rd ed.; WB Saunders: London, UK, 2001.
2. De Antonio, M.; Dogan, C.; Hamroun, D.; Mati, M.; Zerrouki, S.; Eymard, B.; Katsahian, S.; Bassez, G. French Myotonic Dystrophy Clinical Network Unravelling the myotonic dystrophy type 1 clinical spectrum: A systematic registry-based study with implications for disease classification. *Rev. Neurol.* **2016**, *172*, 572–580. [CrossRef] [PubMed]
3. Lanni, S.; Pearson, C.E. Molecular genetics of congenital myotonic dystrophy. *Neurobiol. Dis.* **2019**, *132*, 104533. [CrossRef] [PubMed]
4. Campbell, C.; Sherlock, R.; Jacob, P.; Blayney, M. Congenital myotonic dystrophy: Assisted ventilation duration and outcome. *Pediatrics* **2004**, *113*, 811–816. [CrossRef] [PubMed]
5. Meola, G.; Cardani, R. Myotonic dystrophies: An update on clinical aspects, genetic, pathology, and molecular pathomechanisms. *Biochim. Biophys. Acta Mol. Basis Dis.* **2015**, *1852*, 594–606. [CrossRef] [PubMed]
6. Douniol, M.; Jacquette, A.; Cohen, D.; Bodeau, N.; Rachidi, L.; Angeard, N.; Cuisset, J.-M.; Vallée, L.; Eymard, B.; Plaza, M.; et al. Psychiatric and cognitive phenotype of childhood myotonic dystrophy type 1. *Dev. Med. Child Neurol.* **2012**, *54*, 905–911. [CrossRef]
7. Echenne, B.; Bassez, G. Congenital and infantile myotonic dystrophy. *Handb. Clin. Neurol.* **2013**, *113*, 1387–1393. [CrossRef] [PubMed]
8. Ho, G.; Carey, K.A.; Cardamone, M.; Farrar, M.A. Myotonic dystrophy type 1: Clinical manifestations in children and adolescents. *Arch. Dis. Child.* **2019**, *104*, 48–52. [CrossRef] [PubMed]
9. Mathieu, J.; Allard, P.; Potvin, L.; Prévost, C.; Bégin, P. A 10-year study of mortality in a cohort of patients with myotonic dystrophy. *Neurology* **1999**, *52*, 1658–1662. [CrossRef] [PubMed]
10. De Die-Smulders, C.E.; Höweler, C.J.; Thijs, C.; Mirandolle, J.F.; Anten, H.B.; Smeets, H.J.; Chandler, K.E.; Geraedts, J.P. Age and causes of death in adult-onset myotonic dystrophy. *Brain* **1998**, *121*, 1557–1563. [CrossRef]
11. Chen, H.; Chen, H. Myotonic Dystrophy Type 1. In *Atlas of Genetic Diagnosis and Counseling*; Springer: Cham, Switzerland, 2017; pp. 1999–2011.
12. Groh, W.J.; Groh, M.R.; Saha, C.; Kincaid, J.C.; Simmons, Z.; Ciafaloni, E.; Pourmand, R.; Otten, R.F.; Bhakta, D.; Nair, G.V.; et al. Electrocardiographic abnormalities and sudden death in myotonic dystrophy type 1. *N. Engl. J. Med.* **2008**, *358*, 2688–2697. [CrossRef] [PubMed]
13. Berger, S.L.; Kouzarides, T.; Shiekhattar, R.; Shilatifard, A. An operational definition of epigenetics. *Genes Dev.* **2009**, *23*, 781–783. [CrossRef] [PubMed]
14. Jones, P.A. Functions of DNA methylation: Islands, start sites, gene bodies and beyond. *Nat. Rev. Genet.* **2012**, *13*, 484–492. [CrossRef] [PubMed]
15. Carrió, E.; Díez-Villanueva, A.; Lois, S.; Mallona, I.; Cases, I.; Forn, M.; Peinado, M.A.; Suelves, M. Deconstruction of DNA methylation patterns during myogenesis reveals specific epigenetic events in the establishment of the skeletal muscle lineage. *Stem Cells* **2015**, *33*, 2025–2036. [CrossRef]
16. Reik, W. Stability and flexibility of epigenetic gene regulation in mammalian development. *Nature* **2007**, *447*, 425–432. [CrossRef]
17. Gardiner-Garden, M.; Frommer, M. CpG islands in vertebrate genomes. *J. Mol. Biol.* **1987**, *196*, 261–282. [CrossRef]

18. Bird, A.P. CpG-rich islands and the function of DNA methylation. *Nature* **1986**, *321*, 209–213. [CrossRef] [PubMed]
19. Deaton, A.M.; Bird, A. CpG islands and the regulation of transcription. *Genes Dev.* **2011**, *25*, 1010–1022. [CrossRef]
20. Filippova, G.N.; Thienes, C.P.; Penn, B.H.; Cho, D.H.; Hu, Y.J.; Moore, J.M.; Klesert, T.R.; Lobanenkov, V.V.; Tapscott, S.J. CTCF-binding sites flank CTG/CAG repeats and form a methylation-sensitive insulator at the DM1 locus. *Nat. Genet.* **2001**, *28*, 335–343. [CrossRef]
21. Barbé, L.; Lanni, S.; López-Castel, A.; Franck, S.; Spits, C.; Keymolen, K.; Seneca, S.; Tomé, S.; Miron, I.; Letourneau, J.; et al. CpG Methylation, a Parent-of-Origin Effect for Maternal-Biased Transmission of Congenital Myotonic Dystrophy. *Am. J. Hum. Genet.* **2017**, *100*, 488–505. [CrossRef] [PubMed]
22. Brouwer, J.R.; Huguet, A.; Nicole, A.; Munnich, A.; Gourdon, G. Transcriptionally Repressive Chromatin Remodelling and CpG Methylation in the Presence of Expanded CTG-Repeats at the DM1 Locus. *J. Nucleic Acids* **2013**, *2013*, 567435. [CrossRef]
23. Spits, C.; Seneca, S.; Hilven, P.; Liebaers, I.; Sermon, K. Methylation of the CpG sites in the myotonic dystrophy locus does not correlate with CTG expansion size or with the congenital form of the disease. *J. Med. Genet.* **2010**, *47*, 700–703. [CrossRef] [PubMed]
24. Breton, É.; Légaré, C.; Overend, G.; Guay, S.P.; Monckton, D.; Mathieu, J.; Gagnon, C.; Richer, L.; Gallais, B.; Bouchard, L. DNA methylation at the DMPK gene locus is associated with cognitive functions in myotonic dystrophy type 1. *Epigenomics* **2020**, *12*, 2051–2064. [CrossRef] [PubMed]
25. Hildonen, M.; Knak, K.L.; Dunø, M.; Vissing, J.; Tümer, Z. Stable Longitudinal Methylation Levels at the CpG Sites Flanking the CTG Repeat of DMPK in Patients with Myotonic Dystrophy Type 1. *Genes* **2020**, *11*, 936. [CrossRef] [PubMed]
26. Morales, F.; Vásquez, M.; Corrales, E.; Vindas-Smith, R.; Santamaría-Ulloa, C.; Zhang, B.; Sirito, M.; Estecio, M.R.; Krahe, R.; Monckton, D.G. Longitudinal increases in somatic mosaicism of the expanded CTG repeat in myotonic dystrophy type 1 are associated with variation in age-at-onset. *Hum. Mol. Genet.* **2020**, *29*, 2496–2507. [CrossRef] [PubMed]
27. Morales, F.; Corrales, E.; Zhang, B.; Vásquez, M.; Santamaría-Ulloa, C.; Quesada, H.; Sirito, M.; Estecio, M.R.; Monckton, D.G.; Krahe, R. Myotonic dystrophy type 1 (DM1) clinical sub-types and CTCF site methylation status flanking the CTG expansion are mutant allele length-dependent. *Hum. Mol. Genet.* **2021**, *31*, 262–274. [CrossRef]
28. Santoro, M.; Fontana, L.; Masciullo, M.; Bianchi, M.L.E.; Rossi, S.; Leoncini, E.; Novelli, G.; Botta, A.; Silvestri, G. Expansion size and presence of CCG/CTC/CGG sequence interruptions in the expanded CTG array are independently associated to hypermethylation at the DMPK locus in myotonic dystrophy type 1 (DM1). *Biochim. Biophys. Acta Mol. Basis Dis.* **2015**, *1852*, 2645–2652. [CrossRef]
29. Steinbach, P.; Gläser, D.; Vogel, W.; Wolf, M.; Schwemmle, S. The DMPK gene of severely affected myotonic dystrophy patients is hypermethylated proximal to the largely expanded CTG repeat. *Am. J. Hum. Genet.* **1998**, *62*, 278–285. [CrossRef] [PubMed]
30. Yanovsky-Dagan, S.; Avitzour, M.; Altarescu, G.; Renbaum, P.; Eldar-Geva, T.; Schonberger, O.; Mitrani-Rosenbaum, S.; Levy-Lahad, E.; Birnbaum, R.Y.; Gepstein, L.; et al. Uncovering the Role of Hypermethylation by CTG Expansion in Myotonic Dystrophy Type 1 Using Mutant Human Embryonic Stem Cells. *Stem Cell Rep.* **2015**, *5*, 221–231. [CrossRef] [PubMed]
31. Buckley, L.; Lacey, M.; Ehrlich, M. Epigenetics of the myotonic dystrophy-associated DMPK gene neighborhood. *Epigenomics* **2016**, *8*, 13–31. [CrossRef] [PubMed]
32. Ballester-Lopez, A.; Linares-Pardo, I.; Koehorst, E.; Núñez-Manchón, J.; Pintos-Morell, G.; Coll-Cantí, J.; Almendrote, M.; Lucente, G.; Arbex, A.; Magaña, J.J.; et al. The need for establishing a universal CTG sizing method in myotonic dystrophy type 1. *Genes* **2020**, *11*, 757. [CrossRef] [PubMed]
33. Koehorst, E.; Núñez-manchón, J.; Ballester-lópez, A.; Almendrote, M.; Lucente, G.; Arbex, A.; Chojnacki, J.; Vázquez-manrique, R.P.; Gómez-escribano, A.P.; Pintos-morell, G.; et al. Characterization of RAN Translation and Antisense Transcription in Primary Cell Cultures of Patients with Myotonic Dystrophy Type 1. *J. Clin. Med.* **2021**, *10*, 5520. [CrossRef]
34. Miller, S.A.; Dykes, D.D.; Polesky, H.F. A simple salting out procedure for extracting DNA from human nucleated cells. *Nucleic Acids Res.* **1988**, *16*, 1215. [CrossRef] [PubMed]
35. Carrió, E.; Magli, A.; Muñoz, M.; Peinado, M.A.; Perlingeiro, R.; Suelves, M. Muscle cell identity requires Pax7-mediated lineage-specific DNA demethylation. *BMC Biol.* **2016**, *14*, 30. [CrossRef]
36. Mallona, I.; Díez-Villanueva, A.; Peinado, M.A. Methylation plotter: A web tool for dynamic visualization of DNA methylation data. *Source Code Biol. Med.* **2014**, *9*, 11. [CrossRef] [PubMed]
37. Légaré, C.; Overend, G.; Guay, S.-P.; Monckton, D.G.; Mathieu, J.; Gagnon, C.; Bouchard, L. DMPK gene DNA methylation levels are associated with muscular and respiratory profiles in DM1. *Neurol. Genet.* **2019**, *5*, e338. [CrossRef]
38. Groh, W.J.; Groh, M.R.; Shen, C.; Monckton, D.G.; Bodkin, C.L.; Pascuzzi, R.M. Survival and CTG repeat expansion in adults with myotonic dystrophy type 1. *Muscle Nerve* **2011**, *43*, 648–651. [CrossRef]
39. Logigian, E.L.; Moxley, R.T.; Blood, C.L.; Barbieri, C.A.; Martens, W.B.; Wiegner, A.W.; Thornton, C.A.; Moxley, R.T. Leukocyte CTG repeat length correlates with severity of myotonia in myotonic dystrophy type 1. *Neurology* **2004**, *62*, 1081–1089. [CrossRef]
40. Nichol, K.; Pearson, C.E. CpG methylation modifies the genetic stability of cloned repeat sequences. *Genome Res.* **2002**, *12*, 1246–1256. [CrossRef] [PubMed]
41. Yanovsky-Dagan, S.; Cohen, E.; Megalli, P.; Altarescu, G.; Schonberger, O.; Eldar-Geva, T.; Epsztejn-Litman, S.; Eiges, R. DMPK hypermethylation in sperm cells of myotonic dystrophy type 1 patients. *Eur. J. Hum. Genet.* **2021**, *online ahead of print*. [CrossRef]

42. Antequera, F.; Boyes, J.; Bird, A. High levels of de novo methylation and altered chromatin structure at CpG islands in cell lines. *Cell* **1990**, *62*, 503–514. [CrossRef]
43. Jones, P.A.; Wolkowicz, M.J.; Rideout, W.M.; Gonzales, F.A.; Marziasz, C.M.; Coetzee, G.A.; Tapscott, S.J. De novo methylation of the MyoD1 CpG island during the establishment of immortal cell lines. *Proc. Natl. Acad. Sci. USA* **1990**, *87*, 6117–6121. [CrossRef] [PubMed]

iScience

CellPress
OPEN ACCESS

Article

Immortalized human myotonic dystrophy type 1 muscle cell lines to address patient heterogeneity

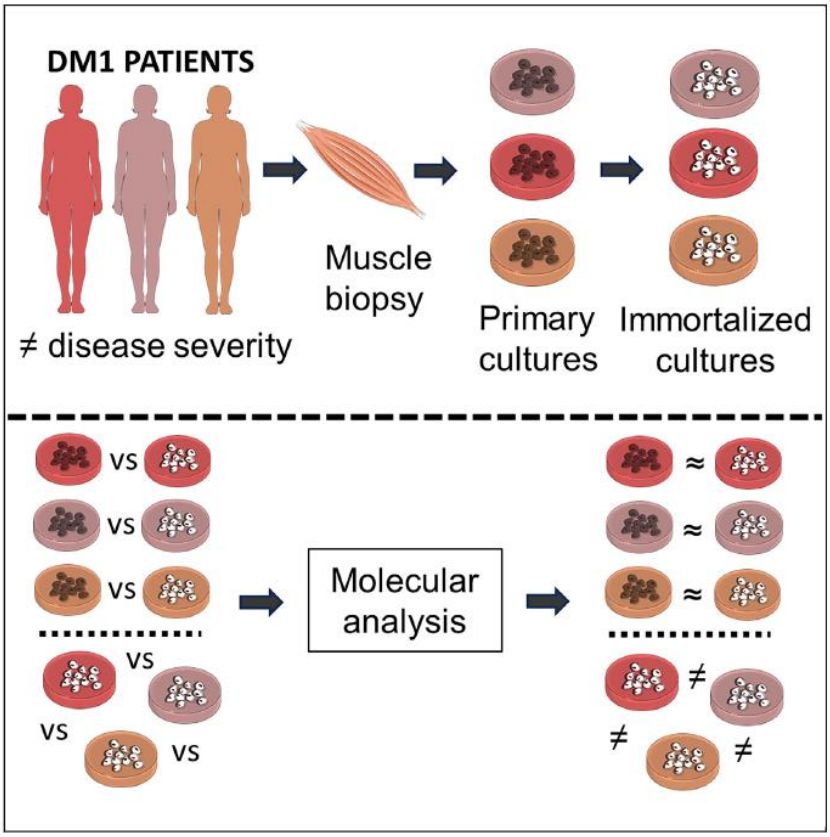

Judit Núñez-Manchón, Júlia Capó, Alicia Martínez-Piñeiro, ..., Vincent Mouly, Mònica Suelves, Gisela Nogales-Gadea

gnogales@igtp.cat

Highlights

Three DM1 immortalized muscle cell models have been generated

The models reproduce the main DM1 molecular hallmarks

There is molecular heterogeneity between the three models

The models are adequate to assess the efficacy of therapies

Núñez-Manchón et al., iScience 27, 109930
June 21, 2024
https://doi.org/10.1016/j.isci.2024.109930

iScience

CellPress
OPEN ACCESS

Article

Immortalized human myotonic dystrophy type 1 muscle cell lines to address patient heterogeneity

Judit Núñez-Manchón,[1] Júlia Capó,[1] Alicia Martínez-Piñeiro,[1,2] Eduard Juanola,[1,2] Jovan Pesovic,[3] Laura Mosqueira-Martín,[4] Klaudia González-Imaz,[4] Pau Maestre-Mora,[1] Renato Odria,[1] Dusanka Savic-Pavicevic,[3] Ainara Vallejo-Illarramendi,[4] Kamel Mamchaoui,[5] Anne Bigot,[5] Vincent Mouly,[5] Mònica Suelves,[1,6] and Gisela Nogales-Gadea[1,6,7,*]

SUMMARY

Historically, cellular models have been used as a tool to study myotonic dystrophy type 1 (DM1) and the validation of therapies in said pathology. However, there is a need for *in vitro* models that represent the clinical heterogeneity observed in patients with DM1 that is lacking in classical models. In this study, we immortalized three DM1 muscle lines derived from patients with different DM1 subtypes and clinical backgrounds and characterized them at the genetic, epigenetic, and molecular levels. All three cell lines display DM1 hallmarks, such as the accumulation of RNA foci, MBNL1 sequestration, splicing alterations, and reduced fusion. In addition, alterations in early myogenic markers, myotube diameter and CTCF1 DNA methylation were also found in DM1 cells. Notably, the new lines show a high level of heterogeneity in both the size of the CTG expansion and the aforementioned molecular alterations. Importantly, these immortalized cells also responded to previously tested therapeutics. Altogether, our results show that these three human DM1 cellular models are suitable to study the pathophysiological heterogeneity of DM1 and to test future therapeutic options.

INTRODUCTION

Myotonic dystrophy type 1 (DM1) is an autosomal dominant multisystemic disease caused by a CTG expansion in the 3′ untranslated region of the myotonic dystrophy protein kinase (*DMPK*) gene. It is the most prevalent muscular dystrophy in adults affecting 1 in 8000. It causes a variety of symptoms that include, but are not limited to: muscle weakness, myotonia, cardiac defects, respiratory failure, endocrine alterations such as diabetes, and cognitive impairment. The presence of these symptoms and their severity differs between patients. They can appear at any age and there is an earlier onset of clinical manifestations in successive generations, which is known as genetic anticipation. According to the age of onset, patients with DM1 can be classified as congenital, childhood, juvenile, adult, or late-onset. An earlier age of onset is associated with a greater disease severity and higher CTG expansion sizes.[1]

The CTG expansion length varies in the range between 50 and thousands of repeats[2] and it has a high degree of instability biased toward expansions in germline and somatic cells. Therefore, the size of the CTG repeat increases over generations in affected pedigrees and through a patients' life.[3–5] Moreover, patients with DM1 present somatic mosaicism in CTG expansion length between different tissues and cell types.[6,7] Altogether, this results in patients presenting heterogeneity at the genetic level, which makes it extremely challenging to determine a precise expansion size for each patient.[8] Currently, CTG expansion size can be determined by small pool PCR which allows researchers to analyze trinucleotide repeat instability[9] in a quantitative manner, detecting common and low abundant CTG sizes in a pool of cells. This technique allows the characterization of the CTG expansion dynamics of this highly unstable repeat expansion.

Epigenetics may have a role in DM1, as the CTG expansion overlaps with a 3.5 kb CpG island.[10–13] The *DMPK* gene is in chromosome 19q surrounded by the *DMWD* (upstream) and *SIX5* (downstream) genes. The *DMPK* locus contains several CpG islands, including the CTCF1 and CTCF2 regions, which are surrounding the CTG expansion. In the case of CTCF1, aberrant methylation patterns have been described by other labs and by ours. For example, DM1 muscle and muscle derived DM1 cells show CTCF1 hypermethylation compared to controls; while blood samples from congenital cases show CTCF1 hypermethylation compared to controls and adult DM1 cases.[12,14,15] However, it is not clear how

[1]Grup de REcerca Neuromuscular de BAdalona (GRENBA), Institut d'Investigació en Ciències de la Salut Germans Trias i Pujol (IGTP), Campus Can Ruti, Universitat Autònoma de Barcelona, 08916 Badalona, Spain
[2]Neuromuscular Pathology Unit, Neurology Service, Neuroscience Department, Hospital Universitari Germans Trias i Pujol, 08916 Badalona, Spain
[3]University of Belgrade - Faculty of Biology, Center for Human Molecular Genetics, Belgrade, Serbia
[4]Group of Neurosciences, Department of Pediatrics, UPV/EHU, Hospital Universitario Donostia - IIS Biodonostia, 20014 San Sebastian, Spain
[5]Sorbonne Université, Inserm, Institut de Myologie, Centre de Recherche en Myologie, F-75013 Paris, France
[6]These authors contributed equally
[7]Lead contact
*Correspondence: gnogales@igtp.cat
https://doi.org/10.1016/j.isci.2024.109930

the hypermethylation of this CpG island contributes to the pathogenesis of the disease, although it has been reported that *DMPK* and the surrounding genes (*DMWD* and *SIX5*) are downregulated in DM1.[16,17]

It has been demonstrated that RNA gain of function[18,19] is the main molecular pathology mechanism in DM1. *DMPK* transcripts containing the CTG expansion accumulate,[20] form hairpin structures[21] and agglomerate in the nucleus. These agglomerations receive the name of RNA foci, whose quantity varies between cells, and patient tissues.[20] We and others have found correlation between RNA foci formation and CTG expansion size, and RNA foci formation and age of onset.[22,23] It is known that foci can bind to important cellular proteins, such as the splicing regulator, muscleblind-like 1 (MBNL1).[24] MBNL1 sequestration and downregulation causes the aberrant splicing of several genes, including insulin receptor (*INSR*),[25] sarcoplasmic reticulum Ca(2+)-ATPase 1 (*ATP2A1*),[26] LIM Domain Binding 3 (*LDB3*),[27] dystrophin (*DMD*),[28] bridging Integrator 1 (*BIN1*),[29] and *MBNL1* (which regulates its own splicing).[30] Some splicing alterations are tightly connected with some of the symptoms that patients with DM1 present: *INSR* is associated with insulin resistance,[31] *BIN1* with muscle weakness,[32] *LDB3* with sudden cardiac death[33] and *ATP2A1* and *DMD* with muscle regeneration.[34,35]

Cellular DM1 models have proven to be a valuable tool for studying the molecular aspects of diseases and for evaluating the efficacy of potential treatments.[36,37] Nowadays, different cellular models have been developed for studying DM1, each with their own pros and cons.[38] Among them, we have cell lines with artificial expressions of exogenous CTG repeats and patient derived cell lines.[39] Cells artificially expressing CTGs, even though they reproduce the hallmarks of the disease,[25,39] lack the genetic context of the *DMPK* gene, including its regulation by the gene promoter and the expression alterations of adjacent genes (*DMWD* and *SIX5*). This inconvenience is overcome in the patient derived cell lines, which can be either primary or immortalized cells. Primary cells are obtained from patient biopsies. The most frequently used are skin fibroblasts, because they are easier to obtain, and myoblasts, as muscle is one of the main affected tissues in DM1, which can fuse into myotubes. However, primary cultures have limitations in the number and type of experiments that can be performed because they have a reduced number of divisions, and it is ethically controversial to take biopsies from patients with DM1. Since skin biopsies are more accessible, skin fibroblasts can be transdifferentiated into myoblasts by *MYOD1* transduction.[31] However, it has been shown that the transdifferentiation does not lead to full muscle cell reprogramming.[40] Another strategy consists in the reprogramming of patient cells into iPSCs.[41] This approach offers the advantage of differentiating iPSCs into any type of cell, including those located in tissues where biopsies are not feasible, such as cardiomyocytes or neurons which are also affected in DM1.[42] The downsides of iPSCs include a highly unstable CTG repeat during reprogramming, incomplete cell maturation, and high maintenance cost. To resolve these problems, immortalized muscle patient cells were developed by inserting lentiviral vectors expressing the catalytic subunit of human telomerase (*TERT*), cydin-dependent kinase 4 (*CDK4*), and cyclin D1 (*CCND1*).[38] With these changes, cells can divide an unlimited number of times, thus diminishing the need to perform muscle biopsies and allowing the execution of experiments that need a high cell number. Nonetheless, it still needs to be proven that the insertion of these transgenes does not produce alterations in cellular behavior.[43] To date, there are only three reports in which four myoblast patient derived cell lines have been generated.[44–46]

In this work, we have immortalized and characterized three DM1 muscle cell lines from patients with adult DM1 that belonged to the juvenile, adult and late onset DM1 subtypes. These patients were clinically heterogeneous in their symptomatology, which is demonstrated by their muscle, heart, and lung pathologies. The immortalized muscle cell models were also heterogeneous in their molecular alterations, but they presented similar alterations to the parental cells from which they were derived. Notably, antisense oligonucleotide treatment rescued a substantial portion of the molecular alterations in these models. In conclusion, the three models generated are adequate models to address the heterogeneity in DM1 and to analyze genetic, epigenetic, transcriptomic, and proteomic alterations, cellular functions, and response to therapies in a more diverse way.

RESULTS

Immortalization of muscle cells derived from patients with myotonic dystrophy type 1 with clinical heterogeneity

In this study, we have immortalized myoblasts from 3 patients with DM1 showing different clinical manifestations and degrees of disability (Table 1). An STR variant analysis of 16 locus was performed for line authentication purposes and it confirmed that the immortalized and primary cell lines of each patient shared the same alleles (Table 2). The samples came from three female patients, ranging in age from 36 to 46 at the moment of sampling. Their ages of onset were 15, 27 and 42, placing them in the juvenile, adult, and late onset DM1 subtypes, respectively. Muscular involvement was determined with the Medical Research Council (MCR) scale in both proximal and distal muscles. Patients JCC-DM1 and ADE-DM1 had moderate muscle involvement; they had an MRC score of 4 for proximal muscles and an MRC score of 3 for distal muscles. In contrast, GPM-DM1 had mild involvement, with an MRC score of 5 for proximal muscles and an MRC score of 4 for distal muscles. Cardiac involvement was mild in patients JCC-DM1 and GPM1-DM1, while in ADE-DM1 it was severe. This patient needed a pacemaker after suffering several bouts of syncope and after being diagnosed with an elongated HV interval. Respiratory involvement was mild in ADE-DM1 who had a forced vital capacity (FVC) of 65%, moderate in JCC-DM1 who had an FVC of 58% and severe in GPM-DM1 who had an FVC of 50% and required mechanical ventilation. Finally, to determine their level of functionality, we used the modified Rankin scale (mRS), which determines DM1 patient's degree of disability and dependence in daily activities. GPM-DM1 had a mRS of 1, implying she did not present significant disability and was able to carry out usual activities. JCC-DM1 had a mRS of 2, implying she suffered a slight disability and even though she could live unassisted, she could not perform all the activities she performed previous to the onset of the disease. ADE-DM1 had a mRS of 4; implying she had a moderately severe disability and wasn't able to attend bodily functions or walk without assistance. Globally, ADE-DM1 was the most affected patient as she suffered from severe cardiac and functional involvement, as well as moderate muscular

Table 1. General data and clinical characterization of the patients with DM1 and controls

Sample	Type of sample	Age at sampling	Gender	Age of onset	Muscle involvement	Cardiac involvement	Respiratory involvement	mRS	Type of cellls derived
JCC-DM1	Patient	36	F	15	moderate	mild	moderate	2	Primary and immortalized
GPM-DM1	Patient	46	F	42	mild	mild	severe	1	Primary and immortalized
ADE-DM1	Patient	39	F	27	moderate	severe	mild	4	Primary and immortalized
C7	Control	66	F						Primary
C9	Control	41	M						Primary
C10	Control	26	M						Primary
AB678	Control	53	M						Immortalized
AB1079	Control	38	M						Immortalized
KM1421	Control	13	F						Immortalized

mRS, modified rankin scale.

involvement. She is followed by JCC-DM1 in severity, who had moderate functional, muscular and respiratory involvement. Lastly, GPM-DM1 had mild involvement in all the parameters studied, except for respiratory function which was severely affected.

A high level of CTG repeats instability characterized all studied myotonic dystrophy type 1 cell lines

CTG expansion was measured in primary and immortalized cell lines from the three patients with DM1 by small pool PCR, which revealed highly heterogeneous CTG expansion patterns within each patient. We created density plots with the results and calculated the estimated progenitor allele (ePAL), the size of the two main expanded populations, and the expansion instability observed in each cell line (Figures 1A and 11B). Primary GPM-DM1 cells had an ePAL of 435 CTGs and showed two expanded main populations with 581 CTGs and 1028 CTGs, while in the immortalized cells the ePAL was 280 CTGs and the two most abundant populations had 379 and 863 CTGs, respectively. Primary JCC-DM1 cells had an ePAL of 663 CTGs and the average sizes of the two main expansion populations were 875 CTGs and 1950 CTG, while the ePAL in the immortalized cells was 654 CTGs, and the two main populations had a size of 953 CTGs and 2080 CTGs. Primary ADE-DM1 cells had an ePAL of 578 CTGs, and the highest expansion sizes of the most abundant populations (1505 CTG and 3075 CTG), while the immortalized cells, had an ePAL of 700 CTGs, and the two most abundant populations had a size of 1224 CTGs and 2301 CTGs. When analysing the expansion instability, GPM-DM1 had the lowest levels both in the primary and the immortalized cell lines, followed by JCC-DM1 and then ADE-DM1 (Figure 1B). All immortalized cell lines had some increase in expansion instability, which was between 6 and 25% of that observed in the parental cell lines, but the expansion instability pattern closely resembled the parental after the immortalization process.

Table 2. STR profiling of the patients from which the cells were isolated and immortalized

Locus	Chromosome location	JCC-DM1	GPM-DM1	ADE-DM1
D8S1179	8	13	10, 14	12, 14
D21S11	21q11.2-21-22	31, 32.2	29, 32.2	30, 33.2
D7S820	7q11.21–22	8, 10	10, 11	10
CSF1PO	5q33.3–34	10, 11	10, 12	11, 13
D3S1358	3p	17, 18	17	16, 17
TH01	11p15.5	6	6	8, 9.3
D13S317	13q22-31	8, 10	11	11
D16S539	16q24-qter	12, 13	12	11
D2S1338	2q35–37.1	17, 19	19, 23	17
D19S433	19q12–13.1	13, 15	12, 13	14, 15
vWA	12p12-pter	14, 16	15, 18	16, 18
TPOX	2p23-2per	9, 11	8, 12	8
D18S51	16q21.3	12, 15	12, 14	14, 15
AMELOGENIN	X: p22.1–22.3 Y: p11.2	X	X	X
D5S818	5q21-31	11, 13	10, 12	11
FGA	4q28	20, 21	25, 26	21, 25

CellPress
OPEN ACCESS

iScience
Article

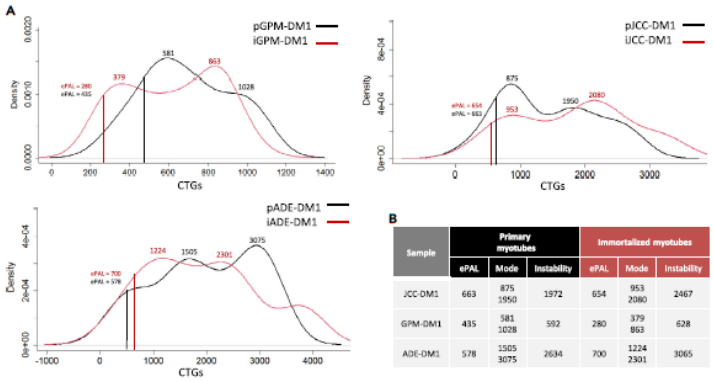

Figure 1. CTG instability is similar between primary and immortalized DM1 cells lines

(A) Density plots showing the distribution of the CTG alleles detected in both the primary (black) and immortalized (red) myotubes derived from the three patients participating in the study. We measured between 41 and 105 alleles per sample.

(B) CTG expansion ePAL, mode and instability in primary and immortalized myotubes of the three patients with DM1 participating in the study. The progenital allele length was estimated as the 10th percentile of allele frequency distribution. The modal allele length was determined as the most frequent allele. The level of somatic instability was calculated by subtracting the 10th percentile from the 90th percentile. "p" and "i" before cell line name mean primary and immortalized, respectively.

Interestingly, the larger the size of the most abundant CTG expansion and the greater degree of instability, the more severely affected the patient was. However, maybe due to the small sample size, no significant correlation was found.

CTCF1 methylation level is increased in the myotonic dystrophy type 1 immortalized cell lines when compared with immortalized control cell lines as observed in primary cell lines

We analyzed DNA methylation levels of the CTCF1 region, which is located upstream of the CTG expansion in the *DMPK* gene (Figure 2A), in myoblasts and in 5 days differentiated myotubes derived from the primary and immortalized cell lines, in both controls and patients with DM1. There were significant differences in the level of methylation between controls and patients; while controls did not show methylation in the analyzed CpG sites of the CTCF1 region, patients with DM1 showed increased levels of methylation, both in myoblasts and in myotubes, in most of the CpG sites (Figure 2B). Moreover, we observed a significant increase in the methylation level in immortalized myoblasts compared to primary ones (Figure 2C). In the case of myotubes, a tendency ($p = 0.06$) was observed. No consistent differences were detected between patients regarding the methylation level of the CTCF1 site (Figure S1). To determine whether the methylation status of this region could change the expression level of neighboring genes, we analyzed the expression of *DMWD*, *DMPK*, and *SIX5* in immortalized myotubes from controls (iCtrls) and patients with DM1 (iDM1). Although significance was not reached due to dispersion in control cell values, all patient cell values were below any of the control values for the three genes (Figure 2D). More data would be needed to confirm the downregulation of DMWD, DMPK and SIX5, which could be a consequence of the hypermethylation in the CTCF1 region in DM1 muscle cells compared to controls.

Myotonic dystrophy type 1 myoblasts show higher cell proliferation and reduction of early myogenic markers

We next sought to characterize the myogenic process in immortalized DM1 myoblasts by using real-time impedance analysis. Figure 3A shows the average real-time impedance curves of control (blue) and DM1 (red) myoblast samples throughout the myogenic process. Initially, all cultures increased their impedance values, which was indicative of myoblast adhesion, spreading, and proliferation, until they reached confluence, which resulted in achieving their maximum impedance values. Notably, at this step DM1 myoblasts showed a significant increase in impedance at 24 and 48 h after seeding, which was indicative of a higher adhesion, spreading, and proliferation levels in comparison to the control cells (Figure 3B). After switching to differentiation medium, a decrease in resistance was observed in both, control and DM1 cells, at 2 days post differentiation (dpd), due to cell reorganisation prior to muscle differentiation/fusion, with this decrease being higher in DM1 cells (Figure 3C). To address whether myogenic process could be altered in DM1 cells, we analyzed the levels of the myogenic regulatory factors Myf5, MyoD and myogenin, in time course experiments by Jess Western blots. Myf5 is expressed during stem cell activation and myoblasts proliferation; MyoD is expressed during myoblast proliferation, commitment to differentiation and myotube fussion; and myogenin is expressed during myotube fussion and maturation into myofiber.[47] As shown in Figure 3D, Myf5 levels were significantly reduced in DM1 cells

iScience
Article

CellPress
OPEN ACCESS

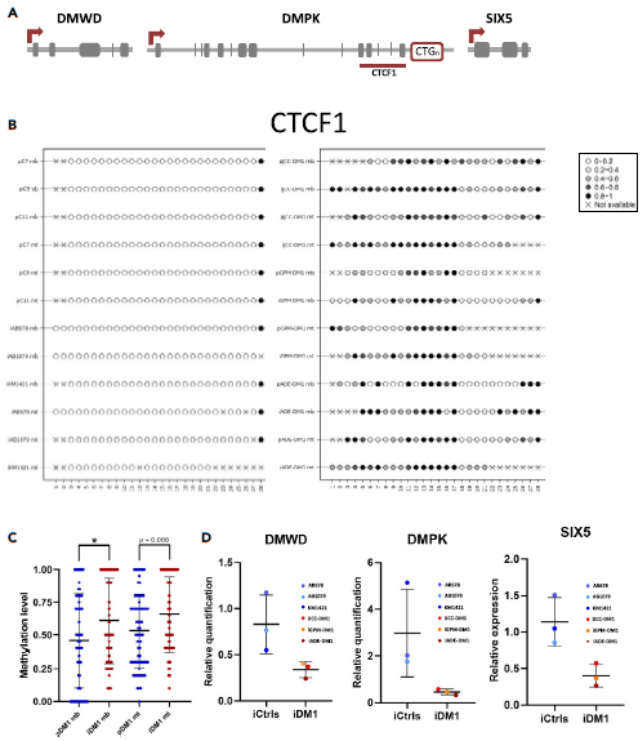

Figure 2. DNA methylation levels in CTCF1 is increased in immortalized cell lines when compared to primary cell lines

(A) Schematic representation of the genomic *DMPK* locus.

(B) Methylation plotter showing the methylation status of the CTCF1 region. Each circle represents a CpG dinucleotide. The level of methylation is represented by the gray gradient.

(C) Graphical representation of the methylation levels in DM1 immortalized and primary myoblasts and myotubes.

(D) Relative expression of *DMWD*, *DMPK* and *SIX5* genes at 5 days of differentiation. HPRT was used as housekeeping gene to normalize the data.

All data are expressed as mean ± SEM. "p" and "i" before cell line name mean primary and immortalized, respectively. "mb" refers to myoblasts and "mt" to myotubes. Means were compared using unpaired two-tail Mann-Whitney test. *$p \leq 0.05$

at 0,2,3 dpd, meanwhile MyoD was also significantly reduced at 3 dpd. No differences were found for Myogenin levels. In conclusion, DM1 cells show alterations in early myogenic markers My5 and MyoD.

Myotonic dystrophy type 1 immortalized cells maintain a reduced fusion index as observed in their parental lines

Next, we investigated the fusion capacity of immortalized DM1 myotubes at 5 days of differentiation by desmin staining (Figure 4A). As shown in Figure 4B, the fusion index was significantly reduced in both primary and immortalized DM1 myotubes compared to the corresponding controls. We also observed that immortalized cells, both control and DM1, showed a higher fusion index than the parental cell lines (Figure 4B). When studied individually, we found significant differences in the fusion index between the three immortalized control cell lines and the three immortalized DM1 cell lines (Figure 4C). Moreover, we found differences in nuclei distribution in the myotubes (Figure 4D). We found a significant difference between patients and controls in the number of myotubes with more than three nuclei. Immortalized patients myotubes with two nuclei were more abundant than immortalized controls with two nuclei, reaching statistical significance. The number of myotubes with more than three nuclei was significantly higher in controls than in patients both in primary and immortalized cell lines (Figure 4D). Furthermore, the diameter of DM1 myotubes was dramatically reduced compared to the control ones (Figure 4E). When analysing individually the cell lines, differences in myotube diameter were found in all cell lines (Figure 4F). iGPM-DM1 was the cell line that had the

CelPress
OPEN ACCESS

iScience
Article

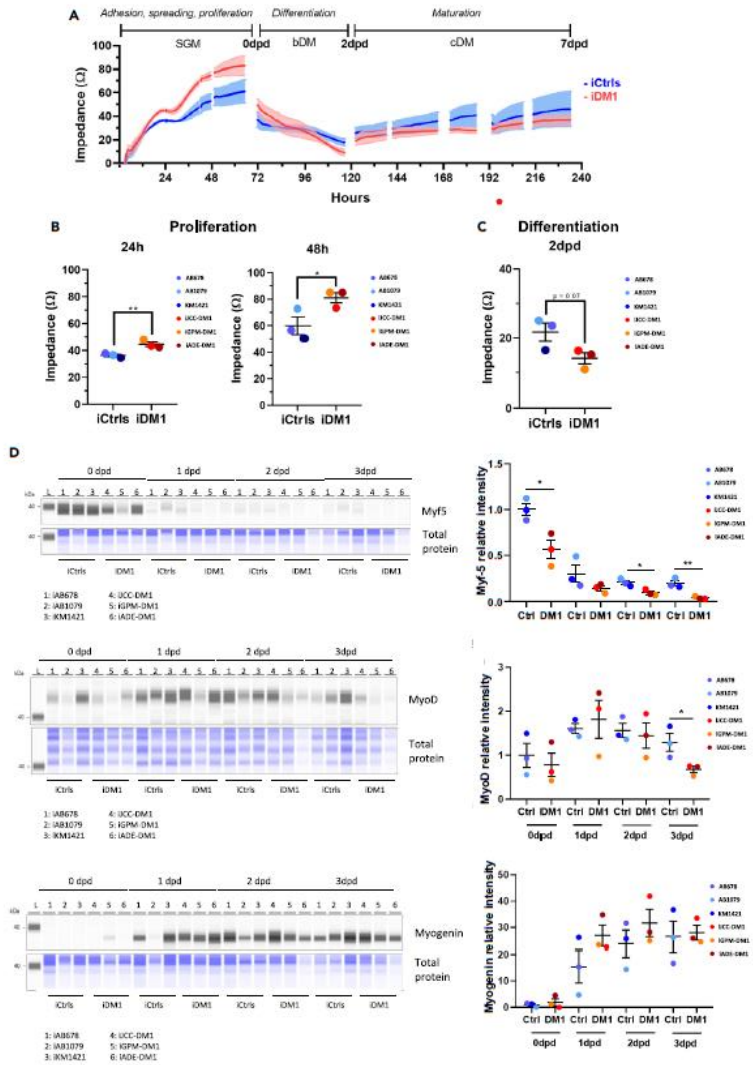

Figure 3. DM1 myoblasts show higher cell proliferation and reduced levels of early myogenic markers

(A) Real-time impedance curves of human iCtrl (blue) and iDM1 (red) myoblasts during culture in proliferation medium (SGM) and differentiation media (bDM and cDM).

(B) Proliferation of iCtrl (blue) and iDM1 (red) myoblasts was analyzed at 24 and 48 h after seeding.

(C) Differentiation of iCtrl and iDM1 myoblasts was analyzed after 2 days in differentiation medium bDM (2dpd).

(D) Jess Western blot analysis of Myf5, MyoD and Myogenin in iCtrl and iDM1 3 differentiating myoblasts at 4 different time-points: 0, 1, 2 and 3 dpd. Values are represented over Ctrl 0 dpd.

Data information: $n = 3$ for iCtrl and iDM1. Dpd, days post differentiation. All data are expressed as mean ± SEM. (A–C) Dots indicate mean values of individual samples from 10 replicates. Means were compared using unpaired two-tail Student's t test. *$p \leq 0.05$, **$p \leq 0.01$. "i" mean immortalized cell line.

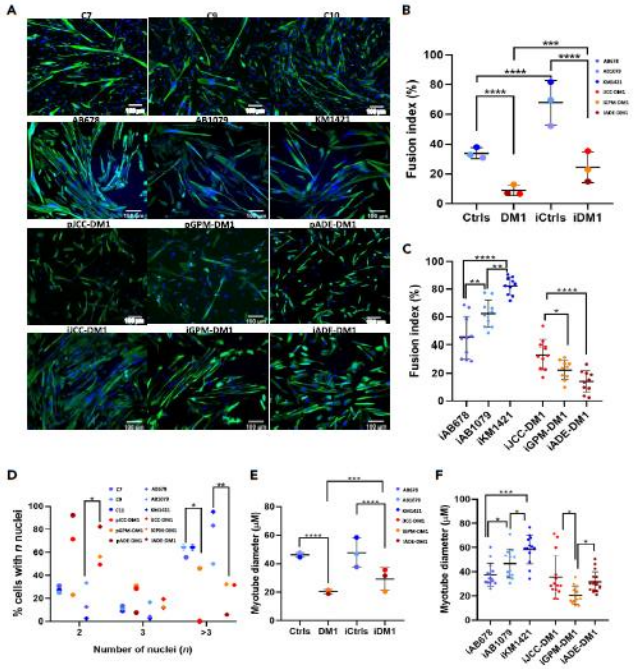

Figure 4. DM1 primary and immortalized myotubes present a lower fusion index compared to controls

(A) Desmin (green) and nuclei (blue) immunofluorescence analysis performed in 5 days differentiated primary and immortalized DM1 or control myotubes.

(B) Fusion index (% of nuclei in desmin positive myotubes with 2 or more nuclei) in primary and immortalized 5 days differentiated DM1 or control myotubes.

(C and D) Fusion index (% of nuclei in desmin positive myotubes with 2 or more nuclei) in individualized immortalized 5 days differentiated DM1 or control myotubes D. Percentage of 5 days differentiated primary and immortalized myotubes containing 2, 3, >3 nuclei.

(E) Myotube diameter (calculated using the maximum diameter value of desmin positive myotubes with 2 or more nuclei) in primary and immortalized 5 days differentiated DM1 or control myotubes.

(F) Myotube diameter in individualized immortalized 5 days differentiated DM1 or control myotubes.

All data are expressed as mean ± SEM. Means were compared using unpaired two-tail t-test. *$p \leq 0.05$, **$p \leq 0.01$, ***$p \leq 0.001$, ****$p \leq 0.0001$. "p" and "i" before cell line name mean primary and immortalized, respectively.

In (B and C), dots indicate mean values of 5 individual analyzed images. In (B and D) at least 350 nuclei/cell line were analyzed.

In (C) at least 850 nuclei/cell line were analyzed.

In (E and F) at least 20 myotubes/cell line were analyzed.

smallest myotube diameter size when compared to the other cell lines. Altogether, the results demonstrate that the immortalized DM1 cell lines also show reduced muscle fusion capacity.

Myotonic dystrophy type 1 immortalized myotubes maintain patient-derived heterogeneity and have equal or greater RNA foci and muscleblind-like 1 co-localization than their primary myotubes

First, we checked for the presence of nuclear RNA foci in 5 days differentiated myotubes. Primary and immortalized control cells did not show RNA foci as expected (Figure S1), whereas primary DM1 myotubes showed variable numbers in the percentage of cells carrying RNA foci and in the number of RNA foci per cell (Figures 5A and 5B). Notably, this patient-derived heterogeneity with respect to the accumulation of RNA foci was greatest in immortalized DM1 cells. Interestingly, the JCC-DM1 and ADE-DM1 immortalized myotubes, which are the cells carrying the longest CTG expansions and derived from the most affected patients, showed not only a significantly higher number of RNA foci per cell compared to GPM-ADE (Figure 5D), but also the highest proportion of cells carrying more than 10 foci per cell (Table 3).

CellPress
OPEN ACCESS

iScience
Article

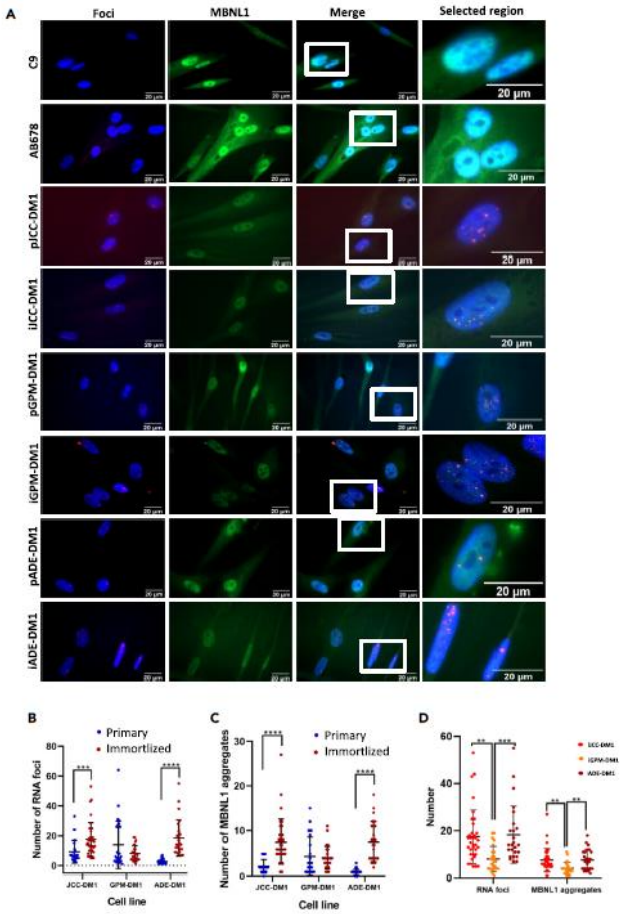

Figure 5. DM1 immortalized myotubes present equal or higher amount of RNA foci and MBNL1 aggregates than the original primary culture

(A) Foci (red), MBNL1 (green) and nuclei (blue) immunofluorescence analysis performed in 5 days differentiated primary and immortalized DM1 myotubes.

(B) Number of RNA foci/nucleus in primary and immortalized 5 days differentiated DM1 myotubes.

(C) MBNL1 aggregates/nucleus in primary and immortalized 5 days differentiated DM1 myotubes.

(D) Comparison of the number of RNA foci/nucleus and MBNL1 aggregates/nucleus between the three immortalized DM1 cell lines.

All data are expressed as mean ± SEM. Between 25 and 35 DM1 nuclei and between 20 and 25 control nuclei were analyzed per cell line. "p" and "i" before cell line name mean primary and immortalized, respectively. Means were compared using unpaired two-tail Mann-Whitney test. $^{**}p \leq 0.01$, $^{***}p \leq 0.001$, $^{****}p \leq 0.0001$.

It is well known that staining with an anti-MBNL1 antibody shows the presence of MBNL-1 aggregates, which co-localize with RNA foci only in DM1 cells. This aggregation of MBNL1 leads to a decrease in cytoplasmic and nuclear fluorescence of MBNL1 compared to that of control cells (Figure 5A). As we observed with RNA foci, primary DM1 cells had a variable number of co-localized aggregates. Immortalized JCC-DM1 and ADE-DM1 myotubes showed a significantly higher mean number of MBNL1 aggregates, as well as a high percentage of cells with more than 10 MBNL1 aggregates when compared to primary cell lines (Figure 5D; Table 3). Altogether, these results indicate that these DM1 immortalized cell lines also show the cell heterogeneity associated with DM1 tissues.

Table 3. Detailed data of the RNA foci and MBNL1 aggregates found in 5 days differentiated primary and immortalized myotubes

Cell line	Foci avg.	% of cells with 0 foci	% of cells with 1–5 foci	% of cells with 6–10 foci	% of cells with 11–15 foci	% of cells with 16–20 foci	% of cells with >20 foci	MBNL1 avg.	% of cells with 0 MBNL1 aggr.	% of cells with 1–5 MBNL1 aggr.	% of cells with 6–10 MBNL1 aggr.	% of cells with 11–15 MBNL1 aggr.	% of cells with 16–20 MBNL1 aggr.	% of cells with >20 MBNL1 aggr.
pJCC-DM1	9,28	0	32	44	8	4	12	2,24	4	96	0	0	0	0
iJCC-DM1	17,51	0	8,6	20	22,9	25,7	22,9	7,63	0	34,3	45,7	14,3	2,85	2,85
pGPM-DM1	13,88	0	48	20	0	0	32	4,4	0	72	20	8	0	0
iGPM-DM1	8,08	0	44	28	12	16	0	4,16	0	76	20	4	0	0
pADE-DM1	2,69	0	91,4	8,6	0	0	0	0,94	20	80	0	0	0	0
iADE-DM1	18,40	0	0	24	36	12	28	7,68	0	40	28	28	4	0

"p" and "i" before cell line name mean primary and immortalized, respectively.

CellPress
OPEN ACCESS

iScience
Article

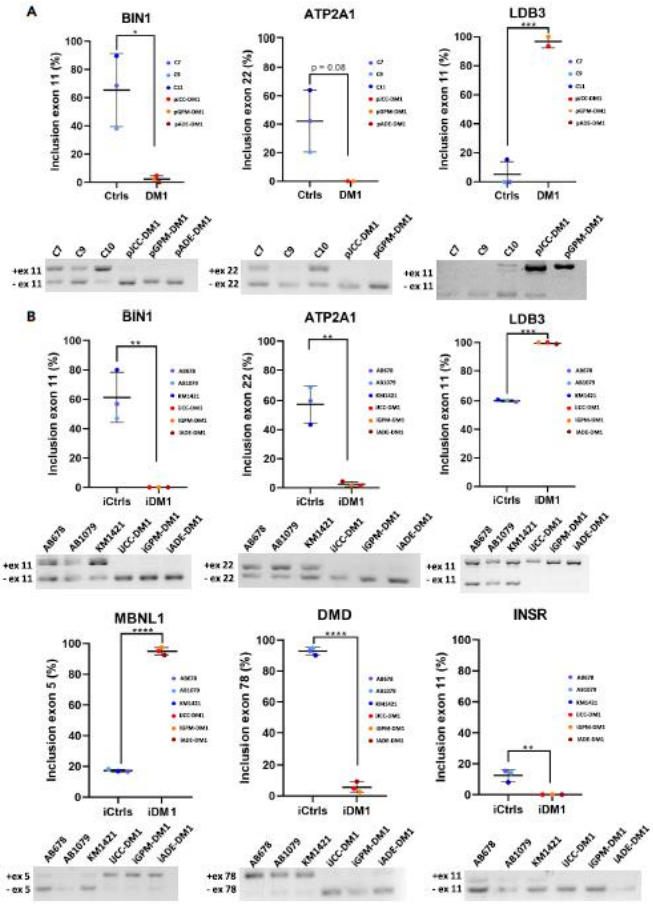

Figure 6. Immortalized DM1 myotubes maintain the splicing defects that characterize DM1 primary myotubes

(A) Exon inclusion analysis of *BIN1*, *LDB3* and *ATP2A1* in primary control and DM1 5 days differentiated myotubes.

(B) Exon inclusion analysis of *BIN1*, *MBNL1*, *LDB3*, *INSR*, *DMD* and *ATP2A1* in immortalized control and DM1 5 days differentiated myotubes.

All data are expressed as mean ± SEM. 3 DM1 samples and 3 control samples were analyzed in each splicing both in primary and immortalized samples, except for *ATP2A1* and *LDB3* in primary samples where 2 DM1 samples and 3 controls were analyzed. Means were compared using unpaired two-tail t-test. *$p \leq 0.05$, **$p \leq 0.01$, ***$p \leq 0.001$, ****$p \leq 0.0001$. "p" and "i" before cell line name mean primary and immortalized, respectively.

Myotonic dystrophy type 1 immortalized myotubes showed the same pathological splicing alterations than their primary myotubes

Next, we analyzed splicing alterations in immortalized DM1 myotubes. We addressed the splicing pattern of transcripts previously described as altered in patients with DM1 (*BIN1* (exon 11), *MBNL1* (exon 5), *LDB3* (exon 11), *INSR* (exon 11), *DMD* (exon 78), and *ATP2A1* (exon 22)). As shown in Figure 6A, DM1 primary myotubes have significantly different *BIN1* and *LDB3* splicing patterns, while a p-value of 0.08 was observed in *ATP2A1* splicing. The same results were obtained when analysing immortalized DM1 myotubes and comparing them with control cells (Figure 6B). Moreover, we found a splicing alteration in the KIF13A gene that was heterogeneously expressed among DM1 immortalized myotubes (Figure 7A). IJCC-DM1 myotubes had a significantly higher exon 32 inclusion than iGPM-DM1 myotubes (Figure 7B), as it can be

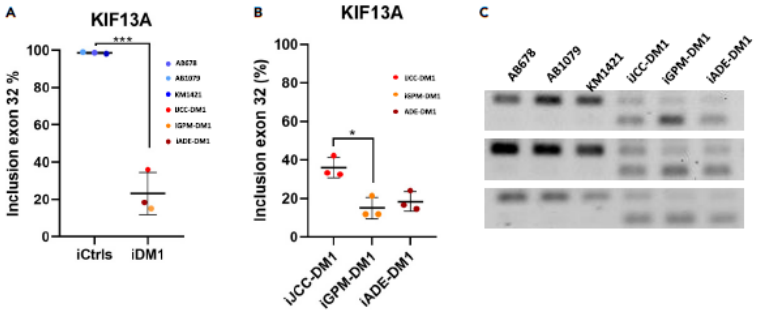

Figure 7. KIF13A splicing defect is heterogeneously expressed among immortalized cell lines

(A) Exon inclusion analysis of KIF13A in immortalized control and DM1 5 days differentiated myotubes.

(B) Exon inclusion analysis of KIF13A in immortalized 5 days differentiated myotubes derived from the three DM1 cell lines.

(C) Gel analysis of *KIF13A* splicing analysis in control and patient DM1 myotubes.

All data are expressed as mean ± SEM. $n = 3$ for each cell line. Means in (A) were compared using unpaired two-tail t-test and in (B) with ANOVA. *$p \leq 0.05$, ***$p \leq 0.001$. "i" before cell line name means immortalized.

observed in the agarose gels (Figure 7C). These results indicate that immortalized DM1 myotubes maintain the splicing defects that characterise this disease, although they can show heterogeneity in the levels of splicing alteration.

Antisense oligonucleotide treatment is equally efficient in myotonic dystrophy type 1 immortalized cell lines as in their original parental lines

To test whether these immortalized cell lines would be suitable for testing DM1 treatments, we treated the cells with an ASO targeting the CTG expansion,[48] previously used in our laboratory (unpublished data). We measured the effect of treatment by analysing the number of RNA foci and colocalizing aggregates of MBNL1 (Figures 8A and S3). Importantly, we observed a significant reduction in both the number of RNA foci (Figure 8B) and the MBNL-1 colocalizing aggregates (Figure 8C) in all immortalized DM1 cell lines. These reductions were also observed in two of the primary cell lines, JCC-DM1 and GPM-DM1, but not in ADE-DM1. Notably, the MBNL-1 colocalizing aggregates decrease was associated in some cases with an increase in the fluorescence signal of MBNL1 in the nucleus. To test whether the RNA foci reduction caused splicing restoration we studied the effect of the ASO treatment in the usual DM1 splicing alterations. Notably, we found a significant reduction in MBNL1 exon 5 splicing alteration. (Figure 8D).

DISCUSSION

Heterogenicity in molecular, clinical, and functional parameters in DM1 is often not represented in the cellular models used to study this disease. The need to generate cellular models that mimic the reported patient differences is increasing, especially with the current development of therapies, and with the necessities to understand pathophysiological mechanisms of DM1. To have more robust results, it is important to work with cell cultures derived from DM1 muscle biopsies, which can show patient heterogeneity and preserve their natural genomic context. However, the accessibility and availability of muscle biopsies from patients with DM1 is very limited, and primary muscle cultures show a reduced proliferative capacity after few passages. In this study, we have generated three immortalized human muscle cell lines derived from three different subtypes of patients with DM1 (juvenile, adult, and late-onset). The genetic, epigenetic, and molecular characterization of these cellular models have shown that all three present the hallmarks of the disease and importantly, they are heterogeneous both from a clinical and molecular point of view.

Given the high instability of the CTG repeat in DM1, we performed SP-PCR to better characterize the genetic expansion variability in our cellular models. Our results revealed high heterogeneity in CTG expansion, with two of the patient-derived cells (ADE-DM1 and JCC-DM1) showing higher ePAL (above 500) and higher instability (above 1900) than the other cell line (GPM-DM1, below 500 and 700, respectively). In addition, the patient-derived muscle cell line with the highest instability (ADE-DM1) was the one whose most abundant populations had the largest CTG expansions and interestingly, corresponded with the most severely affected patient, both from the cardiac and functional points of view. In contrast, the patients with less instability (JCC-DM1 and GPM-DM1) were the mildest affected patients, both cardiacally and functionally. Somatic instability of the CTG expansion has been previously described to be a contributor of disease severity,[49] yet the major contributor of the severity is the ePAL. In this case, the highest ePAL was also found in the immortalized cells of the patient with the highest disease severity (ADE-DM1). However, the primary cells derived from this same patient did not have the highest ePAL, in fact JCC-DM1 had the highest one of the primary cells. These differences between primary and immortalized cells must be derived from the clonal selection that takes place during the immortalization process, in which the CTG expansion tends to expand, but can also contract.

CellPress
OPEN ACCESS

iScience
Article

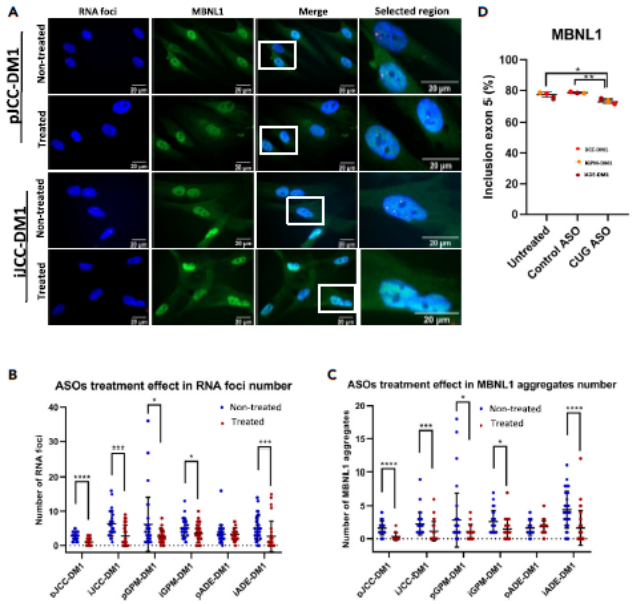

Figure 8. Immortalized DM1 myotubes respond to treatment in a similar way to primary DM1 myotubes

(A) Foci (red), MBNL1 (green) and nuclei (blue) immunofluorescence analysis performed in 9 days differentiated primary and immortalized DM1 myotubes. Rows 1 and 3 correspond to non-treated cells while rows 2 and 4 correspond to 48 h ASO-treated cells.

(B) Number of RNA foci/nucleus in primary and immortalized 48 h ASO-treated or non-treated 9 days differentiated DM1 myotubes.

(C) Number of MBNL1 aggregates/nucleus in primary and immortalized 48 h ASO-treated or non-treated 9 days differentiated DM1 myotubes.

(D) MBNL1 splicing analysis in immortalized 48 h ASO-treated, control-treated or non-treated 9 days differentiated myotubes.

All data are expressed as mean ± SEM. For each cell line in (B and C), it was analyzed between 29 and 43 DM1 nuclei. In (D), 3 DM1 samples were analyzed for each condition. "p" and "i" before cell line name mean primary and immortalized, respectively. Means were compared using unpaired two-tail Mann-Whitney test. *$p \leq 0.05$, ***$p \leq 0.001$, ****$p \leq 0.0001$.

It is indeed remarkable, that clonal cells originating from a single CTG expansion end up having a very similar instability to the primary cells they derived from. It has been hypothesized that individual specific differences, as well as environmental or genetic factors, may contribute to somatic instability.[49] Although 40% of the variance has been reported to be attributed to genetic factors, our results indicate that the contribution of the genetic factors should be above 75% (since only between 6 and 25% variation in instability was found between parental and immortalized cell models). In addition, it is likely that part of the instability was not detected in our study, since measuring these CTG expansions was challenging, and muscle, unlike other tissue such as blood, has larger CTG expansions that are difficult to detect by SP-PCR.[50–52] Deep genomic sequencing techniques[53,54] would probably give more accurate and precise information regarding the larger CTG fragments in muscle and the instability of CTG expansion in DM1 samples.

The CTG expansion overlaps with a 3.5 kb CpG island flanked by two CTCF binding sites, named CTCF1 and CTCF2. We and others have reported changes in the DNA methylation pattern of the CTCF1 region in blood samples from DM1.[10–12] In addition, our group also demonstrated that the CTCF1 region was methylated in a tissue-specific manner only in DM1 muscle biopsies (and not in skin or blood from the same patients), as well as in primary DM1 muscle cells, whereas tissues from unaffected individuals were completely unmethylated.[12] Importantly, the DM1 immortalized muscle cells showed the previously reported CTCF1 hypermethylation in both myoblasts (muscle progenitor cells) and myotubes (mature muscle cells), indicating that the DNA methylation alterations were conserved. However, we observed a significant difference in the methylation levels between primary and immortalized cell lines. Immortalized cell line methylation levels were increased compared to the primary ones. This can be explained by the observation that cellular models, especially immortalized cell lines that have been in culture for a substantial amount of time (since they are originated from a single cellular done), can increase DNA methylation levels[55,56] and/or because of the purity of cell cultures. The presence of a small portion of fibroblasts in the primary cultures, which have an unmethylated CTCF1 region, can have an impact in these CTCF1 methylation studies. DNA methylation is considered a repressive epigenetic mark that plays a role in gene silencing.[57–59] Although we did not find a significant reduction of DMPK, SIX5, and DMWD in our study,

probably due to a small sample, it has been previously reported that there has been a decrease in the expression of these genes in DM1.[60–62] This reduction could be suggesting that DNA hypermethylation in the CTCF1 region could alter transcriptional activity in DM1 muscle samples, which could affect muscle functions. Notably, *SIX5* is abundantly expressed in muscle, heart, brain, and eyes, which are tissues that are affected in DM1. It is homologous to the Drosophila eye development gene sine oculis and it has been proven that *SIX5* deficient mice develop cataracts, as observed in patients with DM1.[63] The *DMWD* gene is abundantly expressed in the brain and testis,[64] although its function is still not clear. However, very recently a quadruple mutant mouse was generated in which the expression of *SIX5*, *DMWD*, *DMPK*, and *MBNL1* was reduced, and these mice recapitulate many important manifestations in congenital DM1, suggesting that changes in gene expression in genes at the *DMPK* locus may modulate disease severity.[65]

The immortalized DM1 cellular models showed an increased proliferation rate when compared with immortalized control models. An advantage in growth and proliferation has already been described in immortalized DM1 lymphocyte cell lines.[66] This effect has been termed "mitotic drive" and it explains why the CTG region tends to expand. Khajavi and colleagues demonstrated that immortalized lymphocytes carrying longer CTG expansions had a growing advantage due to increased Ras, Erk1, and Erk2 activity and decreased $p21^{WAF1}$ activity. However, once DM1 immortalized muscle cell models stop growing and are stimulated to differentiate, they start having alterations.[44] In our immortalized cellular models, DM1 immortalized cells showed a decrease in the impedance during the myotube fusion process, reduced levels of early myogenic markers, a diminished fusion capacity with smaller myotubes, and lower nuclei number per myotube. Some of these alterations have also been found in primary muscle derived cells and have been linked to abnormalities in the temporal expression of differentiation regulators, myogenic progression markers, and alternative splicing patterns before and immediately after the onset of differentiation.[67] These alterations are intrinsically linked to the CTG expansion, since the excision of the expanded repeat reverts all these abnormalities.[67] However, some influence may also come from the environment, since studies in 3D models with immortalized cells demonstrated that these differentiation deficiencies were attenuated[68] when a better niche for differentiation was utilized. Moreover, when comparing primary and immortalized myotubes, we observed an increase in the fusion index in immortalized cell lines, both in controls and DM1. As discussed with the methylation pattern in CTCF1, it is likely that this difference is due to the greater purity of immortalized cultures compared to primary ones. Regarding heterogeneity in the fusion index between cell lines, we found differences between both immortalized controls and patients; meaning that other factors may contribute to the fusion capacity.

Analysis of the molecular hallmarks of the disease revealed heterogeneous alterations in the accumulation of RNA foci and in the sequestration of MBNL1 in our immortalized cell models. Importantly, we have observed that the higher the CTG instability, the higher the average RNA foci per cell. ADE-DM1, had an instability of 3068 CTGs, and had a mean of 18,40 foci per nucleus; JCC-DM1 had an instability of 2467 CTGs and a mean of 17,51 foci per nucleus, and GPM-DM1 had an instability of 828 CTGs and an average of 8,08 foci per nucleus. A direct association between CTG size and foci number in muscle cells has been reported before by our group.[23] We hypothesize that although the CTG size would determine the number of RNA foci at the single cell level, the instability of the CTG repeat in the cells of a certain tissue, would determine the mean of the RNA foci in this particular tissue.[18,24,30]

MBNL1 sequestration was also dependant on the RNA foci average. So, the higher RNA foci/cell, the more MBNL1 aggregates/cell co-localizing with those foci. Again, ADE-DM1 is the cell line carrying more MBNL1 aggregates (7,68 per myotube), followed by JCC-DM1 (7,63 aggregates per myotube), and finally, GPM-DM1 (carrying 4,16 aggregates per myotube). So, it is clear that there is a relationship between CTG expansion, *DMPK* pathological transcript accumulation, and MBNL1 trapping. Heterogeneity in RNA foci accumulation and MBNL1 sequestration can be modified by different experimental conditions. A lower number of RNA foci was observed in the immortalized patient cell lines with 9 differentiation days, when compared to 5 differentiation days. We hypothesize that the heterogeneity could be due to the higher mortality rate observed after 9 days of differentiation, which may difficult the detection of RNA foci.

Splicing alterations were also found in our cellular models. We observed alterations in the splicing of *ATP2A1* and *SERCA1*, which is observed only in mature skeletal muscle cells and is sometimes hard to detect in patient primary cultures[34,69] and in patient derived iPSCs that are differentiated to myotubes.[70] Our cell models showed alterations in *BIN1*, *ATP2A1*, *MBNL1*, *LDB3*, *INSR*, *DMD* and *KIF13A*, which have previously been found altered in DM1 muscle cell models.[44] We found heterogenicity in the alterations of *KIF13A* with JCC-DM1 having significantly less alterations than GPM-DM1. *KIF13* codes for a gene involved in the positioning of endosomes.[71] It is likely that heterogenicity is present in other splicing alterations, but more global transcriptomic studies would be needed to further determine this heterogenicity.

The generation of specific therapies[72] targeting either the gene through CRISPR-Cas9,[73–75] the foci,[76,77] or the increase in MBNL1 availability[78,79] would make these cells an attractive cellular model in which the heterogeneous defects are present in different proportions, which can be quantified after treatments. Notably, the three models showed a significant reduction of RNA foci and MBNL1 aggregates after being treated with an ASO directed against the CTG expansion.[48] Moreover, a significant recovery of the *MBNL1* splicing alteration was observed. Overall, these models would allow treatments to be tested on a larger and more heterogeneous sample than was previously possible.

Prior to this publication, only four DM1 immortalized muscle cellular models have been developed by different research groups (Table 4).[44,45] These cellular models have been a powerful tool used to discover knowledge, develop therapeutic strategies, and overcome the challenges presented by artificial, primary, or transdifferentiated disease models. However, heterogenicity in molecular, clinical, and functional parameters was not represented even though it is a hallmark of the disease.

In this article, we have presented three immortalized muscle cell models for the study of DM1. We have demonstrated that these immortalized cell models behave similarly to the parental cells from which they derive. However, they are heterogeneous, and harbor different molecular alterations that are linked to the presentation of different clinical symptoms in patients. These models will offer new possibilities to understand DM1 from a more diverse point of view. The cells will serve as a tool to study and quantify the degree of certain molecular

Table 4. Comparative table of the characterization of the immortalized DM1 myoblasts/myotubes models available

Cell line	Age of onset/Clinical subtype	Disease progression at sampling	CTG expansion	Epigenetics	RNA foci number	MBNL1 aggregates	Splicing alterations	Differentiation studies	Treatment assessment	Publication
JCC-DM1	15	✓	✓	✓	✓	✓	✓	✓	✓	Núñez-Manchón et al. 2023
GPM-DM1	42	✓	✓	✓	✓	✓	✓	✓	✓	Núñez-Manchón et al. 2023
ADE-DM1	27	✓	✓	✓	✓	✓	✓	✓	✓	Núñez-Manchón et al. 2023
DM1	Infantile	NA	✓	NA	✓	✓	✓	✓	✓	Arandel et al. 2017[44]
DM#1	NA	NA	✓	NA	✓	NA	✓	✓	✓	Pantic et al. 2016[45]
DM#2	NA	NA	✓	NA	✓	NA	✓	✓	✓	Pantic et al. 2016[45]
DM1	Congenital	NA	✓	NA	NA	NA	NA	NA	NA	Bigot et al. 2009[46]

NA, not available.

alterations, and to assess the efficacy of different therapies in a context of different molecular alterations in different genetic backgrounds. Overall, we have generated three cellular models for DM1 that we expect will contribute to the better understanding of this pathology from a more diverse point of view.

Limitations of the study

The main limitation of this study was the limited amount of immortalized cell lines that we were able to generate as it makes it challenging to obtain significant statistical results. Furthermore, these cells were only obtained from females, so there was a sex bias in the data obtained from these three immortalized models.

Another limitation of the study was the unfeasibility of working with the same passage for all the analyzed DM1 cells, which might affect the outcome of some experiments. We observed that the primary cell line with 7 passages, ADE-DM1 was the one that had significantly less RNA foci accumulation and less MBNL1 aggregates than any other (Figure 5). In addition, this cell line was also not responding to the treatment (Figures 8 and S3). Previous unpublished data from our lab showed that this patient-derived primary cell line responded well to this same treatment but at earlier passages. Working with passage 7 may involve cellular alterations, like senescence, which could affect transcriptional activity and response to antisense oligonucleotide treatment.

STAR★METHODS

Detailed methods are provided in the online version of this paper and include the following:

- KEY RESOURCES TABLE
- RESOURCE AVAILABILITY
  - Lead contact
  - Materials availability
  - Data and code availability
- EXPERIMENTAL MODEL AND STUDY PARTICIPANT DETAILS
  - Sample collection and patient characterization
  - Cell culture and immortalization
- METHOD DETAILS
  - CTG expansion sizing
  - DNA methylation analysis
  - Expression analysis by qPCR
  - Impedance measurements
  - Jess Western blot
  - Fluorescence *in situ* hybridization (FISH) and immunocytochemistry (ICC)
  - Splicing analysis
  - Treatment
- QUANTIFICATION AND STATISTICAL ANALYSIS
  - Statistical analysis

SUPPLEMENTAL INFORMATION

Supplemental information can be found online at https://doi.org/10.1016/j.isci.2024.109930.

ACKNOWLEDGMENTS

This research was funded by Instituto de Salud Carlos III grant number PI18/00713 and PI22/00104 (G. Nogales-Gadea), Grants (#21108; #24757) from AFM-Telethon (G. Nogales-Gadea), Ministerio de Ciencia e Innovación grant numbers PID2020-118730RB-I00 (M. Suelves) and PID2020-119780RB-I00 (A. Vallejo-Illarramendi). This work was funded by the Grant CPP2022-009960 and the Grant CNS2022-135519 by MICIU/AEI/10.13039/501100011033 and, by the "European UnionNextGenerationEU/PRTR" (Gisela Nogales Gadea). Departamento de Salud del Gobierno Vasco grant number 2022111045 (A. Vallejo-Illarramendi), IDEA Grant (#7754217 – READ-DM1) funded by the Science Fund of the Republic of Serbia (J. Pesovic, D. Savic-Pavicevic), and Grant Project (#23557) from AFM-Telethon (M. Suelves), and co-financed by Fondos FEDER. J. Núñez-Manchón is funded by Instituto de Salud Carlos III I-PFIS fellowship (grant number IFI20/00022). G. Nogales-Gadea is supported by a Miguel Servet research contract (Instituto de Salud Carlos III CPII19/00021, and FEDER). Pau Maestre is supported by an Investigo Program from Generalitat de Catalunya (100008TC1). Laura Mosqueira-Martin is supported by a PhD fellowship from UPV/EHU. E. Juanola is funded by Rio Hortega Instituto de Salud Carlos III (grant number CM21/00041). We thank Dr. Eduard Gallardo for kindly providing Myf5 antibody. We also thank the IGTP Microscopy Core Facility and staff for their contribution to this publication. The authors wish to acknowledge MyoLine, the platform for the immortalization of human cells from the Institute of Myology in Paris. Artwork shown in the graphical abstract was taken from or adapted from pictures provided by Servier Medical Art (Servier; https://smart.servier.com/), licensed under a Creative Commons Attribution 4.0 Unported License.

CellPress
OPEN ACCESS

iScience
Article

AUTHOR CONTRIBUTIONS

Conceptualization, G.N.G and M.S; methodology, A.B, K.M, and V.M; formal analysis, J.N.M; investigation, J.N.M, J.C; J.P; E.J; L.M.M; P.M.M; and K.G.I; resources, A.M.P; writing – original draft, J.N.M, L.M.M, K.G.I, and G.N.G; writing – review and editing, A.M.P, A.B, V.M, M.S, D.S.P, J.P, R.O; and A.V.L; visualization, J.N.M; supervision, G.N.G and M.S.; funding acquisition, G.N.G and M.S.

DECLARATION OF INTERESTS

The authors declare no competing interests.

Received: July 10, 2023
Revised: March 21, 2024
Accepted: May 3, 2024
Published: May 7, 2024

SUPPORTING CITATIONS

The following references appear in the supplemental information: [81–82].

REFERENCES

1. Bird, T. (1999). Myotonic Dystrophy Type 1 (GeneReviews).
2. Brook, J.D., McCurrach, M.E., Harley, H.G., Buckler, A.J., Church, D., Aburatani, H., Hunter, K., Stanton, V.P., Thirion, J.P., Hudson, T., et al. (1992). Molecular basis of myotonic dystrophy: Expansion of a trinucleotide (CTG) repeat at the 3′ end of a transcript encoding a protein kinase family member. Cell *68*, 799–808. https://doi.org/10.1016/0092-8674(92)90154-5.
3. Ashizawa, T., Anvret, M., Baiget, M., Barcelo, J.M., Brunner, H., Cobo, A.M., Dallapiccola, B., Fenwick, R.G., Grandell, U., Harley, H., et al. (1994). Characteristics of Intergenerational Contractions of the CTG Repeat in Myotonic Dystrophy.
4. Martorell, L., Martinez, J.M., Carey, N., Johnson, K., and Baiget, M. (1995). Comparison of CTG repeat length expansion and clinical progression of myotonic dystrophy over a five year period. J. Med. Genet. *32*, 593–596. https://doi.org/10.1136/jmg.32.8.593.
5. Wong, L.J.C., Ashizawa, T., Monckton, D.G., Caskey, C.T., and Richards, C.S. (1995). Somatic heterogeneity of the CTG repeat in myotonic-dystrophy is age and size-dependent. Am. J. Hum. Genet. *56*, 114–122.
6. Ballester-Lopez, A., Koehorst, E., Linares-Pardo, I., Núñez-Manchón, J., Almendrote, M., Lucente, G., Arbex, A., Alonso, C.P., Lucia, A., Monckton, D.G., et al. (2020). Preliminary findings on ctg expansion determination in different tissues from patients with myotonic dystrophy type 1. Genes *11*, 1–8. https://doi.org/10.3390/genes11111321.
7. Kinoshita, M., Takahashi, R., Hasegawa, T., Komori, T., Nagasawa, R., Hirose, K., and Tanabe, H. (1996). (CTG)n expansions in various tissues from a myotonic dystrophy patient. Muscle Nerve *19*, 240–242. https://doi.org/10.1002/(SICI)1097-4598(199602)19:2<240::AID-MUS21>3.0.CO;2-X.
8. Ballester-Lopez, A., Linares-Pardo, I., Koehorst, E., Núñez-Manchón, J., Pintos-Morell, G., Coll-Cantí, J., Almendrote, M., Lucente, G., Arbex, A., Magaña, J.J., et al. (2020). The need for establishing a universal CTG sizing method in myotonic dystrophy type 1. Genes *11*, 1–9. https://doi.org/10.3390/genes11070757.
9. Gomes-Pereira, M., Bidichandani, S.I., and Monckton, D.G. (2004). Analysis of unstable triplet repeats using small-pool polymerase chain reaction. Methods Mol. Biol. *277*, 61–76. https://doi.org/10.1385/1-59259-804-8:061.
10. Barbé, L., Lanni, S., López-Castel, A., Franck, S., Spits, C., Keymolen, K., Seneca, S., Tomé, S., Miron, I., Letourneau, J., et al. (2017). CpG Methylation, a Parent-of-Origin Effect for Maternal-Biased Transmission of Congenital Myotonic Dystrophy. Am. J. Hum. Genet. *100*, 488–505. https://doi.org/10.1016/j.ajhg.2017.01.033.
11. Morales, F., Corrales, E., Zhang, B., Vásquez, M., Santamaría-Ulloa, C., Quesada, H., Sirito, M., Estecio, M.R., Monckton, D.G., and Krahe, R. (2021). Myotonic dystrophy type 1 (DM1) clinical sub-types and CTCF site methylation status flanking the CTG expansion are mutant allele length-dependent. Hum. Mol. Genet. *31*, 262–274. https://doi.org/10.1093/HMG/DDAB243.
12. Koehorst, E., Odria, R., Capó, J., Núñez-Manchón, J., Arbex, A., Almendrote, M., Linares-Pardo, I., Benito, D.N.D., Saez, V., Nascimento, A., et al. (2022). An Integrative Analysis of DNA Methylation Pattern in Myotonic Dystrophy Type 1 Samples Reveals a Distinct DNA Methylation Profile between Tissues and a Novel Muscle-Associated Epigenetic Dysregulation. Biomedicines *10*, 1372. https://doi.org/10.3390/BIOMEDICINES10061372.
13. Boucher, C.A., King, S.K., Carey, N., Krahe, R., Winchester, C.L., Rahman, S., Creavin, T., Mehji, P., Bailey, M.E.S., Chartier, F.L., et al. (1995). A novel homeodomain-encoding gene is associated with a large CpG island interrupted by the myotonic dystrophy unstable (CTG)n repeat. Hum. Mol. Genet. *4*, 1919–1925. https://doi.org/10.1093/HMG/4.10.1919.
14. Barbé, L., Lanni, S., López-Castel, A., Franck, S., Spits, C., Keymolen, K., Seneca, S., Tomé, S., Miron, I., Letourneau, J., et al. (2017). CpG Methylation, a Parent-of-Origin Effect for Maternal-Biased Transmission of Congenital Myotonic Dystrophy. Am. J. Hum. Genet. *100*, 488–505. https://doi.org/10.1016/j.ajhg.2017.01.033.
15. Morales, F., Corrales, E., Zhang, B., Vásquez, M., Santamaría-Ulloa, C., Quesada, H., Sirito, M., Estecio, M.R., Monckton, D.G., and Krahe, R. (2022). Myotonic dystrophy type 1 (DM1) clinical subtypes and CTCF site methylation status flanking the CTG expansion are mutant allele length-dependent. Hum. Mol. Genet. *31*, 262–274. https://doi.org/10.1093/hmg/ddab243.
16. Inukai, A., Doyu, M., Kato, T., Liang, Y., Kuru, S., Yamamoto, M., Kobayashi, Y., and Sobue, G. (2000). Reduced expression of DMAHP/SIX5 gene in myotonic dystrophy muscle. Muscle Nerve *23*, 1421–1426. https://doi.org/10.1002/1097-4598(200009)23:9<1421::AID-MUS14>3.0.CO;2-Y.
17. Alwazzan, M., Newman, E., Hamshere, M.G., and Brook, J.D. (1999). Myotonic dystrophy is associated with a reduced level of RNA from the DMWD allele adjacent to the expanded repeat. Hum. Mol. Genet. *8*, 1491–1497. https://doi.org/10.1093/hmg/8.8.1491.
18. Kanadia, R.N., Johnstone, K.A., Mankodi, A., Lungu, C., Thornton, C.A., Esson, D., Timmers, A.M., Hauswirth, W.W., and Swanson, M.S. (2003). A Muscleblind Knockout Model for Myotonic Dystrophy. Science *302*, 1978–1980. https://doi.org/10.1126/science.1088583.
19. Mankodi, A., Logigian, E., Callahan, L., Mcclain, C., White, R., Henderson, D., and Krym, M. (2000). Myotonic Dystrophy in Transgenic Mice Expressing an Expanded CUG Repeat. Science *289*, 1769–1772. https://doi.org/10.1126/science.289.5485.176.
20. Taneja, K.L., McCurrach, M., Schalling, M., Housman, D., and Singer, R.H. (1995). Foci of trinucleotide repeat transcripts in nuclei of myotonic dystrophy cells and tissues. J. Cell Biol. *128*, 995–1002. https://doi.org/10.1083/jcb.128.6.995.
21. Michalowski, S., Miller, J.W., Urbinati, C.R., Paliouras, M., Swanson, M.S., and Griffith, J. (1999). Visualization of double-stranded RNAs from the myotonic dystrophy protein kinase gene and interactions with CUG-binding protein. Nucleic Acids Res. *27*, 3534–3542. https://doi.org/10.1093/nar/27.17.3534.
22. Botta, A., Rinaldi, F., Catalli, C., Vergani, L., Bonifazi, E., Romeo, V., Loro, E., Viola, A., Angelini, C., and Novelli, G. (2008). The CTG repeat expansion size correlates with the splicing defects observed in muscles from

myotonic dystrophy type 1 patients. J. Med. Genet. *45*, 639–646. https://doi.org/10.1136/JMG.2008.058909.

23. Ballester-Lopez, A., Núñez-Manchón, J., Koehorst, E., Linares-Pardo, I., Almendrote, M., Lucente, G., Guanyabens, N., Lopez-Osias, M., Suárez-Mesa, A., Hanick, S.A., et al. (2020). Three-dimensional imaging in myotonic dystrophy type 1: Linking molecular alterations with disease phenotype. Neurol. Genet. *6*, e484. https://doi.org/10.1212/NXG.0000000000000484.
24. Miller, J.W., Urbinati, C.R., Teng-Umnuay, P., Stenberg, M.G., Byrne, B.J., Thornton, C.A., and Swanson, M.S. (2000). Recruitment of human muscleblind proteins to (CUG)(n) expansions associated with myotonic dystrophy. EMBO J. *19*, 4439–4448. https://doi.org/10.1093/emboj/19.17.4439.
25. Ho, T.H., Charlet-B, N., Poulos, M.G., Singh, G., Swanson, M.S., and Cooper, T.A. (2004). Muscleblind proteins regulate alternative splicing. EMBO J. *23*, 3103–3112. https://doi.org/10.1038/sj.emboj.7600300.
26. Hino, S.I., Kondo, S., Sekiya, H., Saito, A., Kanemoto, S., Murakami, T., Chihara, K., Aoki, Y., Nakamori, M., Takahashi, M.P., et al. (2007). Molecular mechanisms responsible for aberrant splicing of SERCA1 in myotonic dystrophy type 1. Hum. Mol. Genet. *16*, 2834–2843. https://doi.org/10.1093/hmg/ddm239.
27. Yamashita, Y., Matsuura, T., Kurosaki, T., Amakusa, Y., Kinoshita, M., Ibi, T., Sahashi, K., and Ohno, K. (2014). LDB3 splicing abnormalities are specific to skeletal muscles of patients with myotonic dystrophy type 1 and alter its PKC binding affinity. Neurobiol. Dis. *69*, 200–205. https://doi.org/10.1016/j.nbd.2014.05.026.
28. Rau, F., Lainé, J., Ramanoudjame, L., Ferry, A., Arandel, L., Delalande, O., Jollet, A., Dingli, F., Lee, K.Y., Peccate, C., et al. (2015). Abnormal splicing switch of DMD's penultimate exon compromises muscle fibre maintenance in myotonic dystrophy. Nat. Commun. *6*, 7502. https://doi.org/10.1038/ncomms8205.
29. Fugier, C., Klein, A.F., Hammer, C., Vassilopoulos, S., Ivarsson, Y., Toussaint, A., Tosch, V., Vignaud, A., Ferry, A., Messaddeq, N., et al. (2011). Misregulated alternative splicing of BIN1 is associated with T tubule alterations and muscle weakness in myotonic dystrophy. Nat. Med. *17*, 720–725. https://doi.org/10.1038/NM.2374.
30. Lin, X., Miller, J.W., Mankodi, A., Kanadia, R.N., Yuan, Y., Moxley, R.T., Swanson, M.S., and Thornton, C.A. (2006). Failure of MBNL1-dependent post-natal splicing transitions in myotonic dystrophy. Hum. Mol. Genet. *15*, 2087–2097. https://doi.org/10.1093/hmg/ddl132.
31. Savkur, R.S., Philips, A.V., and Cooper, T.A. (2001). Aberrant regulation of insulin receptor alternative splicing is associated with insulin resistance in myotonic dystrophy. Nat. Genet. *29*, 40–47. https://doi.org/10.1038/ng704.
32. Fugier, C., Klein, A.F., Hammer, C., Vassilopoulos, S., Ivarsson, Y., Toussaint, A., Tosch, V., Vignaud, A., Ferry, A., Messaddeq, N., et al. (2011). Misregulated alternative splicing of BIN1 is associated with T tubule alterations and muscle weakness in myotonic dystrophy. Nat. Med. *17*, 720–725. https://doi.org/10.1038/nm.2374.
33. Yamamoto, T., Miura, A., Itoh, K., Takeshima, Y., and Nishio, H. (2019). RNA sequencing reveals abnormal LDB3 splicing in sudden cardiac death. Forensic Sci. Int. *302*, 109906. https://doi.org/10.1016/j.forsciint.2019.109906.
34. Kimura, T., Nakamori, M., Lueck, J.D., Pouliquin, P., Aoike, F., Fujimura, H., Dirksen, R.T., Takahashi, M.P., Dulhunty, A.F., and Sakoda, S. (2005). Altered mRNA splicing of the skeletal muscle ryanodine receptor and sarcoplasmic/endoplasmic reticulum Ca2+-ATPase in myotonic dystrophy type 1. Hum. Mol. Genet. *14*, 2189–2200. https://doi.org/10.1093/hmg/ddi223.
35. Rau, F., Lainé, J., Ramanoudjame, L., Ferry, A., Arandel, L., Delalande, O., Jollet, A., Dingli, F., Lee, K.Y., Peccate, C., et al. (2015). Abnormal splicing switch of DMD's penultimate exon compromises muscle fibre maintenance in myotonic dystrophy. Nat. Commun. *6*, 7205. https://doi.org/10.1038/ncomms8205.
36. Lee, J.E., Bennett, C.F., and Cooper, T.A. (2012). RNase H-mediated degradation of toxic RNA in myotonic dystrophy type 1. Proc. Natl. Acad. Sci. USA *109*, 4221–4226. https://doi.org/10.1073/pnas.1117019109.
37. Wojtkowiak-Szlachcic, A., Taylor, K., Stepniak-Konieczna, E., Sznajder, L.J., Mykowska, A., Sroka, J., Thornton, C.A., and Sobczak, K. (2015). Short antisense-locked nucleic acids (all-LNAs) correct alternative splicing abnormalities in myotonic dystrophy. Nucleic Acids Res. *43*, 3318–3331. https://doi.org/10.1093/nar/gkv163.
38. Matloka, M., Klein, A.F., Rau, F., and Furling, D. (2018). Cells of matter-In vitro models for myotonic dystrophy. Front. Neurol. *9*, 1–9. https://doi.org/10.3389/fneur.2018.00361.
39. Philips, A.V., Timchenko, L.T., and Cooper, T.A. (1998). Disruption of splicing regulated by a CUG-binding protein in myotonic dystrophy. Science *280*, 737–741. https://doi.org/10.1126/science.280.5364.737.
40. Manandhar, D., Song, L., Kabadi, A., Kwon, J.B., Edsall, L.E., Ehrlich, M., Tsumagari, K., Gersbach, C.A., Crawford, G.E., and Gordân, R. (2017). Incomplete MyoD-induced transdifferentiation is associated with chromatin remodeling deficiencies. Nucleic Acids Res. *45*, 11684–11699. https://doi.org/10.1093/nar/gkx773.
41. Spitalieri, P., Talarico, R.V., Caioli, S., Murdocca, M., Serafino, A., Girasole, M., Dinarelli, S., Longo, G., Pucci, S., Botta, A., et al. (2018). Modelling the pathogenesis of Myotonic Dystrophy type 1 cardiac phenotype through human iPSC-derived cardiomyocytes. J. Mol. Cell. Cardiol. *118*, 95–109. https://doi.org/10.1016/j.yjmcc.2018.03.012.
42. Ueki, J., Nakamori, M., Nakamura, M., Nishikawa, M., Yoshida, Y., Tanaka, A., Morizane, A., Kamon, M., Araki, T., Takahashi, M.P., et al. (2017). Myotonic dystrophy type 1 patient-derived iPSCs for the investigation of CTG repeat instability. Sci. Rep. *7*, 1–7. https://doi.org/10.1038/srep42522.
43. Maqsood, M.I., Matin, M.M., Bahrami, A.R., and Ghasroldasht, M.M. (2013). Immortality of cell lines: Challenges and advantages of establishment. Cell Biol. Int. *37*, 1038–1045. https://doi.org/10.1002/cbin.10137.
44. Arandel, L., Espinoza, M.P., Matloka, M., Bazinet, A., De Dea Diniz, D., Naouar, N., Rau, F., Jollet, A., Edom-Vovard, F., Mamchaoui, K., et al. (2017). Immortalized human myotonic dystrophy muscle cell lines to assess therapeutic compounds. DMM Dis. Model. Mech. *10*, 487–497. https://doi.org/10.1242/dmm.027367.
45. Pantic, B., Borgia, D., Giunco, S., Malena, A., Kiyono, T., Salvatori, S., De Rossi, A., Giardina, E., Sangiuolo, F., Pegoraro, E., et al. (2016). Reliable and versatile immortal muscle cell models from healthy and myotonic dystrophy type 1 primary human myoblasts. Exp. Cell Res. *342*, 39–51. https://doi.org/10.1016/j.yexcr.2016.02.013.
46. Bigot, A., Klein, A.F., Gasnier, E., Jacquemin, V., Ravassard, P., Butler-Browne, G., Mouly, V., and Furling, D. (2009). Large CTG repeats trigger p16-dependent premature senescence in myotonic dystrophy type 1 muscle precursor cells. Am. J. Pathol. *174*, 1435–1442. https://doi.org/10.2353/ajpath.2009.080560.
47. Romagnoli, C., and Brandi, M.L. (2021). Muscle Physiopathology in Parathyroid Hormone Disorders. Front. Med. *8*, 1–7. https://doi.org/10.3389/fmed.2021.764346.
48. Manning, K.S., Rao, A.N., Castro, M., and Cooper, T.A. (2017). BNANC Gapmers Revert Splicing and Reduce RNA Foci with Low Toxicity in Myotonic Dystrophy Cells. ACS Chem. Biol. *12*, 2503–2509. https://doi.org/10.1021/ACSCHEMBIO.7B00416/SUPPL_FILE/CB7B00416_SI_001.PDF.
49. Morales, F., Couto, J.M., Higham, C.F., Hogg, G., Cuenca, P., Braida, C., Wilson, R.H., Adam, B., del Valle, G., Brian, R., et al. (2012). Somatic instability of the expanded CTG triplet repeat in myotonic dystrophy type 1 is a heritable quantitative trait and modifier of disease severity. Hum. Mol. Genet. *21*, 3558–3567. https://doi.org/10.1093/hmg/dds185.
50. Cumming, S.A., Jimenez-Moreno, C., Okkersen, K., Wenninger, S., Daidj, F., Hogarth, F., Littleford, R., Gorman, G., Bassez, G., Schoser, B., et al. (2019). Genetic determinants of disease severity in the myotonic dystrophy type 1 OPTIMISTIC cohort. Neurology *93*, e995–e1009. https://doi.org/10.1212/WNL.0000000000008056.
51. Pešović, J., Perić, S., Brkušanin, M., Brajušković, G., Rakočević -Stojanović, V., and Savić-Pavić Ević, D. (2018). Repeat Interruptions Modify Age at Onset in Myotonic Dystrophy Type 1 by Stabilizing DMPK Expansions in Somatic Cells. Front. Genet. *9*, 1–14. https://doi.org/10.3389/FGENE.2018.00601.
52. Ballester-Lopez, A., Koehorst, E., Linares-Pardo, I., Núñez-Manchón, J., Almendrote, M., Lucente, G., Arbex, A., Alonso, C.P., Lucia, A., Monckton, D.G., et al. (2020). Preliminary Findings on CTG Expansion Determination in Different Tissues from Patients with Myotonic Dystrophy Type 1. Genes *11*, 1–8. https://doi.org/10.3390/GENES11111321.
53. Tsai, Y.C., de Pontual, L., Heiner, C., Stojkovic, T., Furling, D., Bassez, G., Gourdon, G., and Tomé, S. (2022). Identification of a CCG-Enriched Expanded Allele in Patients with Myotonic Dystrophy Type 1 Using Amplification-Free Long-Read Sequencing. J. Mol. Diagn. *24*, 1143–1154. https://doi.org/10.1016/J.JMOLDX.2022.08.003.
54. Rasmussen, A., Hildonen, M., Vissing, J., Duno, M., Tümer, Z., and Birkedal, U. (2022). High Resolution Analysis of DMPK Hypermethylation and Repeat Interruptions in Myotonic Dystrophy Type 1. Genes *13*, 970. https://doi.org/10.3390/GENES13060970.
55. Jones, P.A., Wolkowicz, M.J., Rideout, W.M., Gonzales, F.A., Marziasz, C.M., Coetzee, G.A., and Tapscott, S.J. (1990). De novo methylation of the MyoD1 CpG island during

the establishment of immortal cell lines. Proc. Natl. Acad. Sci. USA *87*, 6117–6121. https://doi.org/10.1073/pnas.87.16.6117.

56. Antequera, F., and J Boyes, A.B. (1990). High levels of de novo methylation and altered chromatin structure at CpG islands in cell lines. Cell *62*, 503–514. https://doi.org/10.1016/0092-8674(90)90015-7.
57. Jones, P.A. (2012). Functions of DNA methylation: islands, start sites, gene bodies and beyond. Nat. Rev. Genet. *13*, 484–492. https://doi.org/10.1038/NRG3230.
58. Carrió, E., Díez-Villanueva, A., Lois, S., Mallona, I., Cases, I., Forn, M., Peinado, M.A., and Suelves, M. (2015). Deconstruction of DNA methylation patterns during myogenesis reveals specific epigenetic events in the establishment of the skeletal muscle lineage. Stem Cell. *33*, 2025–2036. https://doi.org/10.1002/STEM.1998.
59. Reik, W. (2007). Stability and flexibility of epigenetic gene regulation in mammalian development. Nature *447*, 425–432. https://doi.org/10.1038/NATURE05918.
60. Fu, Y.H., Friedman, D.L., Richards, S., Pearlman, J.A., Gibbs, R.A., Pizzuti, A., Ashizawa, T., Perryman, M.B., Scarlato, G., Fenwick, R.G., et al. (1993). Decreased expression of myotonin-protein kinase messenger RNA and protein in adult form of myotonic dystrophy. Science *260*, 235–238. https://doi.org/10.1126/SCIENCE.8469976.
61. Klesert, T.R., Otten, A.D., and T D Bird, S.J.T. (1997). Trinucleotide repeat expansion at the myotonic dystrophy locus reduces expression of DMAHP. Nat. Genet. *16*, 402–406. https://doi.org/10.1038/ng0897-402.
62. Alwazzan, M., Newman, E., and M G Hamshere, J.D.B. (1999). Myotonic dystrophy is associated with a reduced level of RNA from the DMWD allele adjacent to the expanded repeat. Hum. Mol. Genet. *8*, 1491–1497. https://doi.org/10.1093/hmg/8.8.1491.
63. Klesert, T.R., Cho, D.H., Clark, J.I., Maylie, J., Adelman, J., Snider, L., Yuen, E.C., Soriano, P., and Tapscott, S.J. (2000). Mice deficient in Six5 develop cataracts: implications for myotonic dystrophy. Nat. Genet. *25*, 105–109. https://doi.org/10.1038/75490.
64. Westerlaken, J.H.A.M., Van Der Zee, C.E.E.M., Peters, W., and Wieringa, B. (2003). The DMWD protein from the myotonic dystrophy (DM1) gene region is developmentally regulated and is present most prominently in synapse-dense brain areas. Brain Res. *971*, 116–127. https://doi.org/10.1016/S0006-8993(03)02430-2.
65. Yin, Q., Wang, H., Li, N., Ding, Y., Xie, Z., Jin, L., Li, Y., Wang, Q., Liu, X., Xu, L., et al. (2020). Dosage effect of multiple genes accounts for multisystem disorder of myotonic dystrophy type 1. Cell Res. *30*, 133–145. https://doi.org/10.1038/S41422-019-0264-2.
66. Khajavi, M., Tari, A.M., Patel, N.B., Tsuji, K., Siwak, D.R., Meistrich, M.L., Terry, N.H., and Ashizawa, T. (2001). "Mitotic drive" of expanded CTG repeats in myotonic dystrophy type 1 (DM1). Hum. Mol. Genet. *10*, 855–863. https://doi.org/10.1093/hmg/10.8.855.
67. André, L.M., van Cruchten, R.T.P., Willemse, M., Bezstarosti, K., Demmers, J.A.A., van Agtmaal, E.L., Wansink, D.G., and Wieringa, B. (2019). Recovery in the myogenic program of congenital myotonic dystrophy myoblasts after excision of the expanded (CTG)n repeat. Int. J. Mol. Sci. *20*, 5685. https://doi.org/10.3390/ijms20225685.
68. Fernández-Garibay, X., Ortega, M.A., Cerro-Herreros, E., Comelles, J., Martínez, E., Artero, R., Fernández-Costa, J.M., and Ramón-Azcón, J. (2021). Bioengineered in vitro 3D model of myotonic dystrophy type 1 human skeletal muscle. Biofabrication *13*, 035035. https://doi.org/10.1088/1758-5090/abf6ae.
69. Guglielmi, V., Vattemi, G., Gualandi, F., Voermans, N.C., Marini, M., Scotton, C., Pegoraro, E., Oosterhof, A., Kósa, M., Zádor, E., et al. (2013). SERCA1 protein expression in muscle of patients with Brody disease and Brody syndrome and in cultured human muscle fibers. Mol. Genet. Metab. *110*, 162–169. https://doi.org/10.1016/j.ymgme.2013.07.015.
70. Kawada, R., Jonouchi, T., Kagita, A., Sato, M., Hotta, A., and Sakurai, H. (2023). Establishment of quantitative and consistent in vitro skeletal muscle pathological models of myotonic dystrophy type 1 using patient-derived iPSCs. Sci. Rep. *13*, 1–17. https://doi.org/10.1038/s41598-022-26614-z.
71. Nakamori, M., Sobczak, K., Puwanant, A., Welle, S., Eichinger, K., Pandya, S., Dekdebrun, J., Heatwole, C.R., McDermott, M.P., Chen, T., et al. (2013). Splicing biomarkers of disease severity in myotonic dystrophy. Ann. Neurol. *74*, 862–872. https://doi.org/10.1002/ana.23992.
72. Pascual-Gilabert, M., Artero, R., and López-Castel, A. (2023). The myotonic dystrophy type 1 drug development pipeline: 2022 edition. Drug Discov. Today *28*, 103489. https://doi.org/10.1016/j.drudis.2023.103489.
73. Batra, R., Nelles, D.A., Roth, D.M., Krach, F., Nutter, C.A., Tadokoro, T., Thomas, J.D., Sznajder, Ł.J., Blue, S.M., Gutierrez, H.L., et al. (2021). The sustained expression of Cas9 targeting toxic RNAs reverses disease phenotypes in mouse models of myotonic dystrophy type 1. Nat. Biomed. Eng. *5*, 157–168. https://doi.org/10.1038/s41551-020-00607-7.
74. Lo Scrudato, M., Poulard, K., Sourd, C., Tomé, S., Klein, A.F., Corre, G., Huguet, A., Furling, D., Gourdon, G., and Buj-Bello, A. (2019). Genome Editing of Expanded CTG Repeats within the Human DMPK Gene Reduces Nuclear RNA Foci in the Muscle of DM1 Mice. Mol. Ther. *27*, 1372–1388. https://doi.org/10.1016/j.ymthe.2019.05.021.
75. Raaijmakers, R.H.L., Ripken, L., Ausems, C.R.M., and Wansink, D.G. (2019). CRISPR/Cas Applications in Myotonic Dystrophy: Expanding Opportunities. Int. J. Mol. Sci. *20*, 3689. https://doi.org/10.3390/IJMS20153689.
76. Hu, N., Antoury, L., Baran, T.M., Mitra, S., Bennett, C.F., Rigo, F., Foster, T.H., and Wheeler, T.M. (2018). Non-invasive monitoring of alternative splicing outcomes to identify candidate therapies for myotonic dystrophy type 1. Nat. Commun. *9*, 5227. https://doi.org/10.1038/s41467-018-07517-y.
77. Hsieh, W.C., Bahal, R., Thadke, S.A., Bhatt, K., Sobczak, K., Thornton, C., and Ly, D.H. (2018). Design of a "mini" Nucleic Acid Probe for Cooperative Binding of an RNA-Repeated Transcript Associated with Myotonic Dystrophy Type 1. Biochemistry *57*, 907–911. https://doi.org/10.1021/acs.biochem.7b01239.
78. Arandel, L., Matloka, M., Klein, A.F., Rau, F., Sureau, A., Ney, M., Cordier, A., Kondili, M., Polay-Espinoza, M., Naouar, N., et al. (2022). Reversal of RNA toxicity in myotonic dystrophy via a decoy RNA-binding protein with high affinity for expanded CUG repeats. Nat. Biomed. Eng. *6*, 207–220. https://doi.org/10.1038/s41551-021-00838-2.
79. Cerro-Herreros, E., González-Martínez, I., Moreno-Cervera, N., Overby, S., Pérez-Alonso, M., Llamusí, B., and Artero, R. (2020). Therapeutic Potential of AntagomiR-23b for Treating Myotonic Dystrophy. Mol. Ther. Nucleic Acids *21*, 837–849. https://doi.org/10.1016/J.OMTN.2020.07.021.
80. Ketley, A., Chen, C.Z., Li, X., Arya, S., Robinson, T.E., Granados-Riveron, J., Udosen, I., Morris, G.E., Holt, I., Furling, D., et al. (2014). High-content screening identifies small molecules that remove nuclear foci, affect MBNL distribution and CELF1 protein levels via a PKC-independent pathway in myotonic dystrophy cell lines. Hum. Mol. Genet. *23*, 1551–1562. https://doi.org/10.1093/HMG/DDT542.
81. François, V., Klein, A.F., Beley, C., Jollet, A., Lemercier, C., Garcia, L., and Furling, D. (2010). Selective silencing of mutated mRNAs in DM1 by using modified hU7-snRNAs. Nat. Struct. Mol. Biol. *18*, 85–87. https://doi.org/10.1038/nsmb.1958.
82. Wang, Y., Hao, L., Wang, H., Santostefano, K., Thapa, A., Cleary, J., Li, H., Guo, X., Terada, N., Ashizawa, T., et al. (2018). Therapeutic Genome Editing for Myotonic Dystrophy Type 1 Using CRISPR/Cas9. Mol. Ther. *26*, 2617. https://doi.org/10.1016/J.YMTHE.2018.09.003.
83. Mamchaoui, K., Trollet, C., Bigot, A., Negroni, E., Chaouch, S., Wolff, A., Kandalla, P.K., Marie, S., Di Santo, J., St Guily, J.L., et al. (2011). Immortalized pathological human myoblasts: towards a universal tool for the study of neuromuscular disorders. Skelet. Muscle *1*, 34. https://doi.org/10.1186/2044-5040-1-34.
84. Mallona, I., Díez-Villanueva, A., and Peinado, M.A. (2014). Methylation plotter: a web tool for dynamic visualization of DNA methylation data. Source Code Biol. Med. *9*, 11. https://doi.org/10.1186/1751-0473-9-11.

STAR★METHODS

KEY RESOURCES TABLE

REAGENT or RESOURCE	SOURCE	IDENTIFIER
Antibodies		
Mouse anti-MBNL1	DSHB	Cat# MB1a(4A8), RRID:AB_2618248)
Mouse monocolonal anti-Desmin	Abcam	Cat# ab8470, RRID:AB_306577
Rabbit polyclonal MyoD Antibody	Santa Cruz Biotechnology	Cat# sc-304, RRID:AB_631992
Mouse monocolonal anti- myogenin	Santa Cruz Biotechnology	Cat# sc-12732, RRID:AB_627980
Rabbit polyclonal Myf-5 antibody	Santa Cruz Biotechnology	Cat# sc-302, RRID:AB_631994
Bacterial and virus strains		
hTERT lentiviral vectors	Mamchaoui et al.[83]	NA
Cdk4 lentiviral vectors	Mamchaoui et al.[83]	NA
Critical commercial assays		
EZ DNA Methylation Gold kit	Zymo Research	Cat#D5005
Experimental models: Cell lines		
Human primary DM1 myoblasts: JCC-DM1, GPM.DM1, ADE-DM1	This paper	NA
Human primary control myoblasts: C7, C9, C11	This paper	NA
Human immortalized DM1 myoblasts: iJCC-DM1, iGPM.DM1, iADE-DM1	This paper	NA
Human immortalized control myoblasts: AB678, AB1079, KM1421	This paper	NA
Oligonucleotides		
DIG-labelled LNA $(CAG)_7$	MOLBIOL	NA
CTCF1 Fwd1 5′-TGTYGTYGTTTTGGGTTGTATTG-3′	ThermoFisher	NA
CTCF1 Rev1 5′-TTCCYGACTACAAAAACCCTTYG-3′	ThermoFisher	NA
CTCF1 Fwd2 5′-GTTGTATTGGGTTGGTGGTTTA-3′	ThermoFisher	NA
CTCF1 Rev2 5′-CTACAAAAACCCTTYGAACCC-3′	ThermoFisher	NA
Primers for qPCR, see Table S1	ThermoFisher	NA
Primers for splicing analysis, see Table S2	ThermoFisher	NA
BNANC gapmer with the sequence AGCagcagcagCAG	Bio-Synthesis	NA
101 Rev 5′-CTTCCCAGGCCTGCAGTTTGCCCATC-3′	ThermoFisher	NA
102 Fwd 5′-GAACGGGGCTCGAAGGGTCCTTGTAGC-3′	ThermoFisher	NA
Software and algorithms		
GelAnalyzer 19.1	GelAnalyzer	http://www.gelanalyzer.com/?i=1
Chromas version 2.6.6.	Technelysium	https://technelysium.com.au/wp/chromas/
LightCycler 480	Roche	https://diagnostics.roche.com/global/en/products/instruments/lightcycler-480-ins-445.html
AxIS Z	Axion Biosystems	https://www.axionbiosystems.com/resources/product-brochure/axis-z-21-cfr-part-11-statement
ZEN blue	ZEISS	https://www.zeiss.com/microscopy/es/productos/software/zeiss-zen.html

(Continued on next page)

Continued

REAGENT or RESOURCE	SOURCE	IDENTIFIER
GraphPad Prism 8	Graphpad	https://www.graphpad.com/
ImageJ	NIH	https://imagej.nih.gov/ij/download.html
Other		
Methylation Plotter web tool	Mallona et al.[84]	http://maplab.imppc.org/methylation_plotter/

RESOURCE AVAILABILITY

Lead contact

Further information and requests for resources and reagents should be directed to and will be fulfilled by the lead contact, Gisela Nogales-Gadea (gnogales@igtp.cat).

Materials availability

Immortalized cell lines iJCC-DM1, iGPM-DM1 and iADE-DM1 are available upon reasonable request.

Data and code availability

- All data reported in this paper will be shared by the lead contact upon request.
- This paper does not report original code.
- Any additional information required to reanalyse the data reported in this paper is available from the lead contact upon request.

EXPERIMENTAL MODEL AND STUDY PARTICIPANT DETAILS

Sample collection and patient characterization

This study was approved by the Ethics Committee of the University Hospital Germans Trias i Pujol and was performed in accordance with the Declaration of Helsinki for Human Research. Written informed consent was obtained from all participants. Three genetically confirmed DM1 patients with different clinical features aged 36, 39 and 42 were selected to perform the immortalization of biopsy-derived primary myoblasts. The biopsies from the patients were obtained from left biceps. Two different types of controls, obtained from different individuals, were used: primary controls, whose biopsies were obtained from intrinsic hand muscles and immortalized controls that were obtained from healthy individuals quadriceps (AB678, AB1079) and paravertebral muscles (KM1412). Clinical information of DM1 patients was obtained from medical records.

Cell culture and immortalization

Primary myoblasts were isolated from muscle biopsy explants on culture plates treated with human plasma and gelatin 1.5% and then purified by CD56 magnetic separation according to manufacturer's instructions (Miltenyi Biotec; Bergisch Gladbach). Primary myoblasts were grown on 0.1% gelatin-coated flasks in proliferation medium containing Dulbecco's Modified Eagle's Medium (DMEM) supplemented with 10% FBS, 22% M-199, PSF 1x, 10 µg/mL insulin, L-glutamine 2 mM, 25 ng/mL FGF and 5 ng/mL EGF. At 80–90% confluence proliferation medium was substituted by differentiation medium containing DMEM supplemented with 2% FBS, 22% M-199, PSF 1×, 10 µg/mL insulin and L-glutamine 2 mM. For immortalization, 50.000 primary myoblasts were transduced with hTERT and Cdk4 lentiviral vectors with a MOI of 3 in the presence of 4 µg/mL of polybrene (Sigma-Aldrich) overnight. 48 h after, transduced cell cultures were selected with puromycin (1 µg/mL, LifeTechnologies) for 6 days and neomycin (0.1 mg/mL, Life Technologies) for 10 days. Cells were then seeded at clonal density (2 cells per cm2) for 10 days. Selected individual myogenic clones were isolated from each population, using glass cylinders, and their proliferation and differentiation capacities were evaluated. We selected clones which were able to proliferate and to differentiate correctly (we tested their ability to differentiate into myotubes, using immunostaining with MF20 antibody, which recognizes all skeletal-muscle myosin heavy chains (MyHCs). We removed the non-myogenic clones. [83] Immortalized myoblasts were grown on uncoated flasks in proliferation medium containing DMEM supplemented with 16% M-199, 20% FBS, Gentamycin 50 µg/mL, fetuin 25 µg/mL, hEGF 5 ng/mL, bFGF 0.5 ng/mL, Insulin 5 µg/mL and dexamethasone 0,2 µg/mL. For differentiation experiments cells were grown in 1:100 matrigel matrix (Corning) coated surfaces until 80–90% confluence. Proliferation medium was substituted by differentiation medium containing DMEM supplemented with 10 µg/mL of insulin and 50 µg/mL Gentamycin. Both primary and immortalized myoblasts were differentiated into myotubes for 5 or 9 days, depending on the experiment. Pellets for RNA and DNA analysis were collected and coverslips for FISH and ICC were fixed with 4% PFA and permeabilized with 0.3% Triton. We performed an STR variant analysis of 16 locus for cell authentication purposes. Mycoplasma test was performed both before and after the immortalization and it turned out negative for all the cell lines.

METHOD DETAILS

CTG expansion sizing

DNA from the primary and immortalized myotube cultures was extracted using the PureLink Genomic DNA Mini Kit (Invitrogen) according to the manufacturer's instructions. To determine CTG expansion size we performed a small-pool PCR from EcoRI digested DNA followed by Southern blotting. The PCR was performed with 5 ng of digested DNA, using Expand Long Template PCR System (Roche) and primers 102 (5′-GAACGGGGCTCGAAGGGTCCTTGTAGC-3′) and 101 (5′-CTTCCCAGGCCTGCAGTTTGCCCATC-3′). The conditions of the PCR were divided in four steps: 1) 3′ at 96°C. 2) 30″ at 65°C followed by 3′ at 68°C and 30″ at 95°C for 10 cycles. 3) 30″ at 65°C followed by 3′ at 68°C, which increase the duration 30″ each cycle and 30″ at 95°C for 15 cycles. 4) 1′ at 65°C and 8′ at 68°C. PCR products were run in an agarose gel (Serva) ON at 4°C and transferred into a nylon membrane. The membrane is cross-linked and incubated with a DIG-labelled $(CAG)_7$ LNA probe at 65°C for 2 h. The membrane is finally developed using anti-DIG alkaline phosphatase and CDP-star (Roche) according to the manufacturer's instructions. The progenital and modal alleles of each culture were estimated through comparison against the molecular weight ladder GeneRuler 1Kb (ThermoScientific) using GelAnalyzer 19.1 software. The progenital allele length was estimated as the 10th percentile of allele frequency distribution. The modal allele length was determined as the most frequent allele. The level of somatic instability was calculated by subtracting the 10th percentile from the 90th percentile.

DNA methylation analysis

DNA was bisulphite converted using the EZ DNA Methylation Gold kit (Zymo Research), according to the manufacturer's protocol. Bisulphite-converted DNA was amplified by nested PCR for the CTCF1 region (located upstream of the CTG repeat in the *DMPK* gene) with the TaKaRa Taq DNA polymerase (TaKaRa Bio Inc.). For the first PCR, 50 ng of bisulphite-converted DNA were used, while for the second PCR 3 μL of the first PCR product were used. Primers sequences were the following: CTCF1 F1 5′-TGTYGTYGTTTTGGGTTGTATTG-3′, CTCF1 R1 5′-TTCCY GACTACAAAAACCCTTYG-3′, CTCF1 F2 5′-GTTGTATTGGGTTGGTGGTTTA-3′, CTCF1 R2 5′-CTACAAAAACCCTTYGAACCC-3′. PCR conditions for both amplifications were: 5 min of initial denaturation at 94°C, 40 cycles of 30 s denaturation at 94°C, 30 s annealing at 57°C, and 30 s of extension at 72°C and a final extension of 5 min at 72°C. Amplicons were purified using Illustra ExoProStar 1-Step (Merck), according to the manufacturer's instructions. Purified products were sequenced using the BigDye Terminator v3.1 cycle sequencing kit (Thermo Fisher Scientific), following the manufacturer's guidelines. Sequencing products were run on an ABI Prism 3130 Genetic Analyzer (Applied Biosystems) and were analyzed with Chromas software version 2.6.6. The data obtained was represented with the Methylation Plotter web tool.[84]

Expression analysis by qPCR

RNA was extracted from 5 days differentiated myotubes using PureLink RNA Mini Kit (Invitrogen) according to the manufacturer's instructions. 500 ng of RNA was retrotranscribed using SuperScript IV reverse transcriptase (Thermo Fisher Scientific). cDNA was amplified by qPCR in a LightCycler 480 using the Lightcycler 480 SYBR Green I Master (Roche). The primers used are listed in Table S1. Amplification consisted of 40 cycles with the following conditions: 10 s at 95°C for denaturation, 10 s at 65°C for annealing and 15 s at 72°C for extension. Results were analyzed with the LightCycler 480 software.

Impedance measurements

Real-time impedance measurements were used for addressing myogenic behavior of control and DM1 immortalized human myoblasts, by using the Maestro Edge equipment with the impedance module (Axion BioSystems). Prior to cell seeding, Cytoview Z 96-well plates (Axion BioSystems) were overlaid with 100 μL of culture media and placed into the Maestro Edge to record baseline readings of the background impedance without cells. Afterward, myoblasts were seeded on the plates at 20,000 cells per well and left 1 h at room temperature to ensure homogeneous distribution of cells. Impedance was measured every minute at 41.5 kHz for the entire duration of cell culture, by the exposure of cells to small electrical currents delivered by electrodes on the plate surface. Cells were kept at 37°C and 5% CO2 inside the Maestro Edge throughout the experiment for impedance recording. Impedance data (resistance in ohms) was obtained with the AxIS Z software. Cells were grown in Skeletal Muscle Cell growth medium (SGM, PeloBiotech) and differentiated. First in basic differentiation media (bDM) and then in complete differentiation media (cDM), which includes different growth factors and extracellular matrix proteins to promote high myotube maturation (Toral-Ojeda et al., 2018, Lasa-Elgarresta et al., 2022).

Jess Western blot

RIPA lysis buffer (50 mM Tris-HCl pH 7.2, NaCl 0.9%, NP40 1%, EGTA 1 mM, EDTA 1 mM) with proteinase and phosphatase inhibitor cocktails (Thermo Fisher Scientific) and Cell-permeable inhibitor of calpain I, calpain II, cathepsin B and cathepsin L (Merck) was used to extract proteins. A Bovine Serum Albumin (BSA) concentration curve was used to quantify protein. Reagents and equipment for Jess Western blotting were all purchased from Protein Simple. Cell lysates were diluted at a final concentration of 0.5ug/ul with 0.1X sample buffer. 5X Fluorescent Master Mix was added to each sample at a 4:1 ratio (final concentrations of 1% (v/v) SDS and 40 mM DTT) and samples were incubated at 95°C for 5 min 3 mL of each sample were loaded into the cartridge. Subsequent rows of the plate were filled with blocking buffer (antibody diluent 2), primary and secondary antibody solutions, chemiluminescence reagents, and wash buffer according to the manufacturer's instructions. Previously optimized primary antibodies were diluted in antibody diluent at different ratios (1:10 MyoD Antibody (C-20): sc-304, 1:10 sc-12732 - myogenin (F5D), 1:10 Myf-5 (C-20): sc-302), followed by HRP-conjugated secondary antibodies. Finally, the plate was spun down for

5 min at 1000 × g. Plates and capillaries were loaded into a Jess machine, and assays were carried out using the standard 12- to 230-kDa or 66-440 kDa separation range protocol. Compass reports data as spectra of chemiluminescence signals versus apparent MW by assigning ladder peaks to capillary positions. Peak area calculations were performed using the Gaussian method.

Fluorescence *in situ* hybridization (FISH) and immunocytochemistry (ICC)

ICC was performed on fixed and permeabilized cell coverslips. They were blocked (PBS Triton 0.1% with 1% BSA and 1% horse serum) and incubated with anti-MBNL1 (1:200, MB1a(4A8), DSHB) or anti-desmin (1:50, D33, Abcam) overnight at 4°C. Next, the coverslips were washed with PBS-T and cells were then incubated with biotinylated horse anti-mouse-IgG (1:150, Vector) for 1 h at RT. Elite ABC kit (VECTASTAIN) was used for 30′ at RT to amplify the signal, followed by some PBS-T washes and a 2-h incubation at RT with streptavidin-FITC (1:200, Vector). In the anti-MBNL1 incubated cells we subsequently performed FISH. For that, the cells were washed and incubated with acetylation buffer (1.16% triethanolamine, 0.25% acetic anhydride) for 10 m at RT. After pre-hybridization (SSC2X, 30% formamide) the cells were incubated with 1 μM Cy3-labelled (CAG)10 probe diluted 1:100 in hybridization buffer (40% formamide, 2× SSC, 0.2% BSA, dextransulfate 100 mg/mL, vanadyl 2 Mm, tRNA 1 ug/mL, herring sperm 1 mg/mL) for 2 h at 37°C. Finally, the coverslips were washed and mounted in slides with Diamond Anti-Fade mounting medium with DAPI (Thermo Fisher Scientific). Images were taken with Zeiss AxioObserver Z1 microscope at 63× and analyzed with ZEN blue software and ImageJ.

Splicing analysis

Total RNA from primary and immortalized myotube cultures was extracted with the PureLink RNA Mini Kit (Invitrogen) according to the manufacturer's instructions. 500 ng of RNA was retrotranscribed to cDNA using SuperScript IV Reverse Transcriptase (Invitrogen) according to the manufacturer's protocol. One microliter of cDNA was used for the subsequent PCRs to analyze splicing alterations. Primers and PCR conditions are described in Table S2.

Treatment

To study treatment effect in the immortalized cell lines, we differentiated both primary and immortalized myoblasts into myotubes. On differentiation day 7 we added an antisense oligonucleotide (ASO), targeting the expansion repeat, for 48 h. The ASO used was a BNA^{NC} gapmer with the sequence AGCagcagcagCAG (Bio-Synthesis) in which capital letters mean BNA^{NC} modifications. The ASO concentration used was 30 nM.[48] Transfection was performed in differentiation media containing 0.2% lipofectamine 2000 (Thermo Fisher Scientific) and 25% Opti-Mem (Gibco).

QUANTIFICATION AND STATISTICAL ANALYSIS

Statistical analysis

Statistical analysis was performed with GraphPad Prism 8 software. Normality was determined with ShapiroWilk test. T-test or Mann-Whitney test were used for two-group comparison analysis while one-way ANOVA with Dunn's post-test or Kruskal-Wallis test was used for comparison analysis between the three cell lines. *$p \leq 0.05$, **$p \leq 0.01$, ***$p \leq 0.001$, ****$p \leq 0.0001$.